THE
PHYSICAL REVIEW

*A journal of experimental and theoretical physics established by E. L. Nichols in 1893*

SECOND SERIES, VOL. 72, NO. 4 AUGUST 15, 1947

# Nuclear Quadrupole Moment Effects in the Inversion Spectrum of Ammonia*

RICHARD J. WATTS AND DUDLEY WILLIAMS
*Ohio State University, Columbus, Ohio*

(Received April 28, 1947)

Satellite lines have been observed near lines 11, 22, 21, 33, 44, 55, 66, and 76 in the inversion spectrum of ammonia. The relative intensities and displacements of these satellites are in excellent agreement with Van Vleck's recent theory. From the observed separations of the satellites from the main lines can be calculated the interaction energy between the electrical quadrupole moment of the nitrogen nucleus and the electric field of the ammonia molecule.

THE presence of satellite lines constituting a hyperfine structure in the "inversion spectrum" of ammonia was first reported by Good.[1] These satellite lines were observed close to the fine-structure lines in the neighborhood of 0.8 $cm^{-1}$. Their existence has been confirmed by further experiments in other laboratories. The presence of these satellite lines has been explained by the recent theories developed by Van Vleck *et al.*[2] and by Coles and Good.[3] According to these theories, the observed satellite lines result from the interaction of the electrical quadrupole moment of the $N^{14}$ nucleus and the electric field of the other charges in the ammonia molecule.

Van Vleck's equations for the separations of satellites from the central line are as follows:

$$h\Delta\nu = \pm\frac{3}{16}Q\frac{\partial^2 V}{\partial z^2}\left[1-\frac{3K^2}{J(J+1)}\right]\left[\frac{J+1}{2J+3}\right],$$

$$h\Delta\nu' = \pm\frac{3}{16}Q\frac{\partial^2 V}{\partial z^2}\left[1-\frac{3K^2}{J(J+1)}\right]\left[\frac{J}{2J-1}\right],$$

where $\Delta\nu$ and $\Delta\nu'$ denote frequency separations of satellites from the main line, $Q$ is the nuclear quadrupole moment of $N^{14}$ as defined by the expression $\{\rho(3z^2-r^2)\}_{Av}$, and $J$ and $K$ are rotational quantum numbers associated with the total molecular angular momentum and angular momentum about the figure axis of the molecule, respectively.

The agreement of predicted separations with the experimentally observed values was found to be excellent for lines 11, 22, 33, and 44.[2] Another aspect of Van Vleck's theory indicates that the intensity of the satellite lines should decrease rapidly with increasing values of $J$. The experimental results thus far published in detail[2] are in agreement with this prediction, and no satellite lines have been reported for lines with $J$ greater than 4.

The purpose of the present note is to report the results of recent studies conducted in this laboratory, in which satellite lines have been observed for $J$ values as high as 7. The techniques are similar in essentials to those used earlier by other investigators. A modulated Klystron oscillator was used as a source of radiation, and single-crystal detection was employed. The ammonia under study was in a rectangular wave guide equipped with mica

* A research contribution of the Ohio State University Research Foundation under Contract No. W28-099-ac-179 with the Watson Laboratory of Army Air Forces Air Materiel Command, Red Bank, New Jersey.

[1] W. E. Good, Phys. Rev. **70**, 213 (1946).

[2] B. P. Dailey, R. L. Kyhl, M. W. P. Strandberg, J. H. Van Vleck, and E. B. Wilson, Jr., Phys. Rev. **70**, 984 (1946).

[3] D. E. Coles and W. E. Good, Phys. Rev. **70**, 979 (1946).

windows. The length of the section of wave guide forming the "absorption cell" was 100 ft., and pumping was accomplished through a $\frac{1}{16}$-in. slot in the wall. The length of this slot was 5 ft. With an oil diffusion pump, pressures as low as $5\times10^{-3}$ mm of mercury could be attained; these pressures could be maintained for several hours after the absorbtion section was isolated from the pumps.

Spectral lines were observed from an oscillograph trace. The modulating voltage was plotted horizontally and transmitted power vertically on the cathode-ray screen. The results obtained for lines 11, 22, 33, 44, 55, 66, 21, and 76 are given in Fig. 1 in which photographs of the oscilloscope trace are shown. The satellite lines are readily discernible for all these lines except 21 and 76, in which they are barely discernible in the noise. The 21 line itself is rather weak, and the intensities of the satellites relative to the main lines are comparable with the relative intensities of the satellites near the 22 line. However, the intensity of satellites relative to the strong 76 is extremely low.

Measurements of the relative separations $\Delta\nu$ and $\Delta\nu'$ were made by two methods. The first involved measurements of separations of the satellite lines from the main lines on the oscillograph trace; ratios of the separations were then taken to give $\Delta\nu'/\Delta\nu$. This method requires that the oscilloscope separation be directly proportional to frequency difference. Measurements made under different conditions of modulating voltage, horizontal amplifier gain, etc., gave fairly consistent results for the $\Delta\nu'/\Delta\nu$ ratio. Since the satellite pattern is found by other methods to be symmetrical in frequency, it is simple to detect radical departures from linearity. The second method of determining $\Delta\nu'/\Delta\nu$ involves determination of the actual frequency separations by introducing modulating radiofrequency signals from a variable-frequency oscillator. If such a radiofrequency modulation of the order of a few megacycles is applied to the Klystron repeller, small "ghosts" appear near an absorption line on the oscillograph trace. The frequency separation of the "ghost" and the main line is a multiple of the modulation frequency. By comparison of "ghost" and satellite positions, the absolute values of $\Delta\nu$ and $\Delta\nu'$ may be determined. This method of measuring frequency differences has been used by Strandberg *et al.*[2] The accuracy with which frequency differences can be measured by this method is $\pm0.05$ megacycles.

The results obtained for satellite separations

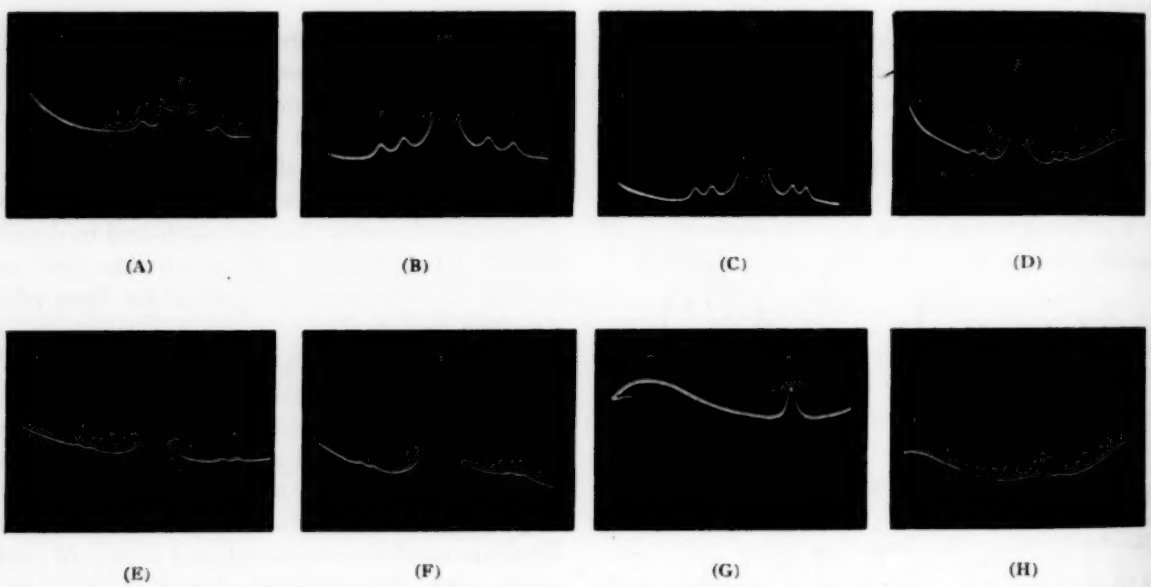


FIG. 1. Photographs of oscilloscope traces showing ammonia absorption lines as follows: A, line 11; B, line 22; C, line 33; D, line 44; E, line 55; F, line 66; G, line 76; H, line 21. All photographs except G and H were obtained with ammonia at identical pressure $\sim10^{-2}$ mm Hg; the pressure was only slightly different when photographs G and H were taken.

TABLE I. Separations of satellites from main lines.

| Line | $\Delta\nu$ | $\left(\frac{\Delta\nu_{JK}}{\Delta\nu_{11}}\right)_{obs.}$ | $\left(\frac{\Delta\nu_{JK}}{\Delta\nu_{11}}\right)_{calc.}$ | $\Delta\nu'$ | $\left(\frac{\Delta\nu_{JK'}}{\Delta\nu_{11'}}\right)_{obs.}$ | $\left(\frac{\Delta\nu_{JK'}}{\Delta\nu_{11'}}\right)_{calc.}$ | $\left(\frac{\Delta\nu'}{\Delta\nu}\right)_{obs.}$ | $\left(\frac{\Delta\nu'}{\Delta\nu}\right)_{calc.}$ |
|---|---|---|---|---|---|---|---|---|
| 11 | 0.62[5] Mc | 1.00 | 1.00 | 1.61 Mc | 1.00 | 1.00 | 2.55 | 2.50 |
| 22 | 1.33 | 2.13 | 2.14 | 2.10 | 1.30 | 1.33 | 1.56 | 1.56 |
| 21 | 0.72 | 1.15 | 1.07 | 1.07 | 0.66 | 0.66 | 1.52 | 1.54 |
| 33 | 1.74 | 2.79 | 2.78 | 2.39 | 1.48[5] | 1.50 | 1.36 | 1.35 |
| 44 | 1.98 | 3.17 | 3.18 | 2.54 | 1.58 | 1.60 | 1.28 | 1.26 |
| 55 | 2.31 | 3.70 | 3.47 | 2.79 | 1.67 | 1.67 | 1.21 | 1.20 |
| 66 | 2.28 | 3.65 | 3.67 | 2.64 | 1.64 | 1.72 | 1.18 | 1.17 |
| 76 | 1.38 | 2.21 | 2.19 | 1.72 | 1.07 | 1.00 | 1.20 | 1.14 |

are summarized in Table I. It will be noted that the experimental results are in agreement with Van Vleck's theory within the limits of experimental error. The values given in the table for $\Delta\nu'/\Delta\nu$ combine the results obtained by the two methods listed above.

The experimentally obtained results can be fitted to Van Vleck's equations to give a value for the interaction energy $Q\partial^2V/\partial z^2$ between the nuclear quadrupole moment and the electric field. In obtaining the value for the interaction energy, we have obtained the frequency which when multiplied by $h$ gives $Q\partial^2V/\partial z^2$ as defined above. This frequency is:

$$\frac{1}{h}Q\frac{\partial^2V}{\partial z^2}=17.05\pm0.11 \text{ megacycles.}$$

Stated in wave numbers, this frequency is

$$5.67\pm0.04\times10^{-4} \text{ cm}^{-1}.*$$

*_Note added in proof:_ This frequency should be divided by 4 for direct comparison with the "quadrupole coupling" terms given by Townes [Phys. Rev. 71, 909 (1947)].

# On the Origin of the Soft Component of Cosmic Radiation

W. HEITLER AND S. POWER
*Dublin Institute for Advanced Studies, Dublin, Ireland*
(Received April 24, 1947)

The intensity of the soft component in the upper atmosphere is calculated on grounds of an improved version of an earlier theory, assuming that the soft component is produced by a short-lived meson which, along with ordinary mesons, is produced by primary protons. The position of the maximum is largely influenced by the mean free path of the primary protons. The results (which are largely independent of the details of the theory), including the latitude effect, are in good agreement with the experiments, thus showing that the bulk of the soft component can be understood by this mechanism. The absence of the east-west effect must be explained by a large angular straggling.

## 1. INTRODUCTION

RECENTLY a theory of the soft component of cosmic rays has been given[1] in which it is assumed that the incoming primary radiation consists solely of protons.

On interacting with matter at the top of the atmosphere, these protons produce mesons. The symmetrical theory of a mixture of pseudoscalar and transverse mesons was used, the former being responsible for the penetrating component, whereas the latter give rise to the major part of the soft component, through rapid $\beta$-decay.

This "mixed" meson theory was chosen as the one which leads to the best understanding of the nuclear forces. In fact, the $\beta$-decay of the heavier nuclei seems incomprehensible unless we assume the existence of a short-lived kind of meson. Since the mesons at sea level are probably pseudoscalar it seems likely that these short-lived mesons are the transverse mesons required by the theory. The existence of a short-lived kind of meson seems equally indispensable for an explanation of the soft component, for the following reasons:

It has been shown[2] that if the total primary radiation consisted solely of electrons, the soft component could be explained completely by the cascade theory. This, however, cannot be true. A large fraction of the primary radiation must consist of protons in order to account for the hard component. Recent rocket experiments[3] also seem to indicate that at least 70 percent of the incoming primaries are protons. Of the remaining 30 percent, some at least must be slow protons, which fail to penetrate a thickness of 15.2 cm of lead used in the experiments or produce only slow mesons which cannot penetrate the lead. Therefore, the fraction of primaries which may be electrons is likely to be something less than 30 percent.

This small fraction of the primaries alone cannot explain the intensity of the soft component. Some other origin is at least partly necessary. Thus, it is important to know whether the soft component can be explained, through secondary and tertiary effects, by a primary radiation of protons only. In the present theory, the major contribution is supplied by the transverse mesons which, decaying at once, produce primary electrons. These in turn increase by cascade multiplication, thus giving rise to the soft component. We shall see that the soft component can indeed be accounted for in this way. It may be added that the results would be practically the same if any other kind of short-lived meson exists (for instance neutrettos) which decays into electrons or photons.

We shall be concerned in this paper only with the bulk of the soft component in the higher part of the atmosphere, which will be seen to consist mainly of comparatively slow electrons. In particular the origin of the large extensive air showers will not be investigated here. It may well be that these necessitate a small energetic primary electron component. By assuming a primary proton component solely, we do not wish to exclude the possibility that a certain

[1] J. Hamilton, W. Heitler, and H. W. Peng, Phys. Rev. **64**, 78 (1943). (In the following quoted as HHP.)
[2] W. Heitler, Proc. Roy. Soc. **161**, 261 (1937); L. W. Nordheim, Phys. Rev. **51**, 1110 (1937).
[3] S. E. Golian, E. H. Krause, and G. J. Perlow, Phys. Rev. **70**, 776 (1946).

fraction of the primaries may be electrons. It is clear that this would not alter anything essential in our results: Since both primary electrons and primary protons give rise to about the same intensity (relative to the number of primary particles), any mixture of primary components would do the same.

Since the publication of the HHP paper,[1] certain modifications have become necessary in the theory, and this is the reason the work has been resumed. One of these modifications has been dealt with in detail in a recent paper by one of us.[4] It refers to the expressions for the cross sections for the production of a meson in a proton-nucleon collision. In order to calculate these cross sections, the method of Weizsäcker-Williams was used, according to which the field of a fast-moving particle, energy $E$, is considered as equivalent to a spectrum of virtual quanta, of various energies. One of these quanta, with energy $\epsilon$, is then scattered by a second particle at rest. The process appears as an emission of a quantum of energy $\epsilon'$, while $\epsilon$ is lost by the fast particle, and the energy $\epsilon-\epsilon'$ is transferred to the particle at rest. There are two distinct contributions to the cross sections derived by this method: (I) where the virtual mesons $\epsilon$ are attributed to the actually moving nucleon, and (II) where the virtual mesons are those belonging to the nucleon actually at rest but considered from a Lorentz frame where the roles of the two nucleons are interchanged. It was the inclusion of contribution (II) which was not considered in HHP.[1]

[4] W. Heitler, Proc. Roy. Irish Acad. **50A**, 155 (1945); W. Heitler and P. Walsh, Rev. Mod. Phys. **17**, 252 (1945). A slightly different interpretation of the Weizsäcker-Williams method has recently been suggested by H. A. Bethe, Phys. Rev. **70**, 787 (1946). The fact that the number of virtual mesons accompanying a fast nucleon is greater than unity has led Bethe to assume that one has to deal here with a multiple emission of mesons. We think it rather doubtful that interpretation is really correct. The number of virtual quanta has no physical meaning other than the strength of force acting on the nucleon at rest, and there is no upper limit for it. In other words, in intermediate states "probabilities" larger than unity may occur, and do occur in theories of particles with integral spin. It is the nucleon at rest which emits the meson (but owing to the exchange character of the forces the fast nucleon loses the charge). We remark that, unless the cross section for meson production is smaller by an order of magnitude than is at present believed, or else the Weizsäcker-Williams method is completely wrong, it follows from the experiments directly that the number of virtual mesons must be larger than unity. A discussion of this fact on different lines has been given by one of us (H) in Proc. Roy. Irish Acad. **50A**, 1 (1944).

These two contributions $\Phi^{I}$ and $\Phi^{II}$ must then be added to give the actual cross sections for meson production. The detailed discussion of this modification has been given in reference 4. The resulting cross sections will merely be quoted in Section 2.

There is a further important modification. It has been remarked by Janossy[5] that the cross section for meson production in a nucleon-nucleon collision, is of the same order of magnitude as the average area occupied by a nucleon in the nucleus. Thus, in its passage through a nucleus, a proton will, on the average, produce more than one meson. Thus the mesons are not produced uniformly, but in small groups. So we can no longer consider the nucleons of matter as being distributed at random, but as being concentrated in groups in the nuclei. An incoming proton will thus travel on the average a distance $l$ before coming in contact with a nucleus, $l$ being the mean free path of a proton in air. The mesons are then produced during the passage of the proton through the nucleus. This modification has the very important effect of shifting the position of the maximum intensity of the soft component (as function of depth) to greater depths. This is very satisfactory, as it will be remembered that previously (HHP) the maximum occurred too near the top of the atmosphere, when compared with the experimental results.

## 2. CROSS SECTIONS FOR MESON PRODUCTION

We quote the formulas of reference 4 for the two contributions $\Phi_t^{I}$ and $\Phi_t^{II}$ for the production of a transverse meson, of energy $\epsilon$, by a nucleon with energy $E$:

$$\Phi_{tNR}{}^{I}d\epsilon=\frac{8}{3}f^2(D_t+D_p)\frac{d\epsilon}{\epsilon^3}\left(1-\frac{\epsilon}{M}\right),\qquad \frac{1}{f}<\epsilon<\frac{M}{2} \tag{1a}$$

$$\Phi_{tER}{}^{I}d\epsilon=\frac{16}{3}\frac{f^2}{M}D_p d\epsilon\left[\frac{1}{\epsilon^2}-\epsilon\left(\frac{2}{E}\right)^3\right],\qquad \frac{M}{2}<\epsilon<\frac{E}{2} \tag{1b}$$

[5] L. Janossy, Phys. Rev. **64**, 345 (1943).

$$\Phi_{tNR}{}^{II}d\epsilon=\frac{4}{9}Mf^2(D_t+D_p)\frac{E-\epsilon}{E^2}d\epsilon$$

$$\times\begin{cases}\left(f^3-\dfrac{8}{M^3}\right) & 1<\epsilon<\dfrac{2E}{Mf}\\ \dfrac{8}{M^3}\left(\dfrac{E^3}{\epsilon^3}-1\right), & \dfrac{2E}{Mf}<\epsilon<E\end{cases} \quad (1c)$$

$$\Phi_{tER}{}^{II}d\epsilon=\frac{32f^2}{M}D_t\frac{d\epsilon}{E^3}(E-\epsilon)\left[\frac{E-\epsilon}{M}-1\right],$$

$$1<\epsilon<E-M. \quad (1d)$$

Each formula is valid only for the energy regions indicated: where they overlap, all contributions must be added. $D_t$ and $D_p$ are certain constants of which, however, our results will be practically independent, $f^2=0.13$ from the theory of nuclear forces. We also use the same natural meson units $c=\hbar=\mu=1$. Cross sections, therefore, are in units of $(\hbar/\mu c)^2=4.3\times10^{-26}$ cm$^2$ and energies in units of $\mu c^2=0.94\times10^8$ ev. In the absence of any conclusive information about the mass of the vector meson we have assumed it to be equal to that of the ordinary meson. The first part of our considerations will be independent of the unit for the thickness of matter traversed. In the section which depends on the cascade theory, we use cascade units. With this unit of length, cascade processes take place in the same way in all materials. In these units, the height of the atmosphere is 24, one cascade unit equaling 3.2 cm. Hg.

There are now two additional contributions to the cross sections (1b) and (1d) which were omitted previously (because of a numerical error in an earlier paper[6]) dealing with the cross section for scattering of a transverse meson by a nucleon in the extreme relativistic region. These contributions are:

$$\Phi_{tER}{}^{I'}d\epsilon=2f^2D_td\epsilon\left[\frac{3K}{7\epsilon^{4/3}}-\frac{2}{M\epsilon^2}\right.$$

$$\left.-\frac{3K}{7}\frac{2^{7/3}}{E^{7/3}}\epsilon+\frac{16\epsilon}{ME^3}\right], \quad \left(\frac{M}{2}<\epsilon<\frac{E}{2}\right) \quad (2b)$$

$$\Phi_{tER}{}^{II'}d\epsilon=2f^2D_td\epsilon\left[-3K2^{1/3}\left\{\frac{E-\epsilon}{E^{7/3}}-\frac{1}{M^{1/3}}\right.\right.$$

$$\left.\left.\cdot\frac{(E-\epsilon)^{4/3}}{E^{7/3}}\right\}+\frac{12}{M}\left\{\frac{E-\epsilon}{E^3}-\frac{(E-\epsilon)^2}{M\cdot E^3}\right\}\right],$$

$$(1<\epsilon<E-M) \quad (2d)$$

where

$$K=\frac{8\sqrt{3}\cdot2^{2/3}\cdot\pi\cdot f^{4/3}}{9M^{1/3}}.$$

In this earlier paper,[6] the total cross section $\Phi$ for the scattering of a transverse meson by a nucleon into a meson of any polarization, in the center of gravity system, was given as

$$\Phi=8\pi(\tfrac{1}{2}+2\bar{\lambda})/\epsilon^2$$

(total charge of system $=2$, $-1$, symmetrical theory), where $\bar{\lambda}$ was incorrectly given as

$$\bar{\lambda}=\pi f^4\tau^{2/3}/6\sqrt{3}$$

with

$$\tau=f^2\epsilon^2.$$

Although $\bar{\lambda}$ was seen to increase with $\epsilon$, it was remarked that the smallness of $f^2=0.13$ made the term negligible, up to large values of $\epsilon$ (actually $\epsilon\sim60$). Thus in (HHP), $2\bar{\lambda}$ was neglected, and $\Phi$ was simply given the value $4\pi/\epsilon^2$.

The true value for $\bar{\lambda}$ is, however,

$$\lambda=\frac{\pi}{3\sqrt{3}}\cdot\frac{\tau^{2/3}}{2^{2/3}}-\frac{3}{16} \quad (3a)$$

for the scattering of a positive meson by a proton and

$$\bar{\lambda}=\frac{\pi}{3\sqrt{3}}\tau^{2/3}\cdot\frac{2^{2/3}}{3}\begin{pmatrix}1-\dfrac{1}{2^{4/3}} & \dfrac{1}{2^{1/3}}-\dfrac{1}{2}\\ \dfrac{1}{2^{1/3}}-\dfrac{1}{2} & \dfrac{3}{4}\end{pmatrix}$$

$$-\frac{3}{16}\begin{pmatrix}1 & 0\\ 0 & 1\end{pmatrix} \quad (3b)$$

for the scattering of a negative meson by a proton. The first row and column refer to a scattered negative meson, the second to a neutretto. The quantity $2\bar{\lambda}$ is now comparable with $\frac{1}{2}$ for all energies and cannot be neglected.

[6] W. Heitler and H. W. Peng, Proc. Roy. Irish Acad. **49A7**, 101 (1943).

The additional contributions to the cross sections (1) for meson production due to the inclusion of these $\bar{\lambda}$ terms are (2b) and (2d).

Now, it must be remarked that the formulas for the cross sections for meson scattering in the extreme relativistic region are already rather doubtful, as they have been derived under the assumption that the existence of multiple processes does not influence the scattering of a single meson. This fact has only been proved mathematically to be true for low energies;[7] for high energies it is not at all mathematically certain and may not be true, because at high energies a large number of possible multiplicities may occur, and even if each of them may have a small influence, the total effect may be large. Although $\Phi_{NR}$ arising from the non-relativistic energy region of meson scattering is unaffected (and the main contribution to the production of mesons of all energies comes from this region), there is an uncertainty of $\Phi_{ER}$ arising from the extreme relativistic region. In particular it may be doubtful whether the cross sections for scattering of a meson are really as large as is indicated by the $\bar{\lambda}$-terms, or whether the influence of multiple processes causes a large damping, making them much smaller. Furthermore, the expressions (3) are asymptotic, valid for $\epsilon \to \infty$. They are needed, however, mainly in the region $\epsilon = M - 5M$, say. If (3) were valid down to the boundary between the non-relativistic and extreme relativistic regions ($\sim M$), the formulas for the scattering of a transverse meson valid in the two regions would differ by a factor almost 10 at the boundary. It is, therefore, highly probable that $\bar{\lambda}$ assumes its asymptotic value (3) only at extremely high energies and is much smaller than (3) in the energy region needed. For this reason, the calculations have been performed twice, with and without these extra terms. It will be seen that there is not much difference between the two results, for the following reason: Although the cross section for the production of mesons is considerably increased by including the $\bar{\lambda}$-terms, the energy loss, $\Phi_{\text{en. loss}}$, is also increased. The total number of mesons (and hence electrons) produced depends, however, on the ratio of the production cross section and the energy loss of the primary proton. This ratio does not change much. We shall need the modified expression for $\Phi_{\text{en. loss}}$ caused by the $\bar{\lambda}$-terms.

The original expression for the energy loss[4] was

$$E\Phi'_{\text{en. loss}} = [1.5E + 22\log(E/M) - 1.0]D_t \cdot 10^{-2} \quad (4)$$

and was approximated by the first term, so that[5]

$$E\Phi'_{\text{en. loss}} = D_t(1.5 \times 10^{-2}E). \quad (4')$$

The extra energy loss due to the inclusion of the $\bar{\lambda}$-terms is computed to be

$$E\Phi''_{\text{en. loss}} = D_t \times 10^{-2}(6.7E - 4.7E^{\frac{1}{2}} - 12\log(E/M) - 88). \quad (5)$$

This, in turn, is approximated by the formula

$$E\Phi''_{\text{en. loss}} = D_t(4.9 \times 10^{-2}E), \quad (5')$$

for the values of $E$ which are most important. Equation (5′) has to be added to (4′). Then

$$(-dE/dx) = NE\Phi_{\text{en. loss}},$$

where $N$ equals the number of nucleons contained in a cylinder of unit length, and of cross section $(\hbar/\mu c)^2$. Thus the distance traveled by a fast nucleon while losing energy from $E_0$ to $E$ is

$$x_{E_0,\,E} = k^{-1}\log(E_0/E), \quad (6)$$

where $k = N \cdot \Phi_{\text{en. loss}}$ and has the value $N \cdot D_t 6.4 \times 10^{-2}$ and $N \cdot D_t 1.5 \times 10^{-2}$, respectively, according to whether the $\bar{\lambda}$-terms are included or not.

There is one further remark to be made about the numerical values of the constants $D$. These values depend on the lower limit of the impact parameter $b_{\min}$ used in deriving the number of virtual quanta. In particular, the number of transverse mesons, with energy $\epsilon$, was found to be[6]

$$q_{t,}d\epsilon = (d\epsilon/\pi\epsilon)(f^2D_t + g^2C),$$

where both $D_t$ and $C$ are functions of $\epsilon$ and of the impact parameter $b_{\min}$. Now $b_{\min}$ is certain to be of the order $\hbar/\text{Mc} = 0.1$ in our units. If $b_{\min}$ is identified with this value then $D_t$ was found to be 165. $C$ was found to be negligible. Now the

[7] W. Heitler and H. W. Peng, Proc. Camb. Phil. Soc. 38, 296 (1942).

[8] Eqs. (4) and (4′) are in fact not directly proportional to $D_t$, but are proportional partly to the factor $(D_t + D_p)$ and partly to $(D_t + 2D_p)$. However, since $D_t$ and $D_p$ depend on the impact parameter in such a way (see below) that the ratio $D_p/D_t$ is virtually constant, and $D_t$ is very much larger than $D_p$, $E \cdot \Phi_{\text{en. loss}}$ is roughly proportional to $D_t$.

actual value of $D_t$ depends rather sensitively on $b_{\min}$ and decreases when $b_{\min}$ is taken larger. If $b_{\min}$ is taken to be $2\hbar/\mathrm{Mc}$, the value of $D_t$ would decrease by roughly a factor 3. However, it will be seen that this dependence of the number of virtual mesons, on the impact parameter does not affect the results. For $D_t$ occurs in all formulas relating to the total number of mesons produced only in the ratio

$$D_t/\Phi_{\text{en. loss}}$$

where $\Phi_{\text{en. loss}}$ is the cross section for energy loss. Since $\Phi_{\text{en. loss}}$ itself is directly proportional to $D_t$,[2] this ratio is quite independent of $b_{\min}$, provided that the order of magnitude of $b_{\min}$ is correct.

On account of this fact, the absolute values of the cross section for meson production and the energy loss of the proton are very uncertain as long as one is forced to use the Weizsäker-Williams method, and both may be considerably smaller than the values given in references 1 and 4, if it should turn out that $b_{\min}$ is to be taken larger than $\hbar/\mathrm{Mc}$. Nevertheless, the total number of mesons appearing at any depth lower than the meson producing layer is more reliably given by the theory as it is independent of the actual value of $b_{\min}$.

### 3. THE TOTAL NUMBER OF ELECTRONS PRODUCED

We assume a spectrum of primary incoming protons, whose energy distribution at the top of the atmosphere we denote by

$$F(E_0)dE_0.$$

The actual process of meson production is roughly as follows: a primary proton on colliding with a nucleus produces a number of pseudoscalar and vector mesons during its passage through the nucleus. If its energy is not very high, the proton is probably brought to rest in one collision. If its energy is high, however, the proton may travel through two or three or even more nuclei, on an average, before being stopped. Since, however, our knowledge of the mean free path of a proton in air is very uncertain, and the accuracy of the theory not sufficient to compute it reliably, we simplify this rather complicated process, as follows: We assume that the proton is brought to rest in its passage through one (say, rather big) nucleus, and the mean free path of the proton is readjusted. This we introduce at a later stage of the considerations. During the passage through this one nucleus all the mesons are then assumed to be produced. Clearly, the total number of mesons produced by a proton is quite independent of the density of the matter traversed (in our case nuclear matter), and is quite independent of any unit of length. The above simplification of the picture can hardly affect the results appreciably. In particular, the position of the maximum and its height should be given correctly if for the mean free path of the proton its actual experimental value is taken.

Thus a proton, in its passage through the nucleus, will by (3) lose energy uniformly with distance according to the law $e^{-kx}$. We assume further that the primary spectrum is of the form

$$F(E_0)=A/E_0^{\alpha+1}. \tag{7}$$

$A$ is a normalization factor. The constant $\alpha$ is determined from the meson intensities at great depths. The value $\alpha=1.5$ represents the facts quite well. The number of primary nucleons at a depth $x$, with energy $E$, is given by (6) and (7)

$$F(E, x)dE=Ae^{-k\alpha x}(dE/E^{\alpha+1}). \tag{8}$$

Then the number of transverse mesons produced at a depth $x$ of nuclear matter within an energy interval $d\epsilon$ is

$$N\cdot d\epsilon\int_{\epsilon}^{\infty}\Phi_t(E, \epsilon)F(E, x)dE, \tag{9}$$

$N$ is the number of nucleons per unit volume. $\Phi_t$ is the cross section (1) and (2) for production of a meson $\epsilon$ by a nucleon of energy $E$, and $F(E, x)$ is the number of nucleons of energy $E$, at depth $x$, given by Eq. (8). These transverse mesons, having an extremely short lifetime, decay at once, each producing an electron and a neutrino. The probability of an electron of energy $\bar{\epsilon}$, being produced by a meson of energy $\epsilon$ in this way is $d\bar{\epsilon}/\epsilon$. The total number of electrons, within the energy interval $d\bar{\epsilon}$, produced in a layer $d$ of nuclear matter is

$$N\cdot Ad\bar{\epsilon}\int_{\bar{\epsilon}}^{\infty}d\epsilon/\epsilon\int_{\epsilon}^{\infty}\Phi_{tr}(E, \epsilon)\int_{0}^{d}e^{-k\alpha x}(dE/E^{\alpha+1}).$$

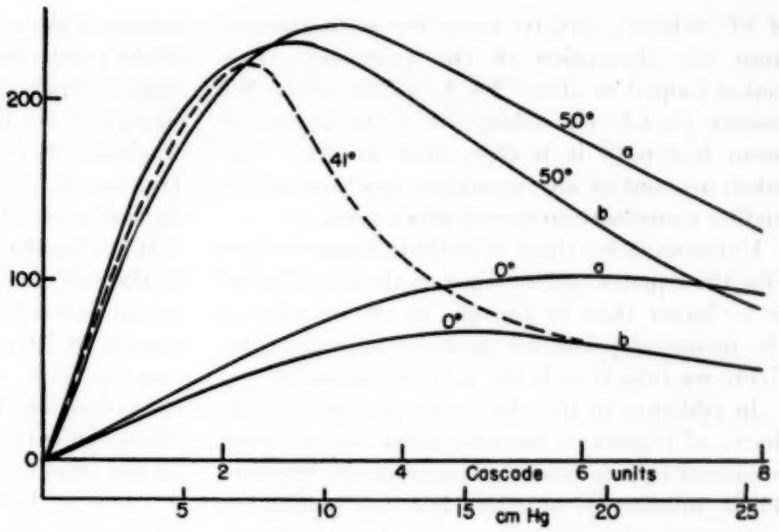


FIG. 1. Intensity of the soft component in the high atmosphere, at 50° and 0° latitude. Curve *a* with, and *b* without inclusion of the $\lambda$-terms. Dotted curve experimental at 41°. For the equator the mean free path of the primary protons was assumed to be 4.5 cascade units, at 50°, 2.5 cascade units. Normalization: 100 incoming primaries.

Obviously, only very small values of $x$ contribute to this integral, so that one may extend the integration over $x$ to infinity. There is a further point to be considered in integrating over $x$: the fact that the primary proton spectrum is cut off at a value $E_\vartheta$ of $E_0$ which depends on the geomagnetic latitude $\vartheta$, imposes the following conditions

$$x>(1/k)\log(E_\vartheta/E), \quad E<E_\vartheta,$$
$$>0, \quad E>E_\vartheta.$$

Having performed the integration over $x$, we get the total number of electrons of energy $\bar{\epsilon}$

$$N(\bar{\epsilon})d\bar{\epsilon}=\begin{cases}\dfrac{N\cdot A}{k\alpha}\cdot\dfrac{d\bar{\epsilon}}{(E_\vartheta)^\alpha}\displaystyle\int_{\bar{\epsilon}}^{\infty}\frac{d\epsilon}{\epsilon}\int_{\epsilon}^{\infty}\Phi_{tr}(E,\epsilon)\frac{dE}{E}, & (E<E_\vartheta)\quad (10a)\\[2ex] \dfrac{N\cdot A}{k\cdot\alpha}d\bar{\epsilon}\displaystyle\int_{\bar{\epsilon}}^{\infty}\frac{d\epsilon}{\epsilon}\int_{\epsilon}^{\infty}\Phi_{tr}(E,\epsilon)\frac{dE}{E^{\alpha+1}}. & (E>E_\vartheta)\quad (10b)\end{cases}$$

For $\Phi$ we insert the cross sections (1) and (2). The limits $\epsilon\cdots\infty$, and $\bar{\epsilon}\cdots\infty$ have to be replaced by narrower limits, according to the regions of validity of the formulas (1) and (2). The integration can then be performed by simple analytical methods.

#### 4. CASCADE MULTIPLICATION

The formulas (10) give the total number of electrons produced in the energy interval $d\bar{\epsilon}$ by the passage of a primary proton averaged over the primary energy spectrum through our "model nucleus," which we have assumed to be so large that the proton is stopped. If we now denote the mean free path of the proton in air by $l$, the chance of its colliding with a nucleus in a distance $d\xi$ is

$$e^{-\xi/l}d\xi/l.$$

Therefore, with the above assumptions, the number of electrons of energy $\bar{\epsilon}$ produced at a depth $\xi$ from the top of the atmosphere because of the decay of transverse mesons is

$$N(\bar{\epsilon})\cdot e^{-\xi/l}\cdot d\xi\cdot d\bar{\epsilon}/l.$$

We measure $\xi$ now in cascade units.

If $C(\bar{\epsilon}, x-\xi)$ be the cascade multiplication function (i.e., the number of electrons produced at a depth $x$, by a single primary electron, energy $\bar{\epsilon}$, at depth $\xi$) the total number of electrons of all energies, observed at depth $x$, because of the decay of transverse mesons, is

$$Z_t(x)=\int_0^x e^{-\xi/l}\frac{d\xi}{l}\cdot\int_0^\infty d\bar{\epsilon}\cdot N(\bar{\epsilon})C(\bar{\epsilon}, x-\xi). \quad (11)$$

This integral has been worked out by numerical integration for two different latitudes, $\vartheta=50^0$ and $\vartheta=0°$ (equator). For $C$ we have used the figures given by Bhabha.

As we do not know with sufficient accuracy, from theoretical considerations, the value of the mean free path $l$, we have taken, for a latitude

of 50°, Schein's effective mean free path, derived from the absorption of the primaries.[9] This makes $l$ equal to about 2.4–3 cascade units. We assume $l=2.5$. By taking for $l$ the measured mean free path it is clear that we have also taken account of any secondary nucleons which further contribute to meson production.

Unfortunately, there is nothing known about $l$ for the equator: all we know is that it is bound to be larger than in Europe, as the energies of the incoming primaries must be larger. Tentatively we take it as being 4.5 cascade units.

In addition to the electrons produced by the decay of transverse mesons, there are electrons produced by the decay of pseudoscalar mesons. Their number is smaller, but not negligible, compared with those caused by transverse mesons. As remarked in (HHP), their number is about $\frac{1}{3}$ of the total number of electrons produced in the upper layers of the atmosphere. They are therefore included by multiplying (11) by a factor $\frac{3}{2}$. (When the $\bar{\lambda}$-terms are included we have added half of the contribution without $\bar{\lambda}$.)

In Fig. 1, the intensity of the soft component for the top part of the atmosphere (normalized for 100 incoming protons) is plotted for $\vartheta=50°$ and the equator and calculated both with (curve *a*) and without (curve *b*) the $\bar{\lambda}$-terms. It is seen that there is very little difference between them. We have also plotted a recent experimental curve for the intensity measured by rocket experiments at White Sands, New Mexico, ($\vartheta=41°$N). The agreement between these curves is as good as can be expected, considering the inaccuracies of the theory. The position of the maximum has been shifted to lower heights than in (HHP), and appears to agree now with the experimental curve rather well. This is due mainly to the fact that a proper account was taken of the mean free path of the primaries, whereas in (HHP) the nucleons of air were considered as uniformly distributed. The electrons produced according to the theory are mainly of low energies, the vector mesons which produce them having themselves, on an average, comparatively low energies. If these alone are multiplied by the cascade process, they give a maximum too near the top of the atmosphere. The introduction of the mean free path causes the necessary shift towards lower heights.

It is clear from Fig. 1, that the latitude effect of the soft component is very large. The theoretical intensity at the equator is about 30 percent at 7.6 cm Hg of that at 50°. This agrees roughly with the measurements of the total ionization by Bowen, Millikan, and Neher.[10] Measurements of the soft intensity at the equator do not seem to exist.

There is, however, a difficulty in our theory which was already referred to in (HHP), and which still persists: the soft component does not seem to show an east-west effect. This seems to suggest that it must arise from an equal number of positive and negative primaries. It was suggested in (HHP) that since the soft component is produced by the protons in such an indirect way, and arises mainly from mesons and therefore electrons of low energy, the east-west effect may be blurred by a large angular spread of the electrons, as it would indeed follow from the theory.

The same view must be taken here—and in any theory that accounts for the soft component as arising indirectly from a primary proton component only. This point requires further clarification from the experimental side.

The results of this paper can be stated as follows: If the existence of a short-lived meson (transverse meson or neutretto) is assumed, the bulk of the soft component can be accounted for as due to a primary proton component only. The same will be the case if the primary radiation consists of any mixture of protons and primary electrons with similar energy spectra, but, of course, the meson component can only be accounted for if the primary proton component is not too weak. The absence of an east-west effect, if confirmed, must be explained by a large angular spread.

[9] M. Schein, M. Iona, and J. Tabin, Phys. Rev. **64**, 253 (1943). These experiments may not be sufficiently accurate yet. One may, *vice versa*, from the position of the maximum conclude that the mean free path of the protons in air must be between two and three cascade units.

[10] I. S. Bowen, R. A. Millikan, and H. V. Neher, Phys. Rev. **53**, 855 (1938).

# Decay Scheme of $Sb^{124}$

WALTER E. MEYERHOF AND GERTRUDE SCHARFF-GOLDHABER
*Department of Physics, University of Illinois, Urbana, Illinois*

(Received June 23, 1947)

The beta- and gamma-rays emitted by $Sb^{124}$ (60d) have been investigated with the help of Geiger-counter coincidences. We find that the hard beta-ray of 2.4 Mev is followed by one gamma-ray, while the soft beta-ray of 0.7 Mev is followed by two gamma-rays. The intensity ratio of the hard to the soft beta-rays is found to be about 1:1.

## INTRODUCTION

THE beta- and gamma-radiations of $Sb^{124}$ have been studied by a number of investigators, but a few questions deserving further investigation remained. Mitchell, Langer, and McDaniel,[1] who studied these beta- and gamma-radiations by means of Geiger-counter coincidences, concluded that it decays with emission of a single $\beta$-ray of 1.54-Mev maximum energy, followed by a $\gamma$-ray of 1.82 Mev and probably a second $\gamma$-ray of $\leq 0.069$ Mev. A lower value for the energy of the hard gamma-ray, namely, $1.75 \pm .04$ Mev was obtained by Klaiber and Scharff-Goldhaber,[2] based on a measurement of the energy of the photo-neutrons from $Sb^{124}+Be$ with a hydrogen-filled ionization chamber. From O'Neal's[3] work on the slowing down of photo-neutrons in water, a value of $1.73 \pm .04$ Mev can be deduced for the $Sb^{124}$ $\gamma$-ray. Kruger and Ogle[4] determined the gamma-ray energy by observing electron pairs produced in a Wilson cloud chamber and found a value of $1.70 \pm .02$ Mev. Hales and Jordan[5] resolved the beta-rays with a magnetic spectrograph into two spectra of maximum energies $0.74 \pm .03$ and $2.45 \pm .07$ Mev. The energy difference of 1.71 Mev agrees fairly well with the average value for the gamma-ray energy. Hales and Jordan suggested, therefore, that $Sb^{124}$ decays partly by emission of a "hard" beta-ray of 2.45 Mev and partly by emission of a "soft" beta-ray of 0.74 Mev followed by a 1.71-Mev gamma-ray. They left the possibility open that in both cases the 0.069-Mev gamma-ray observed by Mitchell, Langer, and McDaniel may follow in the end. Recently Miller and Curtiss,[6] also using a beta-spectrograph, obtained

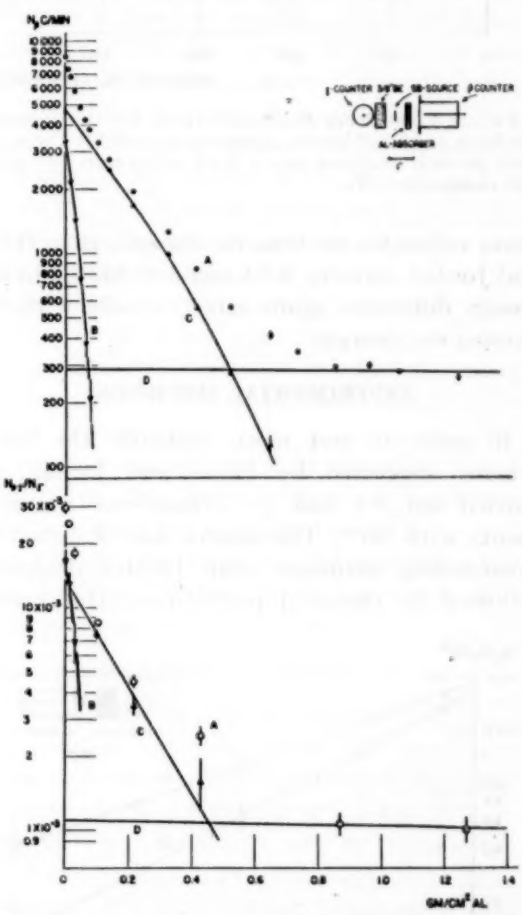

FIG. 1. Top: absorption of the radiation from $Sb^{124}$ in Al. (*A*) measured points, (*B*) "soft" beta-rays, (*C*) "hard" beta-rays, (*D*) gamma-ray background (drawn using additional points beyond 1.4 g/cm² Al). Bottom: Absorption in Al of beta-gamma coincidences per recorded gamma-ray. (*A*) measured points, (*B*) coincidences with "soft" beta-rays, (*C*) coincidences with "hard" beta-rays, (*D*) gamma-gamma coincidences.

[1] A. C. G. Mitchell, L. M. Langer, and P. W. McDaniel, Phys. Rev. **57**, 1107 (1940).
[2] G. S. Klaiber and G. Scharff-Goldhaber, Phys. Rev. **61**, 733A (1942).
[3] R. D. O'Neal, Phys. Rev. **70**, 1 (1946).
[4] P. G. Kruger and W. E. Ogle, Phys. Rev. **67**, 273 (1945).
[5] E. B. Hales and E. B. Jordan, Phys. Rev. **64**, 202 (1943).
[6] L. C. Miller and L. F. Curtiss, Phys. Rev. **70**, 983 (1946).

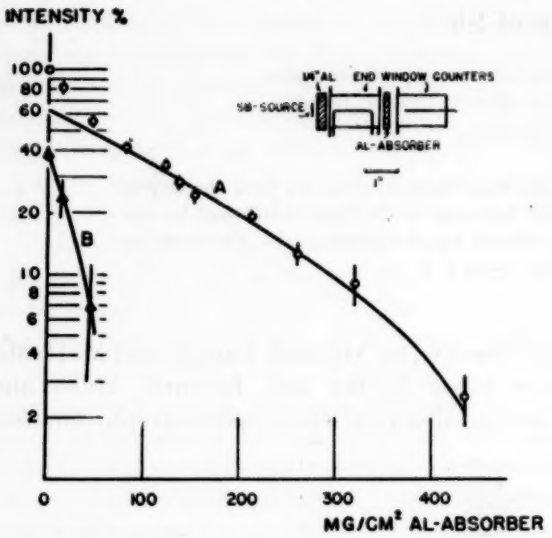


FIG. 2. Coincidence-absorption curve for the Compton electrons produced by the gamma-rays of $Sb^{124}$. The measured curve is analyzed into a hard component ($A$) and a soft component ($B$).

lower values for the beta-ray energies than Hales and Jordan, namely, 0.53 and 2.25 Mev, but the energy difference again agreed closely with the gamma-ray energy.

## EXPERIMENTAL METHODS

In order to test more explicitly the decay scheme suggested by Hales and Jordan, we carried out $\beta$-$\gamma$ and $\gamma$-$\gamma$ coincidence measurements with $Sb^{124}$. This source was obtained by bombarding antimony with 10-Mev deuterons followed by chemical purification. Our coincidence circuit had a resolving time of 1 $\mu$sec. The beta-rays were detected with a mica-window counter, the mica having a thickness of 4 mg/cm². For the detection of the gamma-rays a Geiger counter with a cylindrical gold electrode was used. A beryllium block was placed in front of this counter to filter out the beta-radiation. Schematic drawings added to the figures indicate the arrangement used for each type of measurement.

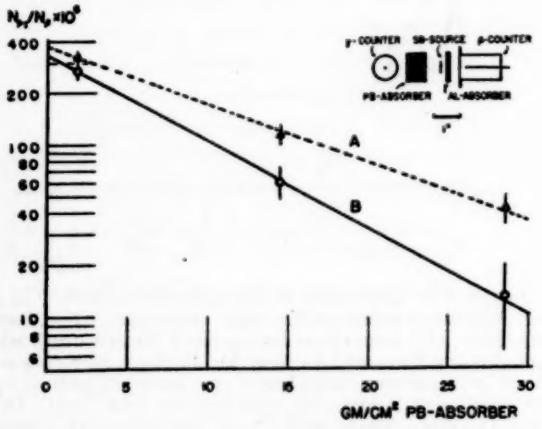


FIG. 3. Beta-gamma coincidences as function of gamma-ray absorber thickness. ($A$) No absorber between source and beta-ray counter. ($B$) 82 mg/cm² Al between source and beta-ray counter.

## RESULTS

The absorption of the beta-rays in aluminum was first studied. An analysis of the absorption curve (Fig. 1, top, curve $A$) shows two distinct $\beta$-ray components (curves $B$ and $C$) corresponding to the soft and hard beta-rays found with the magnetic spectrograph. The intensity ratio of the hard beta-rays to soft beta-rays was $1.0\pm0.2$. To obtain this figure a correction for the mica-window thickness (4 mg/cm²) and the thickness of the source (15 mg/cm²) was applied. Curve $D$ represents the gamma-ray background.

We next studied the beta-gamma coincidences for the two beta-ray components (Fig. 1, bottom) with the result that both coincide with gamma-rays. The coincidence rates found were $1.3\times10^{-3}$ per soft beta-ray and $0.68\times10^{-3}$ per hard beta-ray, i.e., approximately in the ratio 2:1. We can understand this result if we assume that the hard beta-ray is followed by a single gamma-ray, ($\gamma_1$), and that the soft beta-ray is followed by two gamma-rays ($\gamma_2$ and $\gamma_1$).

We first believed[7] that $\gamma_1$ and $\gamma_2$ were of comparable energy, since we were unable to see any structure in a lead absorption curve taken in "poor" geometry. Drs. Miller, Curtiss, and Feister then drew our attention to the fact that a gamma-ray of 0.61 Mev, which was possibly identical with $\gamma_1$, was reported by Rall and Wilkinson[8] and tentatively ascribed to $Te^{122,124}$? (30 $d$ ?).*

By measuring the energy of the Compton electrons produced in Al by the gamma-rays from $Sb^{124}$, using the method of coincidence absorption,

[7] W. E. Meyerhof and Gertrude Scharff-Goldhaber, Bull. Am. Phys. Soc. May 1947, Washington meeting.

[8] W. Rall and R. G. Wilkinson, Phys. Rev. **71**, 321 (1947).

* *Note added in proof:* Drs. Curtiss and Feister have kindly informed us that the 0.6-Mev $\gamma$-ray decays with a 60 $d$ half-life.

we confirmed the presence of two gamma-rays of approximately 1.7 and 0.6 Mev (see Fig. 2). This conclusion was reached by analyzing the absorption curve according to Bleuler and Zünti's method.[9] For the measurement, one counter with mica windows on both ends and a conventional mica end-window counter were used, as sketched in Fig. 2. In our previous coincidence absorption measurements, for which two Eck and Krebs counters had been used, the 0.6-Mev component could not be detected.

Figure 3 shows the result of beta-gamma coincidence measurements for varying thicknesses of the gamma-ray absorber. Curve *A* was measured with no absorber between source and beta-ray counter, while for curve *B* 82 mg/cm² Al were interposed, which absorbed the soft beta-rays. The slope of curve *B*, corresponding to a half-value thickness of 6 g/cm² Pb, is compatible with a gamma-ray energy of 0.6 Mev. Curve *A* has a half-value thickness of 8.5 g/cm² Pb, corresponding to a "weighted" average of the 0.6- and 1.7-Mev gamma-rays.

TABLE I.

| $\beta_1$(Mev) | $\beta_2$(Mev) | $\gamma$(Mev) | Method |
|---|---|---|---|
| 1.54 | | 1.82 | Absorption in Al and Pb, reference 1. |
| | | $\leqslant$.069 | |
| | | 1.75±.04 | Photo-neutrons* detected by proton recoils, reference 2. |
| | | 1.73±.04 | Slowing down of photo-neutrons* in water, reference 3. |
| | | 1.70±.02 | Electron pairs observed in Wilson chamber, reference 4. |
| | | 1.72±.03 | Photoelectrons. Magnetic lens spectrometer, reference 8. |
| 2.45±.07 | 0.74±.03 | | Semicircular magnetic spectrograph, reference 5. |
| 2.25 | 0.53 | | Magnetic lens spectrometer, reference 6. |
| | | 1.67 | Photo-neutrons ($n$-$p$ scattering cross section), reference† |
| | | 1.67 | Photo-neutrons detected by proportional counter, reference‡ |

† A. Wattenberg, Phys. Rev. **71**, 497 (1947).
‡ A. O. Hanson, private communication.

[9] E. Bleuler and W. Zünti, Helv. Phys. Acta **19**, 375 (1946).

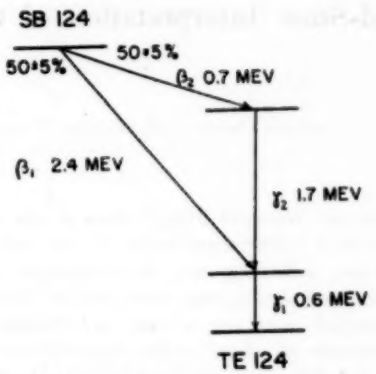


FIG. 4. Proposed decay scheme for $Sb^{124}$.

From these results it can be concluded that the 2.4-Mev beta-ray coincides with the 0.6-Mev gamma-ray, while the 0.7-Mev beta-ray coincides with the 1.7-Mev gamma-ray and the 0.6-Mev gamma-ray.

As we were unable to detect a gamma-ray of $<$0.069 Mev, the decay scheme of Hales and Jordan was modified as shown in Fig. 4.

The energies of the beta- and gamma-radiations of $Sb^{124}$, as obtained by the various investigators, are summarized in Table I.

## ACKNOWLEDGMENTS

We should like to thank Professor M. Goldhaber for much valuable advice. Our thanks are also due to Professor P. G. Kruger and the cyclotron group of the University of Illinois for producing the antimony source, and to Professor R. B. Duffield and Mrs. Ira Pullman for its chemical purification. Mr. Ira Pullman aided materially by constructing the mica-window counters. This research was supported in part by the Office of Naval Research.

# A Solid-State Interpretation of the Structure Near the Limit of the Continuous X-Ray Spectrum

JESSE W. M. DUMOND
*Norman Bridge Laboratory of Physics, California Institute of Technology, Pasadena, California*
(Received May 12, 1947)

P. Ohlin has reported irregularities in his continuous x-ray spectrum isochromats taken at low voltage (3000 to 5000 volts) indicating that the continuous x-ray spectrum from thick targets may have, within 10 or 20 volts of the quantum limit, one or more indentations in which actual *reversals* of slope occur. Unpublished work of Bearden and Schwarz agrees with this. Much less pronounced irregularities about the same distance from the limit were observed at higher voltages (10,000 and 20,000 volts) by DuMond and Bollman much earlier. The present paper interprets these irregularities in terms of the permitted and excluded energy states for the electron in the crystal lattice in its final state after having radiated the x-ray photon. The paper explains (1) how negative slopes in the isochromats from a thick target are possible, (2) why the irregularities are much more pronounced for low than for high voltage isochromats, (3) how the observed isochromat curves may be corrected for the varying retardation of the cathode-ray electrons at varying depths beneath the surface of the target to obtain information regarding the transition probabilities and energy levels for the excluded and permitted empty energy bands for electrons in the target crystal lattice. Some of Ohlin's isochromats are reproduced giving their shapes before and after correction by this method. Confirming evidence from recent work of Davisson and Germer of entirely different nature regarding the position of the first excluded energy band above the Fermi conduction levels is cited.

## THE IRREGULARITIES IN THE LOW VOLTAGE ISOCHROMATS EXHIBITING REVERSALS IN SLOPE

P. OHLIN at Uppsala, in a series of studies of the continuous x-ray spectrum for the purpose of determining the constant $h/e$, has observed curious irregularities[1] in his x-ray isochromats taken at long wave-lengths and low voltages. These occur within ten or fifteen volts of the short wave-length limit and appear in many cases as complete reversals of slope resulting in a sharply defined valley in which there may, in some cases, exist a saw-tooth structure. Schwarz and Bearden[2] have also observed just such structures in isochromats *taken at low voltages comparable with Ohlin's*.

The present author along with many others had long supposed that *a reversal in slope* in a thick target isochromat was an impossibility. The thick target spectrum is usually conceived as a superposition of thin target spectra coming from successively deeper and deeper elementary layers below the front surface of the target. Each successive thin target contribution has sensibly constant intensity per unit $d\nu$ extending from very low frequencies up to the quantum limit, but has lower and lower values of the high frequency quantum limit because the deeper layers are bombarded by electrons that have been retarded by greater penetration from the front surface.[3] On the basis of this somewhat idealized picture one cannot see how there can occur a reversal of slope in the profile of the spectrum or of the isochromat, for such a reversal seems at first to imply *negative intensity contributions* from some of the layers—an absurd impossibility. The spectrum from an ideal *thin target*, on the other hand, might well have such a structure near the short wave-length limit because of the permitted and excluded energy bands for the state of the final electron after the radiative transition. (Such a target must be "thin" in the sense of giving negligible cathode-ray retardation but not so thin as to destroy its crystal-lattice character and the resulting banded energy structure.) In a thick target the superposition of many such contributions progressively displaced in the manner suggested above would surely wash out such banded structural features. At the very best only plateaus could be expected *but no reversals of slope*. It was precisely this point which led the author to look more closely at the mechanism. Something must operate when isochromats are taken at low voltages to make

[1] P. Ohlin, Arkiv. f. Mat. Astr. Fysik **29A**, No. 3 (1942); **31A**, No. 9 (1944); **33A**, No. 23 (1946).

[2] Their complete work has never yet been published, at least to the author's knowledge. It was performed about six years ago.

[3] J. W. M. DuMond and V. Bollman, Phys. Rev. **51**, 409–410 (1937); *ibid.*, Figs. 8 and 9.

the observed spectra (or their images, the isochromats) *more nearly like thin target spectra*, and this must be less operative at higher voltages because such irregularities are much less marked there.[4]

## SELF-ABSORPTION IN THE TARGET MATERIAL GIVES EFFECTIVELY THIN TARGETS AT LOWER VOLTAGES

The absorption of the radiation in the target material itself, as it emerges from layers beneath the front surface, limits the thickness of the total layer from which radiation is observable *to a far greater extent at low voltages than at high*. This is clearly demonstrated by the curves of Fig. 1 referring to copper and tungsten, two of the target materials used by Ohlin. Note that the curves giving the thickness of a target layer sufficient to retard electrons by 10 volts are convex *upward*, while the curves representing the order of depth from which the bulk of the observed radiation must come (limitation by fluorescent absorption in the target itself) *are convex downward*. The ratio of the x-ray path to the electron path in Ohlin's targets was estimated from the geometry shown in Fig. 10 of Ohlin's inaugural dissertation.[5] The curves marked "1/*e* x-ray absorption layer" are therefore applicable as they stand only to this case of Ohlin's x-ray tube with direction of the observed x-ray approximately normal to the cathode-rays and with the target bevelled at approximately $\tan^{-1} 0.5$. Referring now to the abscissa scale, it is clear that, at Ohlin's voltages, absorption of the emerging radiation limits observations to layers in a tungsten target so thin that the electron retardation in those layers is of the order of 6 to 12 volts only, whereas even at the lower of DuMond and Bollman's two voltages (10 kv) the retardation in the observable layer would be of order 30 volts or more. Now it is also clear that such electron retardation exerts *a blurring effect*

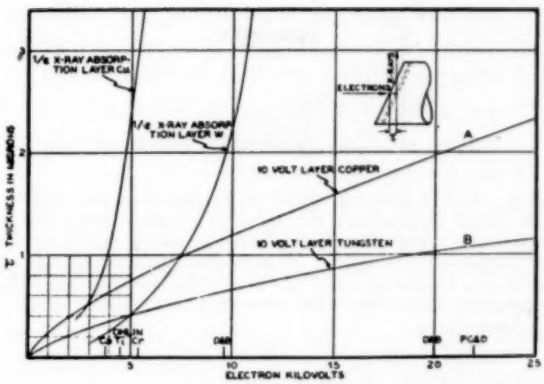


FIG. 1. The ordinates of the curves for copper and for tungsten, curves *A* and *B*, show the depth in microns that electrons of different initial energies (abscissae) must penetrate behind the face of a target of each material in order to be retarded by 10 volts. The curves marked $1/e$ absorption layer give on the same ordinate scale the depth, measured along the direction of the impinging electrons, from which the hardest continuous spectrum x-rays in Ohlin's targets must have come in order to be reduced in intensity by a factor $1/e$. This depth is assumed to be half the actual path of the x-rays in Ohlin's targets for the geometrical reasons illustrated in the small insert. For small retardations such as 10 volts in several kilovolts the electron retardation may be assumed to vary linearly with depth of penetration. These curves show that the layer from which the x-rays can be observed will produce much less electron retardation at low voltages, such as Ohlin's, than at higher voltages such as those of the observations of DuMond and co-workers. Ohlin's voltages, and also those of DuMond and Bollman, and Panofsky, Green, and DuMond are marked on the abscissa scale.

on the spectrum because the different parts of the total observed layer have been bombarded by electrons whose voltages vary over the entire range from that of the initially impinging electrons at the front surface to that of the most retarded electrons at the deepest observable depths. And the curves of Fig. 1 make it clear why this blurring effect will obliterate rugosities of profile such as those observed by Ohlin much more effectively at higher than at lower voltages. They also suggest that, even at Ohlin's low voltages and especially with his lower atomic number targets, such as copper, even *his* observed profiles have already suffered considerable blurring from the effect of electron retardation. It seems likely that if this effect could be completely removed Ohlin's corrected profiles might appear even more rugged. Fortunately this kind of blurring turns out to be rather readily amenable to analytical treatment so that we can pass beyond the qualitative considerations just presented above and actually effect a reasonably accurate quantitative cor-

[4] The reader is referred to the isochromats of the DuMond and Bollman paper (reference 3), Fig. 14, page 416, taken at 10 kv and 20 kv. He will find there in the observed points *slight vestiges of the Ohlin valley just above the knee* $K_2$. Although they are clearly evident and the author remembers distinctly that repeated observations in this region failed to remove these irregularities, they represented such small deviations from the smooth curve that at the time no important significance was attached to them.

[5] P. Ohlin, Dissertation (Uppsala, 1941).

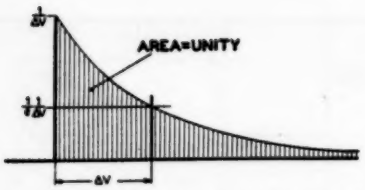


FIG. 2. The $g$ curve which is folded into the ideal or thin target isochromat to give the observed thick target isochromat. The blurring effect of this $g$ curve is the mathematical equivalent of the combined effects of (1) electron retardation and (2) absorption of the emerging continuous radiation. This $g$ curve is normalized so as to have unit area.

rection of the observed curves when the initial blurring effect is not too extreme. (Let it be clearly understood that the blurring effect here referred to has nothing to do with "straggling" of electrons in speed or direction. For the thin layers and voltages here involved straggling is negligible.)

## A METHOD OF CORRECTING ISOCHROMATS FOR THE EFFECTS OF ELECTRON RETARDATION AND SELF-ABSORPTION OF THE EMITTED CONTINUOUS RADIATION

Let us call $f(V)$ the ideal thin target isochromat that would be observed if the effects of electron retardation and absorption of the emerging continuous spectrum could be made completely negligible. Let $F(V)$ represent the actual observed isochromat which has undergone a certain amount of blurring from these two effects.

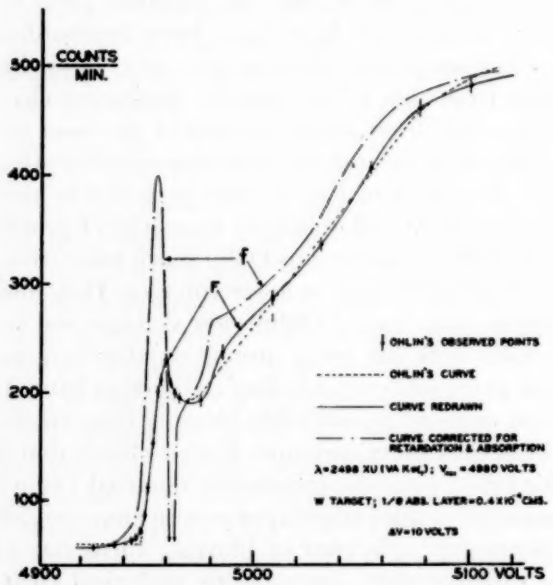


FIG. 3. One of Ohlin's isochromats taken with a tungsten target showing the profile both before and after correction for the blurring effects of electron retardation and absorption of the emerging continuous x-radiation.

It is essential to realize that the combined effects of electron retardation and absorption of the emerging continuous spectrum transform the thin target isochromat $f(V)$ by "folding" [6] it with an exponential function $g(V)$ which is pictured in Fig. 2. The observed isochromat $F(V)$ is a weighted sum of many isochromats of the same shape as $f(V)$, which are successively displaced more and more to the right and at the same time weighted with exponentially diminishing weights according to the $g$ curve of Fig. 2. Only one parameter is required to describe this weighting function $g$, namely, the displacement or retardation in volts $\Delta V$ at the point where the exponential curve has fallen to $1/e$ of its initial value. Clearly $\Delta V$ corresponds to the retardation suffered by electrons that have penetrated into the target to such a depth that the observed emerging radiation is reduced in intensity through fluorescent absorption by a factor $1/e$. For each target material and voltage, $\Delta V$ is a constant which depends on the ratio of the electron and x-ray paths in the target. $\Delta V$ will decrease with increasing x-ray absorption and increase with increasing electron retardation. The author has computed the value $\Delta V$ for each of the targets and voltages used by Ohlin in his studies of the isochromat structures. $\Delta V$ ranges from 6 volts to 25 volts in Ohlin's work.

The inverse operation of divesting a given folded function $F=f*g$ of the blurring effects of one of the folding factors $g$ to obtain the other factor $f$ is *in the present case fortunately both easy in theory and reasonably accurate in application.* From the physical situation we have that

$$F(V)=\frac{1}{\Delta V}\int_0^\infty f(V-u)e^{-u/\Delta V}du \qquad (1)$$

wherein the normalizing factor $(\Delta V)^{-1}$ has been

[6] The mathematical operation of "folding" one function into another usually comes under the theory of integral equations. The fold $F$ of a function $f$ by a function $g$ is sometimes written symbolically as $F=f*g$. It may be defined as

$$F(t)=f*g=\int_A^B f(t-x)g(x)dx.$$

The limits $A$ and $B$ are defined to fit each particular case.

inserted to make the area under the exponential $g$ curve unity so that ordinates and areas of the $F$ and $f$ curves will be comparable in magnitudes and as to physical dimensions. The variable $u$ represents the retardation in volts of the cathode-ray electrons at any specified depth in the target. The significant depths over which the integral is extended are so small that straggling and changes in direction are negligible. The exponential factor in the integrand is the absorption factor for the emerging radiation generated at the depth for which the retardation is $u$. Now integrating (1) by parts

$$F(V)=-f(V-u)e^{-u/\Delta V}\Big]_0^\infty + \int_0^\infty \left\{\frac{\partial}{\partial u}[f(V-u)]\right\} e^{-u/\Delta V}du \quad (2)$$

$$=f(V)-\frac{\partial}{\partial V}\left\{\int_0^\infty f(V-u)e^{-u/\Delta V}du\right\} \quad (3)$$

$$=f(V)-\Delta V\frac{\partial F}{\partial V}; \text{ from Eq. (1).} \quad (4)$$

Solving for $f$ we obtain

$$f(V)=F(V)+\Delta V\, dF/dV. \quad (5)$$

It is obviously very easy to apply formula (5) graphically to the profiles observed by Ohlin, without any numerical computations whatever, once $\Delta V$ has been computed for each curve. Ordinates are erected at intervals along the abscissa scale which are convenient submultiples of $\Delta V$. A tangent fitted by means of a straight edge to the $F$ curve at each of these ordinate points, is then projected to the right over an abscissa interval $\Delta V$ where its intersection with an ordinate gives the corrected value $f(V)$ which must then be replotted on the original ordinate where the tangent was constructed. The operation proceeds very rapidly on a drafting board using a T-square or a "universal" drafting machine.

The author has corrected a number of Ohlin's observed curves in this way, two of which are reproduced in Figs. 3 and 4. A slight uncertainty exists as to whether all of Ohlin's targets were such as to give just the same angle of grazing x-ray emergence as the one described in his dissertation. Small changes in this respect will chiefly change the heights of the peaks and depths of the valleys in the corrected curves but will not greatly affect the positions on the voltage scale at which these features occur.

The author has redrawn Ohlin's profile slightly in Figs. 3 and 4 so as to follow the observed points even a little more literally and with less smoothing out of apparent irregularities than did Ohlin. This is the curve represented with a full line and labelled $F$. The curve labelled $f$ and represented with dots and dashes is the result of applying the correction of formula (5). This is then the profile that would be observed if the effects of electron retardation and absorption of the emerging radiation were completely removed.

The method of formula (5) obviously has its limitations. If $\Delta V$ is very large the term containing the derivative $dF/dV$ dominates the expression and the corrected result becomes so sensitive to small local changes in slope of the observed isochromat that all accuracy is lost unless the precision of the original observations is much higher than can at present be attained.[7]

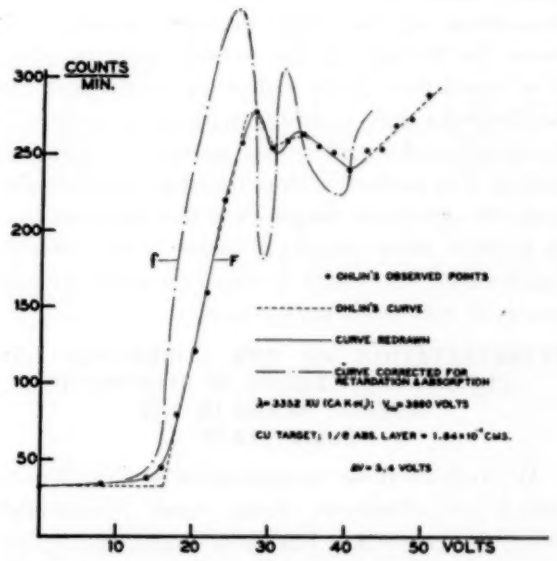


FIG. 4. Isochromat obtained by Ohlin with a copper target showing profiles before and after correction for electron retardation and x-ray absorption.

[7] When $\Delta V$ becomes so large that the cathode electrons, after a retardation $\Delta V$, exhibit considerable straggling in speed and direction, formula (5) will cease to give a reliable correction. There may also be some error introduced even when $\Delta V$ is small by "rediffused" electrons returning from deeper layers of the target to the surface layer of "thick-

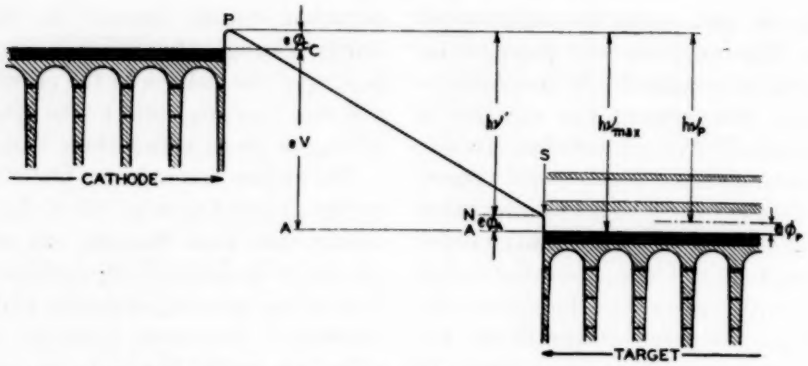


FIG. 5. Idealized energy diagram for transitions of electrons from the cathode to the anode of an x-ray tube. Energy is plotted vertically and a single space coordinate horizontally. The cathode is on the left, the target on the right. The arches and the line sloping downward from cathode to target represent the potential energy of an electron. The horizontal lines refer to the total energy and show the quantized energy levels or bands. Forbidden bands are cross-hatched. Permitted bands are white, save where they are occupied with electrons, in which case they are black. $\phi_C$ is the work function of the cathode, $\phi_A$ the work function of the target. The highest probability of transition corresponding to the first peak on the corrected isochromat is supposed to occur at some point $\phi_P$ volts above the uppermost Fermi levels in the target.

Even in the cases illustrated in Figs. 3 and 4 the derivative term introduces considerable uncertainty, especially in those regions of Ohlin's profile where his observed points are more widely spaced, since one cannot be quite certain of the true shape of the profile between the observations. In the light of the present interpretation it is hoped that Ohlin and others can repeat the isochromats very carefully with great attention to details and a still denser spacing of observed points. *The present evidence indicates pretty clearly near the short wave-length limit that there are one, or perhaps more, regions or bands in the corrected spectrum or isochromat in which the intensity falls nearly or even completely to zero.*

## INTERPRETATION OF THE CORRECTED ISOCHROMATS IN TERMS OF ELECTRONIC ENERGY BANDS IN THE SOLID STATE

We believe these irregularities or dark bands, which are obviously much more pronounced after the correction has been made, reflect the fact that the final energy state of the cathode electron *after* the radiative transition has occurred *must be a permitted electronic energy state of the crystal lattice in which the transition occurs, and that there is here evidence for a banded structure of permitted and excluded energy states above the filled levels of the Fermi conduction electrons in the target.* We thus see in the profiles of the continuous spectrum a new means of studying the electronic energy bands of the solid state.

Figure 5 is a somewhat idealized energy diagram for the potential energy and also for the total energy of an electron in the cathode, the target, and in the electrical field between them in an x-ray tube. The excluded energy bands are shown in diagonal cross-hatching. The remaining regions are the permitted energy bands and where they are occupied by electrons, they are shown in black. In an electrical conductor there is always an unoccupied permitted energy region *above* the top of the densely filled Fermi levels. Above this in turn there may be an exluded or forbidden energy band followed again by a permitted band, etc. As one rises in this energy spectrum the excluded bands in all probability become narrower and narrower and eventually disappear altogether. One sees then that the initial sharp peak in the corrected isochromat of Figs. 3 and 4 in all probability corresponds to the transitions in Fig. 5, in which the final state of the electron is somewhere in the permitted band just above the top of the Fermi levels. The succeeding deep valley in the corrected isochromat probably corresponds to an excluded

ness" $\Delta V$. Since such rediffused electrons would have suffered considerable retardation, errors of this type would probably affect the shape of the corrected isochromats chiefly in regions considerably distant from the short wave-length limit.

energy band immediately above this. A more accurate and detailed study of the isochromat profile may reveal, after correction, further successive bands of exclusion alternating with permitted bands.

It should be pointed out that the method of formula (5) corrects the isochromat only for the combined effects of electron retardation and absorption of the emerging radiation. After this correction has been made, there still remains the blurring effect of the "window curve" of the monochromator which is probably substantial. The author has made no attempt to correct Ohlin's isochromats for the effect of the monochromator window curve because (1) this is much more difficult, and (2) no data on the shape and width of the window are available to him. It is not inconceivable that some of the details of the corrected profile, now obscured by this further blurring effect, would later be revealed with improved resolving power.

Figure 4 shows that for the copper target the first deep dip or excluded energy band commences about ten or eleven volts above the short wave-length limit. Now the author has recently learned from Dr. C. J. Davisson[8] that in very recent work done with Dr. L. H. Germer at the Bell Telephone Laboratories (still unpublished) *there is clear evidence for just such an excluded energy band about ten volts above the topmost energy of the Fermi conduction electrons in copper.* Davisson and Germer bombarded a copper crystal with very slow electrons projected normally against the (111) planes. They found that when the cathode is six volts more negative than the copper target, the electrons refuse to enter the latter and are strongly reflected from the surface although they do enter at lower voltages. With increasing voltage, successive higher energies are found at which electrons are successively accepted and rejected according to a banded structure. To Davisson and Germer's measured voltage between their cathode and target (the difference in the energy levels $A$ and $C$ in Fig. 5) the present author believes there must be added the work function of their cathode ($\phi_C$, Fig. 5, or 4.5 volts approximately) *to find the energy of their impinging electrons relative to the uppermost Fermi levels in their target.* The sum then (4.5 volts plus 6 volts or 10.5 volts) thus gives remarkable confirmation to the present observations regarding the first deep valley in the curve *f* of Fig. 4.

[8] The author is much indebted to Dr. W. Shockley for first informing him of this most interesting confirmation. Dr. Davisson himself described the results to the author.

## COMPARISON OF PRESENT THEORY WITH THAT OF NIJBOER

The author is indebted to Dr. P. Kirkpatrick of Stanford University who examined an advance copy of the present paper for calling his attention to B. R. A. Nijboer's recent paper[9] in which the idea is proposed that the Ohlin structures under discussion may be ascribed to the banded structure of the empty permitted energy levels for electrons in the target crystal lattice. J. A. Bearden also informs the author that the same idea occurred to him but that he rejected it because of the rather large energy jump indicated in his *uncorrected* isochromats measured from the short wave limit to the dip or valley. Thus the simple and primitive idea of associating these dips with banded energies in the solid state is not new. It has doubtless occurred to many. What *is* new and significant, however, in the present author's ideas is:

(1) The explanation of why these dips are so much more pronounced in low voltage isochromats than in high.

(2) The explanation of how *reversals in slope* in the isochromats from thick targets are possible at all.

(3) The development of formula (5) giving the quantitative method of correcting the observed isochromats so as to divest them of the blurring effects of electron retardation and absorption of emerging x-radiation. This correction makes possible the important interpretation of the corrected curves as reliable information on the banded structure of the electron energy levels in the target crystal lattice and, therefore, brings to bear a new tool for the study of the solid state.

Nijboer in his short paper admits his inability to explain the reversals in slope in the isochromats. This is because it did not occur to him to take into account the effects of target absorption and electron retardation in the way that we have explained here. Nijboer, on the other hand, tries to explain the Ohlin structures by calling into play the banded energy level structure of the target, not only in its effect on the x-ray transitions near the quantum limit *but once again*

[9] B. R. A. Nijboer, Physica **12**, No. 7, 461 (Oct. 1946).

*in its effect on the retardation of the electrons entering the target.* He points out that for small energy losses of the cathode-ray electrons these energy losses must also have a banded structure. *This is probably not the primary explanation of the Ohlin valleys, however, for if it were there would be no explanation for the fact that the valleys are far more pronounced in low voltage isochromats than in high voltage ones.* Furthermore, the banded structure of electron energy losses could hardly be observed *as a function of depth or thickness* of a layer of solid copper or tungsten of several microns and, therefore, many atom diameters thickness. This is because *multiple losses* in traversing such a solid layer are extremely likely. It must be recalled that energy losses communicated by the primary cathode electron to very distant electrons in the solid account for a good part of the retardation. For the Fermi (4*s*) electrons alone in solid copper these losses have zero volts as their lower limit and about 9.5 volts as their upper limit, and they can have all intermediate values with a very smooth probability distribution. The 3*d* electrons can accept energies which also have a fairly smooth distribution covering a range of energy losses from about 6 volts to 11 volts with only one very narrow excluded band at losses of about 10 volts.[10] One must also remember that if multiple collisions are likely to occur with a multiplicity $n$, then the probability distribution curve for multiple losses will be the result of *folding* the already rather smooth curve for single collision losses into itself $n$ times. This should surely wash out its banded structural features almost completely even if $n$ were only equal to 2. The author knows of no experimental evidence favorable to the idea that the retardation of a beam of fast electrons penetrating a thin layer of matter is not substantially *proportional to the thickness* of the layer for the first few volts or tens of volts retardation. On this assumption rests the validity of the author's theory of the Ohlin dips and his method of correcting the curves for electron retardation. Small deviations from a linear dependence of retardation on thickness will of course only introduce small corrections into the result. The $g$ curve of Fig. 2 may not have the perfectly smooth idealized exponential profile there shown but the errors so introduced will probably be small.

Ohlin's published isochromats do not extend very far back from the short wave-length limit. If the present interpretation is correct, an application of the correction of formula (5) over a somewhat larger range of voltage should result in a corrected isochromat which eventually and rather rapidly levels off to a nearly flat plateau in the manner that theory[11] and experiment[12] lead us to expect for a thin target isochromat or spectrum. In order that this may occur the observed thick target spectrum at low voltages, such as Ohlin's, must itself bend over and level off rather rapidly. It would be interesting to know whether this actually occurs if Ohlin's low voltage isochromats are explored to greater distance. Reference 7, however, suggests that such a process must be interpreted with caution.

## SUGGESTED TESTS AND APPLICATIONS OF THIS NEW INTERPRETATION

The present interpretation of the irregularities in Ohlin's isochromats lends itself to the following predictions which may afford a test of its correctness and a program for further investigation. (1) By varying the angle of the target face so as to change the obliquity of the angle of grazing emergence of the observed continuous x-radiation one can readily vary $\Delta V$. A more grazing emergence gives a smaller $\Delta V$, and it should thus be possible to exaggerate greatly and at will the ruggedness of the profile. (The target face must of course be smooth and free from pits.) (2) A *liquid* target would probably not manifest the same irregularities in the isochromat, nor to the same degree, if at all.[13] Little is known about the electronic energy states in liquid metallic conductors. (3) Comparison of the corrected isochromat profiles from targets of different conducting and even semiconducting materials with

[10] See Krutter's work described in Frederick Seitz, *Modern Theory of Solids, International Series in Physics* (McGraw-Hill Book Company, New York, 1940), p. 423.

[11] See W. Heitler *Quantum Theory of Radiation* (Clarendon Press, New York, 1936), pp. 161–171 and Fig. 14, taking into account corrections for Sommerfeld factor, etc. Also A. Sommerfeld, Ann. d. Physik **11**, 257 (1931), and P. Kirkpatrick and L. Wiedmann, Phys. Rev. **67**, 336 (1945).

[12] See W. W. Nicholas, J. Research Nat. Bur. Stand. **2**, 837 (1929).

[13] In the third of Ohlin's papers cited in reference 1 the curves for a lead target show much less pronounced dips. It is quite possible that the lead in the immediate vicinity of the focal spot was molten.

the already known facts from other sources[14] regarding the widths and patterns of the electronic energy bands of these same materials in the solid state, might reveal supporting evidence for the proposed interpretation. (4) Perhaps the easiest and most significant test of the proposed ideas might be made by exploring two isochromats at closely adjacent monochromatizing wave-lengths, $\lambda_1$ and $\lambda_2$, selected so that the critical $K$-absorption wave-length $\lambda_K$ for the target material would lie between them. Under these circumstances $\Delta V$ would be much larger for the longer of the two wave-lengths because of the decreased absorption of the emerging radiation so that, of the two isochromat profiles, *the one for shorter wave-length should appear markedly more rugged.* The angle of grazing emergence of the radiation should obviously be selected so as to keep $\Delta V$ appropriately small in both cases. A corollary to this is that for best definition of the corrected profiles the isochromats should be taken at a wave-length just shorter than the $K$-absorption edge of the target material.

It is of some interest to discuss the bearing of the present conclusions on the original objective which motivated the investigations: the determination of $h/e$. The author's corrected isochromats obtained by applying formula (5) to Ohlin's curves show very little shift of the short wave-length limit after correction. These shifts, which are of the order of only one or two volts at most, *are all in a direction to lower the values of $h/e$ obtained by Ohlin.* Since they are so small, however, relative to other uncertainties in his work and since, as already pointed out, even the present "corrected" isochromats have not been corrected for the monochromator window curve, it seems inappropriate at present to dwell in detail on this point.

It may be valuable, however, to recognize a new possibility that the present ideas suggest for improving precision in future $h/e$ determinations. If the present interpretation is correct, that the first sharply defined peak or maximum in the corrected isochromat corresponds to transitions of the electron to final energy states in the band of permitted energies just above the top of the uppermost Fermi conduction electron energies, *then it may be possible to determine $h/e$ with higher precision by determining the voltage where this corrected isochromat peak occurs* (instead of the voltage at the extreme limit of the isochromat). If we call this voltage at the first peak on the corrected isochromat $V_P$, and if the energy level where it occurs is $\phi_P$ volts higher than the top of the Fermi levels in the target, then

$$\frac{h}{e}=\frac{(V+\phi_C-\phi_P)\lambda}{c},$$

where $\phi_C$ is the work function of the cathode and $\lambda$ is the wave-length for which the center of the monochromator window is set (see Fig. 5). One advantage in using the center of this permitted energy band as a reference point, rather than the top of the Fermi distribution, is that by so doing we are, so to speak, *matching a symmetrical exploring tool (the monochromator window curve) against a nearly symmetrical spectral feature (the permitted energy band)* as contrasted with the highly unsymmetrical feature (the lower limit of that permitted band) used at present. The advantage in interpretation of the results is that the center of the first peak of the isochromat can be ascertained much more accurately than the position of the limit itself, blurred as it is by the window curve.

It should be noted that, even if $\phi_P$ is not known, this new method for determining $h/e$ can still be used *by running two isochromats at two different voltages and measuring the voltage difference between the peaks on the corrected curves* because $\phi_P$ (and also $\phi_C$) will be substantially the same in both cases and will cancel out in taking the difference. Needless to say, both isochromats must be taken at sufficiently low voltage to permit effective correction of the curve without too great an uncertainty from the derivative term of Eq. (5).

**ACKNOWLEDGMENTS**

The author wishes gratefully to acknowledge his debt to J. Robert Oppenheimer, Richard C. Tolman, W. V. Houston, E. Richard Cohen, W. K. H. Panofsky, P. Kirkpatrick, Wm. Shockley, C. J. Davisson, and P. Ohlin for very helpful discussions with them on various topics related to the present subject.

[14] See, for example, the interpretative studies of fine structures of absorption edges, such as those of R. de L. Kronig, Zeits. f. Physik **70**, 293 (1931), and experiments such as those of C. H. Shaw, Phys. Rev. **70**, 643 (1946) on gases.

# The Infra-Red Spectrum and Molecular Constants of $C^{12}O^{16}$ and $C^{13}O^{16}$

ROBERT T. LAGEMANN,* ALVIN H. NIELSEN,** AND FRED P. DICKEY***
*The Ohio State University, Columbus, Ohio*

(Received May 5, 1947)

The infra-red spectrum of carbon monoxide has been investigated with a 7200 line-per-inch grating. The fundamental bands of $C^{12}O^{16}$ and $C^{13}O^{16}$ and the overtone of $C^{12}O^{16}$ were measured. The rotational structure has been analyzed by means of combination relations, and the following new values of the molecular constants have been obtained: $\omega_e = 2169.60$ cm$^{-1}$, $\omega_e' = 2121.33$ cm$^{-1}$, $x_e\omega_e = 13.22$ cm$^{-1}$, $(x_e\omega_e)' = 12.64$ cm$^{-1}$, $B_e = 1.9238$ cm$^{-1}$, $B_e' = 1.8465$ cm$^{-1}$, $\alpha = 0.0175$ cm$^{-1}$, $\alpha' = 0.0169$ cm$^{-1}$, $I_e = 14.548\times10^{-40}$ g cm$^2$, $I_e' = 15.157\times10^{-40}$ g cm$^2$, $r_e$ (average for both molecules) $= 1.1291\times10^{-8}$ cm. The primed constants refer to the isotopic molecule.

## 1. INTRODUCTION

THE infra-red spectrum of carbon monoxide has been examined by a number of investigators,[1] using spectrometers with various amounts of resolving power. The most complete of these investigations was that of Whitcomb and Lagemann who used 3600 and 4800 line-per-inch gratings to resolve the rotational structure of the fundamental and overtone bands of $C^{12}O^{16}$.

TABLE I. The rotation lines in the fundamental band of $C^{12}O^{16}$.

| Positive ($R$) branch (cm$^{-1}$) | | | | Negative ($P$) branch (cm$^{-1}$) | | | |
|---|---|---|---|---|---|---|---|
| Identification | $\nu$ Obs. | $\nu$ Calc. | Difference | Identification | $\nu$ Obs. | $\nu$ Calc. | Difference |
| $R(0)$ | 2147.05 | 2146.94 | +0.11 | | | | |
| $R(1)$ | 2150.83 | 2150.70 | +0.13 | $P(1)$ | 2139.32 | 2139.33 | −0.01 |
| $R(2)$ | 2154.44 | 2154.44 | 0.00 | $P(2)$ | 2135.48 | 2135.46 | +0.02 |
| $R(3)$ | 2158.13 | 2158.13 | 0.00 | $P(3)$ | 2131.49 | 2131.56 | −0.07 |
| $R(4)$ | 2161.83 | 2161.79 | +0.04 | $P(4)$ | 2127.61 | 2127.63 | −0.02 |
| $R(5)$ | 2165.44 | 2165.41 | +0.03 | $P(5)$ | 2123.62 | 2123.66 | −0.04 |
| $R(6)$ | 2169.05 | 2168.99 | +0.06 | $P(6)$ | 2119.64 | 2119.65 | −0.01 |
| $R(7)$ | 2172.63 | 2172.54 | +0.09 | $P(7)$ | 2115.56 | 2115.61 | −0.05 |
| $R(8)$ | 2176.12 | 2176.06 | +0.06 | $P(8)$ | 2111.48 | 2111.54 | −0.06 |
| $R(9)$ | 2179.57 | 2179.53 | +0.04 | $P(9)$ | 2107.33 | 2107.43 | −0.10 |
| $R(10)$ | 2183.14 | 2182.98 | +0.16 | $P(10)$ | 2103.12 | 2103.28 | −0.16 |
| $R(11)$ | 2186.47 | 2186.39 | +0.08 | $P(11)$ | 2099.01 | 2099.10 | −0.09 |
| $R(12)$ | 2189.84 | 2189.77 | +0.07 | $P(12)$ | 2094.69 | 2094.89 | −0.20 |
| $R(13)$ | 2193.19 | 2193.11 | +0.08 | $P(13)$ | 2090.56 | 2090.64 | −0.08 |
| $R(14)$ | 2196.53 | 2196.41 | +0.12 | $P(14)$ | 2086.27 | 2086.35 | −0.08 |
| $R(15)$ | 2199.77 | 2199.68 | +0.09 | $P(15)$ | 2081.95 | 2082.03 | −0.08 |
| $R(16)$ | 2202.96 | 2202.92 | +0.04 | $P(16)$ | 2077.57 | 2077.68 | −0.11 |
| $R(17)$ | 2206.19 | 2206.12 | +0.07 | $P(17)$ | 2073.19 | 2073.29 | −0.10 |
| $R(18)$ | 2209.31 | 2209.28 | +0.03 | $P(18)$ | 2068.69 | 2068.86 | −0.17 |
| $R(19)$ | 2212.46 | 2212.41 | +0.05 | $P(19)$ | 2064.31 | 2064.40 | −0.09 |
| $R(20)$ | 2215.66 | 2215.51 | +0.15 | $P(20)$ | 2059.79 | 2059.91 | −0.12 |
| $R(21)$ | 2218.67 | 2218.57 | +0.10 | $P(21)$ | 2055.31 | 2055.38 | −0.07 |
| $R(22)$ | 2221.56 | 2221.59 | −0.03 | $P(22)$ | 2050.72 | 2050.81 | −0.09 |
| $R(23)$ | 2224.63 | 2224.58 | +0.05 | $P(23)$ | 2046.14 | 2046.21 | −0.07 |
| $R(24)$ | 2227.55 | 2227.54 | +0.01 | | | | |
| $R(25)$ | 2230.49 | 2230.46 | +0.03 | | | | |
| $R(26)$ | 2233.34 | 2233.34 | 0.00 | | | | |
| $R(27)$ | 2236.06 | 2236.19 | −0.13 | | | | |
| $R(28)$ | 2238.89 | 2239.01 | −0.12 | | | | |

More recently, Lagemann,[2] using the same spectrometer, observed the fine structure of the $C^{13}O^{16}$ fundamental band superposed on the fundamental band of $C^{12}O^{16}$.

The present paper is the result of an attempt to observe the complete spectrum of both $C^{12}O^{16}$ and $C^{13}O^{16}$ and to compute new values for the constants from these data. The bands observed were the fundamental and overtone of $C^{12}O^{16}$, and the fundamental of $C^{13}O^{16}$. The overtone of the isotopic molecule, though detected, could not be measured with the gas samples available. A sample of gas enriched with $C^{13}O^{16}$ is being obtained, and the overtone will be reported in a future note. Several of the stronger lines of this band were, however, observed, and their position agreed with line positions predicted from the constants given in Table IV.

## 2. EXPERIMENTAL

Two absorption cells fitted with rocksalt windows containing pure carbon monoxide were used in observing these bands: one was 8 cm long and filled to a pressure of 12 cm of mercury, and the other was 20 cm long and filled to atmospheric pressure. The 8-cm cell was found to be of the proper length for the fundamentals, while the 20-cm cell was required to observe the overtone.

The same spectrometer as was used by Whitcomb and Lagemann was equipped with a 7200 line-per-inch replica grating and used for these measurements. Mercury lines in several orders were used to calibrate the instrument. All line positions and frequencies have been reduced to

* Emory University, Emory University, Georgia.
** The University of Tennessee, Knoxville, Tennessee.
*** The Ohio State University, Columbus, Ohio.

[1] E. F. Lowry, J. Optical Soc. Am. **8**, 647 (1924); C. P. Snow and E. K. Rideal, Proc. Roy. Soc. **A125**, 462 (1929); S. E. Whitcomb and R. T. Lagemann, Phys. Rev. **55**, 181 (1939).

[2] R. T. Lagemann, J. Chem. Phys. **10**, 193 (1942).

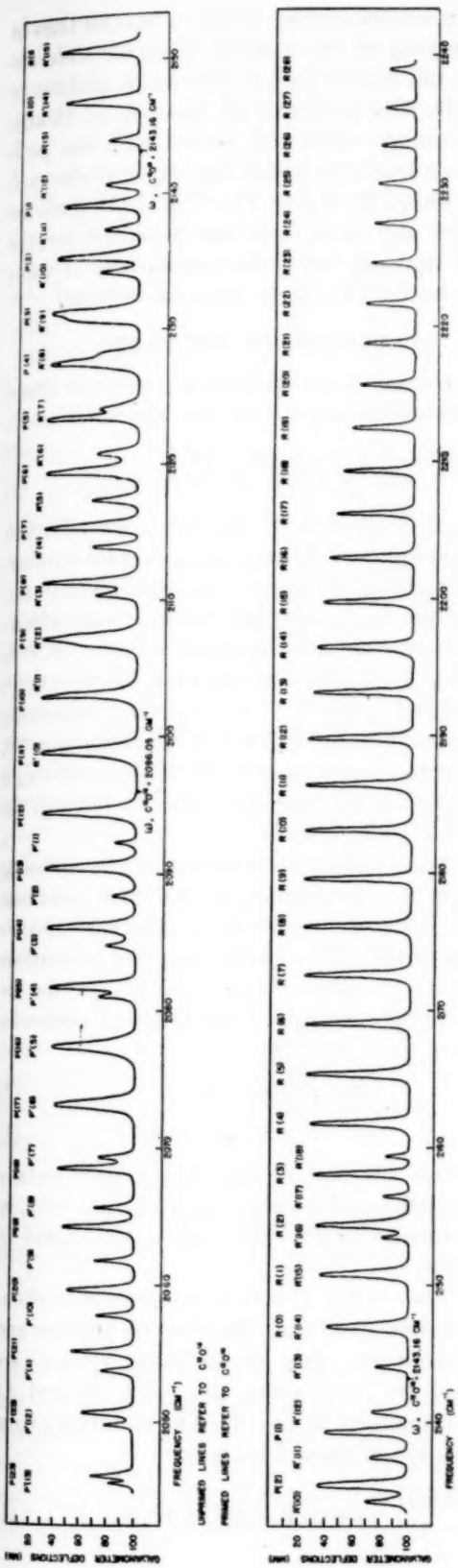

FIG. 1. Fundamental vibration-rotation band of $C^{12}O^{16}$ and $C^{13}O^{16}$.

vacuum. A vacuum thermocouple was used as a radiation detector. The thermocouple output voltage was amplified by a Moll relay and finally observed as deflections of a Leeds and Northrup high sensitivity galvanometer. Angular positions of the grating were recorded and converted to frequencies by the usual relation $\nu(\text{cm}^{-1}) = K_r \csc\theta$ where $K_r$ is the instrument constant. Observations were made at spectral intervals of about 0.07 $\text{cm}^{-1}$, and the slits of the spectrometer were set to include a spectral interval of about 0.25 $\text{cm}^{-1}$. It is believed that the line positions are, in general, reliable to about $\pm 0.07$ $\text{cm}^{-1}$.

### 3. FUNDAMENTAL BANDS

In Fig. 1 is shown a somewhat idealized curve representing the galvanometer deflections in cm as ordinates plotted *versus* frequencies in $\text{cm}^{-1}$ as abscissae for the fundamental bands. Several complete sets of observations were made over the whole region, and only those lines appearing in all sets of observations have been represented in the figure. This has the effect of eliminating from the final curve the thermal agitation errors. In this figure a decrease in galvanometer deflections indicates increased absorption of the incident radiation by the gas. The unprimed lines in Fig. 1 are due to $C^{12}O^{16}$ and are much more intense than the primed lines which are due to $C^{13}O^{16}$.

The double space at the band center caused by the missing line, a characteristic of infra-red spectra of diatomic molecules, was less easily identified for $C^{13}O^{16}$ than for $C^{12}O^{16}$ because some of the isotopic lines were obscured by the much more intense $C^{12}O^{16}$ lines. It was, therefore, not difficult to assign the rotational quantum number, $J$, to the levels, in the case of $C^{12}O^{16}$. After a little study the isotopic lines were also identified without ambiguity. Tables I and II list the frequencies of the lines in $\text{cm}^{-1}$ for both molecules. The appropriate $J$ values for the initial levels are given in adjacent columns. Frequencies computed from Eq. (4) and the constants in Table IV are also listed. The agreement between observed and computed values is within the experimental error in most cases.

### 4. OVERTONE BAND

In Fig. 2 is shown the curve for the overtone band of $C^{12}O^{16}$ plotted in galvanometer deflec-

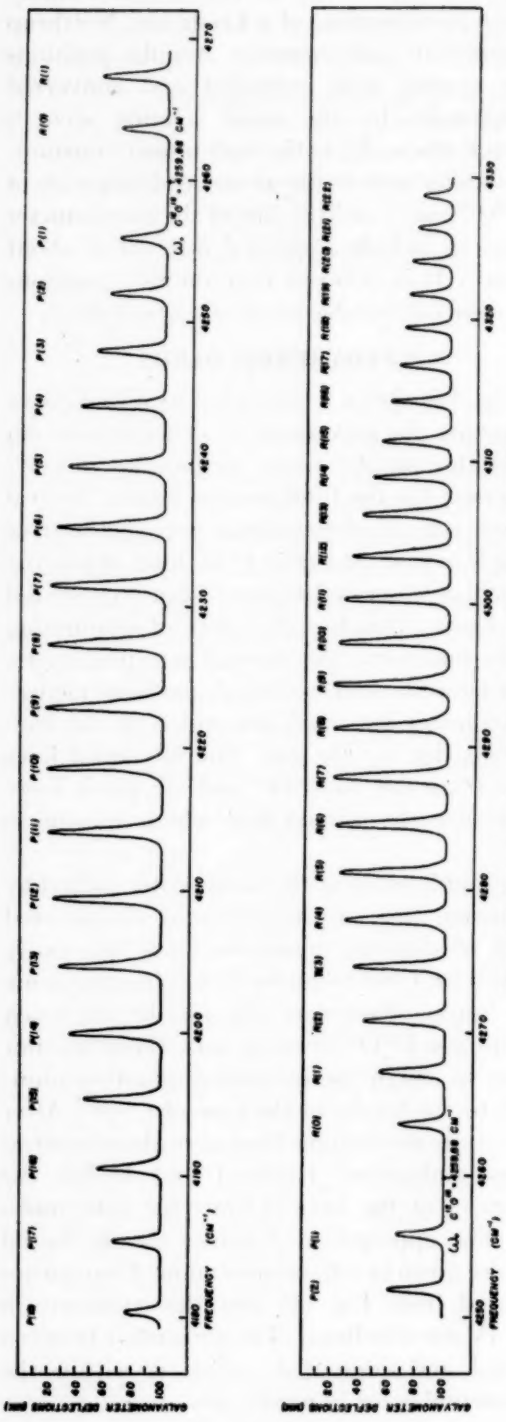

FIG. 2. First overtone vibration-rotation band of $C^{12}O^{16}$.

tions *versus* frequencies in $cm^{-1}$. Several lines of the overtone of the isotopic molecule were observed, but not enough to enable an analysis to be made. The positions of these lines, though not absolutely identified, agreed with line positions predicted by using Eq. (4) and the constants found in Table IV. Table III lists the observed and computed line positions for the normal molecule with the appropriate $J$ value for the initial level in an adjacent column.

### 5. ANALYSIS OF THE BANDS

The energy of an oscillating rotator in quantum mechanics is given by the expression:

$$E_{v,J}/hc=\omega_e(v+\tfrac{1}{2})-x_e\omega_e(v+\tfrac{1}{2})^2+\cdots +B_vJ(J+1)-D_vJ^2(J+1)^2+\cdots, \quad (1)$$

where $E_{v,J}/hc$ = energy in $cm^{-1}$, $v$ = vibration quantum number, $J$ = rotation quantum number, $\omega_e$ = vibrational frequency for infinitesimal amplitude ($cm^{-1}$), i.e., $v=0$, $J=0$, $x_e\omega_e$ = the anharmonic term in the vibration ($cm^{-1}$), $B_v=B_e-\alpha(v+\frac{1}{2})$, the principal rotation term ($cm^{-1}$), $B_e=h/8\pi^2cI_e$ ($cm^{-1}$), $\alpha$ = a constant measuring the dependence of $B_v$ on the vibration ($cm^{-1}$), $D_v$ = a rotational term related to the centrifugal stretching of the molecule ($cm^{-1}$). $D_v$ may be neglected in the present case.

The band center, or position of the "missing line" of the fundamental and first overtone $\nu(v=0-1)$ and $\nu(v=0-2)$ in diatomic spectra may be obtained by considering the transitions $v=0$ to $v=1$, and $v=0$ to $v=2$ in Eq. (1) for the non-rotating molecule $J=0$. These frequencies are given by

$$\nu(0-1)=\omega_e-2x_e\omega_e, \quad (2)$$

$$\nu(0-2)=2(\omega_e-3x_e\omega_e). \quad (3)$$

With Eqs. (2) and (3) and the experimentally determined band centers, $\omega_e$ and $x_e\omega_e$ may be determined directly. The values are found in Table IV.

The lines of the $P$ and $R$ branches in a vibration-rotation band (i.e., the lines on the low and high frequency sides of the band center) are obtained by considering the $\Delta J=-1$ and $\Delta J=+1$ transitions in Eq. (1). The equation giving the position of these lines is

$$\left.\begin{matrix}P(m)\\R(m-1)\end{matrix}\right\}=\nu\mp m(B'+B'')+m^2(B'-B''), \quad (4)$$

where $\nu$ is the frequency of the band center, $B''$ and $B'$ are the $B$ values in the initial and final states, and where $m=1, 2, 3, \cdots$, is the ordinal number of the line. The number in parenthesis $P(m)$ and $R(m-1)$ in Eq. (4) is the $J$ value of the initial rotational state for a line of ordinal number $m$. For the fundamental $\nu=\nu(0-1)$, $B''=B(v=0)=B_e-\alpha/2$, and $B'=B(v=1)=B_e-3\alpha/2$. For the first overtone $\nu=\nu(0-2)$, $B''=B(v=0)=B_e-\alpha/2$, and $B'=B(v=2)=B_e-5\alpha/2$.

The expressions represented by (4) may be combined to give relations which yield the constants $\nu$, $B''$, and $B'$. These informative equations are:

$$\tfrac{1}{2}[R(m-1)+P(m)]=\nu+(B'-B'')m^2, \quad (5)$$

$$\tfrac{1}{2}[R(m-1)-P(m+1)]=(2m+1)B'', \quad (6)$$

$$\tfrac{1}{2}[R(m)-P(m)]=(2m+1)B'. \quad (7)$$

Equation (5) when plotted with $\frac{1}{2}[R(m-1)+P(m)]$ in $cm^{-1}$ as ordinates *versus* $m^2$ as abscissae gives a straight line. The ordinate intercept of this line is $\nu$, the band center, and the slope is $B'-B''$. From a consideration of the $B$ values it may be seen that $[B'(v=1)-B''(v=0)]=-\alpha$. Graphs of Eqs. (6) and (7) when plotted with $\frac{1}{2}[R(m-1)-P(m+1)]$ and $\frac{1}{2}[R(m)-P(m)]$ in $cm^{-1}$ as ordinates *versus* $(2m+1)$ as abscissae are straight lines, the slopes of which are respectively $B''$ and $B'$. In Fig. 3 is shown the graph of $[R(m-1)-P(m+1)]$ *versus* $2(2m+1)$ from which $B''(v=0)$ for $C^{12}O^{16}$ was determined. The data from both fundamental and overtone bands were plotted on the same curve to show that the points fit very accurately the relation (6). The curves for relations (5) and (7) are not shown.

## 6. THEORETICAL

The kinetic and potential energy for the diatomic molecule may be written as

$$T=\tfrac{1}{2}\mu\dot{Q}'^2,$$
$$V=\tfrac{1}{2}KQ'^2+hcK_{111}Q'^3+hcK_{1111}Q'^4+\cdots, \quad (8)$$

where $Q'$ represents the displacement coordinate and $\mu$ the reduced mass, $m_1m_2/(m_1+m_2)$. It is convenient to introduce the dimensionless coordinate $q=(\mu^2\lambda/\hbar^2)^{\frac{1}{4}}Q'$, where $\lambda=4\pi^2c^2\omega_e^2$. This leads to the quantum-mechanical relation for $T$ and $V$ given in (9) and (10).

TABLE II. The rotation lines in the fundamental band of $C^{13}O^{16}$.

| Positive ($R$) branch ($cm^{-1}$) | | | | Negative ($P$) branch ($cm^{-1}$) | | | |
|---|---|---|---|---|---|---|---|
| Identification | $\nu$ Obs. | $\nu$ Calc. | Difference | Identification | $\nu$ Obs. | $\nu$ Calc. | Difference |
| $R(0)$ | * | 2099.69 | | | | | |
| $R(1)$ | * | 2103.30 | | $P(1)$ | 2092.35 | 2092.37 | −0.02 |
| $R(2)$ | * | 2106.87 | | $P(2)$ | 2088.57 | 2088.67 | −0.10 |
| $R(3)$ | 2110.44 | 2110.41 | +0.03 | $P(3)$ | 2084.85 | 2084.92 | −0.07 |
| $R(4)$ | 2113.98 | 2113.92 | +0.06 | $P(4)$ | 2081.12 | 2081.14 | −0.02 |
| $R(5)$ | 2117.46 | 2117.39 | +0.07 | $P(5)$ | * | 2077.33 | |
| $R(6)$ | 2120.92 | 2120.83 | +0.09 | $P(6)$ | * | 2073.49 | |
| $R(7)$ | 2124.20 | 2124.24 | −0.04 | $P(7)$ | 2069.52 | 2069.61 | −0.09 |
| $R(8)$ | * | 2127.61 | | $P(8)$ | 2065.73 | 2065.70 | +0.03 |
| $R(9)$ | * | 2130.94 | | $P(9)$ | 2061.81 | 2061.75 | +0.06 |
| $R(10)$ | 2134.30 | 2134.25 | +0.05 | $P(10)$ | 2057.81 | 2057.77 | +0.04 |
| $R(11)$ | 2137.49 | 2137.52 | −0.03 | $P(11)$ | 2053.79 | 2053.76 | +0.03 |
| $R(12)$ | 2140.83 | 2140.95 | −0.12 | $P(12)$ | 2049.75 | 2049.71 | +0.04 |
| $R(13)$ | 2144.03 | 2143.95 | +0.08 | $P(13)$ | 2045.61 | 2045.63 | −0.02 |
| $R(14)$ | * | 2147.12 | | | | | |
| $R(15)$ | * | 2150.26 | | | | | |
| $R(16)$ | 2153.43 | 2153.36 | +0.07 | | | | |
| $R(17)$ | 2156.50 | 2156.42 | +0.08 | | | | |
| $R(18)$ | 2159.43 | 2159.46 | −0.03 | | | | |

* These lines were obscured by the $C^{12}O^{16}$ lines and were not observed.

$$T=-(hc\omega_e/2)(\partial^2/\partial q^2), \quad (9)$$

$$V=hc[(\omega_e/2)q^2+k_{111}q^3+k_{1111}q^4+\cdots], \quad (10)$$

where

$$k_{111}=K_{111}(\hbar^2/16\pi^4c^2\mu^2\omega_e^2)^{\frac{1}{2}}, \quad (11)$$

and

$$k_{1111}=K_{1111}(\hbar^2/16\pi^4c^2\mu^2\omega_e^2).$$

In considering the isotopic molecule it is reasonable to assume that the potential energy constants $K$, $K_{111}$, $K_{1111}$ are the same as in the normal molecule, but as the reduced mass is different, the frequencies are different. It is possible to verify this assumption for the CO molecule since it leads to the following relations

TABLE III. The rotation lines in the overtone band of $C^{12}O^{16}$.

| Positive ($R$) branch ($cm^{-1}$) | | | | Negative ($P$) branch ($cm^{-1}$) | | | |
|---|---|---|---|---|---|---|---|
| Identification | $\nu$ Obs. | $\nu$ Calc. | Difference | Identification | $\nu$ Obs. | $\nu$ Calc. | Difference |
| $R(0)$ | 4263.66 | 4263.64 | +0.02 | | | | |
| $R(1)$ | 4267.36 | 4267.33 | +0.03 | $P(1)$ | 4255.95 | 4256.05 | −0.10 |
| $R(2)$ | 4270.84 | 4270.95 | −0.11 | $P(2)$ | 4252.05 | 4252.15 | −0.10 |
| $R(3)$ | 4274.63 | 4274.50 | +0.13 | $P(3)$ | 4248.11 | 4248.18 | −0.07 |
| $R(4)$ | 4277.93 | 4277.99 | −0.06 | $P(4)$ | 4244.12 | 4244.14 | −0 02 |
| $R(5)$ | 4281.31 | 4281.40 | −0.09 | $P(5)$ | 4239.90 | 4240.03 | −0.13 |
| $R(6)$ | 4284.59 | 4284.74 | −0.15 | $P(6)$ | 4235.74 | 4235.86 | −0.12 |
| $R(7)$ | 4287.98 | 4288.01 | −0.03 | $P(7)$ | 4231.57 | 4231.61 | −0.04 |
| $R(8)$ | 4291.39 | 4291.22 | +0.17 | $P(8)$ | 4227.39 | 4227.29 | +0.10 |
| $R(9)$ | 4294.45 | 4294.35 | +0.10 | $P(9)$ | 4223.00 | 4222.90 | +0.10 |
| $R(10)$ | 4297.40 | 4297.42 | −0.02 | $P(10)$ | 4218.57 | 4218.45 | +0.12 |
| $R(11)$ | 4300.47 | 4300.41 | +0.06 | $P(11)$ | 4214.05 | 4213.92 | +0.13 |
| $R(12)$ | 4303.47 | 4303.34 | +0.13 | $P(12)$ | 4209.47 | 4209.33 | +0.14 |
| $R(13)$ | 4306.34 | 4306.19 | +0.15 | $P(13)$ | 4204.75 | 4204.66 | +0.09 |
| $R(14)$ | 4308.94 | 4308.98 | −0.04 | $P(14)$ | 4199.99 | 4199.93 | +0.06 |
| $R(15)$ | 4311.55 | 4311.69 | −0.14 | $P(15)$ | 4195.25 | 4195.12 | +0.13 |
| $R(16)$ | 4314.32 | 4314.34 | −0.02 | $P(16)$ | 4190.40 | 4190.25 | +0.15 |
| $R(17)$ | 4316.87 | 4316.92 | −0.05 | $P(17)$ | 4185.39 | 4185.30 | +0.09 |
| $R(18)$ | 4319.50 | 4319.43 | +0.07 | $P(18)$ | 4180.36 | 4180.29 | +0.07 |
| $R(19)$ | 4321.83 | 4321.86 | −0.03 | | | | |
| $R(20)$ | 4324.13 | 4324.23 | −0.10 | | | | |
| $R(21)$ | 4326.56 | 4326.53 | +0.03 | | | | |
| $R(22)$ | 4329.75 | 4329.76 | −0.01 | | | | |

TABLE IV. Molecular constants of $C^{12}O^{16}$ and $C^{13}O^{16}$.

| | $C^{12}O^{16}$ Fundamental | $C^{12}O^{16}$ Overtone | $C^{12}O^{16}$ Herzberg[1] | $C^{13}O^{16}$ Fundamental |
|---|---|---|---|---|
| $\nu(0-1)$ | 2143.16 cm$^{-1}$ | | | 2096.05 cm$^{-1}$ (obs.) |
| $\nu(0-2)$ | | 4259.88 cm$^{-1}$ | | |
| $\omega_e$ | 2169.60 cm$^{-1}$ | | 2168.2 cm$^{-1}$ | 2121.33 cm$^{-1}$ (calc.)* |
| | | | | 2121.24 cm$^{-1}$ (calc.)** |
| $x_e\omega_e$ | 13.22 cm$^{-1}$ | | | 12.64 cm$^{-1}$ (calc.)*** |
| $\alpha$ | 0.0175 cm$^{-1}$ | 0.0174 cm$^{-1}$ | 0.01744 cm$^{-1}$ | 0.0169 cm$^{-1}$ (obs.) |
| | | | | 0.0168 cm$^{-1}$ (calc.)**** |
| $B''(v=0)$ | 1.9150 cm$^{-1}$ | 1.9150 cm$^{-1}$ | | 1.8380 cm$^{-1}$ (obs.) |
| $B'(v=1)$ | 1.8975 cm$^{-1}$ | | | 1.8211 cm$^{-1}$ (obs.) |
| $B'(v=2)$ | | 1.8802 cm$^{-1}$ | | |
| $B_e$ | 1.9238 cm$^{-1}$ | | 1.9310 cm$^{-1}$ | 1.8465 cm$^{-1}$ |
| $I_e$ | $14.548\times10^{-40}$ g cm$^2$ | | | $15.157\times10^{-40}$ g cm$^2$ |
| $r_e$ | 1.1303A | | 1.1284A | 1.1280A |
| $k_{111}$ | $-62.78$ cm$^{-1}$ | | | $-60.70$ cm$^{-1}$ |
| $k_{1111}$ | 13.35 cm$^{-1}$ | | | 12.77 cm$^{-1}$ |

* Calculated from Eq. (2) using $\nu(0-1)'$ and $(x_e\omega_e)'$.
** Calculated from Eq. (12).
*** From Eq. (13) using $B_e'$, $\omega_e'$, and $k_{111}'$, or Eq. (15).
**** From Eq. (12) using $k_{111}'$, $k_{1111}'$, and $\omega_e'$.
[1] G. Herzberg, *Molecular Spectra and Molecular Structure*, Part I, "Diatomic Molecules" (Prentice Hall, Inc., New York, 1939), p. 486.

between the frequencies and the $k$'s:

$$(\omega_e'/\omega_e)=(\mu/\mu')^{\frac{1}{2}},$$
$$k_{111}'=k_{111}(\omega_e'/\omega_e)^{\frac{1}{2}}, \qquad (12)$$
$$k_{1111}'=k_{1111}(\omega_e'/\omega_e)^2,$$

where the prime refers to the isotopic molecule.

In the solution of the quantum-mechanical problem to second order of approximations for the energy,[3] it is found that the constants $x_e\omega_e$ and $\alpha$ in (1) may be expressed in terms of the constants $k_{111}$ and $k_{1111}$ as follows:

$$x_e\omega_e=\tfrac{1}{4}[6k_{1111}-15(k_{111}^2/\omega_e)], \qquad (13)$$

$$\alpha=-6(B_e/\omega_e)[B_e+2k_{111}(2B_e/\omega_e)^{\frac{1}{2}}]. \qquad (14)$$

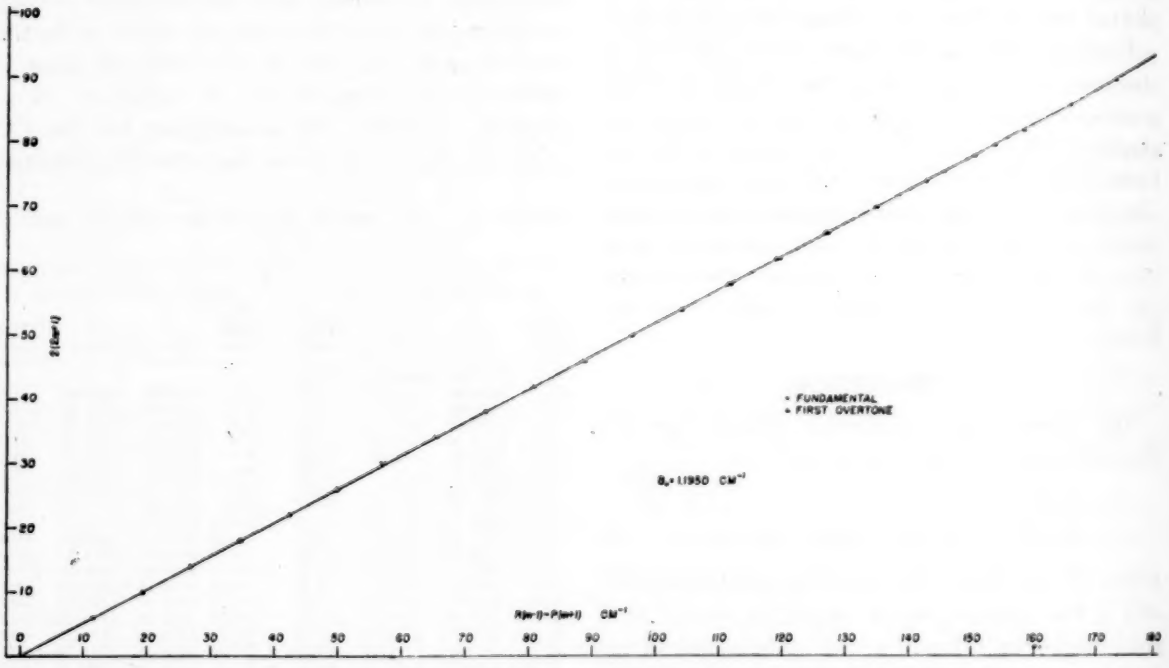


FIG. 3. Plots of $R(m-1)-P(m+1)$ *versus* $2(2m+1)$ for fundamental and first overtone vibration-rotation bands of $C^{12}O^{16}$.

[3] A. H. Nielsen, J. Chem. Phys. **11**, 160 (1943), see $x_{11}$ and $\alpha_1$ of Eq. (15).

By substituting the experimental values of $x_e\omega_e$, $\omega_e$, $B_e$, and $\alpha$ into (13) and (14), $k_{111}$ and $k_{1111}$ were found and are given in Table IV. The corresponding $k_{111}'$ and $k_{1111}'$ were then found from Eqs. (12) and are also listed in Table IV. By substituting the values of $k_{111}'$, $B_e'$, $\omega_e$ into (14), the value of $\alpha'$ was found to be 0.0168 $cm^{-1}$ as compared with the experimental value of 0.0169 $cm^{-1}$. $(x_e\omega_e)'$ found in Table IV was computed by substituting $k_{111}'$ and $k_{1111}'$ and $\omega_e'$ into Eq. (13). This is equivalent to the relation

$$(x_e\omega_e)'/(x_e\omega_e)=(\omega_e'/\omega_e)^2. \quad (15)$$

The equilibrium value $\omega_e'$ was computed from the ratio of the reduced masses and $\omega_e$, Eq. (12). All the constants computed have been tabulated in Table IV.

PHYSICAL REVIEW VOLUME 72, NUMBER 4 AUGUST 15, 1947

# Negative Corona in Freon-Air Mixtures

G. L. WEISSLER AND E. I. MOHR
*Department of Physics, University of Southern California, Los Angeles, California*

(Received April 7, 1947)

In order to gain information as to the importance of negative space charges in coronas, studies of negative corona in freon-air mixtures were undertaken. The mixtures used ranged from $10^{-4}$ to $10^{2}$ percent of freon-12 in dry air. The onset potentials of the intermittent corona region were constant in all mixtures, approximately 6 to 7 kv with $X/p$ about 100; only in pure freon it changed to 12,600 volts with $X/p$ about 200. Concentrations of freon up to one percent revealed corona characteristics very similar to those of air. From one to 20 percent mixtures showed rapidly decaying Trichel pulses. Upon analysis this seems due to the formation of $Cl^-$ and $F^-$, which are shown to be still stable at values of $X/p \geqq 200$. As a consequence, negative space charges will be stable in regions much closer to the corona point than in air and will, therefore, be more efficient in suppressing the discharge as is indicated by decaying pulse sizes. At still higher concentrations the more stable $Cl^-$ and $F^-$ formed heavier space charges, inhibiting the formation of large electron avalanches to such an extent that only incipient Trichel bursts were produced. Thus the range of potential of the intermittent corona region was extended to higher values, and the corona current *vs.* potential curves showed rapidly decreasing slopes with increasing amounts of freon.

## INTRODUCTION

THIS investigation was undertaken for two reasons: to explain in more detail the mechanism that is active in the suppression of sparks because of the presence of gases which form very stable negative ions; and to investigate the character of space-charge pulses in such coronas in order to further our understanding of the more general mechanisms active in spark breakdown in any gas. It is essential to state the reasons for utilizing corona studies for this purpose rather than studies of sparking potentials with plane parallel electrodes. The propagation of a discharge at or near atmospheric pressure is mainly based on the formation of streamers proceeding from the anode or the mid-gap region. This occurs only near a threshold value. A plane parallel gap does not lend itself easily to a detailed study of the mechanisms involved because of the rapidity of events succeeding the initiating streamer. In a corona, however, the range of potentials from onset to spark breakdown is wide. In addition, there are the inherent advantages of strongly divergent electric fields and differences in mechanisms between positive and negative coronas. The proper choice of the geometry of corona gaps, i.e., confocal paraboloids or a hyperboloid point electrode opposite a plane enables one to make field calculations and to observe space-charge phenomena which are obscured in experiments on plane parallel gaps.

The characteristic curves of any point-to-plane corona, plotting the gap current against the applied potential, are made up of three ranges of specific interest. The "dark-current" range occurs well below the onset of any visible corona, and the sharper the point the narrower this range will be. It depends most strongly on the first Townsend coefficient $\alpha$ and to a lesser degree

on the secondary mechanism near the point. The latter is caused chiefly by the efficiency of liberation of electrons from the point surface by positive ion bombardment and also to some photoelectric liberation from the cathode. The currents in this range vary from $10^{-14}$ ampere to about $10^{-8}$ ampere. Photo-ionization and excitation in the gas as well as space-charge distortion of the static electric fields are negligible.

In the "intermittent-corona" range the currents vary from $10^{-8}$ to about $10^{-6}$ ampere, and the corona becomes visible. In addition to the coefficient $\alpha$, the secondary actions at the cathode point become more prominent. The most characteristic aspect of this range is the flickering or intermittent, visible corona. Associated with it are large current fluctuations at any fixed potential and transient space-charge pulses in the immediate vicinity of the point. Space-charge distortion of the electric field occurs intermittently. The corona is not self-sustaining and requires electrons from external ionizing sources to re-initiate it.

The third range is that of the "continuous corona" where the currents for a given potential are steady and reproducible and where the visible character is not erratic. The corona is self-sustaining, and the currents vary smoothly from about $10^{-5}$ ampere until this form of discharge is finally terminated by a disruptive spark or arc.

It should be noted that the transitions from the first to the second, and from the second to the third range do not always occur at a fixed and reproducible potential for a given gap geometry and gas, since the mechanisms active in the second range are subject to strong statistical fluctuations. We have tried to minimize these by providing external ionization from a weak Ra source placed in the vicinity of the gap. The results discussed here are mainly concerned with the second range and partly with the third.

## APPARATUS AND TECHNIQUE

These experiments were carried out in freon-dry-air mixtures near atmospheric pressure (745 mm Hg) in a closed Pyrex system described elsewhere.[1] A 3.1-cm point-to-plane gap was used, employing a hemispherically-capped, smoothly polished Pt point (0.5-mm in diameter) opposite a circular Pt plane of 4-cm diameter with rounded edges. A 70-kv transformer supplied the high voltage through a half-wave rectifier and a one mfd filter condenser. The potential was determined with a 50 megohm, corona-shielded, Taylor resistor in series with an accurate microammeter. Freon-12, dichloro-difluoro-methane, obtained from commercial tanks, was used without further purification since the manufacturer's[2] specifications of purity seemed adequate for this work. The freon-air mixtures ranged $10^{-4}$ to $10^{2}$ percent by volume of freon and were obtained by successive dilutions. Test observations with room air, dried over a $CO_2$ snow-alcohol mixture, were made before and after the work on freon-air mixtures. By the use of liquid air traps, mercury vapor from the diffusion pump and manometer was carefully excluded from the discharge chamber.

Potential *versus* current characteristics were taken up to voltages which were safely below the breakdown limit. Constant gap geometry was thus maintained throughout. A tele-microscope (30×) enabled good visual observation of the discharge, and the transient space-charge pulses at the point were observed with an oscilloscope[3] which was connected across a $3\times10^{4}$ ohms resistor between the plate electrode and ground. A weak radium source was placed 6 inches from the gap in order to facilitate the observation of pulse formation preceding onset of the steady corona.

## EXPERIMENTAL RESULTS

One hundred percent dry air and mixtures up to 0.1 percent of freon showed similar results. The first space-charge pulses (termed by Loeb[4] "Trichel" pulses and explained subsequently in the discussion) were observed in the oscillograph at about 6000 volts and were accompanied by faintly visible light flashes at currents of approximately $10^{-8}$ ampere. These pulses never attained the regularity of frequency nor the uniformity of amplitude observed by Trichel[5] in an open air

[1] G. L. Weissler, Phys. Rev. **63**, 96 (1942).

[2] Kinetic Chemicals, Inc., 10th and Market Streets, Wilmington, Delaware, Technical Paper No. 6 on Freon-12 (Underwriter's Report), and Technical Paper No. 8.

[3] A. F. Kip, Phys. Rev. **55**, 549 (1939), Fig. 1B.

[4] L. B. Loeb, A. F. Kip, G. G. Hudson, and W. H. Bennett, Phys. Rev. **60**, 714 (1941).

[5] G. W. Trichel, Phys. Rev. **54**, 1078 (1938), Figs. 2, b-f.

gap, but showed the same irregular characteristics that Hudson[4] found with an enclosed gap using clean, dry air free from dust particles, and other sources of triggering electrons which were found essential in the production of regular Trichel pulses. The irregular Trichel-pulse bursts were of varying duration, from $10^{-3}$ to $10^{-2}$ second. The amplitude and number of individual peaks in each burst varied, but in general they are represented in Fig. 2A. At higher potentials the number of bursts and the frequency of pulses in each burst increased. Since no "single-sweep" mechanism was available, a detailed study of the pattern, i.e., the exact frequency and shape, was impossible, but the general trends were the same as those reported previously.[4,5]

At about 12,500 volts and a current of 12 microamperes the transition to the continuous corona occurred, showing the same visual characteristics observed previously.[5] The current *versus* potential curve of dry air and mixtures of less than 0.1 percent of freon for the continuous corona is shown in Fig. 1. Although the current was continuous, fluctuations and irregular Trichel pulses were observed in the oscilloscope throughout this third region, and they decreased in amplitude with increasing currents.

With mixtures of from 0.1 to one percent of freon in dry air the only notable difference occurred with the appearance in the intermittent corona region of what might be termed a hysteresis effect. After several minutes at relatively high currents in the continuous corona region, a decrease of the potential below 12.5 kv produced average current values in the intermittent corona region which were much lower than those during the upward run. A few minutes after the first run, with the voltage off during the interval, a second run was started. The first Trichel pulses and faint light flashes then were observed at 9 to 10 kv at a current of about $10^{-5}$ ampere rather than at 6 kv as in the first run. This hysteresis effect became more pronounced with a larger amount of charge passing across the gap and with a shorter time interval between the first and second runs. An interval of 30 minutes or more gave results duplicating those of the first run.

As the freon content was increased from one to 20 percent, the shape of the Trichel bursts

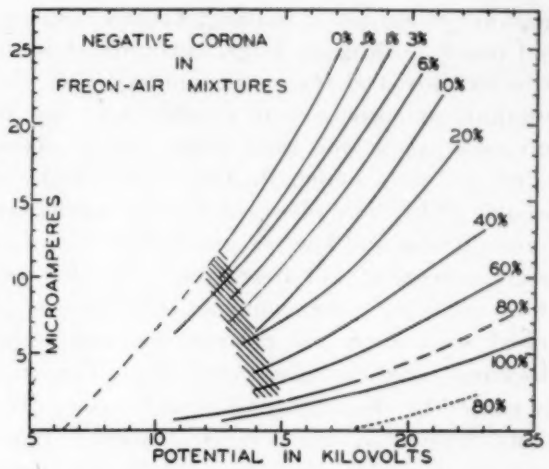


FIG. 1. Current *vs.* potential curves for negative corona in freon-air mixtures. The percentage number indicates the amount of freon by volume in dry, clean air. Total gas pressure: 745 mm of Hg. To the left of the shaded area and below the dotted continuation of the pure air curve (0 percent), the current values for all mixtures fluctuate violently. The dotted 80 percent curve below the 100 percent one is due to the formation of several secondary corona spots 1 to 2 cm from the tip of the point electrode on the stem.

changed from that of Fig. 2A to the decaying ones of Figs. 2B and 2C. This may be caused by the production of increasing amounts of $Cl^-$ and $F^-$ by the discharge. Mixtures of over 20 percent freon showed similar pulses with reduced amplitudes. At concentrations of 60 percent freon and above it was difficult to distinguish the bursts because of their reduced size. These incipient Trichel pulses showed the same regularity as the original Trichel pulses, and they also disappeared at higher potentials.

With mixtures of freon of one to 100 percent the current *versus* potential curves showed successively decreasing slopes with increasing amounts of freon (Fig. 1). Similar results were found for

FIG. 2. A: Irregular Trichel-pulse burst in dry, clean air near onset of negative corona (7000 volts). B: The same in 6 percent freon in air, $p = 745$ mm of Hg. C: The same in 10 percent freon in air, $p = 745$ mm of Hg. It is possible that the individual pulses in B and C return to the zero line. Because of the high speed of pulse formation (less than one microsecond) the details of this oscillograph trace must be instrumental, but the general decay of the pulses seems to be real.

sparking potentials by Skilling, Trump, Nonken, and others.[6] Although larger amounts of freon reduced currents, the onset potentials of the intermittent coronas were roughly 6 kv for all mixtures except for pure freon, where about 12.65 kv were required. Onset potentials of around 13 kv were observed for the continuous corona for air and low percentage mixtures. For larger percentages of freon, onset for the continuous corona region could not be clearly established since both the current and the visual discharge were changing erratically. (This may be caused by fluctuating $Cl^-$ and $F^-$ concentrations caused by the electrical wind.) When plotting these data as in Fig. 1, however, it was possible to obtain current *versus* potential curves for the higher concentrations by using average values except for the region to the left of the shaded line (Fig. 1). In the intermittent corona region the potential range became progressively larger with increasing amounts of freon.

The visual appearance of the discharge gradually changed with increasing amounts of freon from the glow-discharge type in air,[4] with negative glow, Faraday dark space, and narrow positive column, to a larger, diffuse discharge with no dark space. (Loeb[7] gives an excellent analysis of the glow-discharge characteristics of the negative corona and the active ionizing function, contrasting Townsend's $\alpha$ with Morton's[8] proposal.) Intermediate concentrations of freon, 40 to 80 percent, showed alternately at the same potential the wide, diffuse-discharge characteristic of freon, and the narrow type observed in air. A change from the first to the second form was accompanied by an increase in current with a corresponding decrease on changing back to the first type. In the second, more concentrated form, an active cathode spot was formed, and therefore the discharge moved less readily over the point surface than did the diffuse type.

[6] J. G. Trump, F. J. Safford, and R. W. Cloud; Trans. A.I.E.E. **60**, 132 (March 1941); G. C. Nonken, Trans. A.I.E.E. **60**, 1017 (Dec. 1941); H. H. Skilling and W. C. Brenner, Trans. A.I.E.E. **61**, 191 (April, 1942).

[7] L. B. Loeb, "The mechanism of the negative corona at atmospheric pressure in relation to the first Townsend coefficients," Phys. Rev. **71**, 712 (1947),

[8] P. L. Morton, Phys. Rev. **70**, 358 (1946); G. W. Johnson, Phys. Rev. **71**, 278A (1947).

## DISCUSSION

In a gas in which electrons attach readily, Trichel pulses represent the major space-charge phenomena of the negative point corona. (In pure, free electron gases such as A, $H_2$, and $N_2$, however, it has been found[1] that the Trichel-pulse mechanism is not applicable.) In order to understand the observations in freon it is necessary to discuss first the mechanism in air. When a sufficient negative potential is applied to a point in air at atmospheric pressure, an electron, generated in the high field region, travels away from the point and by cumulative ionization by collision produces $\exp[\int_0^{x_0}\alpha dx]$ new electrons and positive ions. At a distance $x_0$ from the point surface the electric field $X$ is decreased to such a low value that ionization by electron impact becomes negligible ($\alpha<1$). In this region ($X/p=90$) electrons attach readily and form relatively slow negative ions. During the development of the first avalanche new ones are generated by the liberation of triggering electrons from the point surface by three processes: (a) positive ion bombardment; (b) the photoelectric effect at the cathode; and (c) electron emission from rough spots and dust specks. When the electrons in these avalanches have traveled beyond $x_0$, they enhance the negative-ion space-charge cloud so much that the field in the immediate vicinity of the point is insufficient to permit effective ionization by collision about the point, and the discharge is suppressed. After $10^{-3}$ to $10^{-4}$ second the negative ions have traveled sufficiently far into the gap toward the anode to diffuse the limiting negative space charge. The original field is then restored, and if sufficient triggering electrons are furnished by field emission or by the Paetow-Malter effects[9] the process will be repeated. Since it depends only on the clearing time required for the negative ions, it produces regular Trichel pulses in the oscillograph.[5] If, however, the corona point is carefully polished, and dust-free air is used, field emission will be absent. For re-ignition the discharge then depends on triggering electrons liberated from the point by those few positive ions which are still available. (The majority of positive ions are drawn into the point and

[9] L. Malter, Phys. Rev. **49**, 478 (1936); **50**, 48 (1936); H. Paetow, Zeits. f. Physik **111**, 770 (1939).

neutralized during or before the choking-off period.) As a result of the low efficiency of secondary emission by positive ions of relatively low energy, this repetitive process will be subjected to strong statistical fluctuations, giving rise to the irregular Trichel pulse-bursts[4] (Fig. 2A).

In flame-decomposition tests performed on freon-12 by the manufacturers,[2] HF, HCl, and other electro-negative gases were produced. A similar and more efficient decomposition process including the production of Cl and F will be initiated by electron impacts. The electron affinity of the oxygen atom is about 2.2. ev, but since O does not exist long in air, most of the attachment is to the $O_2$ molecules which have an affinity of 0.07 to 0.19 ev. This is markedly lower than the affinities of Cl (3.8 ev) and F (4 ev).

One should, therefore, expect that with freon added in increasing amounts to air, the negative-ion space charges will be formed closer to the point surface. This means a smaller $x_0$ for avalanche formation, with correspondingly lower currents, and also a greater effectiveness in suppressing the discharge (Fig. 2B, C). The negative ions of chlorine and fluorine must therefore be stable at higher values of the ratio of $X/p$ (field-strength in volts/cm divided by pressure in mm of Hg) than those of oxygen, and efficient electron capture[10] may be possible at values of $X/p$ as high as 200. This value seems to be substantiated by the following calculations:

On the assumption that the corona point was shaped in the form of a hyperboloid of revolution and that the plane electrode was large in diameter compared with the gap, the electric fields at the surface of the point and at different distances from the point were calculated by established methods.[11] (The surface field at the point was calculated to be $X_s = 65$ kv/cm (Fig. 3A) at 5 kv, which is only 54 percent of the value of $X_s' = 120$ found by Kip[12] to be necessary for streamer formation in air. Since he made his observations and calculations with confocal paraboloid electrodes assuring him of much greater accuracy, our values of $X$ and $X/p$ in Fig. 3A indicate only order of magnitudes and relative quantities. Since $X_s = kV_s$ it is possible to replace the calculated factor $k = 13$ by a factor $k' = 120$ (kv/cm)/5 (kv) = 24 obtained from direct comparison with Kip's data. The curves for $X/p = f(x)$ given there must thus be shifted by this fraction, and results shown in Fig. 3B are based on this correction.) Values of $X/p = 200$ at a distance of only 0.3 mm from the point surface for an applied potential of 12 kv were found (Fig. 3B). The very low corona currents in pure freon and the absence of normal size Trichel-pulse bursts appear to be mainly due to the absence of large avalanche formation. It is possible that the triggering electrons have only 6 or 7 ionizing free paths over a distance $x_0$, say 0.3 mm before attachment occurs, instead of 13 or 14 as in air over the same $x_0$, and their energy is dissipated in dissociation, vibrational levels, etc. It is interesting that the onset potentials of the intermittent corona region for pure air and freon mixtures up to 80 percent are approximately the same (6 to 7 kv). The corresponding value of $X/p$ at the point surface is about 100 (Fig. 3A), which is close to $X/p = 90$ when the negative $O_2$ ion sheds its electron.[13] For 100 percent freon,

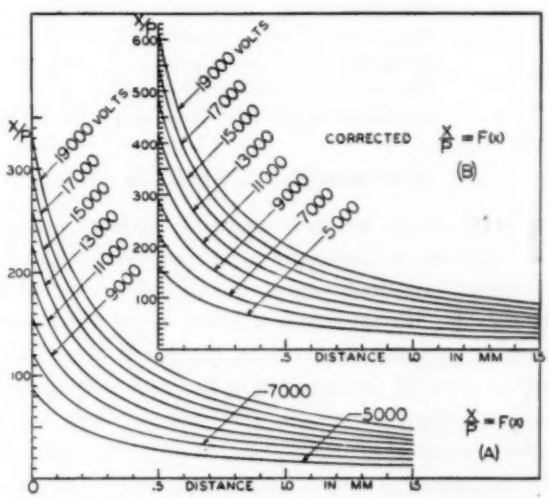


FIG. 3. A: $X/p$ as a function of distance $x$ in mm from the point surface: $X_s = kV_s$ and $X_x = (RX_s)/(R+x)$; $2R = 0.5$-mm diam.; $k = 13$, when hyperboloid point is assumed; $p = 745$ mm of Hg. B: Corrected values of $X/p = f(x)$, using Kip's data; see text.

[10] H. S. W. Massey, *Negative Ions* (Cambridge University Press, New York, 1938), Chapters III and IV.
[11] C. F. Eyring, S. S. Mackeown, and R. A. Millikan, Phys. Rev. **31**, 900 (1928); (see also reference (4) page 715).
[12] A. F. Kip, Phys. Rev. **55**, 551 (1939).
[13] L. B. Loeb, Phys. Rev. **48**, 684 (1935); see also Loeb, *Fundamental Processes of Electrical Discharge in Gases* (John Wiley and Sons, Inc., New York, 1939), pp. 291–293.

the onset potential is 12.65 kv with a value of $X/p=200$ at the point surface. (The same values of $X/p$ are found along a vertical line above 0.3 mm in Fig. 3B for the respective point potentials of 6 and 12 kv.) This indicates the threshold of stability of the negative ions produced in freon. The negative ion formation and the relatively inelastic electron impacts in freon tend to decrease materially the first Townsend coefficient $\alpha$.

The hysteresis effect of increased onset potentials for the intermittent corona may be explained by the accumulation of decomposition products of freon which are particularly effective in electron capture. Since free atoms like Cl and F will recombine to form molecules, it is not surprising to find that the effect disappears with time. Such reactive gases can also be absorbed by electrode materials and similar substances. In an enclosed, air-filled chamber a transient lowering of the sparking potential was observed as a result of the formation of nitrous oxides after the passage of several sparks,[14] but in freon the reverse is true.

We wish to express our appreciation to Professor L. B. Loeb for the loan of the discharge chamber used in this work and for his assistance in the interpretation of the results in the light of recent data from his research group.

[14] W. R. Haseltine, Phys. Rev. **58**, 188 (A) (1940).

PHYSICAL REVIEW VOLUME 72, NUMBER 4 AUGUST 15, 1947

# Positive Corona in Freon-Air Mixtures

E. I. MOHR AND G. L. WEISSLER
*Department of Physics, University of Southern California, Los Angeles, California*

(Received April 7, 1947)

In this investigation of positive corona, streamer pulses increased in frequency and strength to a maximum at one percent of freon in air. The visual characteristic of the corona changed markedly indicating also that the discharge sustained itself largely by the streamer mechanism. The dissociation of freon by the discharge created stable $Cl^-$ and $F^-$ ions which neutralized the positive space charges and therefore stimulated streamers. As the freon content was increased, streamers degenerated until they could not be distinguished from burst pulses. The onset potentials were shifted to higher values and the current *vs.* potential curves showed decreasing slopes with increasing amounts of freon.

## EXPERIMENTAL RESULTS

THE data on the positive point-to-plane corona in freon-air mixtures were obtained by using the techniques described previously.[1] In air the intermittent corona region (Geiger-counter regime) began with the onset of streamers[2] at a point potential of 5 kv, and it extended over a range of about 200 volts. Some burst pulses were also observed. At 5.2 kv onset of the continuous corona occurred, and streamers no longer were present. The current was 0.25 microampere, and the visual appearance of the discharge was steady. Further increase in potential resulted in monotonically increasing currents (Fig. 1). At between 20 and 25 kv occasional "breakdown" streamers were observed. Since these only occur close to the sparking potential, the runs were terminated. The visual character of the discharge was that of a uniform glow which extended over a larger surface area of the point as the potential was raised.

It has been pointed out before[3] that the addition of small amounts of impurities to the gas strongly influences streamer formation and thereby sparking potentials. Therefore, after several runs with the same dry air filling, streamers were observed in the continuous corona region. They did not occur in this region after the refilling of the chamber, and the results of

[1] G. L. Weissler and E. I. Mohr, preceding paper on negative corona.
[2] A. F. Kip, Phys. Rev. **55**, 551 (1939).
[3] G. L. Weissler, Phys. Rev. **63**, 96 (1943); R. W. Haseltine, Phys. Rev. **58**, 188A (1940).

the first run were duplicated. The addition of from $10^{-4}$ to $10^{-1}$ percent of freon to pure air gave essentially the same results as those just described for *old* air: streamers were formed in the lower potential region of the continuous corona, and they disappeared at around 10 kv.

The characteristics in a one-percent freon-air mixture changed markedly. The onset potential of the intermittent corona region was again 5 kv, but the range was extended to about 9 kv. Visible, strong streamers were observed, and the currents fluctuated between zero and three microamperes. Streamers were still present after the onset of the continuous corona at 9.15 kv and were active throughout this entire region. The visual appearance of the continuous corona underwent a significant change from the uniform glow in air, which covered the point like a closely adhering sheath of about 0.05 to 0.1 mm in thickness, to a very localized discharge like a narrow and intense luminous channel or spindle (Fig. 2). The area of contact between the spindle and the corona point was very bright and about 0.05 mm in diameter. The maximum diameter of the spindle was never greater than two to three times the diameter at contact. As the potential was raised the spindle increased in brilliance, seemed to decrease in diameter, and grew in length up to six mm at 21 kv. Its tip swayed laterally and gave the impression of streamers feeding into it. The current *versus* potential curve was only very slightly below that of pure air.

The concentration of freon in dry air was gradually increased to 100 percent. The onset potentials of the intermittent corona region were raised to higher values, reaching 13 kv for 100 percent freon. The potential range became progressively larger with increasing amounts of freon, i.e., extending beyond 25 kv for 100 percent freon, and the current *vs.* potential curves decreased in slope (Fig. 1). The visual appearance of the discharge changed from a pinkish-purple color typical of air to bluish-white. It retained the general form of a spindle, at least at the higher potentials, but it decreased in length and increased in diameter as the freon content was increased. The discharge gradually lost its well-defined shape and became more diffuse (Fig. 2).

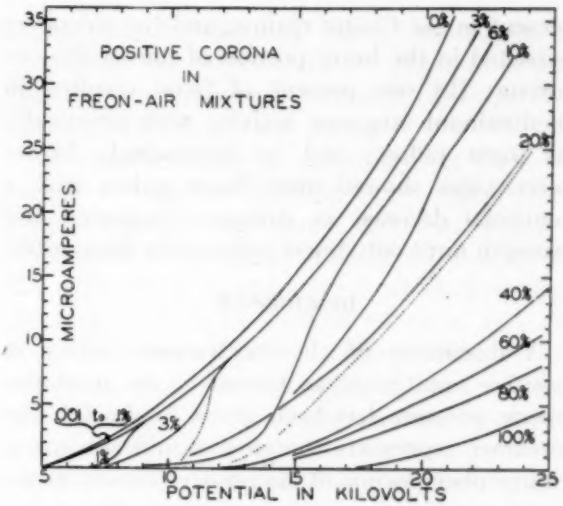


FIG. 1. Current *vs.* potential curves for positive corona in freon-air mixtures. The percentage number indicates the amount of freon by volume in dry, clean air. Total gas pressure: 745 mm of Hg. The dotted curves are representative of the values obtained in a second run, about 15 minutes after the first one was finished.

With large amounts of freon the general trend of streamer formation in both the intermittent and the continuous corona regions seemed to be one of degeneration. In mixtures containing three percent of freon streamers were immediately followed by burst pulses as indicated by decaying saw-tooth patterns in the oscillograph.[4] When the percentage of freon was increased further, streamers became weaker, formed less frequently, and assumed the characteristics of burst pulses which gradually decreased in amplitude.

The corona characteristics of each gas filling were checked by two or more runs. If the time interval between runs was of the order of a few minutes only, a hysteresis effect similar to that in negative corona[1] was observed. For mixtures of $10^{-2}$ to 100 percent of freon the onset potentials of the intermittent corona region were shifted several thousand volts higher than those of the first run. This effect seemed to depend only slightly on the concentration. In the lower part of the intermittent corona region the current *vs.* potential values of the second run were far below those of the first, and they gradually converged toward the point of onset of the continuous corona, i.e., the broken line curves in Fig. 1.

To summarize: (a) In from zero to 0.1 percent freon streamers and occasional burst pulses were

[4] A. F. Kip, Phys. Rev. **55**, 549 (1939), Fig. 6.

present in the Geiger regime, and the streamers persisted in the lower portion of the continuous corona; (b) one percent of freon resulted in predominant streamer activity with practically no burst pulses; and (c) increasingly higher percentages showed more burst pulses with a continual decrease in streamer frequency and strength until only burst pulses were discernible.

## DISCUSSION

A discussion of the mechanisms active in positive point-to-plane corona in air at atmospheric pressure has been given by Loeb.[5] The streamer represents the most significant space-charge phenomenon of the positive corona in air, and it occurs in a very narrow potential region termed the Geiger-counter regime.[6] Streamers disappear at the onset of the continuous corona and are replaced by the self-sustaining burst-pulse corona, which is composed of many rapid current fluctuations caused by a continuous succession of burst pulses.

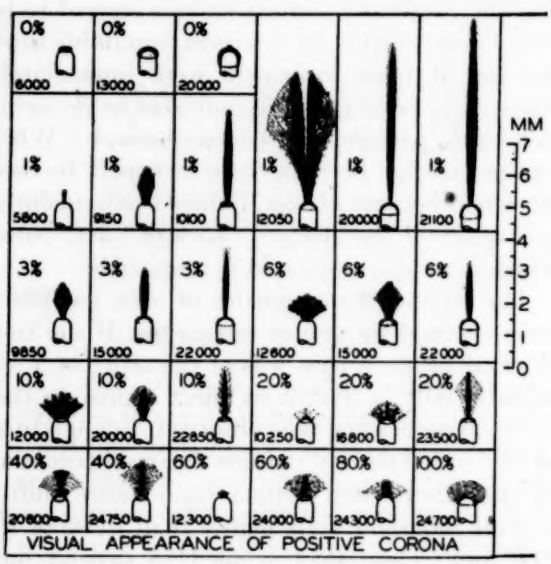


FIG. 2. Visual appearance of positive corona in freon-air mixtures. The percentage number indicates the amount of freon by volume in dry, clean air, the other number the point potential in volts. With a point diameter of $\frac{1}{2}$ mm, it was attempted to make the drawings to scale.

In the Geiger region the static field about the point is of sufficient magnitude so that a chance electron produces an avalanche of $\exp[\int \alpha dx]$ positive ions and electrons. Most of the positive ions form a concentrated space-charge boss near the point surface. Photons produced in the avalanche ionize the gas photoelectrically[7] and thereby create additional avalanches which feed into the space-charge boss as a result of its highly directive field. Thus the positive space charge extends into the gap well beyond the high field region about the point, and produces a streamer which dies out when the combined gradients become too weak. The production of a second streamer must await the clearance from the gap of residual positive space charges which decrease the field below the minimum value at which streamers may form. For this reason, at or above the onset of continuous corona, the field is only sufficient for the production of lateral avalanches which form a burst pulse. An extended glow spreads uniformly over the point surface in contrast to the extremely narrow channel of light characteristic of the streamer. In the intermittent corona region either streamers or burst pulses may occur, depending on the statistical distribution of the positive space charge at any instant. They are observed more frequently in mixed gases or in gases where metastable states are abundant,[3] since their mechanisms depend strongly on efficient photo-ionization in the gas.

In mixtures of low freon content the state of a mixed gas with intense photo-ionization was more fully realized than in air. This condition reached a maximum value for concentrations of about one percent, and streamers which were easily visible in the tele-microscope persisted over the entire potential range of our observations. The abundant formation of streamers in the continuous corona region may be explained by the presence of negative ions which neutralize the positive space charges in the streamer channels. The persistence of streamers and the radical change in the visual characteristics from an extended burst pulse corona in air to the narrow and brilliant channel in the one percent

[5] L. B. Loeb and A. F. Kip, J. App. Phys. **10**, 142 (1939); L. B. Loeb and J. M. Meek, *ibid.* **11**, 438 (1940); L. B. Loeb and J. M. Meek, *The Mechanism of the Electric Spark* (Stanford University Press, Stanford University, California, 1941), Chapter II.

[6] C. G. Montgomery and D. D. Montgomery, J. Frank. Inst. **231**, 447 (1941).

[7] E. Greiner, Zeits. f. Physik **81**, 543 (1933); A. M. Cravath, Phys. Rev. **47**, 254 (A) (1935); with L. B. Loeb, *ibid.* **47**, 259 (A) (1935); C. Dechene, J. de phys. et rad. **7**, 533 (1936).

freon mixture (Fig. 2) suggest that the discharge is propagated mainly by the streamer mechanism.

The spindle consisted of a highly conducting plasma of positive and negative ions and electrons, and it showed current densities varying from $1.7\times10^{-2}$ amp./cm² at a potential of 10 kv near onset of the continuous corona to one amp./cm² at 21 kv. The narrowness of this form of discharge can be explained by the following: When a strong streamer forms in a gas, lateral branching is reduced; also the existence of stable negative ions in the plasma of the streamer channel causes an increase in the lifetime of the channel, and therefore it will be re-used by succeeding streamers and appear as an intensely bright spindle. In pure $N_2$, in which negative ions do not form, a similar spindle-shaped corona has been observed at potentials close to breakdown. In $N_2$ the discharge channel is maintained because of the presence of atoms in the metastable state. In pure $H_2$, on the other hand, negative ions and metastable states are absent and, therefore, no such corona has been observed.[3]

Electron avalanches at higher freon concentrations do not develop to the size attained in air because of the greater stability and numbers of the negative ions. The positive ion space charges are consequently not strong enough to distort the field sufficiently for streamer formation and the discharge, therefore, develops into laterally spreading burst pulses.

At concentrations of 40 percent of freon or higher it became impossible to differentiate clearly between streamers and burst pulses. These results are similar to those found in air by Kip using sharp needle points,[8] which attenuate the high field region rapidly. Since $x_0$ and the number of ionizing free paths within $x_0$ are reduced, the $\int_0^{x_0}\alpha dx$ is smaller, and the positive space charges are insufficient to sustain streamer propagation. In the work on negative corona in freon[1] it has been shown that the negative ions formed are stable at values of $X/p\geqq200$, compared to an $X/p=90$ where the negative $O_2$ ions shed their electron. Therefore the high field region in which effective ionization by collision can take place with freon is confined much closer to the positive point and thus gives rise to similar phenomena to those observed with needle points in air.

We again wish to express our thanks to Professor L. B. Loeb for his assistance in the interpretation of our data.

[8] A. F. Kip, Phys. Rev. **55**, 552 (1939), Fig. 8.

# Statistical Geometry and Fundamental Particles

NATHAN ROSEN
*University of North Carolina, Chapel Hill, North Carolina*

(Received May 10, 1947)

To take account of the fact that the existence of a fundamental length $a$, the classical electron radius, sets a limit to the accuracy with which the position of a point can be measured, it is proposed to introduce two spaces, an "abstract" space consisting of points, and an "observable" space in which one deals with elementary volumes correlated to the points of the former by means of a statistical distribution function in the form of a three-dimensional Gaussian error function. Such a function is not Lorentz invariant, but one can obtain Lorentz covariance in the observable space by carrying out the usual Lorentz transformation in the abstract space. If one assumes that the usual equations for wave fields, in which the fundamental particles are regarded as points, are valid in the abstract space, then one can obtain corresponding equations in the observable space, with the particles behaving as if they had finite volumes. The difficulties associated with infinite self-energies and singularities in the interactions between particles, as calculated by the usual perturbation method, disappear, but the difficulty associated with the divergence of the series of successive orders of perturbations remains.

## 1. GENERAL CONCEPTS

THE constant $a$, the "classical electron radius" of the order of $10^{-13}$ cm, is considered to play an important role in limiting the range of validity of the present form of the quantum theory.[1] It has been suggested by various authors[2] that this constant represents the smallest measurable distance, and that it is therefore necessary to alter the ordinary concepts of geometry when one is dealing with regions having dimensions of the order of $a$. Accordingly, March[2] introduced a "granular" geometry in which the smallest distinguishable element of space is a sphere of radius $a$. Recently there appeared a very interesting paper by Snyder,[3] in which the coordinates and time are treated as non-commuting operators, the coordinates having eigenvalues which are integral multiples of $a$.

In the present paper the point of view adopted is somewhat related to that of March. It is assumed that the constant $a$ determines the lower limit to the error in the measurement of the position of a point. If one measures the x-coordinate of a point under the most favorable conditions, because there does not exist an infinitesimally small measuring rod in nature, one will not obtain an exact value, in general. On the basis of the theory of random errors of measurement it is reasonable to expect that repeated measurements will give values distributed about the mean value in a normal or Gaussian distribution. It will be assumed, then, that the probability of getting a value lying between $\xi$ and $\xi+d\xi$ is given by

$$(2\pi)^{-\frac{1}{2}}a^{-1}\exp[-(\xi-x)^2/2a^2]d\xi,$$

where $x$ is the mean value. Extending this idea to the other coordinates, we will assume that, if one measures the position of a point, for example, that of an electron at a certain instant of time, the probability of obtaining values in the ranges $d\xi$, $d\eta$, $d\zeta$ near $\xi$, $\eta$, $\zeta$ is given by

$$dW=\chi(\xi-x, \eta-y, \zeta-z)d\xi d\eta d\zeta, \quad (1)$$

where

$$\chi(u, v, w)=(2\pi a^2)^{-\frac{3}{2}} \times\exp[-(u^2+v^2+w^2)/2a^2], \quad (2)$$

so that

$$\int_{-\infty}^{\infty}\int_{-\infty}^{\infty}\int_{-\infty}^{\infty}\chi(u, v, w)dudvdw=1. \quad (3)$$

In this way we arrive at the idea of a geometry dealing with small regions, "elementary volumes," instead of points, provided we think of the elementary volume associated with mean values of the coordinates $x$, $y$, $z$, as made up of those points (values of $\xi$, $\eta$, $\zeta$) for which the function $\chi(\xi-x, \eta-y, \zeta-z)$ has an appreciable value. Such an elementary volume differs from the kind considered by March in that it does not have a definite boundary.

The basic physical principle associated with such a geometry is that only a physical quantity

[1] W. Heisenberg, Zeits. f. Physik **120**, 513 (1943).
[2] A. March, Naturwiss. **26**, 649 (1938), where references are given to papers by himself and other authors.
[3] H. S. Snyder, Phys. Rev. **71**, 38 (1947).

associated with an elementary volume can be observed, while the value at a point is not directly observable. If one wishes to have physical laws in terms of observable quantities, it is therefore necessary to express them in terms of physical quantities which refer to elementary volumes.

When one attempts to formulate laws in this way, taking account of the basic indeterminacy of position, it is convenient to work with two spaces, an "abstract" or point space and an "observable" space, made up of elementary volumes, as described above. To every point of the abstract space one can correlate an elementary volume of the observable space by taking the mean values of the coordinates of the latter equal to the corresponding coordinates of the former. In the observable space, no meaning will be assigned to the value of a physical quantity, such as a field variable, at a point, but only to the mean value over an elementary volume. The purpose of introducing the abstract space is to help one to obtain such mean values.

In attempting to formulate physical laws in the framework of this statistical geometry it is natural at the outset to try to keep them as nearly as possible in the same form as at present. Thus, in the case where one is dealing with physical variables satisfying linear equations, one might try to retain these equations, but to take them as holding in the *abstract space*. The corresponding equations in the observable space would then be obtained by an averaging process from the latter, so that, for example, a function $f(x, y, z, t)$ would go over into[4]

$$\bar{f}(x, y, z, t) \equiv \langle f(x, y, z, t) \rangle$$

according to the relation

$$\bar{f}(x, y, z, t) = \int\int\int f(\xi, \eta, \zeta, t) \times \chi(\xi - x, \eta - y, \zeta - z) d\xi d\eta d\zeta. \quad (4)$$

Such a transformation has some interesting properties. In the case of a constant, $C$, it follows obviously that

$$\bar{C} = C. \quad (5)$$

One also sees readily that for a coordinate $x$ and the time $t$

$$\bar{x} = x, \quad \bar{t} = t. \quad (6)$$

In the case of any well-behaved function $f(x, y, z, t)$ it follows that

$$\langle Cf \rangle = C\bar{f}, \quad \langle f_1 + f_2 \rangle = \bar{f}_1 + \bar{f}_2 \quad (7)$$

$$\langle \partial f/\partial x \rangle = \partial \bar{f}/\partial x, \quad \langle \partial f/\partial t \rangle = \partial \bar{f}/\partial t, \quad (8)$$

and

$$\int_{-\infty}^{\infty}\int_{-\infty}^{\infty}\int_{-\infty}^{\infty} \bar{f} dx dy dz = \int_{-\infty}^{\infty}\int_{-\infty}^{\infty}\int_{-\infty}^{\infty} f dx dy dz. \quad (9)$$

On the other hand one finds that

$$\langle xf \rangle = x\bar{f} + a^2(\partial \bar{f}/\partial x). \quad (10)$$

It follows that for a function $f(x, y, z, t)$ which satisfies a linear homogeneous partial differential equation with constant coefficients, the equation for $\bar{f}(x, y, z, t)$ will have the same form as that for $f$. It should be noted however that, while we have obtained the form of the equation in the observable space by an averaging process, this does not mean necessarily that each solution $\bar{f}$ must be obtained by first determining a suitable solution $f$ and then getting its mean value over an elementary volume. Once the appropriate equation in the observable space has been found, it is possible to get its solutions directly. Each such solution, however, is subject to the restriction that it must be possible to express it as the mean value of some function over the elementary volume.

## 2. LORENTZ TRANSFORMATION

Before considering applications of the preceding ideas, it is necessary to examine them from the standpoint of the special theory of relativity. If we have two frames of reference moving with a uniform relative velocity, it is to be expected that the same uncertainty in the measurement of position will exist in each of them. In each system one will have "elementary volumes," and an observer in each one will be able to introduce an "abstract" and an "observable" space. Any physical law must be expressible in the same form in each frame of reference.

Now, the special relativity theory was developed without taking account of the limitation on measurement imposed by the existence of the

[4] Owing to typographical difficulties in setting bars over multiple symbols or boldface symbols, the notation with angular brackets will be used where required. *Ed.*

fundamental constant $a$. Hence one should be prepared to find that the introduction of this constant into the theory leads to changes in the usual transformation relations between quantities in the two frames of reference.

In order to be sure of obtaining transformation equations that will lead to physical laws of the same form in the two systems, one can make the following assumption: The usual Lorentz transformation will be assumed to hold in the transformation from the abstract space of one reference frame to that of the other frame moving relative to it with a uniform velocity. The transformation of a physical quantity in the observable space can then be determined from the corresponding transformation in the abstract space, if one knows how to go from the abstract to the observable space.

It may turn out in some cases that the transformation in the observable space will differ from the Lorentz transformation. However, as far as the transformation of coordinates and time is concerned, we see from Eq. (6) that the Lorentz transformation will remain valid. From a consideration of a plane monochromatic wave one can readily see that the frequency and wavelength of a light wave transform in the usual way.

At this point it is appropriate to consider briefly another question suggested by relativistic considerations. In the preceding discussion the time coordinate has been treated quite differently from the space coordinates. In particular, we have considered the uncertainty in the measurement of a space coordinate at a particular moment of time. It might be asked whether one should not introduce an uncertainty in the time (in this case of the order of $a/c$) in the same way as has been done for the coordinates. This would mean having on the right-hand side of Eq. (1) an additional factor

$$(2\pi)^{-\frac{1}{2}}ca^{-1}\exp[-c^2(\tau-t)^2/2a^2]d\tau.$$

However, the objection to such a procedure appears to be that it would be difficult to interpret the formalism from the operational standpoint. In the three-dimensional treatment considered previously the function $\chi$ of Eq. (1) represents the probability distribution of measured values of the coordinates of a point, such as the position of an electron, at a given moment of time, so that the time serves as a parameter to identify what is to be measured. In the four-dimensional treatment, where the time would also be measured and would have an uncertainty, no such parameter would in general be available, so that it would not always be clear what one was measuring or how the measurement could be repeated. The procedure adopted here, of using the time as a parameter is, after all, in agreement with what is generally done in the quantum theory.

### 3. ELECTRON AND RADIATION FIELD

We next consider the problem of the electron and its interaction with the electromagnetic field. In order to avoid lengthy derivations, reference will be made to the book of Heitler[5] for a discussion of the classical and quantum theories of the electromagnetic field.

The electromagnetic field for a given distribution of charges with a density $\rho$ and convective velocity $\mathbf{v}$ can be described classically in terms of the potentials $\phi$, $\mathbf{A}$ by means of the following equations:[6]

$$\Box^2\phi=-4\pi\rho, \tag{11}$$

$$\Box^2\mathbf{A}=-(4\pi/c)\rho\mathbf{v}, \tag{12}$$

$$\nabla\cdot\mathbf{A}+\dot{\phi}/c=0, \tag{13}$$

with a dot denoting differentiation with respect to the time. The electric and magnetic field intensities $\mathbf{E}$ and $\mathbf{H}$ are then given by

$$\mathbf{E}=-\nabla\phi-\dot{\mathbf{A}}/c, \quad \mathbf{H}=\nabla\times\mathbf{A}. \tag{14}$$

If we assume that these equations are to remain valid in the abstract space and then go over to the observable space by transformations of the type of Eq. (4), we get in place of (11)

$$\Box^2\bar{\phi}=-4\pi\bar{\rho}, \tag{15}$$

while the other equations are changed in the same way. We see that in the observable space the equations for the electromagnetic field have the same form as in the abstract space, except for the fact that the charge and current densities refer to mean values over an elementary volume. Hereafter, we shall drop the bars from the field

[5] W. Heitler, *The Quantum Theory of Radiation*, second edition (Oxford Press, England, 1944).

[6] The d'Alembertian operator $\Box^2\equiv\nabla^2-\partial^2/c^2\partial t^2$.

variables, but it will be understood that they refer to the observable space.

It has been suggested[7] that an electron, because of its fundamental character, should be represented by the simplest of all structures, a point. Let us adopt this standpoint, but let us represent the electron by a point in the *abstract space*. The corresponding representation in the observable space, however, will no longer be a point but an elementary volume.

Consider a point charge $e_k$ having at the time $t$ coordinates $x_k$, $y_k$, $z_k$, and an instantaneous velocity $\mathbf{v}_k$ in the $x$ direction. The charge density $\rho$ at a point $x, y, z$, at the time $t$ is then given by

$$\rho = e_k(1-v_k^2/c^2)^{-\frac{1}{2}}\delta([x-x_k][1-v_k^2/c^2]^{-\frac{1}{2}}) \times\delta(y-y_k)\delta(z-z_k), \quad (16)$$

where $\delta$ is the Dirac delta-function. It follows that

$$\bar{\rho} = e_k\chi(x-x_k, y-y_k, z-z_k), \quad (17)$$

so that the "effective charge density" is now given by a Gaussian distribution. It is seen that $\bar{\rho}$ has spherical symmetry about the center. Thus this effective charge distribution does not undergo a Lorentz contraction when it is in motion. This is, of course, attributable to the fact that the charge distribution arises from the geometry of the space and not from any assumed internal structure of the electron. A similar behavior was pointed out by March.[2]

In the same way one obtains in the observable space

$$\langle\rho\mathbf{v}\rangle = e_k\mathbf{v}_k\chi(x-x_k, y-y_k, z-z_k), \quad (18)$$

where $\mathbf{v}_k$ is the velocity of the point charge in the abstract space, or that of the center of the charge distribution in the observable space.

We see then that, on the basis of statistical geometry, one obtains a description of the electron in which many of the previous difficulties have been removed. The electron behaves like a distributed charge without any singularities, as far as its interaction with the electromagnetic field is concerned. At the same time any questions concerning the stability of the electron or the nature of the cohesive forces holding the charge together drop out. It is meaningless to ask about the force exerted on or by a part of the electron, but only the electron as a whole.

The equations for the electromagnetic field associated with a system of electrons can now be written

$$\Box^2\phi = -4\pi\sum_k e_k\chi(x-x_k, y-y_k, z-z_k), \quad (19)$$

$$\Box^2\mathbf{A} = -(4\pi/c)\sum_k e_k\mathbf{v}_k \times\chi(x-x_k, y-y_k, z-z_k), \quad (20)$$

with the remaining equations having the same form as (13) and (14).

Let now expand $\phi$ and $\mathbf{A}$ in series of plane monochromatic waves, following Heitler (reference 5, p. 47) and using his notation. For example, if we write

$$\phi = \sum_\sigma a_\sigma(t)\phi_\sigma(x, y, z), \quad (21)$$

then from (19) we obtain

$$\ddot{a}_\sigma + \omega_\sigma^2 a_\sigma = \sum_k e_k\bar{\phi}_\sigma(k), \quad (22)$$

where $\omega_\sigma$ is the (circular) frequency, and $\bar{\phi}_\sigma(k)$ is given by

$$\bar{\phi}_\sigma(k) = \int\phi_\sigma(\xi, \eta, \zeta) \times\chi(\xi-x_k, \eta-y_k, \zeta-z_k)d\xi d\eta d\zeta, \quad (23)$$

which is the mean value of $\phi_\sigma$ over the elementary volume of the $k$'th particle. Equation (22) is the same as the corresponding equation given by Heitler (reference 5, p. 49) except for the fact that here we have $\bar{\phi}_\sigma$ instead of $\phi_\sigma$ on the right-hand side. In the same way, in the expansion of the vector potential $\mathbf{A}$ in series of transverse and longitudinal plane waves, one gets equations for the coefficients which differ from those given there by Heitler only with respect to this averaging over the elementary volume.

Now the effect of averaging over the elementary volume becomes important as one goes to high frequencies. Consider a plane monochromatic wave, say, of the form

$$\phi = B\exp[i(kx-\omega t)], \quad (24)$$

with $\omega = kc$. Then one finds

$$\bar{\phi} = B[\exp(-k^2a^2/2)]\exp[i(kx-\omega t)] = [\exp(-k^2a^2/2)]\phi = [\exp(-\omega^2a^2/2c^2)]\phi. \quad (25)$$

[7] J. Frenkel, Zeits. f. Physik **32**, 518 (1925); P. A. M. Dirac, Proc. Roy. Soc. **A167**, 148 (1938).

This means that the coupling of an electron with the high frequency components of the electromagnetic field is now weaker than in the classical theory.

If again one follows Heitler (reference 5, p. 50) in writing down a Hamiltonian function for the system and then calculating the energy present in the longitudinal field components, one finds that this can be expressed as a sum of terms of two kinds: (1) interaction energies of pairs of particles, and (2) self-energies of single particles. For the energy of interaction of two particles one obtains, on integrating over the various frequencies and directions of the plane waves,

$$V_{ik}=(e_ie_k/r)\Phi(r/2a), \tag{26}$$

where $e_i$, $e_k$ are the charges of the particles, $r$ is the distance between them, and

$$\Phi(x)=2\pi^{-1}\int_0^x[\exp(-u^2)]du. \tag{27}$$

For $r\gg a$, this goes over into the coulomb interaction, but as $r$ approaches zero, it remains finite, instead of going to infinity as does the coulomb interaction.

The self-energy of a particle $W_k$ one obtains either by going through the same kind of calculation as that leading to Eq. (26) or by getting $\frac{1}{2}V_{kk}$ from (26), letting $r$ approach zero. One finds for the self-energy

$$W_k=\tfrac{1}{2}V_{kk}=e_k^2/2\pi^{\frac{1}{2}}a. \tag{28}$$

Incidentally, the same results for $V_{ik}$ and $W_k$ can be obtained by calculating the electrostatic interaction and electrostatic energy of charge distributions of the form given by Eq. (17).

If one equates the expression (28) for an electron to its rest energy $m_0c^2$ one finds

$$a=0.79\times10^{-13}\text{ cm}$$

based on the way $a$ was defined in Eq. (2). However, it is not clear at present that such a procedure of equating the electrostatic self-energy to the total rest energy is justified.

Let us now consider the question of quantization. In view of what was found for the equation of the electromagnetic field in the observable space it is plausible to take for the quantum-theoretical equations for the system consisting of electrons and radiation field the same equations used up to now (reference 5, Chapters II and III) with the sole modification that in the interaction of an electron with the field, the mean value of the latter over an elementary volume must now be used.

The Hamiltonian for the system can be written

$$H=\sum_k H_k+\sum_\lambda H_\lambda+\sum_{i>k} V_{ik}+\sum_k W_k+H'. \tag{29}$$

Here the Hamiltonian for a particle is given on the basis of the Dirac theory by

$$H_k=c\alpha_k\cdot(\mathbf{p}_k-e_k\langle\mathbf{A}^e\rangle(k))+m_kc^2\beta_k+e_k\tilde{\phi}^e(k), \tag{30}$$

$\tilde{\phi}^e(k)$, $\langle\mathbf{A}^e\rangle(k)$ being the mean values of the potentials of the external field at the $k$'th particle. The Hamiltonian for a transverse radiation wave is given by

$$H_\lambda=2\omega_\lambda^2q_\lambda^*q_\lambda \tag{31}$$

in terms of the quantized amplitudes $q_\lambda$ (a discussion of which will be found in reference 5, p. 59). The term $H'$ represents the interaction between the electrons and the transverse, or radiation, field. It is given in the present case by

$$\begin{aligned}H'&=-\textstyle\sum_k e_k\boldsymbol{\alpha}_k\cdot\langle\mathbf{A}\rangle(k)\\&=-\textstyle\sum e_k\boldsymbol{\alpha}_k\cdot(q_\lambda\langle\mathbf{A}_\lambda\rangle(k)+q_\lambda^*\langle\mathbf{A}_\lambda^*\rangle(k)),\end{aligned} \tag{32}$$

where

$$\begin{aligned}\langle\mathbf{A}_\lambda\rangle(k)=\int&\mathbf{A}_\lambda(\xi,\eta,\zeta)\\&\times\chi(\xi-x_k,\eta-y_k,\zeta-z_k)d\xi d\eta d\zeta,\end{aligned} \tag{33}$$

and $\mathbf{A}_\lambda$ is the vector potential for a plane monochromatic transverse wave, suitably normalized (reference 5, p. 59). It follows from Eq. (25) that

$$\langle\mathbf{A}_\lambda\rangle(k)=\exp[-\omega_\lambda^2a^2/2c^2]\mathbf{A}_\lambda(x,y,z). \tag{34}$$

It might be pointed out that in (31) we are taking the Hamiltonian of the radiation field in the usual form. An alternative procedure is based on the supposition that the quantization of the radiation field is carried out in the abstract space instead of the observable space. This, however, necessitates giving up the proportionality between energy and frequency and leads to the existence of a maximum value for the energy of a photon. Such a situation does not appear satisfactory.

If one treats the coupling term $H'$ as a perturbation and carries out the usual perturbation-theory calculations, one finds that the use of mean values of the radiation field over an elementary volume, as given by Eq. (34), gets rid of the previous "high frequency" divergence difficulties.

We have already seen how one obtains a finite value for the static self-energy, Eq. (28). By means of a second-order perturbation calculation one can calculate the dynamic (or transverse) self-energy (reference 5, p. 181). One finds, on taking account of the negative energy states of the electron, that this is given by

$$W_k' = (e_k^2\hbar c/2\pi a^2 E) - (e_k^2/2a\pi^{\frac{1}{2}}) \times[1-(m_0^2c^3/2pE)\ \ln\{(E+cp)/(E-cp)\}], \quad (35)$$

where $E$ is the unperturbed energy and $p$ the momentum of the electron. This result, while finite, is unsatisfactory, however. The first term, which is the important one for small velocities, turns out to have a value which is much larger than $m_0c^2$, if one takes $a\sim 10^{-13}$ cm.

It appears that this is related to another difficulty: if one calculates the contribution to the self-energy of higher order perturbation terms, one finds that, while the value obtained for each order is finite, the terms of even order (the only non-vanishing terms) keep getting larger as one goes to higher orders, for $a\sim 10^{-13}$ cm. A rough estimate indicates that the ratio of an even-order term to the preceding one is of the magnitude of $e^2\hbar c/a^2(mc^2)^2$, or of 137 for $a$ equal to the classical electron radius. This means, of course, that the perturbation calculation is divergent and hence should not be used in determining the energy of interaction of the electron and the field. It appears that the coupling between the electron and the field is too strong for the perturbation theory to be applicable. It might be pointed out that this difficulty is not peculiar to the present approach. In a sense a similar difficulty also exists in the usual "point-electron" theory, but is masked by the presence of infinities in the individual terms of the perturbation calculation.

As has already been remarked, in the observable space the interaction between a particle and the field involves the mean value of the field over the elementary volume of the particle. Since our knowledge of the field can be obtained only from the observation of its effect on particles, it follows that only such a mean value (a mean of the mean, from the standpoint of the abstract space) can be determined. Hence it is to be expected that in such matters as commutation relations among field variables, etc., one should deal with such mean values over elementary volumes, and not the values at a point.

#### 4. OTHER PARTICLES

In the case of other elementary particles one can use the same method as for electrons: the particle is regarded as a point in the abstract space and, therefore, as an elementary volume in the observable space. This leads to the expectation that all fundamental particles should have the same "size."

The expression for the interaction of a particle with a field in the observable space must take account of the fact that the particle is now an extended source. This can be done as above, by writing down the field equations in the abstract space and then going over to the observable space. From the form of the equations the corresponding Hamiltonian can then be deduced. In general it differs from the Hamiltonian for "point" particles in that the interaction terms involve the average values of the field variables over the elementary volumes of the particles.

In the case of nucleons interacting with a meson field, it is evident that the static interaction between two heavy particles (calculated in first approximation) will not have any singularity. Hence, if such an interaction is used as the potential energy in the Schrödinger equation, no "cutting off" of this interaction energy at small distances between the particles is necessary.

*Note added in proof:*—It has been kindly pointed out to me by Mr. M. F. M. Osborne that in the book by A. S. Eddington, *Fundamental Theory* (Cambridge University Press, 1946), use was made of an "abstract" space and a Gaussian-error transformation function, although in somewhat different applications.

# The Deflection of Charged Particles in a Ferromagnetic Medium

GREGORY H. WANNIER
*Socony-Vacuum Laboratories, Paulsboro, New Jersey**

(Received April 4, 1947)

The deflection is recomputed which a beam of charged particles will undergo when penetrating a ferromagnetic medium whose magnetism is due to electronic spins. The extreme importance of the "interior of the electron" for the effective magnetic field **b** is brought out by a quantum calculation which is analogous to well-known classical considerations. Only if the interpenetration of beam particle and electron has random probability will one find **b**=**B**. Otherwise deviations are to be expected which can be estimated in special cases. A section is added which develops the conditions under which magnetic deflection can be observed in competition with multiple scattering. Very high energy protons and deuterons offer the best possibilities (see Fig. 2).

## 1. GENERAL NATURE OF THE PROBLEM

IN recent years, experiments have come to the fore[1] in which the magnetic deflection of a beam inside a magnet plays a role. Such experiments involve the question of the magnitude of the "effective field" inside a polarized medium. Such a field has to be specified in terms of a process. In the case which is to be studied in this paper a fast charged particle traverses a piece of magnetized matter and experiences a very large number of small magnetic deflections. The resultant effect can be described in terms of an "effective magnetic field" **b** by the formula

$$\mathbf{F}=(ze/c)\mathbf{v}\times\mathbf{b}, \tag{1}$$

where **F** is the force on a beam particle, $ze$ its charge, and **v** its velocity.

There is one simple statement we can make about **b**. If the velocity of the beam particles is increased sufficiently so that their paths can be considered to be straight lines, then **b** will approach the magnetic induction **B**

$$\lim_{v\to\infty}\mathbf{b}=\mathbf{B}. \tag{2}$$

This is a consequence of the generally accepted theory that all magnetic dipoles are in nature equivalent to circulating currents. That this view is correct for the Dirac electron has been shown by Weizsäcker.[2]

Many people believe that (2) is not just a limiting relation, but a generally valid equation. The case against this supposition has been very well stated by Swann.[3] His considerations, although expressed in classical language, are valid in quantum mechanics also. They can be expressed as follows: If the magnetization of a ferromagnet is orbital in nature then there is little doubt that (2) will hold under very wide conditions. However, the more common case is that of ferromagnetism arising from the electron spin. In other words, the magnetization **M** originates in dipoles which are very small even on an atomic scale. The field which they produce varies over a very wide range of magnitudes and even the sign of its component along **M** is variable, with regions of very large negative and positive contributions adjoining near the electron. This situation is schematically represented in Fig. 1. The quantity **b** defined through (1) is an average value of this true field for a beam particle. It is well known that the extreme fields in the neighborhood of a small dipole enter decisively in the determination of such an average. The one simple result mentioned earlier, giving **b**=**B**, results from the averaging process only if there is no force capable of favoring or hindering the interpenetration of the two particles. In addition, it is necessary for a statistical average that each beam particle enter several times the "interior" of an electron. Such interpenetration does not pose any problems of principle in present day physical theory, but it does remain a practical question in each individual case. Among the forces which might enter into play there is of course the Coulomb force

* The greater part of this work was carried out at the University of Iowa, Iowa City, Iowa.

[1] F. Rasetti, Phys. Rev. 66, 1 (1944).

[2] C. F. v. Weizsäcker, Ann. d. Physik 17, 869 (1933).

[3] W. F. G. Swann, Phys. Rev. 49, 574 (1936).

between the two charges. In addition, there is the possibility of short range forces which might not otherwise be observable.

## 2. CALCULATION OF THE AVERAGE FIELD b

Since ferromagnetism is associated with the electron spin we must use Dirac wave functions for the electron. For the beam particles, no structure will be assumed except the possession of a charge. This is not so much an assumption as a definition of what we wish to call the magnetic deflection of a charged particle.

The calculation which follows differs from the standard in that it computes the expectation value of a force rather than an energy. The force is the force **F** in Eq. (1). Reading the latter as an operator equation, we can see that finding the expectation value of the force **F** is equivalent to finding the expectation value of the field **b**, provided the velocity is an approximate constant of the motion; this must necessarily be so if we want to observe a small deflection at all. The correct operator for **b** can be obtained from two independent approaches. Either we take the law of Biot-Savart and make the substitution for the electron velocity **w**

$$\mathbf{w} \rightarrow -\boldsymbol{\alpha} c,$$

where $\alpha_x$, $\alpha_y$, $\alpha_z$ are the three Dirac matrices; or else we take the Breit Hamiltonian, translate it into classical language, compute the magnetic part of the force, and translate back into quantum language. Either approach gives the same result. The operator giving the field $\mathbf{b}(\mathbf{r})$ at the position $\mathbf{r}$ equals

$$\mathbf{b}(\mathbf{r}) = \sum_{\nu=1}^{n} \frac{e\boldsymbol{\alpha}_\nu \times (\mathbf{r} - \mathbf{r}_\nu)}{|\mathbf{r} - \mathbf{r}_\nu|^3}. \tag{3}$$

Here the summation extends over all ferromagnetic electrons in the magnet. In order to obtain the expectation value of (3) we require the knowledge of the spinor wave function

$$\psi(\mathbf{r}_1, \mathbf{r}_2, \mathbf{r}_3, \cdots \mathbf{r}_n; \mathbf{r}),$$

where $\mathbf{r}$ stands for the Cartesian coordinates of a beam particle, and $\mathbf{r}_1$, $\mathbf{r}_2$, $\cdots$ are the Cartesian and spin coordinates of the ferromagnetic electrons.

In looking for a reasonable approximation to $\psi$ we can first convince ourselves that a product

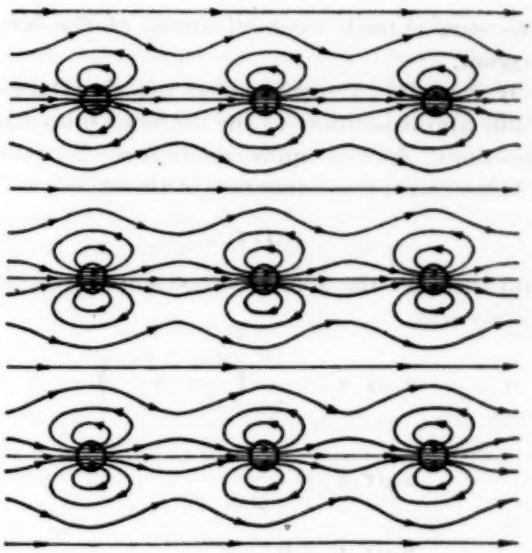

FIG. 1. A schematic picture of the magnetic field inside a ferromagnet.

wave function

$$\psi_1(\mathbf{r}_1, \mathbf{r})\psi_2(\mathbf{r}_2, \mathbf{r})\psi_3(\mathbf{r}_3, \mathbf{r}) \cdots \psi_n(\mathbf{r}_n, \mathbf{r})\chi(\mathbf{r})$$

is adequate. The reason is that the ferromagnetic electrons are inner shell electrons and can be assumed to be localized and independent of each other in their Cartesian coordinates. For their spins, on the other hand, we may assume complete coupling with a pre-assigned field direction. This justifies the product assumption and shows that the individual factors $\psi_\nu$ differ from each other only in the location of their origin. The result should be anti-symmetrized, of course, but as this will have no effect on an interaction of the type (3) we can dispense with it. The factor $\chi(\mathbf{r})$ at the end is added for convenience. It is essentially a modified plane wave which is normalized over the whole ferromagnet. The functions $\psi_\nu$ can then be considered normalized in their first coordinate.

With this type of wave function, the calculation is reduced to a two-body problem. We get for the expectation value **b** of (3)

$$\mathbf{b} = \int_\Omega \chi^*(\mathbf{r}')\chi(\mathbf{r}')d\tau'$$

$$\sum_{\nu=1}^{n} \int_\Omega \left\{ \psi_\nu(\mathbf{r}, \mathbf{r}') \frac{e\boldsymbol{\alpha} \times (\mathbf{r}' - \mathbf{r})}{|\mathbf{r}' - \mathbf{r}|^3} \psi_\nu(\mathbf{r}, \mathbf{r}') \right\} d\tau. \tag{4}$$

The sum extends over all atoms of the ferromagnet.

It is useful at this point to use the Darwin-Pauli approximation to the correct Dirac wave functions.[4] In this approximation we introduce a Schrödinger wave function of the type

$$\varphi_\nu(\mathbf{r}, \mathbf{r}'), \tag{5}$$

and then get the spinor components in the following way

$$u_{\nu 1}(\mathbf{r}, \mathbf{r}') = \frac{ih}{2mc}\left(\frac{\partial \varphi_\nu}{\partial x} - i\frac{\partial \varphi_\nu}{\partial y}\right),$$

$$u_{\nu 2}(\mathbf{r}, \mathbf{r}') = -\frac{ih}{2mc}\frac{\partial \varphi_\nu}{\partial z},$$

$$u_{\nu 3}(\mathbf{r}, \mathbf{r}') = 0,$$

$$u_{\nu 4}(\mathbf{r}, \mathbf{r}') = \varphi_\nu.$$

Substitution of these values into (4) yields

$$\mathbf{b} = \int_\Omega \rho(\mathbf{r}')d\tau' \times \int_\Omega \frac{[\mathbf{I}_o(\mathbf{r}, \mathbf{r}') + \mathbf{I}_s(\mathbf{r}, \mathbf{r}')] \times (\mathbf{r}' - \mathbf{r})}{c|\mathbf{r}' - \mathbf{r}|^3} d\tau, \tag{6}$$

with

$$\rho(\mathbf{r}') = \chi^*(\mathbf{r}')\chi(\mathbf{r}'), \tag{7}$$

$$\mathbf{I}_o(\mathbf{r}, \mathbf{r}') = \frac{ieh}{2m}\sum_\nu (\varphi_\nu^* \nabla \varphi_\nu - \varphi_\nu \nabla \varphi_\nu^*), \tag{8}$$

$$I_{sx} = \frac{eh}{2m}\sum_\nu \frac{\partial}{\partial y}(\varphi_\nu^* \varphi_\nu),$$

$$I_{sy} = -\frac{eh}{2m}\sum_\nu \frac{\partial}{\partial x}(\varphi_\nu^* \varphi_\nu), \tag{9}$$

$$I_{sz} = 0.$$

Equation (6) states the law of Biot-Savart for a beam particle which has a probability density $\rho(\mathbf{r}')$ to be at a given place. $\mathbf{I}_o + \mathbf{I}_s$ is the current density producing the magnetic field. This current density breaks up into two parts. The part (8) is the current produced by the orbital motion of the electrons, part (9) is the contribution of the spin. We shall neglect the contribution (8) in the future.

[4] H. A. Bethe, *Handbuch der Physik*, Vol. XXIV, 1, p. 304.

To facilitate further discussion we shall define as the true magnetization $\mathbf{M}(\mathbf{r}, \mathbf{r}')$ the following quantity

$$\mathbf{M}(\mathbf{r}, \mathbf{r}') = \mathbf{k}(eh/2mc)\sum_\nu \varphi_\nu^* \varphi_\nu, \tag{10}$$

where $\mathbf{k}$ is a unit vector in the $z$-direction. $\mathbf{M}(\mathbf{r}, \mathbf{r}')$ gives the magnetization at the point $\mathbf{r}$. Because of the assumption of perfect ferromagnetism, it has the same direction everywhere and can be treated as a scalar if convenient. Its magnitude varies periodically in the crystal lattice and depends on the location $\mathbf{r}'$ of the beam particle as a parameter. With the help of definition (10), Eq. (9) takes the form

$$\mathbf{I}_s(\mathbf{r}, \mathbf{r}') = c\nabla \times \mathbf{M}(\mathbf{r}, \mathbf{r}') \tag{11}$$

which is a well-known relationship of classical electrodynamics.[5] Using (11) and neglecting (8), we get (6) in the form

$$\mathbf{b} = \int_\Omega \rho(\mathbf{r}')d\tau' \int_\Omega \frac{(\nabla \times \mathbf{M}) \times (\mathbf{r}' - \mathbf{r})}{|\mathbf{r}' - \mathbf{r}|^3} d\tau. \tag{12}$$

In addition to (10) we shall introduce several averages of this true magnetization $\mathbf{M}$. The first will be called the atomic magnetization $M_a(\mathbf{r})$

$$M_a(\mathbf{r}) = \Omega^{-1}\int_\Omega M(\mathbf{r}, \mathbf{r}')d\tau'. \tag{13}$$

This average removes the dependence on the beam particle, but it still varies rapidly within atomic distances. Another average that can be formed is the dynamic magnetization $M_d(\mathbf{r}, \mathbf{r}')$.

$$M_d(\mathbf{r}, \mathbf{r}') = (\Delta\Omega)^{-1}\int_{\Delta\Omega} M(\mathbf{r}+\varrho, \mathbf{r}'+\varrho)d\tau_\varrho. \tag{14}$$

Here $\Delta\Omega$ is a volume large compared to atomic dimensions, but small compared to the size $\Omega$ of the magnet. The final average is the gross magnetization $\bar{M}$ which is obtained by carrying out the missing averaging process on (13) or (14)

$$\bar{M}(\mathbf{r}) = (\Delta\Omega)^{-1}\int_{\Delta\Omega} M_a(\mathbf{r}+\varrho)d\tau_\varrho = \Omega^{-1}\int_\Omega M_d(\mathbf{r}, \mathbf{r}')d\tau'. \tag{15}$$

[5] R. Becker, *Theorie der Elektrizität* (B. G. Teubner, Leipzig, 1933), Vol. 2, Chapter C.

Both $M_d$ and $\bar{M}$ have the crystalline structure averaged out, but (14) still shows the dynamic effect of the beam particle. The final average (15) is variable only in the walls of the magnet; the current (11) reduces for this case to the "equivalent solenoid" current which, in turn, produces a field equal to the induction **B**. Thus Eq. (12) reduces for this case to

$$\mathbf{B}=\int_\Omega \rho(\mathbf{r}')d\tau' \int_\Omega \frac{(\nabla\times\bar{\mathbf{M}})\times(\mathbf{r}'-\mathbf{r})}{|\mathbf{r}'-\mathbf{r}|^3}d\tau. \quad (16)$$

The two last averages can be related to each other through an equation of the form

$$M_d(\mathbf{r},\mathbf{r}')=\bar{M}(\mathbf{r})f(\mathbf{r}-\mathbf{r}'), \quad (17a)$$

where

$$\int_\Omega f(\mathbf{r})d\tau=\Omega, \quad (17b)$$

and

$$f(\mathbf{r})=1, \text{ (if } \mathbf{r} \text{ is larger than atomic dimensions).} \quad (17c)$$

The reason for this is that inside the crystal the only variation of $M_d$ not yet averaged out is that arising from the proximity of the beam particle. This effect involves coordinate differences only as is indicated in (17a) and is necessarily of short range as is shown by (17c); in the walls of the magnet, the two averages vary the same way.

Equations (12) and (16) show that **b** will equal **B** if it is permissible to replace $M$ by its double average $\bar{M}$. The two intermediate averages will have a certain usefulness in the following discussion.

### 3. A GENERAL THEOREM CONCERNING b

A classical calculation of the average field **b** leads[3] to certain general statements emphasizing the importance of the interior of the electron. One introduces as a device the true di-pole type of an elementary magnet. Let us call **h** the average field which would be produced if all the electronic di-poles were of this type. This quantity **h** is of course fictitious, but it is useful in that we can infer that it would be very accidental to find $\mathbf{b}=\mathbf{B}$ unless we find $\mathbf{b}-\mathbf{h}=4\pi\bar{\mathbf{M}}$. Of this difference $\mathbf{b}-\mathbf{h}$, one can show that it arises entirely from contributions inside the magnetic di-poles. The quantum mechanical analog of this calculation will now be carried through.

It has been pointed out that Eq. (12) can be arrived at without the use of Dirac theory. Simple electrodynamics predicts Eq. (11), and Eq. (12) results from it by the law of Biot-Savart. The only assumption needed is that **M** is due to circulating electric charges. Now, if we assume instead that **M** is due to di-poles, then a variable magnetization would produce a pole density $P$ which equals[5]

$$P=-\nabla\cdot\mathbf{M}=-\partial M/\partial z. \quad (18)$$

The average field resulting from the same magnetization (10) would then produce a different field **h**. It equals

$$\mathbf{h}=-\int_\Omega \rho(\mathbf{r}')d\tau' \int_\Omega \frac{\partial M}{\partial z}\frac{\mathbf{r}'-\mathbf{r}}{|\mathbf{r}'-\mathbf{r}|^3}d\tau. \quad (19)$$

Following the reasoning which led from (12) to (16) we get an expression for the conventional magnetic field **H** as due to the pole faces:

$$\mathbf{H}=-\int_\Omega \rho(\mathbf{r}')d\tau' \int_\Omega \frac{\partial \bar{M}}{\partial z}\frac{\mathbf{r}'-\mathbf{r}}{|\mathbf{r}'-\mathbf{r}|^3}d\tau. \quad (20)$$

Now we take (12) and (19) and form their difference. We find

$$b_z-h_z=\int_\Omega \rho(\mathbf{r}')d\tau' \int_\Omega \frac{(\mathbf{r}'-\mathbf{r})\cdot\nabla M}{|\mathbf{r}'-\mathbf{r}|^3}d\tau,$$

or, expressing the second integrand as a divergence,

$$b_z-h_z=\int_\Omega \rho(\mathbf{r}')d\tau' \int_\Omega \nabla\cdot\left[M\nabla\frac{1}{|\mathbf{r}'-\mathbf{r}|}\right]d\tau.$$

We can apply Gauss' theorem provided we exclude the point $\mathbf{r}'=\mathbf{r}$. The expression then reduces to

$$b_z-h_z=\int_\Omega \rho(\mathbf{r}')d\tau' 4\pi M(\mathbf{r}',\mathbf{r}'). \quad (21)$$

In a similar manner we find $b_x-h_x=0$, $b_y-h_y=0$. If the same calculation is applied to (16) and (20), instead of (12) and (19), we get, of course

$$B_z-H_z=4\pi\bar{M}, \quad B_x-H_x=0, \quad B_y-H_y=0, \quad (22)$$

as expected.

On Eq. (21) we can make the following observation. Consider

$$\sum_\nu \varphi_\nu^*(\mathbf{r}, \mathbf{r}')\varphi_\nu(\mathbf{r}, \mathbf{r}')$$

and its average

$$\Omega^{-1}\int_\Omega \sum_\nu \varphi_\nu^*(\mathbf{r}, \mathbf{r}')\varphi_\nu(\mathbf{r}, \mathbf{r}')d\tau'.$$

For physical reasons the two expressions must be equal when $\mathbf{r}'-\mathbf{r}$ is made large in the first one. The second expression gives, therefore, the electron density at $\mathbf{r}$ if the beam particle is very far away. On the other hand

$$\sum_\nu \varphi_\nu^*(\mathbf{r}, \mathbf{r})\varphi_\nu(\mathbf{r}, \mathbf{r})$$

gives the electron density at $\mathbf{r}$ if the beam particle is also at $\mathbf{r}$. We can write, therefore,

$$\sum_\nu \varphi_\nu^*(\mathbf{r}, \mathbf{r})\varphi_\nu(\mathbf{r}, \mathbf{r}) = p(\mathbf{r})\Omega^{-1}\int_\Omega \sum_\nu \varphi_\nu^*(\mathbf{r}, \mathbf{r}')\varphi_\nu(\mathbf{r}, \mathbf{r}')d\tau',$$

where

$$p(\mathbf{r}) = \frac{\text{chance of finding the electron at } \mathbf{r} \text{ if beam particle is also at } \mathbf{r}}{\text{chance of finding the electron at } \mathbf{r} \text{ if beam particle is far away}}. \quad (23)$$

We shall call it the coincidence probability at $\mathbf{r}$. Now, using (10) and (13), the previous considerations give us

$$M(\mathbf{r}, \mathbf{r}) = p(\mathbf{r})M_a(\mathbf{r}).$$

This transforms (20) into

$$\mathbf{b}-\mathbf{h} = 4\pi\int_\Omega \rho(\mathbf{r})p(\mathbf{r})\mathbf{M}_a(\mathbf{r})d\tau, \quad (24)$$

or in words: $\mathbf{b}-\mathbf{h}$ is equal to $4\pi$ times the average value of the atomic magnetization along the path of a beam particle, *provided the atomic magnetization at each point is multiplied with the coincidence probability at that point.*

The same relation was stated in a simpler form in an earlier paper.[6] If the effect of the crystalline field upon the beam is negligible $\rho(\mathbf{r})$ and $p(\mathbf{r})$ become constants in the magnet. The latter is obviously connected with $f(\mathbf{r})$, as defined in (17). It equals

$$p = f(\mathbf{0}). \quad (25)$$

In view of (15) Eq. (24) gives then

$$\mathbf{b}-\mathbf{h} = 4\pi p\bar{\mathbf{M}}, \quad (26)$$

where $\bar{\mathbf{M}}$ is now the gross magnetization. Equation (26), in turn, reduces to (22) if the coincidence probability is unity, that is for undisturbed wave functions.

The conditions under which (24) or (26) holds were enumerated formally in an earlier paper.[6] A short review of them may be in order:

(a) "That the magnetic interaction is sufficiently small to be treated as a first order perturbation." This condition is implicit in picking a wave function (5) not involving the magnetic interaction and computing from it the expectation value of (3). It appears reasonable enough for charged particles, but seems inadmissible for neutrons. It is not possible, of course, to find wave functions containing magnetic effects unless "cut-off" methods are used.

(b) "That the magnetic field is due entirely to the electronic spin." It arises from the neglect of (8) and appears generally accepted for ferromagnetic metals.

(c) "That the ferromagnetic electrons move in orbits independent of each other." This is a reasonable assumption which is necessary to get Eq. (4).

(d) "That it is sufficiently accurate to solve the Dirac equation in the Schrödinger-type approximation of Darwin-Pauli." This assumption transforms (4) into (6) and needs some discussion. The true Dirac wave functions are very weakly infinite at the origin; they will produce divergent results in the present case unless combined with a cut-off procedure. As soon, however, as a cut-off radius of the order of the electron radius is introduced the wave functions differ only insignificantly from those used here. The assumption, therefore, appears to be justified.

(e) "That the test charge is much heavier than the electron." Having a $p$ different from unity in (26) implies scattering. This scattering will affect the beam particle unless it is heavier or much faster than the electron with which it collides. Even if this condition is broken the equations from (3) on may still be applicable;

[6] G. H. Wannier, Phys. Rev. 67, 364 (1945).

but Eq. (1) will break down and make our results meaningless unless a new empirical definition is found justifying (3). This remark applies for instance to the proposal of Webster[7] to apply considerations of this type to conduction electrons in iron.

A further assumption stressed by Swann[3] happens to be unnecessary. The difficulty raised there is that coincidence of beam particle and electron would be so uncommon statistically that a strict average would have little meaning. In quantum theory the "coincidence" part of a wave arises entirely from the $S$-part of the wave function. The chance for such an $S$-collision can be obtained as follows: we estimate the maximum angular momentum possible for a beam particle passing a monatomic layer by taking it to be (reduced mass) × (impact parameter) × (relative velocity), and limiting the impact parameter to one half of the interatomic distance. The maximum quantum number $J$ thus obtained lies between 10 and 100, depending on the velocity. This gives a probability for $S$-collisions lying between $10^{-2}$ and $10^{-4}$. Thus even in a 0.01-mm foil each beam particle experiences at least 10 $S$-collisions.

Under the restrictions just listed, Eqs. (24) and (26) state in quantum language the same thing as the classical considerations of Swann.[3] The difference $\mathbf{b}-\mathbf{h}$ arises entirely from the interior of the electrons and thus depends on the result of head-on collisions. If $\mathbf{b}$ is to equal $\mathbf{B}$ this difference must equal $4\pi\bar{\mathbf{M}}$ in spite of the facts just stated.

## 4. SPECIAL RESULTS FOR THE COULOMB FIELD

The analysis of the previous section shows that there are two effects which may produce a $\mathbf{b}$ which is not equal to $\mathbf{B}$:

(a) The crystalline field will modify the wave function of the beam particle so that encounters between beam particle and ferromagnetic electron no longer have random probability.

(b) When there is an encounter, the chance of interpenetration is not average because of the intervention of repulsive or attractive forces.

The effect (b) opens a possibility of detecting short range forces which may not otherwise be observable. For such hypothetical forces, Eq. (26) goes about as far as we can hope to go. There is, however, such an effect produced by the Coulomb field of the two charges. We shall calculate this effect in the following, assuming effect (a) to be negligible, as it probably is for beams of reasonable energy.

The first thing we can do for this case is to examine the relationship of the previous section. The simpler form (26) applies here. The value of $p$ is given by (25); it is well known for the Coulomb field[8] and equals

$$p=x/(1-e^{-x}), \tag{27a}$$

where

$$x=(4\pi^2ze^2/hv)=1.39\cdot10^9(z/v). \tag{27b}$$

If the absolute value of $x$ is large, $p$ will be very large for positive charges and zero for negative charges. For high velocities, on the other hand, $x$ will be small and $p$ will equal unity. A list of values of $p$ in the transition region is given in Table I of reference 6.

The calculation can be completed without any difficulty to yield $\mathbf{b}$ itself. Our assumptions permit substitution of the smoothed out $M_d$ for $M$ in Eqs. (12) or (19). The quantity $M_d$, in turn, can be expressed through Eq. (17). Taking the difference between Eqs. (12) and (16) or between Eqs. (19) and (20) we get formulas of the form

$$\mathbf{h}-\mathbf{H}=-\int_\Omega \rho(\mathbf{r}')d\tau' \times\int_\Omega \frac{\partial}{\partial z}(\bar{M}\{f(\mathbf{r}'-\mathbf{r})-1\})\frac{\mathbf{r}'-\mathbf{r}}{|\mathbf{r}'-\mathbf{r}|^3}d\tau.$$

$\bar{M}$ can be treated as a constant, because in the region in which it is variable the second factor is zero by virtue of Eq. (17c). The integral then breaks up in two independent factors and gives

$$\mathbf{h}-\mathbf{H}=\bar{M}\int_\Omega \frac{\partial f(\mathbf{r})}{\partial z}\frac{\mathbf{r}}{r^3}d\tau.$$

For Coulomb forces, $f(\mathbf{r})$ is expressible in parabolic coordinates, and the calculation can be made in closed form. The result involves the same quantity $p=f(\mathbf{0})$ that was written down in

[7] D. L. Webster, Am. J. Phys. **14**, 360 (1946).

[8] Mott and Massey, *Theory of Atomic Collisions* (Oxford University Press, New York, 1933), p. 36.

(27). It reads

$$\mathbf{b}=\mathbf{B}+2\pi\bar{\mathbf{M}}(p-1), \tag{28a}$$

or

$$\mathbf{b}=\mathbf{H}+2\pi\bar{\mathbf{M}}(p+1). \tag{28b}$$

Strictly speaking, this equation is only found for the field transverse to the beam, while for the longitudinal field an equation

$$b_l=B_l+4\pi\bar{M}_l(p-1)$$

results. There seems to be no physical application, however, in which this component could be observed.

It is interesting to notice that (28) gives for positive particles an average field which is larger than **B**, while for negative particles it is smaller. This asymmetry gives some hope of observing the effect, which is, unfortunately, not in the range of easy observation (see next section).

Webster[7] has called attention to a consequence of (28) for conduction electrons in a ferromagnet. For them $p$ equals zero and we get

$$\mathbf{b}=\tfrac{1}{2}(\mathbf{B}+\mathbf{H}). \tag{29}$$

This formula has been inferred earlier by Swann.[3] The first objection to this formula is that the crystalline field will certainly modify the chance of encounters at these low speeds. The second difficulty is the lack of an experimental definition of the type (1) which would make **b** at least in principle a measurable quantity. However, Webster[7] suggests some indirect approaches in his paper which may be of value in this situation.

## 5. MAGNETIC DEFLECTION AND MULTIPLE SCATTERING

Observations on magnetic deflection have to compete in practice with multiple scattering. It is therefore useful to study the two effects concurrently. The study is based on the following three equations:

(a) The range-energy formula[9]

$$-\frac{dE}{dx}=\frac{4\pi\epsilon^4z^2ZN}{mv^2}\ln\left(\frac{2mv^2}{I(1-\beta^2)e^{\beta^2}}\right); \tag{30}$$

(b) The magnetic deflection formula

$$\frac{d\varphi}{dx}=\frac{ze\bar{b}}{pc}; \tag{31}$$

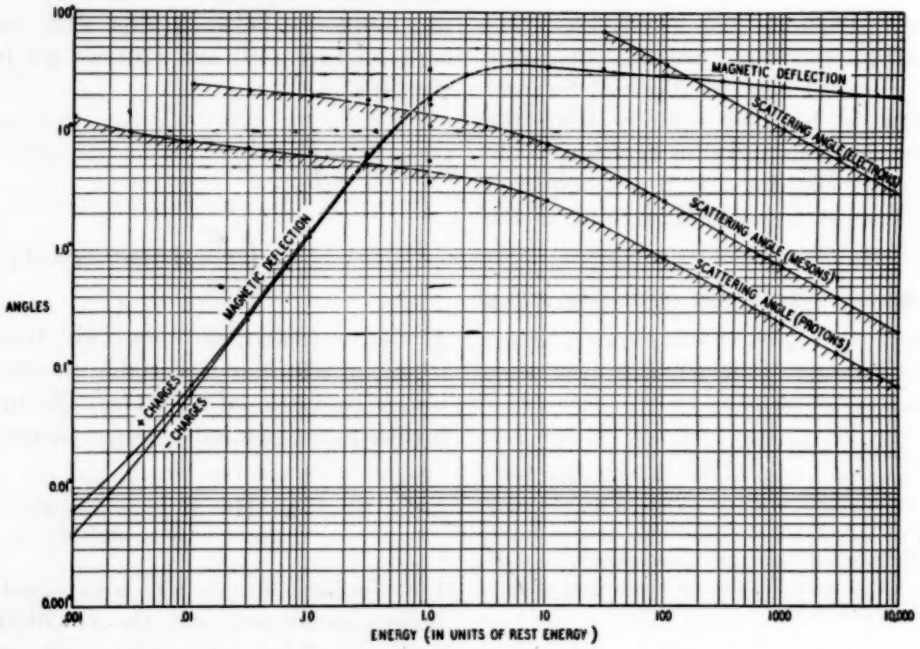


FIG. 2. Angles of magnetic deflection and scattering for various particles as a function of energy. Thickness is picked to maximize the ratio of the two quantities. Results near $E=Mc^2$ are rough interpolations only.

[9] M. Livingston and H. A. Bethe, Rev. Mod. Phys. **9**, 263 (1937), Eqs. (749) and (750).

(c) The multiple scattering formula[10]

$$\frac{d\langle\theta^2\rangle}{dx}=\frac{8\pi z^2Z^2\epsilon^4N}{p^2v^2}\ln(181Z^{-\frac{1}{3}}). \quad (32)$$

Here the symbols have the following meaning:

$e$ = basis of natural logarithms,
$\epsilon$ = elementary charge,
$m$ = electronic mass,
$M$ = mass of beam particle,
$ze$ = charge of beam particle,
$E$ = energy of beam particle,
$\varphi$ = angle of magnetic deflection of beam particle,
$\theta$ = root mean square angle of scattering of beam particles
$p$ = momentum of beam particle,
$v$ = velocity of beam particle,
$\beta=v/c$,
$x$ = path length in foil material,
$Z$ = atomic number of foil material,
$b$ = effective magnetic field inside foil material,
$N$ = number of atoms per unit volume in foil material,
$I$ = mean ionization potential of foil material.

As a preliminary calculation, we can try to determine the thickness of the ferromagnet in such a way as to make the quantity $\varphi/\theta$ a maximum. The result is that the thickness must be chosen in such a way that in the non-relativistic region ($E\ll Mc^2$)

$$E/E_0=0.432,$$

and in the relativistic region ($E\gg Mc^2$)

$$E/E_0=0.203,$$

where $E$ = energy of beam particle when leaving foil, $E_0$ = energy of beam particle when entering foil. A somewhat more complicated result is obtained in the neighborhood of $E=Mc^2$. The maximum of $\varphi/\theta$ is sufficiently flat to make a choice

$$E=\tfrac{1}{4}E_0 \quad (33)$$

reasonable. This choice was made for the numerical results of this section. It determines the thickness of the magnet to be used when the energy $E_0$ of the beam is given. The actual value of the thickness is obtained by integrating (30) and is easily available in the literature.

For the present purpose, it is preferable to eliminate $x$ from the Eqs. (30), (31), and (32) and to get $\varphi$ and $\theta$ as functions of the beam energy.

[10] B. Rossi and K. Greisen, Rev. Mod. Phys. **13**, 263 (1941), Eq. (1.53a).

The integration can be carried out for the ranges $E\ll Mc^2$ and $E\gg Mc^2$. The results are for $E\ll Mc^2$

$$\varphi=\frac{Ib}{16\pi zZ\epsilon^3N}\left(\frac{I}{2mc^2}\right)^{\frac{1}{2}}\times\left[li\left\{\frac{2mv_0^2}{I}\right\}^{\frac{1}{2}}-li\left\{\frac{2mv^2}{I}\right\}^{\frac{1}{2}}\right], \quad (34)$$

$$\theta^2=Z\frac{m}{M}\ln(181Z^{-\frac{1}{3}})\left[\ln\ln\frac{2mv_0^2}{I}-\ln\ln\frac{2mv^2}{I}\right]; \quad (35)$$

for $E\gg Mc^2$

$$\varphi=\frac{mc^2b}{8\pi zZN\epsilon^3}\left[\ln\ln\frac{2mE_0^2}{IM^2c^2e}-\ln\ln\frac{2mE^2}{IM^2c^2e}\right], \quad (36)$$

$$\theta^2=Z\frac{m}{M}\left(\frac{2mc^2}{Ie}\right)^{\frac{1}{2}}\ln(181Z^{-\frac{1}{3}})\left[li\left\{\frac{IM^2c^2e}{2mE_0^2}\right\}^{\frac{1}{2}}-li\left\{\frac{IM^2c^2e}{2mE^2}\right\}^{\frac{1}{2}}\right]. \quad (37)$$

Here $lix$ is the logarithmic integral

$$lix=\int_0^x dx/\ln x$$

or, more properly, its real part.

The numerical evaluation of (34), (35), (36), and (37) is shown in Fig. 2 for the case of iron. On the abscissa axis is plotted the energy in units of $Mc^2$; this gives the same $\varphi$-curve for all particles of unit charge. A somewhat arbitrary connection is made between the regions $E\ll Mc^2$ and $E\gg Mc^2$; it is marked by dotted lines. The value of $b$ was taken as large as possible, namely, 21,900 oersted. A reasonable averaging process[11] was used for $I$ and gave

$$I/mc^2=0.000385.$$

Scattering curves are given for the electron, meson, and proton. The meson mass was taken as 200 electron masses. The proton gives best results; actually the deuteron is still more favorable, as it has the scattering diminished by a factor 0.7 compared to the proton. The Coulomb splitting discussed in Section 4 is shown for the $\varphi$-curve. It appears difficult to observe.

[11] The average is a logarithmic average of the type discussed by Livingston and Bethe (reference 9, p. 265).

In conclusion we can say that the magnetic deflection of a beam of charged particles in magnetized iron should be quantitatively observable if high energy protons or deuterons are used instead of mesons.[1] A modification of the generally accepted result

$$\mathbf{b}=\mathbf{B}$$

may be expected if there are short range forces modifying interpenetration of proton and electron. The Coulomb force alone will give such an effect, but it appears barely at the threshold of observation.

I wish to express my thanks at this point to Dr. John Eldridge, Dr. J. R. Dunning, and Dr. H. A. Bethe for valuable discussions.

PHYSICAL REVIEW VOLUME 72, NUMBER 4 AUGUST 15, 1947

# Interpretation of the Triton Moment*

R. G. SACHS
*Argonne National Laboratory, Chicago, Illinois*

(Received April 29, 1947)

In order to account for the measured magnetic moment of the triton it is necessary to assume that the wave function in the ground state is a linear combination of $^2S$, $^2P$, $^4P$, and $^4D$ functions. An attempt is made to determine the amplitudes of these functions from the magnetic moment on the assumption that the intrinsic nucleon moments are additive and relativistic effects are negligible. With certain reasonable assumptions concerning the nature of the wave functions, it is found that the relative probabilities for finding the system in the $^2P$, $^4P$, and $^4D$ states satisfy the relation shown by the curves in Fig. 1. Wherever the results would otherwise be arbitrary, the wave functions have been chosen in such a way as to minimize the amount of $P$ state, with the exception that only the lowest one-particle configurations have been considered. If the amplitude of the $^2S$ state is taken to be as large as possible, the wave function contains no $^4D$ state, 8 percent $^4P$ state, and 17 percent $^2P$ state. A wave function of this form would seem to indicate that there is a spin-orbit coupling other than the tensor interaction acting among nuclear particles. In the other extreme case that the wave function contains a maximum of the $^4D$ function, the $^2S$ state probability is zero, the $^4D$ probability is 22 percent, the $^4P$ is 30 percent, and the $^2P$ is 48 percent. If the wave function of $He^3$ has the same form as that of $H^3$, the $He^3$ moment would be expected to lie on one of the curves shown in Fig. 2.

## 1. INTRODUCTION

THE recent measurements[1,2] of the magnetic moment of the triton give a value about 6.7 percent greater than that of the proton. If the ground state of the triton were a pure $^2S_{\frac{1}{2}}$ state, it would be expected that the moment would be equal to the proton moment. It is believed, of course, that the ground state is not a pure $^2S$ state but contains an admixture of $^2P$, $^4P$, and $^4D$ states.[3] A theory based on simplifying assumptions leads[4] to the conclusion that the presence of these states should result in a reduction of the moment instead of the observed increase. However, it has been pointed out[5] that cross terms between the various states in the expression for the magnetic moment have been neglected in the simple theory. These may be positive and could, therefore, account for the large moment.

It is the purpose of this paper to obtain a general expression for the magnetic moment in terms of the amplitudes of the various wave functions and thereby to gain some information concerning the nature of the ground state wave

* This work has been carried out under the auspices of the Atomic Energy Commission. It was completed and submitted for declassification on March 14, 1947.

[1] H. L. Anderson and A. Novick, Phys. Rev. **71**, 372 (1947).

[2] F. Bloch, A. C. Graves, M. Packard, and R. W. Spence, Phys. Rev. **71**, 373 and 551 (1947).

[3] E. Gerjuoy and J. Schwinger, Phys. Rev. **61**, 138 (1942).

[4] R. G. Sachs and J. Schwinger, Phys. Rev. **70**, 41 (1946).

[5] R. G. Sachs, Phys. Rev. **71**, 457 (1947).

function of the triton. The expression for the moment will be found to consist of a sum of terms of three different types. The first are the diagonal elements which are uniquely given in terms of the constant amplitudes of the wave functions. The second are cross terms which involve overlap integrals between the "radial" parts of the wave functions. These "radial" wave functions actually are not purely radial but are also functions of the cosine, $q$, of the angle between the vector connecting the two neutrons and the vector connecting the proton to the center of mass of the two neutrons.

The third set of terms consists of cross terms involving overlap integrals between one radial function and the derivative with respect to $q$ of another such function. These may be very large if the wave functions contain very high configurations, that is, if the individual particles have very high orbital angular momenta. However, it seems likely that such high configurations do not occur in the ground state, since in the ground state the wave function adjusts itself in such a way as to minimize the kinetic energy of the system. For that reason, it will be assumed in the final analysis that these cross terms vanish, or, more specifically, that the radial functions do not depend on $q$. This assumption eliminates a great deal of the arbitrariness from the results.

Considering then terms of only the first two types, it is found that the observed moment can be accounted for only if the $D$ state probability is less than that of either the $^2P$ or $^4P$ states. This conclusion appears to be at variance with current ideas concerning the nature of the triton wave function.[3] If it is accepted that the interaction term responsible for the mixing of states is the tensor interaction, then the $^4D$ state would be directly coupled to the $^2S$ state but the $P$ states would not be. Therefore, it might be expected that the $D$ state probability would be larger than the $P$ probabilities.

This expectation is based on the premise that the wave function is predominately a $^2S$ state. There is the possibility that the wave function contains little or no $^2S$ state; that is, that the advantage gained through the large average value of the tensor interaction in the $P$ and $D$ states might be large enough to over-compensate the correspondingly large kinetic energy, in which case the energy would be a minimum for a small $S$ state probability.

Further information concerning these questions may be obtained experimentally by means of a measurement of the moment of $He^3$. This paper includes a discussion of the relation between the moment of $He^3$ and the various possible mixtures of states which are consistent with the observed moment of $H^3$.

In this discussion, no consideration is given to the possibility that the intrinsic moments of the neutron and proton are not additive. Also, the relativistic correction to the triton moment is ignored.[6]

## 2. THE WAVE FUNCTIONS

The possible forms of the triton wave functions, with respect to their dependence on the spins of the particles, have been given by Gerjuoy and Schwinger.[3] We denote by $\rho$, the unit vector in the direction of the distance between the two neutrons and $\mathbf{r}$, the unit vector in the direction of the distance from the center of gravity of the neutrons to the proton. If $\sigma_3$ is the Pauli spin operator for the proton and $\sigma_{12}=(\sigma_1-\sigma_2)/2$, where $\sigma_1$ and $\sigma_2$ are the Pauli operators for the two neutrons, then the wave functions have the following form:

$$^2S: \quad \psi_1=\psi f_1, \tag{1a}$$

$$\psi_2=(\sigma_{12}\cdot\sigma_3)(\mathbf{r}\cdot\rho)\psi f_2, \tag{1b}$$

$$^2P: \quad \psi_3=\sigma_3\cdot(\mathbf{r}\times\rho)(\mathbf{r}\cdot\rho)\psi f_3, \tag{1c}$$

$$\psi_4=[\sigma_{12}\cdot\mathbf{r}\times\rho+i(\sigma_3\cdot\mathbf{r})(\sigma_{12}\cdot\rho) -i(\sigma_3\cdot\rho)(\sigma_{12}\cdot\mathbf{r})]\psi f_4, \tag{1d}$$

$$^4P: \quad \psi_5=\left[\sigma_{12}\cdot\mathbf{r}\times\rho+\frac{i}{2}(\sigma_{12}\cdot\mathbf{r})(\sigma_3\cdot\rho) -\frac{i}{2}(\sigma_3\cdot\mathbf{r})(\sigma_{12}\cdot\rho)\right]\psi f_5, \tag{1e}$$

$$^4D: \quad \psi_6=[(\sigma_{12}\cdot\mathbf{r})(\sigma_3\cdot\mathbf{r})-(\sigma_{12}\cdot\rho)(\sigma_3\cdot\rho)] \times(\mathbf{r}\cdot\rho)\psi f_6, \tag{1f}$$

$$\psi_7=[(\sigma_{12}\cdot\mathbf{r})(\sigma_3\cdot\mathbf{r})+(\sigma_{12}\cdot\rho)(\sigma_3\cdot\rho) -\tfrac{2}{3}(\sigma_{12}\cdot\sigma_3)](\mathbf{r}\cdot\rho)\psi f_7, \tag{1g}$$

[6] H. Margenau, Phys. Rev. 57, 383 (1940). P. Caldirola, Phys. Rev. 69, 608 (1946). G. Breit, Phys. Rev. 71, 400 (1947). R. G. Sachs, Phys. Rev. 72, 91 (1947).

$$\psi_8=[(\sigma_{12}\cdot\mathbf{r})(\sigma_3\cdot\boldsymbol{\varrho})+(\sigma_{12}\cdot\boldsymbol{\varrho})(\sigma_3\cdot\mathbf{r})-\tfrac{2}{3}(\mathbf{r}\cdot\boldsymbol{\varrho})(\sigma_{12}\cdot\sigma_3)]\psi f_8, \quad (1h)$$

$$\psi_9=[(\sigma_{12}\cdot\mathbf{r}\times\boldsymbol{\varrho})(\sigma_3\cdot\mathbf{r}\times\boldsymbol{\varrho})-\tfrac{1}{3}(\mathbf{r}\times\boldsymbol{\varrho})^2(\sigma_{12}\cdot\sigma_3)](\mathbf{r}\cdot\boldsymbol{\varrho})\psi f_9. \quad (1i)$$

The function $\psi$ is given by

$$\psi=(4\pi\sqrt{2})^{-1}(\chi_1{}^+\chi_2{}^- -\chi_1{}^-\chi_2{}^+\chi_3{}^m, \quad (2)$$

where the $\chi$ are the spin wave functions of the indicated particles. The functions $f_j$ are functions of the distances corresponding to $\mathbf{r}$ and $\boldsymbol{\varrho}$, and they are also even functions of the quantity $q=(\mathbf{r}\cdot\boldsymbol{\varrho})$. For simplicity, they will be described as "radial" functions. The extra factors $(\mathbf{r}\cdot\boldsymbol{\varrho})$ which are displayed in these equations, but not in those tabulated by Gerjuoy and Schwinger, are introduced in order to satisfy the Pauli principle for the two neutrons. The normalization conditions for the radial functions take the form

$$\tfrac{1}{2}\int|f_1|^2=1, \quad (3a)$$

$$\tfrac{3}{2}\int q^2|f_2|^2=1, \quad (3b)$$

$$\tfrac{1}{2}\int q^2(1-q^2)|f_3|^2=1, \quad (3c)$$

$$\tfrac{3}{2}\int(1-q^2)|f_4|^2=1, \quad (3d)$$

$$\tfrac{3}{4}\int(1-q^2)|f_5|^2=1, \quad (3e)$$

$$\int q^2(1-q^2)|f_6|^2=1, \quad (3f)$$

$$\tfrac{1}{3}\int(1+3q^2)q^2|f_7|^2=1, \quad (3g)$$

$$\tfrac{1}{3}\int(3+q^2)|f_8|^2=1, \quad (3h)$$

$$\tfrac{1}{3}\int(1-q^2)^2q^2|f_9|^2=1. \quad (3i)$$

The integrals indicated in these conditions are to be taken over the variable $q$ (limits: $-1$ to $+1$) and over the magnitude of the distance between the neutrons and the magnitude of the distance from the center of the neutrons to the proton.

The wave function in the ground state of the triton is expected to be a linear combination of the nine functions given in Eq. (1); that is,

$$\Psi=\sum_{j=1}^{9}\alpha_j\psi_j. \quad (4)$$

The coefficients, $\alpha_j$, and the form of the functions, $f_j$, could only be determined by solving the Schroedinger equation for the three-body problem. It is our purpose to express the magnetic moment of the triton in terms of the $\alpha_j$ and certain integrals over the $f_j$. Then we can hope to get some idea concerning the quantities $\alpha_j$ and $f_j$ from the observed moment. The magnetic moment of the nucleus is given by

$$\mu=\mu_p(\Psi,\sigma_3{}^z\Psi)+\mu_n(\Psi,[\sigma_1{}^z+\sigma_2{}^z]\Psi)+(\Psi,L_3{}^z\Psi), \quad (5)$$

where $L_3{}^z$ is the $z$-component of the orbital angular momentum of the proton, $\mu_p$ is the magnetic moment of the proton, and $\mu_n$ is the magnetic moment of the neutron. In this expression, the wave function, $\Psi$, is taken to be that function for which the magnetic quantum number of the total angular momentum is $+\frac{1}{2}$. By making use of Eq. (4), the magnetic moment can be expressed in terms of the matrix elements of the spin and orbital angular moment operators. Thus

$$\mu=\sum_{j,k}\alpha_j{}^*\alpha_k\{\mu_p(j|\sigma_3{}^z|k)+\mu_n(j|\sigma_1{}^z+\sigma_2{}^z|k)+(j|L_3{}^z|k)\}, \quad (6)$$

where the $j$, $k$ refer to the wave functions $\psi_j$, $\psi_k$. In the next section it will be shown that a considerable fraction of these matrix elements vanish, so that this expression is not quite so formidable as it looks on first sight.

### 3. THE MATRIX ELEMENTS

In evaluating the matrix elements which appear in Eq. (6), it is convenient first to determine which of the elements vanish. The only diagonal elements that would be expected to vanish are those corresponding to the mixing of

two $S$ states by an orbital angular momentum operator. Thus:

$$({}^2S|L_3{}^z|{}^2S)=0, \tag{7}$$

where the indicated ${}^2S$ states refer to an arbitrary linear combination of the functions $\psi_1$ and $\psi_2$.

If the states to be mixed are orthogonal in the space coordinates, then the matrix element of the spin operators vanishes, since the spin operator will not remove the space orthogonality. Similarly, the matrix elements of the orbital angular momentum vanish if the functions are orthogonal in spin. It follows that:

$$\begin{gathered}({}^2S|\sigma_j{}^z|{}^2P)=0, \quad ({}^2S|\sigma_j{}^z|{}^4P)=0,\\ ({}^2S|\sigma_j{}^z|{}^4D)=0, \quad ({}^2P|\sigma_j{}^z|{}^4D)=0,\\ ({}^4P|\sigma_j{}^z|{}^4D)=0,\end{gathered} \tag{8}$$

where $j=1, 2, 3$. Also:

$$\begin{gathered}({}^2S|L_3{}^z|{}^4P)=0, \quad ({}^2S|L_3{}^z|{}^4D)=0,\\ ({}^2P|L_3{}^z|{}^4P)=0, \quad ({}^2P|L_3{}^z|{}^4D)=0.\end{gathered} \tag{9}$$

It is now possible to resort to symmetry arguments to show that other elements vanish. The operators, $\sigma_j{}^z$ and $L_3{}^z$, do not involve $\boldsymbol{\rho}$ (see Eq. (12)), so they are unchanged by the transformation $\boldsymbol{\rho}\rightarrow-\boldsymbol{\rho}$. Therefore, if the functions to be mixed by the matrix element have opposite symmetry under this transformation, the element vanishes. A study of the functions given in Eq. (1) leads to the new results:

$$(1|\sigma_j{}^z|2)=0, \quad (3|\sigma_j{}^z|4)=0, \quad (3|\sigma_j{}^z|5)=0, \tag{10}$$

and

$$(1|L_3{}^z|4)=0, \quad (2|L_3{}^z|3)=0, \quad (3|L_3{}^z|4)=0. \tag{11}$$

It will be noted that, apart from the factors $f_k$, each of the functions $\psi_1\cdots\psi_9$ is either symmetric or antisymmetric under interchange of $\mathbf{r}$ and $\boldsymbol{\rho}$. It has already been pointed out[4] that use can be made of this property, since the operator $L_3{}^z$ is given, in units of $\hbar$, by

$$L_3{}^z=2\left(x\frac{\partial}{\partial y}-y\frac{\partial}{\partial x}\right)\Big/3i, \tag{12}$$

while the $z$-component of the total angular momentum is given by

$$L^z=\left[\left(x\frac{\partial}{\partial y}-y\frac{\partial}{\partial x}\right)+\left(\xi\frac{\partial}{\partial\eta}-\eta\frac{\partial}{\partial\xi}\right)\right]\Big/i, \tag{13}$$

where $x, y, z$ are the components of $\mathbf{r}$ and $\xi, \eta, \zeta$, those of $\boldsymbol{\rho}$. The two terms in Eq. (13) clearly have the same matrix element between two wave functions, both of which are either symmetric or antisymmetric under interchange of $\mathbf{r}$ and $\boldsymbol{\rho}$. Thus the matrix element of either term is one-half the matrix element of $L^z$. It follows that for two such functions, $\psi_l$ and $\psi_m$:

$$(l|L_3{}^z|m)=\tfrac{1}{2}(l|L^z|m). \tag{14}$$

The functions $\psi_5$ and $\psi_6$ are both antisymmetric under interchange of $\mathbf{r}$ and $\boldsymbol{\rho}$, so they satisfy the condition for the validity of Eq. (14). In addition, $\psi_5$ and $\psi_6$ are orthogonal, so that the matrix element of the $z$-component of the orbital angular moment vanishes, since both functions are proper functions of this operator:

$$(5|L^z|6)=0. \tag{15}$$

Then, according to Eq. (14),

$$(5|L_3{}^z|6)=0. \tag{16}$$

Equation (14) may also be used to evaluate the diagonal elements of $L_3{}^z$. Considering first the ${}^2P$ functions, both are seen to be antisymmetric under interchange of $\mathbf{r}$ and $\boldsymbol{\rho}$, so any linear combination has the same property. Thus

$$({}^2P|L_3{}^z|{}^2P)=\tfrac{1}{2}({}^2P|L^z|{}^2P)=2/9. \tag{17}$$

Similarly,

$$({}^4P|L_3{}^z|{}^4P)=\tfrac{1}{2}({}^4P|L^z|{}^4P)=-1/9. \tag{18}$$

The situation is not quite so simple for the ${}^4D$ functions. $\psi_6$ is antisymmetric and $\psi_7$, $\psi_8$, $\psi_9$ are symmetric under the operation being considered. Therefore, there are cross terms between $\psi_6$ and the other three functions which depend on the more detailed properties of the functions. The other terms can be evaluated by the above method. If ${}^4D'$ denotes an arbitrary linear combination of $\psi_7$, $\psi_8$, and $\psi_9$, then:

$$\begin{aligned}(6|L_3{}^z|6)&=({}^4D'|L_3{}^z|{}^4D')\\ &=({}^4D'|L^z|{}^4D')=1/3.\end{aligned} \tag{19}$$

It is also a simple matter to evaluate the diagonal elements of $\sigma_j{}^z$ in the quartet states, since these functions are symmetric in $\sigma_1{}^z$, $\sigma_2{}^z$,

and $\sigma_3^z$. Therefore,[7]

$$(^4P|\sigma_j^z|^4P)=\tfrac{2}{3}(^4P|S^z|^4P)=5/9 \quad (20)$$

and

$$(^4D|\sigma_j^z|^4D)=\tfrac{2}{3}(^4D|S^z|^4D)=-1/3. \quad (21)$$

The values of the diagonal elements of the spin matrices in the states $\psi_1$ and $\psi_3$ may be obtained immediately by noting that both functions are antisymmetric for interchange of $\sigma_1^z$ and $\sigma_2^z$. Therefore,

$$(1|\sigma_1^z+\sigma_2^z|1)=(3|\sigma_1^z+\sigma_2^z|3)=0. \quad (22)$$

On the other hand, the sum of the three $\sigma_j^z$ must be equal to twice the average value of $S^z$, or

$$(1|\sigma_3^z|1)=2(^2S|S^z|^2S)=1 \quad (23)$$

and

$$(3|\sigma_3^z|3)=2(^2P|S^z|^2P)=-1/3. \quad (24)$$

All other matrix elements may be obtained by direct computation. Since the required calculation is tedious and not at all illuminating, it will not be presented here. The results are:

$$\begin{aligned}&(2|\sigma_3^z|2)=-\tfrac{1}{3}, \quad (2|\sigma_1^z+\sigma_2^z|2)=4/3,\\ &(4|\sigma_3^z|4)=\tfrac{1}{9}, \quad (4|\sigma_1^z+\sigma_2^z|4)=-4/9,\\ &(5|\sigma_3^z|4)=\tfrac{2}{3}\int(1-q^2)f_5^*f_4,\\ &(5|\sigma_1^z+\sigma_2^z|4)=-\tfrac{2}{3}\int(1-q^2)f_5^*f_4\end{aligned} \quad (25)$$

for the spin elements. The elements of the orbital angular momentum operator are:

$$(3|L_3^z|1)=\frac{1}{9i}\int(1-q^2)qf_3^*f_1', \quad (26a)$$

$$(4|L_3^z|2)=\frac{1}{3i}\int(1-q^2)f_4^*(f_2+qf_2'), \quad (26b)$$

$$(7|L_3^z|5)=\frac{2}{9i}\int q^2f_7^*f_5-\frac{1}{9i}\int q(1-q^2)f_7^*f_5', \quad (26c)$$

$$(8|L_3^z|5)=\frac{1}{18i}\int(3+q^2)f_8^*f_5-\frac{1}{9i}\int q(1-q^2)f_8^*f_5', \quad (26d)$$

$$(9|L_3^z|5)=-\frac{1}{18i}\int q^2(1-q^2)f_9^*f_5+\frac{1}{9i}\int q(1-q^2)^2f_9^*f_5', \quad (26e)$$

$$(6|L_3^z|7)=\frac{5}{9}\int q^2(1-q^2)f_6^*f_7+\frac{2}{9}\int q^3(1-q^2)f_6^*f_7', \quad (26f)$$

$$(6|L_3^z|8)=\frac{2}{9}\int q(1-q^2)f_6^*f_8', \quad (26g)$$

$$(6|L_3^z|9)=-\frac{1}{9}\int q^2(1-q^2)f_6^*f_9, \quad (26h)$$

where $f_j'$ is the derivative of $f_j$ with respect to $q$.

### 4. THE MAGNETIC MOMENT

In terms of these matrix elements, the magnetic moment is given by Eq. (6). In order to bring out explicitly the symmetry character of the wave functions, we set

$$\begin{aligned}&\alpha_1=a_1S, \quad \alpha_2=a_2S, \quad \alpha_3=a_3\,{}^2P, \quad \alpha_4=a_4\,{}^2P,\\ &\alpha_5=a_5\,{}^4P, \quad \alpha_6=a_6D, \quad \alpha_7=a_7D, \quad \alpha_8=a_8D,\\ &\alpha_9=a_9D,\end{aligned} \quad (27)$$

where $S^2$ is the probability of finding the system in the $^2S$ state, $(^2P)^2$ that of finding it in the $^2P$ state, etc. The numbers $S$, $^2P$, $^4P$, and $D$ are chosen to be real. They must satisfy the normalization condition

$$S^2+{}^2P^2+{}^4P^2+D^2=1. \quad (28)$$

The $a_k$ also must be normalized as follows:

$$|a_1|^2+|a_2|^2=1, \quad (29)$$

$$|a_3|^2+|a_4|^2=1, \quad (30)$$

$$|a_5|^2=1, \quad (31)$$

[7] The factor 2 arises from the fact that the Pauli operator, $\sigma^z$, is twice the spin.

$$|a_6|^2+|a_7|^2+|a_8|^2+|a_9|^2$$
$$+\tfrac{2}{3}\Re\Big\{4a_7^*a_8\int q^2f_7^*f_8$$
$$-a_7^*a_9\int(1-q^2)q^2f_7^*f_9$$
$$-a_8^*a_9\int(1-q^2)q^2f_8^*f_9\Big\}=1. \quad (32)$$

$\Re\{\ \}$ denotes the real part of the quantity contained in the bracket. Equation (32) has a relatively complicated form because the functions $\psi_7$, $\psi_8$, and $\psi_9$ are not orthogonal to one another.

In terms of the coefficients defined by Eq. (27), the magnetic moment is:

$$\mu=\mu_p-\frac{4}{3}|a_2|^2S^2(\mu_p-\mu_n)$$
$$-\frac{4}{3}{}^2P^2[\mu_p-\tfrac{1}{3}|a_4|^2(\mu_p-\mu_n)]$$
$$+\frac{2}{9}{}^4P^2(5\mu_n-2\mu_p)-\frac{2}{3}D^2(2\mu_p+\mu_n)$$
$$+\frac{2}{9}{}^2P^2-\frac{1}{9}{}^4P^2+\frac{1}{3}D^2+\mu_x, \quad (33)$$

where $\mu_x$ contains the cross terms. This last quantity is given by

$$\mu_x=\frac{2}{9}D^2\Re\Big\{a_6^*a_7\Big[5\int q^2(1-q^2)f_6^*f_7$$
$$+2\int q^3(1-q^2)f_6^*f_7'\Big]$$
$$+2a_6^*a_8\int q(1-q^2)f_6^*f_8'$$
$$-a_6^*a_9\int q^2(1-q^2)f_6^*f_9\Big\}$$
$$+\frac{4}{3}(\mu_p-\mu_n)\,{}^4P\,{}^2P\Re\Big\{a_5^*a_4\int(1-q^2)f_5^*f_4\Big\}$$
$$+\frac{2}{3}{}^2PS\mathcal{I}\Big\{\frac{1}{3}a_3^*a_1\int(1-q^2)qf_3^*f_1'$$
$$+a_4^*a_2\int(1-q^2)f_4^*(f_2+qf_2')\Big\}$$
$$+\frac{1}{9}D\,{}^4P\mathcal{I}\Big\{2a_7^*a_8\Big[2\int q^2f_7^*f_8$$
$$-\int q(1-q^2)f_7^*f_8'\Big]$$
$$+a_8^*a_9\Big[\int(3+q^2)f_8^*f_9$$
$$-2\int q(1-q^2)f_8^*f_9'\Big]$$
$$-a_9^*a_9\Big[q^2(1-q^2)f_9^*f_9$$
$$-2\int q(1-q^2)^2f_9^*f_9'\Big]\Big\}. \quad (34)$$

Here, $\mathcal{I}\{\ \}$ is the imaginary part of the expression in the bracket.

The expression Eq. (34) is so complicated that some assumptions concerning the wave function must be made in order to simplify it. We assume that the functions $f_k$ are independent of $q$ or

$$f_k'=0. \quad (35)$$

This assumption appears to be reasonable, since the wave function of the ground state will have such a form that the kinetic energy of the system is as small as possible. Therefore, it should be a very smooth function, in which case Eq. (35) would be approximately valid.

The functions $f_k$ also depend on the magnitudes of the distances between the particles. In accordance with our assumption that these functions are smooth, it seems reasonable to assume that they all have about the same shape. Therefore, we take

$$\int f_j^*f_k=\Big[\int|f_j|^2\int|f_k|^2\Big]^{\frac{1}{2}}. \quad (36)$$

According to the well-known Schwartz inequality, this equation gives an upper limit on the magnitudes of the integrals involved. Consequently, the magnitudes of the coefficients of the cross terms in the expression for the magnetic

moment are no greater than the values given by Eq. (36), so the estimates obtained below of the amount of admixed $^2P$, $^4P$, and $^4D$ states are lower limits.

If we now set

$$a_k = x_k + iy_k, \tag{37}$$

the cross terms in the magnetic moment become

$$\mu_z = \frac{2}{3\sqrt{3}} D^2 \left[ \frac{5}{\sqrt{7}} (x_6x_7 + y_6y_7) - \frac{\sqrt{7}}{2} (x_6x_9 + y_6y_9) \right]$$
$$+ \frac{8\sqrt{2}}{9} (\mu_p - \mu_n)\, {}^4P\, {}^2P (x_5x_4 + y_5y_4)$$
$$+ \frac{2\sqrt{5}}{9} {}^4PD \left[ \frac{2}{\sqrt{7}} (x_7y_5 - x_5y_7) + (x_8y_5 - x_5y_8) \right.$$
$$\left. - \frac{\sqrt{7}}{10} (x_9y_5 - x_5y_9) \right]. \tag{38}$$

Here, use has been made of the normalization conditions given by Eq. (3) as well as the assumption Eq. (36). The normalization condition expressed by Eq. (32) now has the form

$$\sum_{j=6}^{9} (x_j^2 + y_j^2) + \frac{4}{\sqrt{7}} (x_7x_8 + y_7y_8) - (x_7x_9 + y_7y_9)$$
$$- \frac{\sqrt{7}}{5} (x_8x_9 + y_8y_9) = 1. \tag{39}$$

The magnetic moment is still given by Eq. (33), with $|a_2|^2 = x_2^2 + y_2^2$ and $|a_4|^2 = x_4^2 + y_4^2$. The constants, $x_j$, $y_j$, are to be chosen in such a manner that they satisfy the conditions of Eqs. (29) to (31) and Eq. (39), and that they give the correct value of the magnetic moment, i.e.,[1]

$$\mu = 1.067 \mu_p. \tag{40}$$

The eighteen constants are clearly not determined by these five conditions, so some further assumptions may be made in order to make the final results somewhat more specific.

The fact that the coefficient in Eq. (40) is larger than unity does lead to a considerable limitation on the choice of the constants, since the diagonal terms in Eq. (33) tend to reduce the moment below the proton moment. Therefore, it is necessary to take the non-diagonal terms to be positive and rather large. In order to minimize the negative diagonal terms in Eq. (33) we are led to choose

$$a_2 = 0, \quad |a_4|^2 = 1. \tag{41}$$

Since it seems likely that the amount of $S$ state will be as large as possible, we might require that the constants $x_j$, $y_j$ be chosen in such a way as to lead to the largest possible value of $S^2$. There is also some reason to guess that the $D$ state probability will be large compared to the $^2P$ and $^4P$ probabilities.[3] Although it will be found that this condition cannot be satisfied, we will choose the values of the constants in such a way as to make $D^2$ as large as possible just to see how closely we can approach the desired result. No simple analytical method was found for choosing the constants $x_j$, $y_j$ in such a way that $D^2$ would turn out to be a maximum. For this purpose, it is desirable to make the coefficients of the terms containing $D$ in Eq. (38) as large as is consistent with Eq. (39). It was found by examination that the maximum amount of $D$ state resulted when

$$\begin{aligned} &x_6 = y_6 = x_7 = y_7 = x_9 = y_9 = 0, \\ &x_5 = x_4 = -y_8, \\ &y_5 = y_4 = x_8. \end{aligned} \tag{42}$$

With these values of the constants, the relation between the amplitudes of the $P$ and $D$ states which is given by Eq. (40) is

$$2.12\, {}^4P^2P + 0.178\, {}^4PD - [0.50\, {}^2P^2 + 1.25\, {}^4P^2 + 0.759 D^2] = 0.067, \tag{43}$$

where we have taken $\mu_p = 2.79$ and $\mu_n/\mu_p = -0.685$. The values of $^4P^2$, $^2P^2$, and $D^2$ which are given by this equation are shown in Fig. 1. It should be emphasized that these are not the only possible combinations of these constants which will agree with the triton moment because the choice of the $x_j$, $y_j$ which has been made is rather special.

It is to be noted that the $S$ state probability will be a maximum for $D^2 = 0$, $^4P^2 = 8$ percent and $^2P^2 = 17$ percent. $D^2$ is never as large as $^2P^2$, and it is at most equal to $4P^2$ in spite of the fact that the coefficients $x_j$, $y_j$ have been chosen in such a way as to lead to as large a value of $D^2$ as possible. The largest value of $D^2$ is 22 percent with $^4P^2 = 30$ percent and $^2P^2 = 48$ percent. In this case the wave function contains no $S$ state.

It is generally believed that the properties of the wave function of $He^3$ are the same as those of the wave functions of the triton. Therefore, the conclusions drawn here concerning the admixture of states in the triton may be assumed to hold also for $He^3$. This makes it possible to make certain predictions concerning the magnetic moment of $He^3$. It has been shown that the moment of $He^3$ is given in terms of the moment of $H^3$ by the relation[4]

$$\mu(He^3)+\mu(H^3)=\mu_p+\mu_n-2(\mu_p+\mu_n-\tfrac{1}{2}) \times(3D^2-{}^4P^2+2{}^2P^2)/3. \quad (44)$$

The consequences of this equation are demonstrated in Fig. 2 which shows the relation between the moment of $He^3$ and the amounts of $^2P$, $^4P$, and $^4D$ states which satisfy the relationship shown in Fig. 1. These are not the only possible values for the $He^3$ moment, since certain specific assumptions have been made concerning the wave function in order to obtain Fig. 1. The value of the $He^3$ moment to be expected on the basis of the 4 percent of $^4D$ state and 0 percent $P$ state found by Gerjuoy and Schwinger[3] is $\mu(He^3)/\mu_p=-0.763$, a value which seems to be well out of the range of possibilities allowed by the considerations put forth here.[5] Therefore, a measurement of the moment of $He^3$ should prove to be a definitive experiment for distinguishing between the two cases. If the results are in agreement with expectations, it would then be possible to obtain another relation between the probabilities of the various states by taking the horizontal intercept of the observed moment with the various curves in Fig. 2.

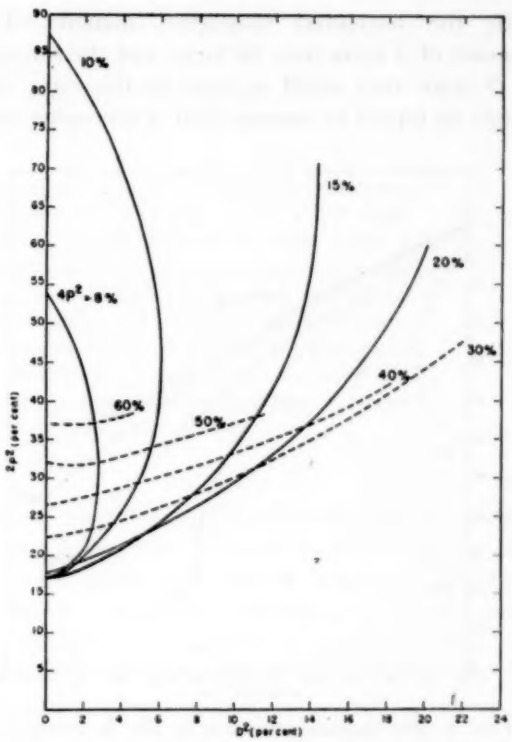


FIG. 1. Relation between $^2P$, $^4P$, and $^4D$ state probabilities required to account for experimental moment of the triton. The special assumptions made in obtaining these curves are expressed by Eqs. (35), (41), and (42).

## 5. CONCLUSION

The conclusion that the amount of $D$ function is small compared to the amount of $P$ function in the ground state of the triton is somewhat surprising if one believes that the tensor interaction is responsible for the admixture of states since, then, it would appear that the $D$ state should play a predominant role. It is possible, of course, that this conclusion is a consequence of erroneous assumptions concerning the nature of the radial wave functions $f_j$. The derivatives of these functions have been neglected, and it can be seen that important terms could be introduced if the derivatives were not negligible. However, it has been found that the values of $f_k'$ required to make these terms appreciable are quite large. To assume that it has such a large value would imply that the wave functions consist of products of one particle wave functions corresponding to high orbital angular momenta of the individual particles. This seems most unlikely. For the present, it seems reasonable to drop such terms.

There appear to be two essentially different wave functions of the triton which are consistent

[5] The Gerjuoy-Schwinger assumption of a small amount of $^4D$ function and even smaller amounts of the $P$ functions is not consistent with the results obtained here because of the condition, Eq. (35). However, if the average value of $f_1'$ happens to be large enough, in contrast to the requirement of Eq. (35), the term Eq. (26a) would give a contribution to the moment sufficient to account for the measured value even if the $^2P$, $^4P$, and $^4D$ probabilities are small. In this sense the measurement of the moment of $He^3$ might be considered as a test of the assumption expressed by Eq. (35). A large average value of $f_1'$ would be rather surprising, since the usual assumption that $f_1$ be a function of $(r_{12}^2+r_{13}^2+r_{23}^2)$, where $r_{mn}$ is the distance between particles $m$ and $n$, would lead to $f_1'=0$.

with the measured magnetic moment. The amount of $S$ state may be large and the amount of $D$ state very small or zero. In this case, one might be forced to assume that a spin-orbit coupling plays an important role in determining nuclear structure. The other alternative is that there is little or no $S$ state. This would imply that the tensor interaction has a sufficiently high average value to compensate the increase in kinetic energy which would appear for such a wave function. There would probably still be some difficulty in understanding the saturation of nuclear forces. A better understanding of this point could be obtained by carrying through a calculation of the binding energy of the triton on the assumption that there is little or no $S$ state.

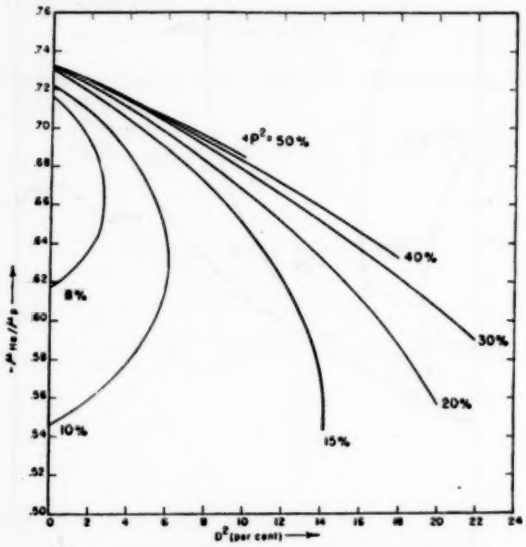


FIG. 2. The magnetic moment of $He^3$ in units of the proton moment. These curves have been obtained on the assumption that the relations shown in Fig. 1 apply also to $He^3$.

The possibility that the simple theory is entirely wrong should not be overlooked. The intrinsic moments of the neutrons and proton may be sufficiently perturbed by their mutual interaction to account for an appreciable fraction of the difference between the triton moment and the proton moment. Finally, relativistic corrections to the triton moment would be expected[4] and these may not be negligible compared to the effects under consideration.

The numerical work required for the construction of Figs. 1 and 2 was carried out by S. Moszkowski.

# Ultrasonic Measurements on Single Crystals*

H. B. HUNTINGTON**
*Massachusetts Institute of Technology, Cambridge, Massachusetts*

(Received April 2, 1947)

A pulse technique at 10 Mc/sec. has been used to measure acoustic velocity and attenuation of several alkali halides and Rochelle salt. Values for the elastic moduli of LiF, NaCl, BRr, and KI have been determined. The attenuation of the ultrasonic beam in these media is small. Corresponding measurements on the elastic moduli of Rochelle salt are reported. Under the assumption of plane wave transmission many of these moduli automatically correspond to those measured on foiled crystals by other methods. Attenuation is considerable in Rochelle salt, and appears to be excessively high for transmission involving the temperature-dependent $c_{44}$ (foiled case). Where this modulus is involved marked effects have been observed from electric bias and mechanical pressure. A complete set of elastic moduli has been obtained and used to calculate the corresponding values for the moduli of compliance.

## 1. INTRODUCTION

THE recent development of short pulse techniques has made available pulsed ultrasonics as a very convenient tool for investigating the mechanical properties of matter. During the war, some work was carried out on liquids at the Radiation Laboratory at Massachusetts Institute of Technology.[1,2] More recently a systematic study of the velocity and absorption of certain organic liquids has been performed by workers[3] in this laboratory. Some research on solids has been done as part of the war effort in England[4] and also in this country.[5] The pulse technique has also been used as a tool for detecting mechanical flaws in solids.[6]

Recently, the most widely used technique for measuring ultrasonic velocity and absorption in single crystals[7] has been the composite oscillator method initiated by Quimby's students,[8] whereby a piezoelectric crystal is cemented to the specimen under test, and the frequency is varied to obtain a resonance. Information on the velocity and elastic constants is obtained from the frequency of resonance. The breadth of the resonance measures the damping or internal friction.

With the pulse technique the same quantities are studied, usually at a much higher frequency at which the specimen is many wave-lengths on a side. Traveling waves replace standing waves.

Briefly, the experimental procedure consists in exciting a piezoelectric crystal, which is also cemented to the specimen under test, by a short pulse of the carrier frequency. The pulse travels down through the specimen and may be detected by a second piezoelectric crystal or reflected from the end surface to the transmitting crystal. In either case successive echoes are converted into electric pulses, amplified, and displayed on a time base sweep.

Actual elapsed times between the signals of successive echoes are measured to give velocity data. For the traveling wave, the velocity is a directly measured quantity whose determination is uncomplicated by boundary conditions or mode coupling.

On the other hand, the measured attenuation of the successive echoes must be interpreted with caution, as there are many possible causes for such attenuation other than direct absorption by the medium itself. In the first place, any sort of

* The research reported in this document was made possible through support extended the Massachusetts Institute of Technology, Research Laboratory of Electronics, jointly by the Army Signal Corps, the Navy Department (Office of Naval Research), and the Army Air Forces (Air Materiel Command) under the Signal Corps Contract No. W36-039 sc-32037.

** Now at the Rensselaer Polytechnic Institute, Troy, New York.

[1] P. Rosenberg, Radiation Laboratory, M.I.T. Report S-56, Nov. 1945.

[2] M. Cefola, M. E. Droz, S. Frankel, E. M. Jones, G. Maslach, and C. E. Teeter, Jr., Radiation Laboratory, M.I.T. Report 963, March 1946.

[3] J. R. Pellam and J. K. Galt, J. Chem. Phys. **14**, 608 (1946).

[4] TRE report T-1539, Aug. 22, 1943.

[5] D. L. Arenberg, Radiation Laboratory, M.I.T. Report 932, April 1946.

[6] F. A. Firestone, Metal Progress **48**, 505 (1945); E. N. Simon, Metal Progress **48**, 518 (1945).

[7] For a review of the measurements of elastic constants for single crystals see R. F. S. Hearmon, Rev. Mod. Phys. **18**, 409 (1946).

[8] L. Balamuth, Phys. Rev. **45**, 715 (1934); F. C. Rose, Phys. Rev. **49**, 50 (1936).

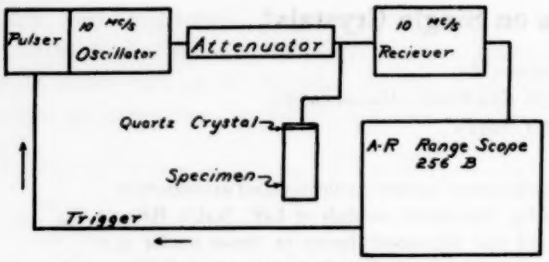


FIG. 1. Block diagram.

inhomogeneity in the specimen under test will give rise to scattering which will break up the intensity of the beam. In the megacycle range minute impurities can cause scattering. Residual thermal stresses also have the same effect. Extensive scattering can also be caused by the individual polycrystals of the specimen if the grain size is not very small compared to the wavelength of the ultrasonics. In the second place, even for homogeneous specimens, there will be some spreading of the beam from ordinary diffraction effects. This spreading is ordinarily not serious because narrow angle beams are obtained at high frequency. However, it is necessary for all specimens to be carefully prepared with two opposite surfaces flat and parallel. Any misalignment of these surfaces will cause a distortion in the pattern of the multiple echoes. As a result, the successive echoes decrease unevenly and may show an oscillatory character where some echoes are actually larger than their immediate predecessor. In the third place, any thermal gradients in the specimens will cause refraction and consequent pulse distortion. Finally, the character of the film between crystal and specimen is increasingly critical at shorter wave-lengths. It is essential that the surfaces be clean so that the film will be uniform. All particles and air bubbles should be carefully excluded. Precaution should be taken to keep the film as thin as possible, and this is particularly important if the film has a low acoustic impedance. Otherwise, the crystal element will not have a sufficiently broad band character to maintain good pulse shape. For work with transverse waves it appears to be impracticable to use liquid or wax films.

The effect of pulse distortion is naturally more pronounced in attenuation measurements. Mainly from this cause the results given here are only of a qualitative nature and tend to represent upper limits rather than actual values. To obtain more precise values would require repeated measurements on the same specimens to evaluate the reproducibility and influence of the film used, and on specimens of different size and shape to eliminate the effects of geometry, beam spreading, reflections, and the like.

The effect of pulse distortion on velocity measurements, though much smaller than on attenuation, was the limiting factor in the accuracy of the results. For successive pulses which maintained essentially the same shape, the precision of the velocity determination was easily as good as 0.1 percent. With the appearance of pulse distortion, for one reason or another, the determination of the time between pulses became difficult. Results varied, depending on procedure and interpretation of the scope pattern, so that the inaccuracy in velocity measurement might be as high as $1\frac{1}{2}$ percent. For this reason the accuracy of measurement varies considerably throughout.

It was decided in this investigation to study single crystals to avoid as far as possible the pulse deterioration arising from polycrystalline inhomogeneities. Many of the alkali halide crystals used were obtained from the Harshaw Development Company. Measurement on these substances was of particular interest as the attenuation was very low. We were fortunate to obtain two single crystals of copper from Mr. L. Gold of the M.I.T. metallurgy department which showed a considerably larger attenuation. Rochelle salt was chosen because of interest in its piezoelectric properties and its Curie point at room temperature. These crystals were supplied by the Brush Development Company.

## 2. EXPERIMENTAL PROCEDURE

The equipment used in these measurements consisted of a DuMont 256B A/R Range Scope, a pulsed 10 Mc/sec. oscillator, a broad band 10 Mc/sec. receiver, and a calibrated 70 ohm attenuator, arranged as shown in the block diagram (Fig. 1). The oscillator was adjustable in frequency, but for this work the frequency was held fixed at 10.6 Mc/sec. The trigger from the A/R scope initiated a video pulse. The pulse cut off a tube which previously loaded the grid

circuit of the oscillator. With the tube cut off, the high frequency pulse started with a rapid rise time. The duration of the pulse could be varied from $\frac{3}{4}$ to $2\frac{1}{2}$ μsec. The 10 Mc/sec. receiver consisted of 5 stages of high frequency amplification followed by a detector and two stages of video amplification. The frequency response was such that the amplifier could pass pulses with 0.1 μsec. rise time with negligible distortion.[9] The attenuator was variable from 0 to 101 db in steps of 1 db.

Quartz crystals were used for electromechanical transducers. In general, the same crystal, attached through a $T$ connector, was used to transmit and receive. The specimen under test was clamped in place on a small brass table with the crystal fastened to the prepared surface. The $T$ junction was physically near the amplifier input, and transforming networks were not employed. Attenuation measurements were made only when sufficient attenuation had been inserted so that the driving impedance at the junction was effectively 70 ohms.

The preparation of electrodes for crystals to be used with alkali-halides and Rochelle salt was complicated by the fact that the surfaces of these materials could not be cleaned by the usual reagents. For this reason it appeared inadvisable to attempt to apply metal electrodes either by evaporation or Brashear's process. The interposition of a metal foil between crystal and specimen was undesirable, since a second binding film would be needed between foil and specimen. Under such circumstances the production of good pulse shapes would have been difficult. Instead, electrodes were deposited on the quartz crystal itself by the Brashear process so that the whole crystal, 1 in. in diameter, was plated everywhere except for a centered ring of bare quartz on one face. The inner and outer diameters of the ring were $\frac{1}{2}$ in. and $\frac{3}{4}$ in., respectively. The completely silvered face was attached to the specimen, while on the other side press-fingers of beryllium copper made ground connection to the outer ring and a steel spring formed a coaxial lead to excite the central, silvered spot.

For the film between quartz and specimen several materials such as oil, vaseline, and Canada balsam were tried with indifferent success. Good pulse shape could be obtained with a thin layer of paraffin that had been allowed to cool under uniform pressure, but at temperatures for which the paraffin would flow freely it was extremely difficult to prevent dehydration of the Rochelle salt. Moreover, satisfactory transmission of transverse waves required a film of rigid material. It was decided to use an organic compound with a sharp melting point in the 40°–50°C range. For this purpose, it was found[10] that phenyl salicylate with a melting point near 42°C was completely satisfactory, and it was used almost exclusively in the later measurements.

All experiments were performed at ambient temperature, except for some measurements on Rochelle salt where the specimen was cooled to a few degrees below the Curie point and allowed to warm up slowly over a period of several hours.

The A/R scope is provided with two long sweeps, one of 122 microseconds and the other 1.22 milliseconds (20,000 yd. and 200,000 yd. radar range), which start with the trigger. There are also available several delayed sweeps of which the fastest has a speed of 1 inch per microsecond. The procedure in taking the data was to put each echo in turn on this delayed sweep. By the use of the calibrated attenuator the echo was adjusted to give a fixed deflection, and the reading of the attenuator was recorded. Next, the attenuation was decreased by a fixed amount which caused the signal to overload. The delay time corresponding to the steep leading edge of the overloaded pulse could be read from a dial

TABLE I. Measurements of elastic constants of alkali halides (in units of $10^{11}$ dynes/cm²).

| Density | | Constant measured | LiF 2.295 | NaCl 2.165 | KBr 2.75 | KI 3.13 |
|---|---|---|---|---|---|---|
| I | (a) | $c_{11}$ | 9.75 | | | 2.69 |
| | (b) | $c_{44}$ | | | | 0.362 |
| II | | $c_{11}$ | 9.96 | 4.79 | 3.54 | |
| III | (a) | $c_{11}$ | 9.74 | 4.85 | 3.45 | |
| | (b) | $c_{44}$ | 5.56 | $1.27_1$ | 0.508 | |
| IV | (a) | $c_{44}$ | 5.52 | $1.26_6$ | 0.515 | |
| | (b) | $\frac{1}{2}(c_{11}-c_{12})$ | 2.85 | $1.80_6$ | $1.45_3$ | |
| | (c) | $c_{12}$ (calc.) | 4.04 | 1.23 | 0.54 | |
| | (d) | $\frac{1}{2}(c_{11}+c_{12})+c_{44}$ | 12.12 | 4.27 | 2.54 | |
| | (e) | $\frac{1}{2}(c_{11}+c_{12})+c_{44}$ | $12.4_8$ | 4.31 | 2.50 | |

[9] The pulser and amplifier units were developed for testing ultrasonic delay lines by R. D. Arnold at the M.I.T. Radiation Laboratory in 1945.

[10] We are much indebted to Mr. C. S. Pearsall of this laboratory for his advice and assistance in this matter.

which measured the angular displacement of a heliopotentiometer. Small corrections had to be applied to the dial readings for both the 122-microsecond and the 1.22-millisecond ranges. The instrument is supplied with an 82 kc crystal which gives markers every 12.192 microseconds. (The repetition rate is synchronized to be a subharmonic of this frequency.) From the markers, the correction curves for the heliopotentiometer could be obtained. When it was possible to make time measurements on both the 122-microsecond and 1.22-millisecond range sweeps, the two agreed to within 0.1 percent. This internal consistency served as a check on the accuracy and stability of the correction curves.

In any long series of successive echoes a gradual deterioration of pulse shape could be observed, so that an originally short flat pulse might appear after many reflections to be rounded off and extended in time. It seems likely that this was caused by diffusing reflections from the film and the back of the quartz as well as from the end of the specimen. Since measurements were made on the front of the pulse, the distance of travel was always measured completely within the specimen.

For any particular series the time intervals between successively recorded echoes have been considered as independent measurements of an experimental quantity, which therefore determine an average value and a root mean error. Actually, the recorded values of the successive time intervals are not strictly independent, but are so interrelated that a deviation from the mean in one interval is likely to be counterbalanced by a deviation in the opposite direction in the next. For this reason the root mean square deviation of these quantities should actually be greater than the error in the average. A more exact treatment seems scarcely justified and, in the presentation of the data, this root mean error has been included in Tables II and III to give a comparative measure of the precision of the respective time measurements.

### 3. ALKALI-HALIDES

To arrive at the dynamic equations of an elastic anisotropic medium one equates the product of the mass of an infinitesimal volume times its acceleration along a coordinate axis to the net force obtained by integrating the stress components over the surface of the volume element. This gives the result

$$\rho\left(\frac{\partial^2 u_i}{\partial t^2}\right)=\sum_j \partial T_{ij}/\partial x_j, \tag{1}$$

where $\rho$ is the density, $u_i$ is the displacement in the $i$th direction, and the $T_{ij}$ are components of the stress tensor. All indices run over the range of the three cartesian coordinates. The stresses can be related to the strains $\epsilon_{kl}$ by a tensor equation involving the moduli of elasticity in the form of a tensor of rank 4.

$$T_{ij}=\sum_{kl} c_{ijkl}\epsilon_{kl}. \tag{2}$$

The strains $\epsilon_{kl}$ are here defined as a symmetric tensor[11] in terms of the displacements

$$\epsilon_{kl}=\tfrac{1}{2}\left(\frac{\partial u_k}{\partial x_l}+\frac{\partial u_l}{\partial x_k}\right). \tag{3}$$

The elastic equations for the medium are obtained by combining Eqs. (1), (2), and (3).

$$\rho\left(\frac{\partial^2 u_i}{\partial t^2}\right)=\tfrac{1}{2}\sum_{jkl}\frac{\partial}{\partial x_j}\left\{c_{ijkl}\left(\frac{\partial u_k}{\partial x_l}+\frac{\partial u_l}{\partial x_k}\right)\right\}. \tag{4}$$

The tensor $c_{ijkl}$ is symmetric with respect to interchange of $i$ and $j$, $k$, and $l$, and the pair $ij$ with the pair $kl$. For a homogeneous medium the moduli of elasticity are independent of position. Therefore

$$\rho\left(\frac{\partial^2 u_i}{\partial t^2}\right)=\sum_{jkl} c_{ijkl}\partial^2 u_k/\partial x_j\partial x_l. \tag{4a}$$

Under the conditions of measurements with pulsed ultrasonics, the wave-length is small compared with dimensions of the specimen. For a pulse of plane waves traveling through a medium in the $x_1$ direction, one may expect all quantities to be independent of $x_2$ and $x_3$. For this reason the elastic equations of motion become simplified,

$$\rho\left(\frac{\partial^2 u_i}{\partial t^2}\right)=\sum_k c_{i1k1}\partial^2 u_k/\partial x_1{}^2. \tag{4b}$$

[11] This definition of the strains is not the traditional one, but is nevertheless widely used. It is more convenient here because of the tensor character.

If the expressions for the displacements of the plane waves are taken to be

$$u_i = A_i \exp[iw(t - x_1/v)],$$

then the equations for the amplitudes become

$$\rho v^2 A_i - \sum_k c_{ijkl} A_k = 0. \tag{4c}$$

One can identify the components of the tensor $c_{ijkl}$ with the moduli of elasticity as usually defined, by combining paired indices.

| | |
|---|---|
| 11→1 | 23→4 |
| 22→2 | 31→5 |
| 33→3 | 12→6 |

In the case of propagation parallel to one of the cubic axes of the alkali-halides the determinantal equation for the allowed values for velocity of propagation takes on a particularly simple form

$$\begin{vmatrix} c_{11}-\rho v^2 & 0 & 0 \\ 0 & c_{44}-\rho v^2 & 0 \\ 0 & 0 & c_{44}-\rho v^2 \end{vmatrix} = 0.$$

With an $X$-cut quartz crystal attached to a (100) face, $c_{11}$ could be obtained directly from measurements of the elapsed time between successive echoes and the distance traveled by the pulse. Density values as listed in Table I were obtained from the *Handbook of Chemistry and Physics*. Replacing the $X$-cut quartz by a $Y$-cut quartz one could generate transverse waves and obtain $c_{44}$.

A second specimen was necessary in each case for the determination of $c_{12}$. These additional specimens were supplied with a pair of plane parallel faces in the (110) direction. The determinantal equation for the values of the velocity becomes[12]

$$\begin{vmatrix} [\frac{1}{2}(c_{11}+c_{12})+c_{44}]-\rho v^2 & 0 & 0 \\ 0 & \frac{1}{2}(c_{11}-c_{12})-\rho v^2 & 0 \\ 0 & 0 & c_{44}-\rho v^2 \end{vmatrix} = 0.$$

With the $X$-cut quartz one measures $\frac{1}{2}(c_{11}+c_{12})+c_{44}$, and with the $Y$-cut quartz one measures $\frac{1}{2}(c_{11}-c_{12})$ and $c_{44}$ simultaneously from two series of echoes. If the $Y$-cut crystal was oriented so that the $x$-axis was parallel to the (1–10) axis in the (110) plane of the alkali-halide, then only the transverse vibration with velocity $[\frac{1}{2}(c_{11}-c_{12}/\rho)]^{\frac{1}{2}}$ was excited. In a similar manner the other beam could be isolated by rotating the quartz through 90°. In addition to supplying values for $c_{12}$, measurements on the 45° alkali-halides gave two internal checks on the accuracy of the measurements.

All the data taken on alkali-halides are listed in Table I. The measurements tabulated in rows I(a) and (b) were taken on specimens kindly supplied by Professor D. C. Stockbarger of the M.I.T. Physics Department. Mr. D. L. Arenberg of the Physics Department of Brown University loaned the specimens from which the measurements given in row II were obtained. The measurements under III and IV refer to specimens purchased from the Harshaw Development Company. The specimens used for III were cut along cleavage planes and allowed ultrasonic propagation in the (100) direction. The measurements IV(a), (b), and (d) were made from a second set of specimens cut to provide flat parallel (110) planes. The values of IV(a) should be compared with III(b) to evaluate the degree of reproducibility of the same measurement in two different specimens. The values for $c_{12}$ in IV(c) are obtained from III(a) and IV(b). The results tabulated in IV(e) are calculated from III(a), (b), and IV(c) and are to be compared with the measured values in IV(d). The internal agreement with the Harshaw crystals is better than 2 percent in all cases except one (where the disagreement is less than 3 percent). These crystals were cut to afford cross sections one inch square (or more) perpendicular to the path of the ultrasonic beam. The active area of the quartz crystals in every case was a circle $\frac{1}{2}$ in. in diameter. Under these conditions good pulse-shape reproduction was maintained, and accurate time determination was possible. The specimens loaned by Mr. Arenberg were also originally prepared by the Harshaw Company, but presented cross sections $\frac{1}{2}$ in. square to the ultrasonic beams. With them the pulse-shape reproduction was poorer with consequent greater inaccuracy in the time measurement. This may have been the result of the smaller cross section or of inexperience in the technique of securing satisfactory

[12] For formulas giving the expressions for elastic constants, after a rotation see W. G. Cady, *Piezoelectricity*, McGraw-Hill Book Company (1946).

TABLE II. Elastic constants of alkali halides (in units of $10^{11}$ dynes/cm$^2$).

| | | Pulse measurement | Bergman[14] | Durand[15] | Bridgman[13] | Hunter and Siegel[16] |
|---|---|---|---|---|---|---|
| LiF | $c_{11}$ | 9.74±0.01 | 11.77 | | | |
| | $c_{12}$ | 4.04±0.02 | 4.33 | | | |
| | $c_{44}$ | 5.54±0.03 | 6.28 | | | |
| NaCl | $c_{11}$ | 4.85 ±0.01 | 4.67 | 4.99 | 4.70 | 4.86 |
| | $c_{12}$ | 1.23 ±0.02 | 1.23 | 1.31 | 1.23 | 1.19 |
| | $c_{44}$ | $1.26_5$±0.025 | 1.19 | $1.27_0$ | $1.28_1$ | 1.28 |
| KBr | $c_{11}$ | 3.45 ±0.07 | | | 3.33 | |
| | $c_{12}$ | 0.54 ±0.03 | | | 0.58 | |
| | $c_{44}$ | 0.508±0.005 | | | 0.621 | |
| KI | $c_{11}$ | 2.690±0.005 | | | 2.67 | |
| | $c_{44}$ | 0.362±0.001 | | | 0.421 | |

[13] P. W. Bridgman, Proc. Am. Acad. **64**, 19 (1929).
[14] L. Bergman, *Der Ultraschall* (J. W. Edwards, 1942).
[15] M. Durand, Phys. Rev. **50**, 449 (1936).
[16] L. Hunter and S. Siegel, Phys. Rev. **61**, 84 (1942).

films as the measurements were of a preliminary nature.

The weighted results of the measurements with the one-inch square specimens are given in Table II together with probable error figures based on the precision of the time measurements. In some cases, the internal checks (see Table I) show greater deviations than would be expected from the indicated precision, and perhaps arise from an unknown source of systematic error. Values obtained by other investigators are also listed in Table II for comparison. The most marked discrepancies appear in the comparison of these measurements for LiF and those of Bergman[14] obtained by an optical method. For KBr and KI the $c_{44}$ constant here measured is about 20 percent less than that measured by Bridgman. For NaCl, however, there appears to be fair agreement among all observers.

TABLE III. Elastic moduli of Rochelle salt (in units of $10^{11}$ dynes/cm$^2$).

| | Pulse measurements | Unstarred values | Mason |
|---|---|---|---|
| | 90° Cuts (100) | | |
| $c_{11}$ | 2.550±0.005 | | 2.64 |
| $c_{22}$ | 3.81 ±0.011 | | 3.18 |
| $c_{33}$ | 3.705±0.013 | | 3.91 |
| $c_{55}$* | 0.286±0.008 | $c_{55}$=0.321±0.008 | 0.304 |
| $c_{66}$* | 0.960±0.027 | $c_{66}$=0.979±0.027 | 0.996 |
| | | $\frac{1}{2}(c_{55}+c_{66})$=0.650±0.014 | |
| | 45° Cuts (110) | | |
| $c_{12}$ | 1.41 ±0.03 | | 1.81 |
| $c_{23}$ | 1.46 ±0.06 | | 2.13 |
| $c_{13}$ | 1.16 ±0.04 | | 2.23 |
| $\frac{1}{2}(c_{44}+c_{66})$* | 1.145±0.003 | $\frac{1}{2}(c_{44}+c_{66})$=1.159±0.003 | |
| | | $c_{44}$=1.34 ±0.03 | 1.25 |
| $\frac{1}{2}(c_{55}+c_{66})$* | 0.637±0.002 | $\frac{1}{2}(c_{55}+c_{66})$=0.644±0.002 | |

A few observations can be made about ultrasonic attenuation and pulse behavior in the alkali-halides. In general the attenuation between successive echoes appeared to be far smaller than we have encountered in most substances. In this respect pulses of compressional vibration moving perpendicular to the cleavage planes made the best showing. In the case of the measurements of $c_{11}$ for rocksalt, over fifty echoes were observed on the 1.22-millisecond sweep. From first to last there was diminution in intensity of less than 15 db. In the potassium bromide specimen for the same period of time there was observed a drop in intensity of about 20 db for thirty-seven echoes. The order of magnitude of the results, rather than the actual values, is the significant quantity in isolated measurements of this sort. The results were very sensitive to the uniformity and character of the connecting film between the specimen and the quartz. Probably film losses account for the fact that transverse waves showed greater attenuation than compressional waves.

With lithium fluoride very marked mode conversion took place. Energy was lost from the main compressional beam on striking the sides of the specimen at small angles by conversion to transverse vibration. Some of the transverse beams so generated were later reconverted to a compressional excitation and detected by the X-cut quartz. It was possible to identify positively these smaller echoes by the times of their arrivals. The pronounced effect of large angle reflection in causing mode conversion, predominantly in LiF, may be accounted for in

part (1) by the longer wave-length which causes a wider diffraction pattern for the same geometry, and (2), possibly by greater efficiency of conversion in the region of an incident angle of 75° (as determined by the dimensions of the specimen). D. L. Arenberg has evaluated the efficiency of conversion as a function of angle and Poisson ratio for isotropic materials[5] and has shown it to be very sensitive to the latter for large angles. The extension of this work to a cubic crystal presents difficulties. It should, however, be remarked that the ratio $c_{11}/c_{44}$ is significantly smaller for LiF than for the other alkali-halides so that a different behavior on reflection may be expected.

### 4. COPPER

We had the good fortune to be able to borrow for test purposes two large copper single crystals from Mr. L. Gold of M.I.T. Metallurgy Department. Previous attempts to make measurements on polycrystalline copper specimens had been unsuccessful because of the very large scattering losses involved. With both single crystals of copper, however, return signals were received which showed well-defined pulse shape and little evidence of scattering. These signals, however, fell off quite rapidly, something of the order of 1 db per cm. This large attenuation is in marked contrast with the behavior of the alkali-halides discussed in the previous section. It should be pointed out that, while the Harshaw crystals had all been carefully annealed, the copper crystals were untreated. The frequency of the measurement is beyond the range of the frequency-dependent types of internal friction usually investigated for metals.[17]

From each of the two copper crystals three ultrasonic velocities were measured in one direction, corresponding to one compressional and two transverse waves. If the crystal orientations had been known, it would have been possible to obtain values for the elastic constants of copper.

### 5. ROCHELLE SALT

For a piezoelectric material additional terms must be added to Eq. (2) for the stresses to include the interactions between mechanical and electrical parameters.

$$T_{ij}=\sum_{kh} c_{ijkh}\epsilon_{kh}+\sum_{m} f_{ijm}P_m, \tag{5}$$

where the $P_m$ are the polarizations, and the $f_{ijm}$ are the piezoelectric constants. Also, the equations for the electric field strengths give

$$E_i=\sum_{kh} f_{khi}\epsilon_{kh}+\sum_{m} \chi_{im}P_m, \tag{6}$$

where the $X_{im}$ are the reciprocal susceptibilities of the clamped crystal. Under this selection of thermodynamic variables, the elastic constants with constant polarization are involved.

If one writes down Maxwell's equations for the piezoelectric crystal, it is practicable to disregard the magnetic quantities and charge concentrations inside the crystal. One then obtains the following equations,

$$\text{curl } \mathbf{E}=0 \quad \text{and} \quad \text{div } \mathbf{D}=0.$$

Under the conditions of the pulsed ultrasonic experiment one can assume that the only spatial variation the field quantities will exhibit will be along the direction of propagation, say the $x_1$ direction. This shows that $E_2$, $E_3$, and $D_1$ are all constants and affect the ultrasonic velocity only by their biasing action. It follows that Eq. (6) becomes

$$E_1=\sum_{kh} f_{kh1}\epsilon_{kh}+\sum_{m} \chi_{1m}P_m=-4\pi P_1, \tag{6a}$$

$$0=\sum_{kh} f_{kh2}\epsilon_{kh}+\sum_{m} \chi_{2m}P_m, \tag{6b}$$

$$0=\sum_{kh} f_{kh3}\epsilon_{kh}+\sum_{m} \chi_{3m}P_m. \tag{6c}$$

These equations can be solved for the components of the polarization and the results substituted back into Eq. (5). The equations of motion which replace (4b) for the non-piezoelectric crystal have the same form

$$\rho\left(\frac{\partial^2 u_i}{\partial t^2}\right)=\sum_{k} c^*_{i1k1}\partial^2 u_k/\partial x_1^2, \tag{7}$$

except that now the starred moduli of elasticity have been altered by the inclusion of the piezoelectric terms. Since the added terms depend in a special way on the direction of propagation, they

[17] C. Zener "Anelasticity of Metals," Trans. A.I.M.E., Aug. (1946).

do not necessarily have the symmetry of the crystal and may make the crystal appear to have a lower symmetry than it is known to possess. This effect was first observed by Atanasoff and Hart[18] in their measurements on standing waves in quartz. The correct explanation of the effect was put forward by A. W. Lawson.[19]

In the case of Rochelle salt the crystal symmetry remains unaffected, but at least one of the added terms has a profound effect of a different sort. For this material the $\chi_{ij}$ is a matrix with no off-diagonal terms, and the $f_{kli}$ connect only polarization parallel to a given axis with the shear stress about that axis. Again use is made of the fact all field quantities are a function of $x_1$ alone so that it remains only to relate the $T_{ii}$ with the $\epsilon_{kl}$,

$$T_{i1}=\sum_k c_{i|k|}\epsilon_{k1}-(f_{i1m}^2/\chi_{mm})_{m\neq i\neq 1}\epsilon_{i1}. \quad (8)$$

As a result, the starred moduli of elasticity can be written

$$c_{ikl}^*=c_{ikl} \text{ for } i\neq k \text{ or for } i=1 \quad (9)$$

and

$$c_{iii}^*=c_{iii}-f_{im}^2/\chi_{mm}$$

for $m$, $i$, and $l$ all different. In the usual nomenclature this last relation would be written

$$c_{55}^*=c_{55}-f_{25}^2/\chi_2, \quad (9a)$$

$$c_{66}^*=c_{66}-f_{36}^2/\chi_3. \quad (9b)$$

It is of interest to note that the starred quantities are identically the reciprocals of the elastic compliances for the foiled crystals.

Since $c_{15}$, $c_{16}$, and $c_{56}$ vanish for Rochelle salt from symmetry conditions (which are not removed by inclusion of piezoelectric terms), the determinantal equation for velocities in the $x_1$ direction is

$$\begin{vmatrix} c_{11}-\rho v^2 & 0 & 0 \\ 0 & c_{55}^*-\rho v^2 & 0 \\ 0 & 0 & c_{66}^*-\rho v^2 \end{vmatrix}=0. \quad (10)$$

It is possible then to generate a pure compressional wave by an $X$-cut quartz crystal or two transverse waves with a $Y$-cut crystal, respectively. In this way one can measure $c_{11}$, $c_{55}^*$, and $c_{66}^*$. By attaching $X$-cut quartz crystals to the faces perpendicular to the $x_2$ and the $x_3$ directions, measurements can also be made of $c_{22}$ and $c_{33}$. These five values are listed in Table III in the first block which refers to the so-called "90° cuts" or those specimens whose sides were perpendicular to the principal axes of the Rochelle salt. In the same table (second column) are given values for $c_{55}$ and $c_{66}$ as calculated from Eq. 9 by using Mason's values:[20]

$$f_{14}=7.8\times 10^4; \quad f_{25}=7.05\times 10^4; \quad f_{36}=5.40\times 10^4$$

and

$$\chi_2=1.43; \quad \chi_3=1.53$$

and

$$K_2=9.8; \quad K_3=9.2.$$

The differences between $c_{55}^*$ and $c_{55}$, $c_{66}^*$ and $c_{66}$ are not large but, while $c_{44}$ varies only slowly with temperature, it is known that the foiled elastic constant for shear about the $x_1$-axis, $c_{44}^*$ effectively vanishes at 23.0°C. For the temperature range −18°C to +23.0°C the Rochelle salt crystal is deformed by a set strain $\epsilon_4$, its symmetry class changes from orthorhombic to monoclinic, and it becomes ferroelectric. This anomalous behavior has been successfully treated by the phenomenological theory of Mueller.[21] We shall return to a discussion of the transverse vibration with velocity $(c_{44}^*/\rho)^{\frac{1}{2}}$ later. It is sufficient to point out here that the quantity was too temperature-dependent to allow precise calculation of $c_{44}$ and values for these quantities are omitted from the upper block of Table III.

The lower part of Table III gives the results obtained from the 45°-cut specimens. These were principally measurements of the off-diagonal elements $c_{12}$, $c_{23}$, and $c_{13}$. For a 45° rotation about the axis in the $x_1$ direction the transformed matrix which relates strains and polarizations to stresses and electric field strength (see Eqs. (5) and (6)) is given in Table IV:[22]

For plane wave propagation in the new $x_2$ direction (actually a (011) axis in the unrotated

[18] John V. Atanasoff and Philip J. Hart, Phys. Rev. **59**, 85 (1941).

[19] A. W. Lawson, Phys. Rev. **59**, 838 (L) (1941).

[20] W. P. Mason, Phys. Rev. **55**, 775 (1939).

[21] H. Mueller, Phys. Rev. **47**, 175 (1935); *ibid.* **57**, 829 (1940); *ibid.* **58**, 565 (1940); *ibid.* **58**, 805 (1940).

[22] W. P. Mason, *Electromechanical Transducers and Wave Filters* (D. Van Nostrand Company, New York, 1942), pp. 315–326. Mason's starred quantities are equivalent to our unstarred quantities.

lattice) the strains $\epsilon_1$, $\epsilon_3$, and $\epsilon_5$ will not be excited. One can solve for the $P_i$ from equations which resemble (6a), (6b), and (6c) after interchange of indices 1 and 2 and obtain

$$P_1=-\frac{f_{14}}{\chi_1}\epsilon_2, \qquad P_2=-\frac{f_{25}\chi_3+f_{36}\chi_2}{2[\chi_3\chi_2+2\pi(\chi_3+\chi_2)]}\epsilon_6, \qquad P_3=\frac{f_{25}(\chi_3+4\pi)-f_{36}(\chi_2+4\pi)}{2[\chi_2\chi_3+2\pi(\chi_2+\chi_3)]}\epsilon_6. \tag{11}$$

It follows that the determining equation for the velocities in this direction is:

$$\begin{vmatrix} \frac{c'+c_{23}+2c_{44}^*}{2}-\rho v^2 & \frac{c_{33}-c_{22}}{4} & 0 \\ \frac{c_{33}-c_{22}}{4} & \frac{c'-c_{23}}{2}-\rho v^2 & 0 \\ 0 & 0 & \frac{(c_{55}+c_{66})^*}{2}-\rho v^2 \end{vmatrix}=0. \tag{12}$$

The quantity $(c_{55}+c_{66})^*$ is accordingly an abbreviation,

$$(c_{55}+c_{66})^*=c_{55}+c_{66}-\frac{\frac{f_{36}^2}{\chi_3}+\frac{f_{25}^2}{\chi_2}+(f_{25}-f_{36})^2\frac{2\pi}{\chi_2\chi_3}}{1+\frac{2\pi}{\chi_2}+\frac{2\pi}{\chi_3}}.$$

Inspection of this determinant indicates that there will be one purely transverse wave propagated in the (011) direction and polarized in the (100) direction. The other transverse mode and the compressional mode are coupled together, but fortunately the coupling is weak enough so that excitation with $X$-cut quartz appears to give only one set of signals. The velocity of this nearly compressional wave has a measured value of $(c_b/\rho)^{\frac{1}{2}}$, where $c_b$ is given as $2.64\times10^{11}$ dyne/cm$^2$ in column 1 of Table V. Excitation with $Y$-cut

TABLE IV. Strain-polarization matrix for a 45° rotation.

| | | | | | | | | |
|---|---|---|---|---|---|---|---|---|
| $c_{11}$ | $\frac{c_{12}+c_{13}}{2}$ | $\frac{c_{12}+c_{13}}{2}$ | $\frac{c_{13}-c_{12}}{2}$ | 0 | 0 | 0 | 0 | 0 |
| $\frac{c_{12}+c_{13}}{2}$ | $\frac{c'+c_{23}+2c_{44}}{2}$ | $\frac{c'+c_{23}-2c_{44}}{2}$ | $\frac{c_{33}-c_{22}}{4}$ | 0 | 0 | $f_{14}$ | 0 | 0 |
| $\frac{c_{12}+c_{13}}{2}$ | $\frac{c'+c_{23}-2c_{44}}{2}$ | $\frac{c'+c_{23}+2c_{44}}{2}$ | $\frac{c_{33}-c_{22}}{4}$ | 0 | 0 | $-f_{14}$ | 0 | 0 |
| $\frac{c_{13}-c_{12}}{2}$ | $\frac{c_{33}-c_{22}}{4}$ | $\frac{c_{33}-c_{22}}{4}$ | $\frac{c'-c_{23}}{2}$ | 0 | 0 | 0 | 0 | 0 |
| 0 | 0 | 0 | 0 | $\frac{c_{55}+c_{66}}{2}$ | $\frac{c_{55}-c_{66}}{2}$ | 0 | $\frac{f_{25}-f_{25}}{0}$ | $\frac{f_{25}+f_{36}}{2}$ |
| 0 | 0 | 0 | 0 | $\frac{c_{55}-c_{66}}{2}$ | $\frac{c_{55}+c_{66}}{2}$ | 0 | $\frac{f_{25}+f_{36}}{2}$ | $\frac{f_{36}-f_{25}}{2}$ |
| 0 | $f_{14}$ | $-f_{14}$ | 0 | 0 | 0 | $\chi_1$ | 0 | 0 |
| 0 | 0 | 0 | 0 | $\frac{f_{25}-f_{36}}{2}$ | $\frac{f_{25}+f_{36}}{2}$ | 0 | $\frac{\chi_2+\chi_3}{2}$ | $\frac{\chi_3-\chi_2}{2}$ |
| 0 | 0 | 0 | 0 | $\frac{f_{25}+f_{36}}{2}$ | $\frac{f_{36}-f_{25}}{2}$ | 0 | $\frac{\chi_3-\chi_2}{2}$ | $\frac{\chi_3+\chi_3}{2}$ |

where $c'$ stands for $\frac{c_{22}+c_{23}}{2}$.

TABLE V. Data and results for the non-diagonal elastic moduli of Rochelle salt (all quantities in units of $10^{11}$ dynes/cm$^2$).

| Crystal surface | (011) | (101) | (110) |
|---|---|---|---|
| $c_d$ | 1.182 | $0.94_2$ | 0.858 |
| $c_b$ | 2.64 | $2.53_2$ | $3.32_8$ |
| $c_b+c_d$ | 3.82 | $3.47_4$ | $4.18_6$ |
| Left side of Eq. 13 | 3.76 | $3.41_4$ | $4.14_9$ |
| Non-diagonal moduli | 1.52−1.40 | 1.19−1.13 | 1.44−1.38 |

quartz oriented to give transverse vibration polarized along the $x_1$ axis led to a measurement of a velocity $(c_d/\rho)^{\frac{1}{2}}$, where $c_d$ is given by $1.182\times10^{11}$ dynes/cm$^2$ in Table V. The quantities given in columns 2 and 3 of Table V, refer to the other 45° cuts as indicated by the Miller indices at the head of each column, respectively. The $c_b$ and $c_d$ in each case refer to quantities experimentally measured from compressional and transverse excitations, respectively. For the moduli of elasticity a cyclic interchange of subscripts is understood on going from column 1 to column 2, and from column 2 to column 3.

The observed data in Table V, namely, the values for $c_b$ and $c_d$, are used to calculate the off-diagonal moduli of elasticity $c_{23}$, $c_{13}$, and $c_{12}$. The internal consistency of the data is checked by the diagonal-sum rule which requires that

$$(c_{22}+c_{33})/2+c_{44}^*=c_b+c_d \text{ for (011) direction,} \quad (13a)$$

$$(c_{11}+c_{33})/2+c_{55}^*=c_b+c_d \text{ for (101) direction,} \quad (13b)$$

$$(c_{11}+c_{22})/2+c_{66}^*=c_b+c_d \text{ for (110) direction.} \quad (13c)$$

These internal checks (see rows 3 and 4 in Table V) show discrepancies of one to three percent, which unfortunately introduce uncertainties in the values of the non-diagonal moduli of the order of 5 or 10 percent. The quantities of Eq. (13a) require special comment because of the temperature sensitivity of $c_{44}^*$. A temperature run was made on the measurement of $c_b$ for the (011) direction, and the velocity of propagation was found to go through a minimum at 23.7°C near the Curie point. The value of $c_b$ at this minimum is given as $2.64\times10^{11}$ dynes/cm$^2$ in Table V. Since $c_{44}^*$ vanishes at the Curie point, only $(c_{22}+c_{33})/2$ or $3.76\times10^{11}$ dynes/cm$^2$ has been used for row 4 col. 1 of Table V.

The evaluation of the non-diagonal elements was carried out twice in every case, by solving the quadratic equation for the desired quantity first with $\rho v^2$ equal to $c_b$ and next with $\rho v^2$ equal to $c_d$. Both values are given in Table V as an indication of the probable error of the results. A first-order approximation to the value for any non-diagonal modulus could be obtained by neglecting the coupling between the modes. The exact value could then be quickly obtained by Horner's method. Only the mean values for $c_{12}$, $c_{23}$, and $c_{13}$ are given in Table III.

The modulus of elasticity as determined from the pure transverse vibrations in the 45° $Y$–$Z$ specimen has been used to give an additional check on $c_{55}$ and $c_{66}$. The result for $\frac{1}{2}(c_{55}+c_{66})$ as given at the bottom of Table III checks to 1 percent the same quantity as calculated from measurements on the (100) specimens, as given in the same table. The value for $\frac{1}{2}(c_{44}+c_{66})$ was also found from the 45° $X$–$Z$ specimen and from it a value for $c_{44}$ was obtained.

Table III also shows for comparison Mason's values for the moduli of elasticity for constant polarization as computed from his measured moduli of compliance. In Table VI are given the values of the moduli of compliance as calculated from the data obtained by the pulse method. Values obtained directly for these quantities by Mason[20] and Hinz[23] are given in adjoining columns. Here the agreement with Mason is quite satisfactory for all the moduli listed except $s_{13}$.

The attenuation of the ultrasonic beam in Rochelle salt was much greater than in the alkali halides. No systematic quantitative measurements were made, but it was observed that the loss was never less than 1 db per inch of travel and sometimes a great deal more. The attenuation was always large in those measurements which involved $c_{44}^*$ and, for the propagation of the transverse wave which involved this modulus alone, the attenuation increased so rapidly as the Curie point was approached that it was not possible to extend our measurements below 26.5°C. An ultrasonic signal which was

[23] H. Hinz, Zeits. f. Physik **111**, 617 (1938). Measurements were made by a static method.

observed after it had transversed a half-inch of Rochelle salt, dropped by some 24 db as the temperature fell by 2°C in this range.

As might be expected, mechanical stress and electrostatic bias along the $X_1$ axis caused marked effects on those waves whose velocity depended on $c_{44}^*$. In general only qualitative information was obtainable concerning the influence of such external forces on the ultrasonic velocity. On the other hand, very pronounced changes in pulse size and shape accompanied the application of stress or bias and indicated clearly changing interference effects from different portions of the ultrasonic beam. These effects were more pronounced the nearer the Curie point.[21] At 24°C the velocity of the compressional wave in the (011) direction increased by 3 percent on the application of a d.c. field 4 e.s.u.

## 6. DISCUSSION AND ACKNOWLEDGMENTS

An ultrasonic pulse technique has been applied to measure the mechanical properties of some single crystals at 10 Mc/sec. The results for the elastic constants in general are self-consistent to 2 percent or better and in most cases agree satisfactorily with previously measured values. The attenuation in the alkali-halide single crystals is small so that one can do little more than put an upper limit on the internal friction as measured by the decrement. Internal friction in the copper single crystal is high in comparison with that found at lower frequencies, even for unannealed specimens.[24] Attenuation in Rochelle salt is also quite high, probably as a result of conversion of mechanical energy into electrical losses. Particularly high attenuation is evident in those cases which involve the shear constant $c_{44}^*$ for the crystal with zero field in the $x_1$ direction. It is known that for this modulus the departure from Hooke's law is appreciable for strains of $10^{-4}$ within a few degrees of the Curie point. It seems possible that anharmonic terms in the stress-strain relation could be responsible for some of the observed loss. By causing an interaction with the Debye waves of the lattice these terms could bring about frequency conversion of the energy of the ultrasonic beam so that its intensity would decrease rapidly with distance traveled.

TABLE VI. Moduli of compliance for Rochelle salt in units of $10^{-12}$ cm²/dynes.

| | Pulsed measurement | Mason[20] | Hinz[23] |
|---|---|---|---|
| $s_{11}$ | 5.24 | 5.18 | 5.23 |
| $s_{22}$ | 3.50 | 3.49 | 3.43 |
| $s_{33}$ | 3.37 | 3.34 | 3.24 |
| $s_{12}$ | −1.54 | −1.53 | −2.18 |
| $s_{13}$ | −0.98 | −2.11 | −1.68 |
| $s_{23}$ | −0.91 | −1.03 | −1.33 |

It is a great pleasure for me to thank Professor Mueller for having pointed out to me the interesting possibilities in Rochelle salt for such investigation and for his advice and lively interest in the research. Also I wish to thank individually Professor Stockbarger, Mr. Arenberg, and Mr. Gold for the use of their single-crystal specimens.

[24] T. A. Read, Phys. Rev. **58**, 371 (1940). Our attenuation corresponds to a value of $\Delta_1 = 8 \times 10^{-3}$ for the logarithmic decrement in Reade's notation.

# Specular Reflection from Mercury Vapor*

JAY M. HANSEN AND HAROLD W. WEBB
*Columbia University, New York, New York*

(Received April 28, 1947)

A quantitative study was made of the variation with vapor pressure of the diffusely scattered (absorbed and re-emitted) radiation from mercury vapor and of the regular reflection from a quartz-mercury vapor surface (specular reflection) which had been observed by Wood. The mercury vapor was contained in a quartz cell, and the intensity measurements were made with a photo-cell, with a stabilized low pressure discharge tube used as a source.

Both scattering and specular reflection were present over the range of vapor densities corresponding approximately to the range of condensed mercury temperatures between 100°C and 300°C. The scattered radiation increased up to 50°C and then fell off rapidly and was less than 0.5 percent at 300°C. Specular reflection was less than 0.5 percent below 100°C, and was measurable at 125°C, at which temperature the product of the cube root of the number of atoms per cubic centimeter and the wave-length was approximately seven. Over the range of densities corresponding to the range 150°C to 300°C, most of the energy of the 2537A radiation incident upon the mercury vapor was dissipated in the vapor.

The a.c. method, previously used in this laboratory for measurement of mean lifetimes, was used to study the persistence of the radiation in the quartz cell. For vapor pressures above 75°C there was no apparent change in the form of the curve giving the relation between the emission by the cell of scattered radiation and the elapsed time. Within the resolution of the timing method, about 1/40 of the lifetime of the excited state, the specular reflection showed no delay.

The optical constants, index of refraction and coefficient of absorption, of dense mercury vapor for the 2537A line were calculated from the reflectivity at two different angles of incidence. Their ratio remained nearly constant as the vapor pressure increased.

IT was shown by Wood[1] that at low vapor pressures mercury vapor irradiated with the resonance line 2537A showed only diffuse scattering, while at high pressures this was replaced by specular reflection. He illuminated with the sharp, unreversed line of a water-cooled mercury arc a small quartz bulb containing mercury vapor at various pressures. At low pressures the vapor throughout the entire bulb emitted radiation, but with increasing pressure the reradiating volume contracted toward the surface of entrance of the resonance line. He found that at a pressure corresponding to a condensed mercury temperature of 270°C the diffuse scattering had completely disappeared. However, at this temperature specular reflection by the quartz-mercury vapor surface was observable, and increased to considerable values with increase of pressure. This specular or metallic reflection occurred only at the resonance wave-length.

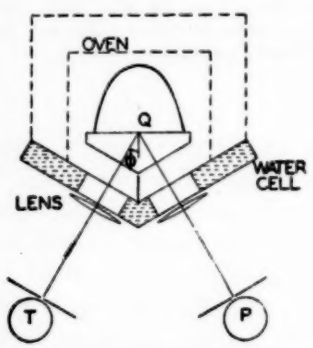


FIG. 1. Apparatus used for measurement of reflectivity. Slit width—1 mm; distance from slit to lens—30 cm. $T$—source; $Q$—quartz cell containing mercury vapor; $P$—photo-cell.

Rump[2] investigated the changes of line form caused by scattering and by reflection as a function of the pressure by means of absorption measurements, and concluded that specular reflection began at a lower temperature than that given by Wood. Schnettler[3] introduced the foreign gases $H_2$ and $O_2$, which quench the resonance radiation, and found that they affected the specular reflection only slightly. He interpreted this result as indicating that the lifetime of the excited atoms is not involved in specular reflection.

This paper describes a more detailed quantitative study of the diffuse scattering and of the

* Publication assisted by the Ernest Kempton Adams Fund for Physical Research of Columbia University.

[1] R. W. Wood, *Researches in Physical Optics*, II (Columbia University Press, New York, 1919).

[2] W. Rump, Zeits. f. Physik **29**, 196 (1924).

[3] O. Schnettler, Zeits. f. Physik **65**, 55 (1930).

specular reflection and their dependence upon pressure. A study was also made of the accompanying persistence or delay of the radiation. The use of the term "specular reflection" was found to be somewhat confusing, since in the experiments to be described the reflection from the inner boundary of the quartz container changed gradually from a "quartz-vacuum" reflection to a "quartz-mercury vapor" reflection and experimentally no distinction was made between them. Consequently in this paper the regular reflection will be referred to simply as "reflection." Diffuse scattering due to absorption and re-emission will be referred to simply as "scattering."

## METHOD

The mercury vapor under study was contained in a quartz cell $Q$ (see Fig. 1) with a plane front face, with provision made for varying the vapor pressure. Radiation of wave-length 2537A excited in a low pressure tube was allowed to fall on this surface and the scattered and reflected radiation studied. The investigation was divided into two parts: (1) A series of measurements to determine the variation in the reflectivity of the quartz-mercury vapor surface and the variation of the intensity of the scattered radiation with vapor pressure and temperature. (2) A study of the time elapsing between the incidence of the radiation on the mercury vapor and its re-emission.

In the first set of tests, radiation from a source $T$ (see Fig. 1) collimated by a slit and lens, was incident upon the plane quartz-mercury vapor surface. When measuring only the reflection a second lens and slit were used before the photo-cell $P$, the scattered radiation being practically eliminated because of the small solid angle subtended at the quartz tube by the slit. By removing the second collimator and putting the photo-cell close to the quartz cell $Q$, intensity measurements were made which included all of the reflected and a considerable fraction of the scattered radiation. Using these two types of measurement the behavior of both the scattered and the reflected radiation could be separately studied.

The measurements of the persistence of the radiation from the mercury vapor in the quartz

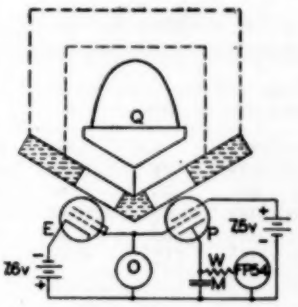


FIG. 2. Apparatus used for measurement of persistence. $E$—source; $O$—oscillator; $P$—photo-cell.

tube $Q$ were made by a modification of the method previously used in this laboratory for measuring the mean lifetimes of excited atoms.[4] Radiation was produced in a thin layer of mercury vapor in the excitation cell $E$ (see Fig. 2) by electron impact. Some of this radiation was incident upon the quartz tube $Q$, and the reradiated energy entered the photo-cell $P$. Alternating voltages were applied by an oscillator $O$ to both the excitation cell $E$ and to the photo-cell $P$ in the same phase. Excitation in $E$ occurred only during the positive half-cycle of the oscillator voltage. The direction of the current in the photo-cell reversed with reversal of the polarity of the oscillator voltage. At low frequencies, for which persistence of radiation had a negligible effect, radiation reached the photo-cell during only the positive half-cycles and there was no reverse photoelectric current. As the frequency was increased, the persistence of the radiation became appreciable and some radiation fell into the negative half-cycles and, since the average output of $E$ was constant, the measured photoelectric current decreased. The result of this measurement is expressed by a curve giving the ratio $R$ of the current at the frequency $f$ to the current at the low frequency for which the effect of persistence was negligible. Such a curve will be referred to as an "$R$-$f$" curve. For the purpose of this investigation we can use the formula $R=1-a(1+S)$. This formula is based on the assumption that the photo-cell current changes sharply from positive saturation to negative saturation at zero voltage, which was approximately true. Here $a$ is the fraction of the total radiation falling on the photo-cell in the

[4] P. H. Garrett, Phys. Rev. **40**, 779 (1932).

TABLE I.

| Temperature (°C) | $N$ (atoms/cm³) | $N^{1/3}\lambda$ | $n$ | $\kappa$ | $L/\lambda$ |
|---|---|---|---|---|---|
| 100 | $6.9\times10^{15}$ | 4.8 | 1.00 | 0.00 | — |
| 215 | $5.4\times10^{17}$ | 21 | 0.98 | 0.045 | 1.8 |
| 300 | $4.1\times10^{18}$ | 43 | 0.94 | 0.165 | 0.48 |
| 350 | $1.0\times10^{19}$ | 62 | 0.89 | 0.33 | 0.24 |
| 400 | $2.2\times10^{19}$ | 85 | 0.84 | 0.53 | 0.15 |
| 450 | $4.5\times10^{19}$ | 112 | 0.81 | 0.69 | 0.12 |

TABLE II.

| Temperature (°C) | $N$ (atoms/cm³) |
|---|---|
| 0 | $6.0\times10^{12}$ |
| 10 | $1.6\times10^{13}$ |
| 26 | $6.5\times10^{13}$ |
| 45 | $2.6\times10^{14}$ |
| 50 | $3.7\times10^{14}$ |
| 75 | $1.8\times10^{15}$ |
| 115 | $1.4\times10^{16}$ |
| 150 | $6.3\times10^{16}$ |

negative half-cycles and $S$ is the ratio of the current in the photo-cell for the same intensity of radiation when negative and positive voltages are applied, respectively. For very high frequencies $a$ approaches 0.5 and $R$ approaches $(1-S)/2$.

Since the radiation from the source $E$ had some persistence, it was necessary to calculate the added persistence due to the quartz cell from the shift of the observed $R$-$f$ curve from the curve obtained from the source $E$ directly.

## APPARATUS

The quartz cell[5] $Q$ had an inside diameter at the front face of 3.2 cm. This face was a fused quartz prism of angle 109° so arranged that while only the quartz-mercury vapor boundary contributed to the reflection into the photo-cell, it was still possible to use a large aperture. A small side tube contained a small quantity of liquid mercury the temperature of which was altered to vary the vapor pressure. The upper part of the cell was maintained about ten degrees hotter than the side tube to prevent condensation of mercury on the surface. The temperatures and corresponding vapor pressures given in this paper are those of the liquid mercury. The corresponding density of the vapor expressed as the number of atoms per cubic centimeter ($N$) is given in Tables I and II.

The quartz cell was placed in a special oven. To protect the other apparatus from heat from the oven, the front wall was a water cell insulated on the inside. The radiation passed into and out of the oven through quartz windows. Each window consisted of a pair of polished, fused quartz plates between which distilled water was circulated. A third polished, fused quartz plate was used inside the furnace and was separated from the inner cooled plate by a thin layer of dead air to eliminate excessive heat losses. At high temperatures it was difficult to prevent the windows from clouding rapidly and quantitative measurements were troublesome. The upper part of the furnace was heated electrically and its temperature regulated manually. The air was stirred by a jet of compressed air. The non-uniformity of temperature throughout this part of the furnace did not exceed twenty degrees at the highest temperature used (450°C). The temperature of the liquid mercury in the side tube was controlled with a thermostat which was designed to allow rapid changes of the operating temperature. The lower part of the furnace was a cylindrical copper block with a hole bored along the axis to receive the side tube containing the liquid mercury. This block was heated by coils wound around it. Its temperature was controlled to about 0.1°C by a thermocouple in circuit with a potentiometer and galvanometer. The galvanometer spot illuminated a photo-cell in such a way as to control an amplifier the output of which was the heater current. The values of the temperature were obtained from the potentiometer settings.

The source $T$ was a mercury vapor arc with a quartz capillary about 1.8 mm in diameter, and was observed transversely to avoid self-reversa of the 2537A line. It was operated at a pressure of 0.009 mm (45°C) and a direct current of about 40 milliamperes. Its output was stabilized by monitoring with a photo-cell which controlled through an amplifier the circuit which furnished the power supply for the arc. The intensity of the arc had no measurable random fluctuation, but showed a steady decrease of about one percent per hour owing to deposits on the surfaces of the capillary. This source was used with a

[5] Made by the Amersil Company, Inc., Hillside, New Jersey.

Corning filter number 791, which absorbed wavelengths shorter than 2200A. The measurements were corrected for current produced in the photocell $P$ by radiation other than the resonance line 2537A, amounting to about four percent of the total current. This arc was used when a high intrinsic intensity without self-reversal was needed for the measurements of reflection.

The photo-cell $P$ was fabricated of nickel, and its active surfaces were coated with a film of magnesium. The envelope was of glass which transmitted about forty percent at 2537A. The photoelectric current approximately saturated at plus or minus one volt, and the ratio $S$ of the sensitivity when the grid was negative to that with the grid positive was 0.28. The photoelectric currents were measured by an FP54 tube (see Fig. 2) used as an electrometer. The high frequency voltage was kept off the grid of the electrometer tube by a resistance $W$ of $10^{10}$ ohms in series with the capacity to ground of the FP54 grid circuit, the impedance of which at the frequencies used was small compared to $W$. A condenser $M$ of about sixty micro-micro farads completed the alternating current circuit through the photo-cell.

The excitation cell $E$ employed a thermionic cathode, and an anode which consisted of a grid placed close to the cathode and a surrounding nickel mesh. The small distance between the cathode and the grid provided a large space current at low positive anode voltage. The direct anode voltage was 7.6 volts (see Fig. 2), the peak alternating voltage about 8.0 volts, the peak current about 100 milliamperes, and the average current 47 milliamperes. Under these operating conditions the curve of excitation as a function of time approximated half-sine waves. The envelope was of the same high transmission glass as was used for the photo-cell. The vapor pressure in the excitation cell was $1.8\times10^{-4}$ mm, corresponding to 0°C. At this pressure the radiation from the cell had a greater persistence than that which would have resulted from only the single lifetime $1.08\times10^{-7}$ second,[4] owing to the fact that about fifty percent of the radiation from the atoms excited by electron impact was absorbed and re-emitted in the cell.

A comparison of the line widths of the radiation from the sources $E$ and $T$ was made by measurements of absorption with a mercury vapor absorption cell. The absorption coefficient was within four percent of the same value for both sources.

## REFLECTION AND SCATTERING

For the measurement of reflection alone, the apparatus of Fig. 1, described above, was used with both collimators. The ratio of the photoelectric current with the mercury vapor in the quartz cell to the current with the vapor frozen out with liquid nitrogen was measured at different temperatures. This gave the ratio of the reflectivity of the quartz-mercury vapor surface to that of the quartz-vacuum surface. Curve $A$ of Fig. 3 shows this ratio as a function of temperature for an angle of incidence, $\phi$, on the quartz-mercury vapor surface of 28.3°.

To find the variation with temperature of the scattered radiation, similar measurements were made with the photo-cell $P$ placed as close as possible to the furnace window so that it would receive a maximum of scattered radiation in addition to that reflected. The same angle of incidence was used. The result is shown as curve $B$ in Fig. 3. Curve $B$ coincides with $A$ within the precision of measurement (0.5 percent) for temperatures above 300°C, has a minimum at about 200°C, a maximum at 50°C, and falls to zero at low pressures. The variation with temperature of the scattered radiation is given by the difference between curves $A$ and $B$, plotted as curve $C$, the scale of ordinates being shown at the right of the figure. This curve coincides with $B$ below about 100°C. It should be noted, however, that only a fraction of the total scattered radia-

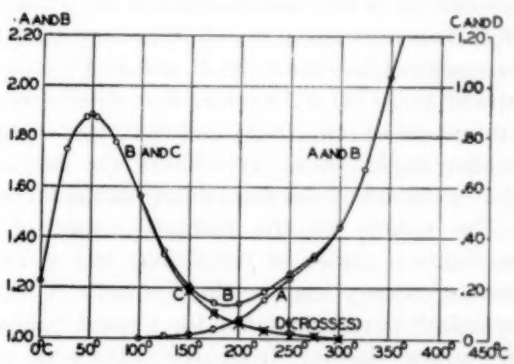


FIG. 3. Curve $A$—reflected radiation. Curve $B$—scattered plus reflected radiation. Curve $C$—difference between $A$ and $B$. Curve $D$—delayed radiation.

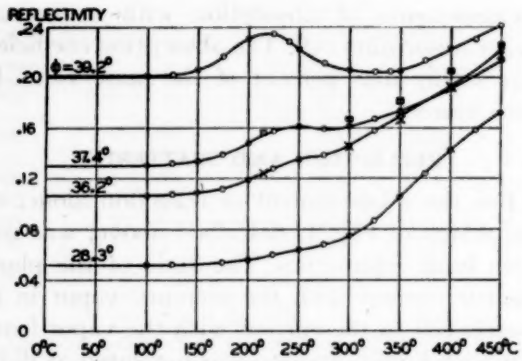


FIG. 4. Reflectivity *vs.* condensed mercury temperature for four values of the angle of incidence $\phi$.

tion is involved in this measurement. This fraction could not be accurately computed since it depended upon the geometry of the system, varying somewhat with the vapor density in the cell.

Curves *C* and *A* show that the effect of the mercury vapor on the reflection was inappreciable (less than 0.5 percent) below 100°C and scattering disappeared (less than 0.5 percent) at 300°C. In the region 150°C to 300°C both were present, though weak, so that most of the energy of the 2537A radiation entering the quartz cell was dissipated in the vapor.

The absolute reflectivity of the quartz-mercury vapor surface was found by multiplying the ordinates of curve *A* by the reflectivity of the quartz-vacuum surface calculated from the index of refraction of the fused quartz. The results are shown in Fig. 4, the reflectivity being plotted as a function of the temperature. Curves for three other values of the angle of incidence, $\phi = 36.2°$, 37.4°, and 39.2°, are also given. These were determined in the same manner as the values for 28.3°. It is interesting to note that the reflectivity for angles of incidence (39.2° and 37.4°) near the critical angle (41.6°) have each a maximum and a minimum of reflectivity and that the curves for smaller angles show reversals of the curvature at approximately the same values of the pressure.

The values for the mercury vapor of the constants $n$ (index of refraction) and $\kappa$ (coefficient of absorption) in the Fresnel's reflection formulas[6] were calculated for several values of the vapor density from the values of total reflectivity obtained for $\phi = 39.2°$ and 28.3°. These values are given in columns four and five of Table I. In the first, second, and third columns are given the temperature, the number of atoms per cubic centimeter, $N$, and $N^{\frac{1}{3}}\lambda$. Here $\lambda$ is the wave-length in the vapor of the 2537A line. In the sixth column is given the distance, $L$, in wave-lengths, in which the intensity of the resonance line was attenuated in the vapor by the factor $e$, as calculated from the values of $\kappa$.

The estimated error in the values of the optical constants was two percent or less for $n$, and for $\kappa$ seven percent at 215°C, and fifteen percent at 400°C. These errors were primarily due to the probable error of 0.3° in determining $\phi$, the effect of which on the optical constants increased with $\phi$ and the reflectivity.

Using the tabulated values of the optical constants, the reflectivities for the angles of incidence 37.4° and 36.2° were calculated. The calculated points for 36.2° are shown in the figure by crosses, which lie close to the experimental curve. The similar points for 37.4° are shown by squares, which lie above the corresponding experimental curve. This discrepancy was attributed to an error of determining the angle $\phi$, and would largely disappear were the angle of incidence increased by 0.4°, which is a little greater than the estimated uncertainty in the measurement of the angle.

The values of $1-n$, $\kappa$, and the reflectivity for $\phi = 28.3°$ are plotted in Fig. 5 as a function of $N^{\frac{1}{3}}\lambda$. From this figure it is seen that the increase of the reflectivity of the surface, caused by the mercury vapor and the attenuation, became measurable at approximately the same density ($N^{\frac{1}{3}}\lambda$ about 5). It shows also that the ratio of

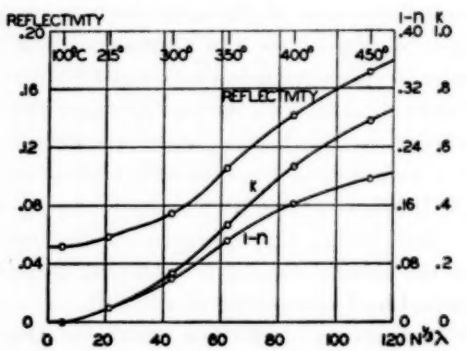


FIG. 5. Reflectivity, $1-n$ and $\kappa$ as a function of $N^{\frac{1}{3}}\lambda$.

[6] M. Born, *Optik* (Edwards Brothers, Inc., Ann Arbor, Michigan, 1943), pp. 29, 260.

$1-n$ to $\kappa$ is almost independent of the increase of vapor pressure. The maxima and minima in the reflectivity curves of Fig. 4 are not dependent upon peculiarities in the variation of $n$ and $\kappa$, but are largely due to the fact that the angles of incidence approach the critical angle.

## PERSISTENCE

The persistence or delay of the radiation, caused by persistence in the quartz cell, was investigated by obtaining ratio-frequency (*R-f*) curves at temperatures ranging from 0°C to 450°C. The results are shown in Fig. 6. The curve marked "aluminum" was taken with an aluminum reflector substituted for the quartz cell. For this curve the only persistence involved was that in the source *E*. When the quartz cell was used, the added persistence, caused by the absorption and re-emission in the cell of some of the radiation from *E*, resulted in a further change in the division between the half-cycles of the illumination of the photo-cell and consequently gave *R-f* curves differing from the aluminum curve. Curves for nine values of the vapor pressure, indicated by the corresponding temperatures, are given in the figure. It is to be noted that as the temperature is increased the curves shift toward lower frequencies until a temperature of approximately 45°C is reached, after which the shift is toward higher frequencies. The 300°C and 450°C curves coincide with the aluminum curve within the precision of measurement of the curves, which was about one-half percent. It will be further noted that the curves differ markedly in shape, especially at the lower frequencies.

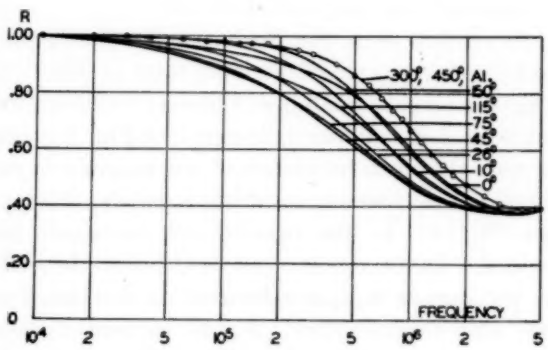


FIG. 6. Observed *R-f* curves for different values of the condensed mercury temperature. Frequency in cycles per second.

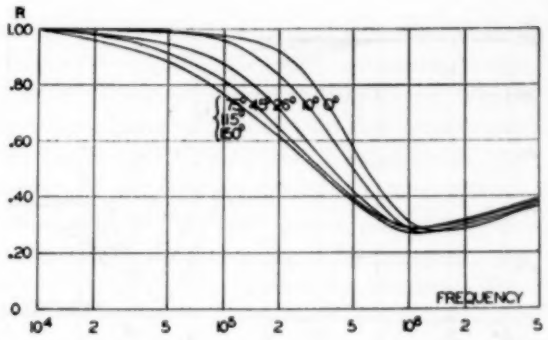


FIG. 7. Observed *R-f* curves for scattered radiation only.

Each of the measured curves, except the aluminum curve, can be considered as the composite of the two curves which would have been obtained if the radiation reflected from the quartz-mercury vapor surface and the radiation absorbed and re-emitted by the vapor in the cell could have been measured separately. The ordinates of the curves are equal to the sum of the corresponding ordinates of these two component curves multiplied by $b$ and $1-b$, respectively, where $b$ is the ratio of the intensity of the reflected energy to the total intensity received by the photo-cell. The values of $b$ for the range 0°C to 150°C were found by measuring the ratio of the photoelectric current with the mercury vapor in the tube to the current when the vapor was frozen out, since below 150°C the reflection was practically the same as from the quartz-vacuum surface. With this data the *R-f* curves, which would have been obtained with the scattered radiation alone, were computed from the curves in Fig. 6, and are shown in Fig. 7. No curves are given for temperatures above 150°C since for these temperatures the scattered radiation was so small a fraction of the total that it was not possible to carry out the calculations with significant results. The 75°C, 115°C, and 150°C curves were indistinguishable, and presumably the curves for the scattered radiation for all higher temperatures would be identical with this limiting curve. Again it will be noted that as the temperature increases the difference between the shape of the curves and of that due to the direct radiation from *E* becomes more marked. This is especially evident in the higher temperature curves in which the ordinates fall off from unity at low frequencies. The precision

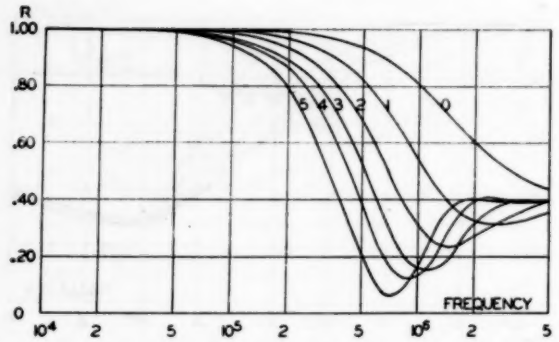


FIG. 8. Calculated *R-f* curves for 0 to 5 absorption re-emission steps.

of the points on the curves of Fig. 7 was estimated to be three percent for the 0°C and 150°C curves, and better for the others.

The maximum of the intensity of the scattered radiation received by the photo-cell occurred at about 50°C (see Fig. 3), which is very nearly the same as the temperature above which all the *R-f* curves have the limiting form and position. For higher temperatures the radiation is absorbed and dissipated in the quartz cell to a large degree, but the relation between the intensity of the radiation which escapes and the elapsed time is apparently unchanged.

It should be noted in discussing Fig. 7 that the forms of these curves for the scattered radiation depend upon the persistence in the source $E$ as well as on the added delays in the quartz cell. The most probable process causing these delays is the simple absorption re-emission process with the lifetime $1.08\times10^{-7}$ second. The explanation of the long persistence as caused by the formation of metastable atoms, which because of collisions of the first kind eventually radiate the resonance line, seems untenable in view of the small probability of this process.[7] Each observed curve is therefore considered as the composite of, first, *R-f* curves for the radiation which, emitted without experiencing absorption and re-emission in $E$, was absorbed and re-emitted once in the quartz cell, second, *R-f* curves for radiation which experienced two absorption re-emission processes in the source and in the quartz cell considered as a single system, third, curves for radiation which experienced three such delays, etc. Since we cannot determine the relative intensity of radiation in each of these groups as is necessary for an exact analysis of the experimental curves, we can only estimate these. In Fig. 8 are shown some *R-f* curves which were calculated from the characteristics of $E$ and the photo-cell. The curve marked *O* is for the radiation emitted by excited atoms which reaches the photo-cell without experiencing absorption. Curve *1* is for radiation which has experienced one absorption re-emission process after its original emission, curve *2* for radiation which has experienced two absorption re-emission steps, etc. From the shape and position of these curves and of those in Fig. 7 it is obvious that for temperatures of 26° and higher a very large number of steps must have been involved if the form of the curves was due solely to these absorption re-emission processes. Computation of such curves as those of Fig. 8 for a large number of steps was impracticable. However, it can be shown that the intensity of radiation from a group of atoms excited at the time $t=0$ and experiencing $m$ absorption re-emission steps will follow the law $t^m e^{-t/\tau}$, where $\tau$ is the lifetime and $m$ is the number of absorption re-emission steps. This expression has a maximum at $t=m\tau$. Since the radiation was excited only during the positive half-cycles, the *R-f* curves will therefore have their minima approximately at the frequencies for which the maxima of $t^m e^{-t/\tau}$ occur one-half period after the excitation, or for $f=1/(2m\tau)$. From this relation it can be estimated that in the case of the limiting curve at least several percent of the radiation must have experienced several hundred absorption re-emission steps. A rough estimate gives the average number of such steps as about 40.

As already seen, the *R-f* curves for aluminum, and for the quartz cell at 450°C and at 300°C in Fig. 6 coincide within 0.5 percent. From the calculated *R-f* curves *0*, *1*, and *2* of Fig. 8 it can be seen that at a frequency of one magacycle the increased persistence resulting from the delay of one lifetime in the quartz cell decreases the ordinate about twenty percent. Since the shift in the curves is approximately proportional to the added persistence, it was estimated from the precision with which the 450°C and 300°C curves were determined, that if any persistence were introduced by the reflection it was less

[7] C. Kenty, Phys. Rev. **42**, 823 (1932).

than one-fortieth of a lifetime. This, together with the fact that the scattered radiation became immeasurable at approximately the same temperature as did persistence of radiation in the quartz cell, leads us to assume that reflection introduces no delay at any temperature.

As an additional check on the behavior of the scattered radiation from the quartz cell in the region 150°C to 300°C, the alternating current method was employed in a somewhat different manner. The ratio, $S$, of the photo-current for negative and positive voltages on the grid of the photo-cell was approximately 0.28, and the persistence of the radiation reflected from the quartz-mercury vapor surface (persistence due only to $E$) resulted in more energy arriving at the photo-cell in the positive half-cycles than in the negative. Hence the reflected radiation $a=a_s\leq\frac{1}{2}$. In this test the phase of the voltage applied to the photo-cell was reversed with respect to that on the excitation cell, so that in the formula for $R$, $S$ was replaced by $1/S$, i.e., $R=1-a_s(1+1/S)=1-4.57a_s$. Hence $R=0$, for the frequency for which $a_s=0.219$. The frequency was then determined for which the photoelectric current was zero with the quartz cell at 300°C, at which temperature there was no measurable persistence in the quartz cell. Using this frequency in the modified circuit, measurements of the photo-current for different vapor pressures were made. The results are shown in Fig. 3 by curve $D$, the observed points being given by crosses. The scale of ordinates of $D$, shown at the right of the figure, is of course arbitrary and was adjusted to coincide with $C$ at 150°C. The two curves are coincident within the precision of measurement. This result agrees with the conclusions that reflection was instantaneous for all pressures, and that the relation between the intensity of the absorbed and re-emitted (scattered) energy and the time which gave the limiting $R$-$f$ curve of Fig. 7 remained unchanged at temperatures above 150°C.

The authors take this opportunity to thank Professor L. J. Hayner for her assistance in this investigation.

PHYSICAL REVIEW VOLUME 72, NUMBER 4 AUGUST 15, 1947

# The Electromagnetic Shift of Energy Levels

H. A. BETHE
*Cornell University, Ithaca, New York*
(Received June 27, 1947)

BY very beautiful experiments, Lamb and Retherford[1] have shown that the fine structure of the second quantum state of hydrogen does not agree with the prediction of the Dirac theory. The $2s$ level, which according to Dirac's theory should coincide with the $2p_{\frac{1}{2}}$ level, is actually higher than the latter by an amount of about 0.033 $cm^{-1}$ or 1000 megacycles. This discrepancy had long been suspected from spectroscopic measurements.[2,3] However, so far no satisfactory theoretical explanation has been given. Kemble and Present, and Pasternack[4] have shown that the shift of the $2s$ level cannot be explained by a nuclear interaction of reasonable magnitude, and Uehling[5] has investigated the effect of the "polarization of the vacuum" in the Dirac hole theory, and has found that this effect also is much too small and has, in addition, the wrong sign.

Schwinger and Weisskopf, and Oppenheimer have suggested that a possible explanation might be the shift of energy levels by the interaction of the electron with the radiation field. This shift comes out infinite in all existing theories, and has therefore always been ignored. However, it is possible to identify the most strongly (linearly) divergent term in the level shift with an electromagnetic *mass* effect which must exist for a bound as well as for a free electron. This effect should

[1] Phys. Rev. **72**, 241 (1947).
[2] W. V. Houston, Phys. Rev. **51**, 446 (1937).
[3] R. C. Williams, Phys. Rev. **54**, 558 (1938).
[4] E. C. Kemble and R. D. Present, Phys. Rev. **44**, 1031 (1932); S. Pasternack, Phys. Rev. **54**, 1113 (1938).
[5] E. A. Uehling, Phys. Rev. **48**, 55 (1935).

properly be regarded as already included in the observed mass of the electron, and we must therefore subtract from the theoretical expression, the corresponding expression for a free electron of the same average kinetic energy. The result then diverges only logarithmically (instead of linearly) in non-relativistic theory: Accordingly, it may be expected that in the hole theory, in which the *main* term (self-energy of the electron) diverges only logarithmically, the result will be *convergent* after subtraction of the free electron expression.[6] This would set an effective upper limit of the order of $mc^2$ to the frequencies of light which effectively contribute to the shift of the level of a bound electron. I have not carried out the relativistic calculations, but I shall assume that such an effective relativistic limit exists.

The ordinary radiation theory gives the following result for the self-energy of an electron in a quantum state $m$, due to its interaction with transverse electromagnetic waves:

$$W=-(2e^2/3\pi hc^3)\times\int_0^K kdk\sum_n|\mathbf{v}_{mn}|^2/(E_n-E_m+k), \quad (1)$$

where $k=h\omega$ is the energy of the quantum and $\mathbf{v}$ is the velocity of the electron which, in non-relativistic theory, is given by

$$\mathbf{v}=\mathbf{p}/m=(h/im)\nabla. \quad (2)$$

Relativistically, $\mathbf{v}$ should be replaced by $c\boldsymbol{\alpha}$ where $\boldsymbol{\alpha}$ is the Dirac operator. Retardation has been neglected and can actually be shown to make no substantial difference. The sum in (1) goes over all atomic states $n$, the integral over all quantum energies $k$ up to some maximum $K$ to be discussed later.

For a free electron, $\mathbf{v}$ has only diagonal elements and (1) is replaced by

$$W_0=-(2e^2/3\pi hc^3)\int kdk\mathbf{v}^2/k. \quad (3)$$

This expression represents the change of the kinetic energy of the electron for fixed momentum, due to the fact that electromagnetic mass is added to the mass of the electron. This electromagnetic mass is already contained in the experimental electron mass; the contribution (3) to the energy should therefore be disregarded. For a bound electron, $\mathbf{v}^2$ should be replaced by its expectation value, $(\mathbf{v}^2)_{mm}$. But the matrix elements of $\mathbf{v}$ satisfy the sum rule

$$\sum_n|\mathbf{v}_{mn}|^2=(\mathbf{v}^2)_{mm}. \quad (4)$$

Therefore the relevant part of the self-energy becomes

$$W'=W-W_0=+\frac{2e^2}{3\pi hc^3}\times\int_0^K dk\sum_n\frac{|\mathbf{v}_{mn}|^2(E_n-E_m)}{E_n-E_m+k}. \quad (5)$$

This we shall consider as a true shift of the levels due to radiation interaction.

It is convenient to integrate (5) first over $k$. Assuming $K$ to be large compared with all energy differences $E_n-E_m$ in the atom,

$$W'=\frac{2e^2}{3\pi hc^3}\sum_n|\mathbf{v}_{mn}|^2(E_n-E_m)\ln\frac{K}{|E_n-E_m|}. \quad (6)$$

(If $E_n-E_m$ is negative, it is easily seen that the principal value of the integral must be taken, as was done in (6).) Since we expect that relativity theory will provide a natural cut-off for the frequency $k$, we shall assume that in (6)

$$K\approx mc^2. \quad (7)$$

(This does not imply the same limit in Eqs. (2) and (3).) The argument in the logarithm in (6) is therefore very large; accordingly, it seems permissible to consider the logarithm as constant (independent of $n$) in first approximation.

We therefore should calculate

$$A=\sum_n A_{nm}=\sum_n|\mathbf{p}_{nm}|^2(E_n-E_m). \quad (8)$$

This sum is well known; it is

$$A=\sum|\mathbf{p}_{nm}|^2(E_n-E_m)=-h^2\int\psi_m^*\nabla V\cdot\nabla\psi_m d\tau$$
$$=\tfrac{1}{2}h^2\int\nabla^2V\psi_m^2d\tau=2\pi h^2e^2Z\psi_m^2(0), \quad (9)$$

[6] It was first suggested by Schwinger and Weisskopf that hole theory must be used to obtain convergence in this problem.

for a nuclear charge $Z$. For any electron with angular momentum $l \neq 0$, the wave function vanishes at the nucleus; therefore, the sum $A=0$. For example, for the $2p$ level the negative contribution $A_{1S,2P}$ balances the positive contributions from all other transitions. For a state with $l=0$, however,

$$\psi_m^2(0) = (Z/na)^3/\pi, \tag{10}$$

where $n$ is the principal quantum number and $a$ is the Bohr radius.

Inserting (10) and (9) into (6) and using relations between atomic constants, we get for an $S$ state

$$W_{ss}' = \frac{8}{3\pi}\left(\frac{e^2}{hc}\right)^3 \mathrm{Ry}\frac{Z^4}{n^3}\ln\frac{K}{\langle E_n - E_m\rangle_{Av}}, \tag{11}$$

where Ry is the ionization energy of the ground state of hydrogen. The shift for the $2p$ state is negligible; the logarithm in (11) is replaced by a value of about $-0.04$. The average excitation energy $\langle E_n - E_m\rangle_{Av}$ for the $2s$ state of hydrogen has been calculated numerically[7] and found to be 17.8 Ry, an amazingly high value. Using this figure and $K=mc^2$, the logarithm has the value 7.63, and we find

$$W_{ss}' = 136\ln[K/(E_n - E_m)]$$
$$= 1040 \text{ megacycles}. \tag{12}$$

This is in excellent agreement with the observed value of 1000 megacycles.

A relativistic calculation to establish the limit $K$ is in progress. Even without exact knowledge of $K$, however, the agreement is sufficiently good to give confidence in the basic theory. This shows

(1) that the level shift due to interaction with radiation is a real effect and is of finite magnitude,

(2) that the effect of the infinite electromagnetic mass of a point electron can be eliminated by proper identification of terms in the Dirac radiation theory,

(3) that an accurate experimental and theoretical investigation of the level shift may establish relativistic effects (e.g., Dirac hole theory). These effects will be of the order of unity in comparison with the logarithm in Eq. (11).

If the present theory is correct, the level shift should increase roughly as $Z^4$ but not quite so rapidly, because of the variation of $\langle E_n - E_m\rangle_{Av}$ in the logarithm. For example, for $He^+$, the shift of the $2s$ level should be about 13 times its value for hydrogen, giving 0.43 $cm^{-1}$, and that of the $3s$ level about 0.13 $cm^{-1}$. For the x-ray levels L$I$ and L$II$, this effect should be superposed upon the effect of screening which it partly compensates. An accurate theoretical calculation of the screening is being undertaken to establish this point.

This paper grew out of extensive discussions at the Theoretical Physics Conference on Shelter Island, June 2 to 4, 1947. The author wishes to express his appreciation to the National Academy of Science which sponsored this stimulating conference.

[7] I am indebted to Dr. Stehn and Miss Steward for the numerical calculations.

PHYSICAL REVIEW VOLUME 72, NUMBER 4 AUGUST 15, 1947

# Spectral Location of the Absorption Due to Color Centers in Alkali Halide Crystals

HENRY F. IVEY
*Research Laboratory, Westinghouse Electric Corporation, Bloomfield, New Jersey*

(Received June 2, 1947)

SEITZ[1] has recently published a paper summarizing the properties of the absorption bands arising from electrons trapped in the lattice of alkali halide crystals. The present writer is not aware of the existence of a compilation of data on the spectral location of these various bands. Table I was prepared to collect this information. The terminology for the bands is that used by Seitz. In this respect it is of interest to point out that the band designated by Seitz as the $M$-band (after Molnar) has been called the $O$-band (after Ottmer) by Kalabuchov.[2]

In addition to the $F$-, $R_1$-, $R_2$-, and $M$-bands occurring in the pure alkali halides, Table I also

[1] F. Seitz, Rev. Mod. Phys. **18**, 384 (1946).

[2] N. Kalabuchov, J. Phys. U.S.S.R. **9**, 41 (1945).

TABLE I. Spectral location of the absorption in alkali halide crystals.

| Inter-ionic salt distance,[a] $d$ (Angstroms) | | Location of absorption peak (Angstroms) (Values in parentheses are calculated) | | | | |
|---|---|---|---|---|---|---|
| | | $U$-Band | $F$-Band | $R_1$-Band | $R_2$-Band | $M$-Band |
| LiF | 2.01 | (1320) | (2540)<br>2570[e]<br>2500[d-f] | (2950) | (3200)<br>3100[e]<br>3060[d] | (4160)<br>4440[e] |
| LiCl | 2.57 | (1740) | (3980)<br>3850[d, f] | (4620) | (5000)<br>5800[d] | (6100)<br>6500[d] |
| LiBr | 2.75 | (1870) | (4520) | (5250) | (5680) | (6790) |
| LiI | 3.00 | (2060) | (5310) | (6160) | (6670) | (7770) |
| NaF | 2.31 | (1550) | (3280)<br>3410[e]<br>3350[d]<br>3400[f] | (3810) | (4120)<br>4150[d] | (5160)<br>5050[e]<br>5100[d] |
| NaCl | 2.81 | (1920)<br>1920[b] | (4710)<br>4580[e]<br>4700[d]<br>4650[f] | (5470)<br>5450*[e] | (5920)<br>5960*[e] | (7010)<br>7250[e]<br>7200[d]<br>7050[b] |
| NaBr | 2.98 | (2040)<br>2100[b] | (5250)<br>5400[d, f] | (6100) | (6600) | (7700) |
| NaI | 3.23 | (2230) | (6090)<br>5880[f] | (7070) | (7650) | (8710) |
| KF | 2.67 | (1810) | (4280)<br>4550[d, f] | (4970) | (5380)<br>5700[g] | (6480) |
| KCl | 3.14 | (2160)<br>2140[b] | (5760)<br>5560[e]<br>5630[d, f] | (6690)<br>6580*[e] | (7250)<br>7270*[e] | (8350)<br>8250[e]<br>8200[d] |
| KBr | 3.29 | (2280)<br>2280[b] | (6300)<br>6250[e]<br>6300[d, f] | (7320)<br>7350*[e] | (7920)<br>7900*[e] | (8970)<br>8920*[e]<br>9200[b] |
| KI | 3.53 | (2460)<br>2440[b] | (7180)<br>6890[e]<br>7200[d]<br>6850[f] | (8340) | (9020) | (10,000) |
| RbF | 2.82 | (1930) | (4740) | (5500) | (5950) | (7070) |
| RbCl | 3.27 | (2260)<br>2300[b] | (6230)<br>6090[d]<br>6240[f] | (7240) | (7830) | (8890) |
| RbBr | 3.43 | (2380)<br>2420[b] | (6800)<br>6940[e]<br>7200[g] | (7900)<br>8050*[e] | (8550)<br>8590*[e] | (9560)<br>9570*[e] |
| RbI | 3.66 | (2560) | (7630)<br>7560[e]<br>7750[f] | (8850) | (9590) | (10,600) |
| CsF | 3.00 | (2060) | (5310) | (6160) | (6670) | (7770) |
| CsCl | 3.56 (s.c.) | | 6200[g] | | | |
| CsBr | 3.71 (s.c.) | | | | | |
| CsI | 3.95 (s.c.) | | | | | |

* Indicates a measurement at −180°C.
(s.c.)=simple cubic.

[a] F. Seitz, *The Modern Theory of Solids* (McGraw-Hill, Book Company, New York, 1940).
[b] R. Hilsch and R. W. Pohl, as quoted by J. H. de Boer, *Electron Emission and Adsorption Phenomena*, p. 277.
[c] See reference 3 in text.
[d] R. Ottmer, Zeits. f. Physik **46**, 798 (1928).
[e] See reference 4 in text.
[f] See reference 6 in text.
[g] This approximate value was taken from a figure given by R. W. Pohl, Proc. Phys. Soc. London **49** (extra part, p. 3) (1937).
[h] See reference 2 in text.

includes data for the $U$-band which arises when hydrogen enters into solid solution with the alkali halides, replacing halogen ions. Some of the measurements reported were made at −180°C, the corresponding values of wave-length at room temperature will be higher by about 100 or 200A than those listed. In addition to the bands tabulated, Molnar[3] found an additional band (with properties similar to the $R$-bands) in NaCl at 8230A (measured at −180°C). Schneider[4] also reported an additional band in LiF at 5200A.

Since the location of all the bands has not yet been measured, estimated values of those as yet unmeasured would be of interest. Fröhlich,[5] from theoretical considerations concerning the $F$-band, derived the relation

$$\nu_{max} d^2 = h/16m = 0.45 \text{ cm}^2\text{-sec.}^{-1}, \quad (1)$$

where $\nu_{max}$ is the frequency of maximum absorption, $d$ is the inter-ionic distance (lattice constant) of the salt considered (in cm), $h$ is Planck's constant, and $m$ is the electronic mass. Mollwo[6] reported that his experimental data agreed with an equation of this form with a constant of 0.50 cm²-sec.⁻¹. If Eq. (1) is rewritten in terms of wave-length, one obtains

$$\lambda_{max} = 667 d^2 \text{A}, \quad (2)$$

where the value of $d$ is now given in angstroms. The writer has fitted empirical equations of this same general type to the data compiled in the table and obtained the following relations[7]

$$U: \quad \lambda_{max} = 615 d^{1.10} \text{A}, \quad (3)$$

$$F: \quad \lambda_{max} = 703 d^{1.84} \text{A}, \quad (4)$$

$$R_1: \quad \lambda_{max} = 816 d^{1.84} \text{A}, \quad (5)$$

$$R_2: \quad \lambda_{max} = 884 d^{1.84} \text{A}, \quad (6)$$

$$M: \quad \lambda_{max} = 1400 d^{1.56} \text{A}. \quad (7)$$

These formulas (and that of Fröhlich above) apply only to those alkali halides crystallizing in the face-centered cubic structure and not to

[3] J. P. Molnar, M.I.T. Ph.D. Thesis, Physics Dept. (October, 1940). The writer is indebted to Dr. Molnar for his kind permission to use his previously unpublished data.
[4] E. G. Schneider, J. Opt. Soc. Am. **27**, 72 (1937).
[5] H. Fröhlich, Zeits. f. Physik, **80**, 819 (1933).
[6] E. Mollwo, as reported by Pohl in reference (3).
[7] These equations were first presented in a Ph.D. Thesis to the M.I.T. Physics Dept., June, 1944.

CsCl, CsBr, and CsI, which have simple cubic structures.

The values enclosed in parentheses in the table are those calculated from the above equations. In the case of the *F*-band the mean error is 130 angstroms, which is less than that for Mollwo's relation. The most serious point of disagreement is in the case of the *R*- and *M*-bands for LiCl. In the case of LiF, the "secondary maxima" reported lie between the predicted $R_1$ and $R_2$ values, possibly indicating that the two separate bands were not resolved. The good agreement in the case of the *U*-band indicates that the claim of Hughes[8] that this band can be represented by an equation of the general type considered here with an exponent of two is certainly in error.

Although no attempt is made to justify the equations presented here on a theoretical basis, the equality of the exponent in the case of the *F*- and *R*-bands seems more than fortuitous. According to the pictures suggested by Seitz,[1] these three bands arise from absorbing centers involving only halogen-ion vacancies in the crystal lattice, while the *M*- and *U*-bands involve an alkali-ion vacancy and a negative hydrogen ion, respectively.

[8] A. L. Hughes, Rev. Mod. Phys. **8**, 294 (1936).

The fact that the spectral location of all the observed absorption bands depends only on the lattice constant (and on the temperature) suggests an interesting possibility. Since solid solutions of the various alkali halides will have lattice constants intermediate to those of the parent salts, it would seem plausible that the position of the absorption peaks could be changed at will, simply by varying the composition of such mixed crystals. This might possibly be of value in the application of this absorption phenomenon to practical problems such as the Skiatron.[9] So far as the writer is aware, no work on color centers in solid solutions of the alkali halides has been reported.

Another interesting implication of the empirical relations presented here is that the absorption spectra due to color centers in LiI and CsF, which have identical lattice constants, should be indistinguishable as far as spectral location is concerned. At present very little is known concerning the variation of the relative intensities and the permanency of the various bands from one salt to another.

[9] A. H. Rosenthal, Proc. Inst. Rad. Eng. **28**, 203 (1940). H. W. Leverenz, R.C.A. Review **7**, 199 (1946). See also Vol. V of the M.I.T. Radiation Laboratory Technical Series to be published.

# Letters to the Editor

*PUBLICATION of brief reports of important discoveries in physics may be secured by addressing them to this department. The closing date for this department is five weeks prior to the date of issue. No proof will be sent to the authors. The Board of Editors does not hold itself responsible for the opinions expressed by the correspondents. Communications should not exceed 600 words in length.*

## Nuclear and Molecular Constants from Microwave Spectra: Methyl Chloride and Methyl Bromide*

WALTER GORDY, JAMES W. SIMMONS, AND A. G. SMITH
*Department of Physics, Duke University, Durham, North Carolina*
July 7, 1947

THE first rotational transition, $J=0$ to $J=1$, of $CH_3Cl^{35}$ and of $CH_3Cl^{37}$ and the second transition, $J=1$ to $J=2$, of $CH_3Br^{79}$ and of $CH_3Br^{81}$ have been measured and analyzed. The detecting system used and the method of analysis have been described in previous notes.[1]

As in methyl iodide,[1] hyperfine structure caused by the nuclear quadrupole moments of the halogens was observed for both methyl chloride and methyl bromide. Figures 1 and 2 give comparisons of the calculated and observed hyperfine patterns. The quadrupole coupling factors, $eQ(\partial^2V/\partial z^2)$, determined from the line spacings are listed in Table I,

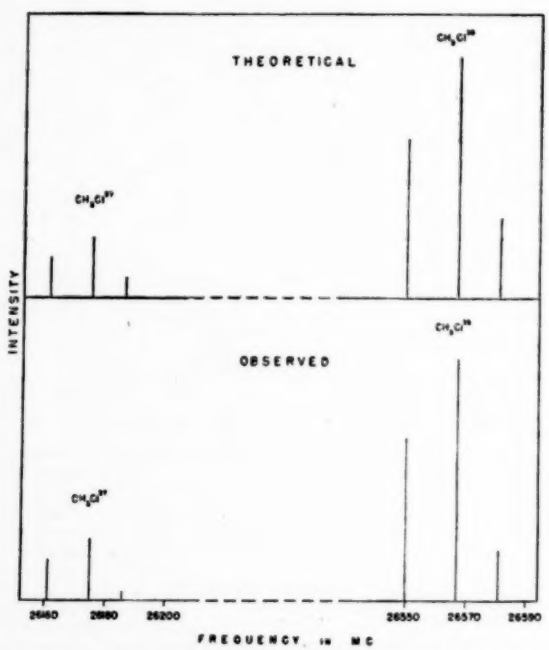


FIG. 1. Calculated and observed hyperfine structure for the $J=0$ to $J=1$ rotational transition of methyl chloride.

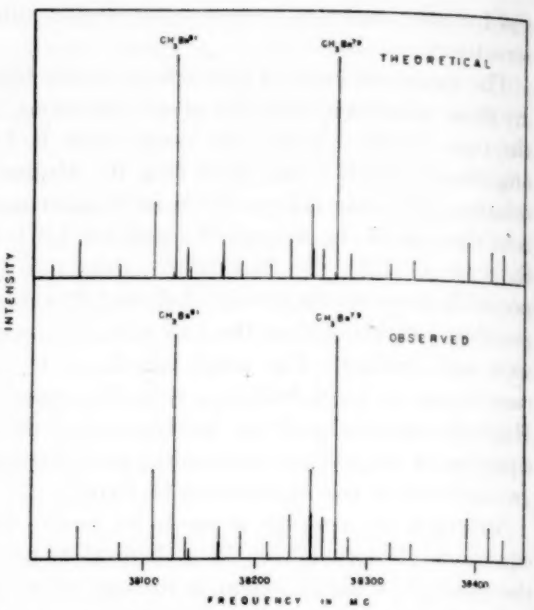


FIG. 2. Calculated and observed hyperfine structure for the $J=1$ to $J=2$ rotational transition of methyl bromide.

where the corresponding coefficients for BrCN and ClCN are given for comparison.

In order to evaluate nuclear quadrupole moments from microwave hyperfine structure the factor $\partial^2V/\partial z^2$ must be determined from other sources. Recently Townes[2] has suggested that for heavy atoms covalently bonded by $p$-orbitals this factor can be calculated from atomic fine structure separations by the same formula[3] as that used in the determinations of quadrupole moments from atomic spectra. In his evaluation of the quadrupole moments of bromine and chlorine from BrCN and ClCN he assumed that the effects of the double-bond character on $\partial^2V/\partial z^2$ in these molecules can be neglected. The comparisons in Table I indicate that this assumption is hardly justified. Since the almost normal bond length of the methyl halides indicate that they are not complicated by appreciable resonance, the atomic spectra determination of $\partial^2V/\partial z^2$

TABLE I. Quadrupole coupling factors.

| Molecule | Nucleus | $\partial^2V/\partial z^2$ (e.s.u.) | Quadrupole coupling $eQ\partial^2V/\partial z^2$ | Quadrupole moment ($Q$ in cm$^2$) |
|---|---|---|---|---|
| $CH_3Cl$ | $Cl^{35}$ | | 69 | $-0.055\times10^{-24}$ |
| | $Cl^{37}$ | | 56 | $-0.045\times10^{-24}$ |
| ClCN | $Cl^{35}$ | $17\times10^{15}$ (a) | 84 (a) | $-0.067\times10^{-24}$ (a) |
| | $Cl^{37}$ | $17\times10^{15}$ (a) | 64 (a) | $-0.051\times10^{-24}$ (a) |
| $CH_3Br$ | $Br^{79}$ | | 573 | $0.17\times10^{-24}$ |
| | $Br^{81}$ | | 485 | $0.14\times10^{-24}$ |
| BrCN | $Br^{79}$ | $48\times10^{15}$ (a) | 720 (a), (670) (b) | $0.21\times10^{-24}$ (a) |
| | $Br^{81}$ | $48\times10^{15}$ (a) | 556 (a), (567) (b) | $0.16\times10^{-24}$ (a) |

[a] From C. H. Townes, ref. 2.
[b] From W. Gordy, W. V. Smith, A. G. Smith, and H. Ring, Phys. Rev. (to be published).

should be more applicable to them than to the halogen cyanides, in which structures of the type $X^+=C=N^-$ contribute significantly to the ground state. Hence, we have evaluated the quadrupole moments of the bromine and chlorine nuclei from our measurements on $CH_3Br$ and $CH_3Cl$, using the $\partial^2V/\partial z^2$ values as determined by Townes.[3] These are also listed in the table.

The moments of inertia, $I_B$, for the lowest vibrational state are: for $CH_3Cl^{35}$, $63.1\times10^{-40}$ g-cm²; for $CH_3Cl^{37}$, $64.0\times10^{-40}$ g-cm²; for $CH_3Br^{79}$, $87.5\times10^{-40}$ g-cm²; and for $CH_3Br^{81}$, $87.9\times10^{-40}$ g-cm². The smaller moments of inertia, $I_A$, in these molecules cannot be determined from pure rotation spectra but have been evaluated to three places from infra-red vibration-rotation spectra. Assuming the CH lengths equal to those in methane and the Hal−C−H angle that determined from the infra-red $I_A$ values, the above $I_B$ values yield 1.79A for the C−Cl length in methyl chloride and 1.94A for the C−Br length in methyl bromide. If a tetrahedral angle, 109° 28′ is assumed for the angle Hal−C−H, the resulting distances would be 1.78A for C−Cl and 1.93A for C−Br.

* The research described in this report was supported by Contract No. W-28-099-ac-125 with the Army Air Forces, Watson Laboratories, Air Materiel Command.

[1] W. Gordy and M. Kessler, Phys. Rev. **71**, 640 (1947); W. Gordy, A. G. Smith, and J. W. Simmons, Phys. Rev. (to be published).
[2] C. H. Townes, Phys. Rev. **71**, 909 (1947).
[3] H. A. Bethe and R. F. Bacher, Rev. Mod. Phys. **8**, 226 (1936).

## Density of Surface States on Silicon Deduced from Contact Potential Measurements

W. H. Brattain and W. Shockley
*Bell Telephone Laboratories, Murray Hill, New Jersey*
July 3, 1947

THE contact potentials of several $N$ and $P$-type silicon surfaces have been measured. The respective numbers of donator and acceptor impurities in each sample were determined by measuring the electrical conductivity and Hall constant. A correlation was found between impurity concentration and contact potential. Each surface was ground flat and then sand-blasted lightly with 180 mesh silicon carbide. The contact potential was then measured in air, in vacuum after heat treatment to 400°C, in high purity $N_2$ and finally in air again. The results are given in Table I. The reference surface was platinum, which probably had a work function between 4 and 5 volts. The data given are averages of several runs and should be accurate to approximately 0.02 volts.

One might expect a contact potential difference between $N$ and $P$-type silicon slightly less than the width of the energy gap in silicon (1.2 volts). That this is not the case has already been reported by W. E. Meyerhof.[1] An explanation of the latter result based on surface states has been given by J. Bardeen.[2] On the basis of the surface state picture one would expect the contact potential between $N$ and $P$-type silicon to increase as the respective impurity concentration was increased approaching 1.2 volts as a limit. The data in Table I shows that after heat treatment in vacuum the contact potential difference between the two types does increase and the difference between $P$-type silicon ($5.7\times10^{20}$ acceptors) and $N$-type silicon ($1.9\times10^{20}$ donators) is the order of 0.6 volts. From these data one can

Table I. Contact potential in volts.

| Type | Impurity $N/cm^3$ | In air after sandblast | In vacuum after heat treatment | After letting in $N_2$ | After exposure to air |
|---|---|---|---|---|---|
| $P$ | $5.7\times10^{20}$ | +0.31 | −0.27 | −0.19 | +0.07 |
| $P$ | $1.5\times10^{20}$ | +0.35 | −0.18 | −0.10 | +0.13 |
| $P$ | $6.5\times10^{18}$ | +0.30 | −0.10 | −0.09 | +0.17 |
| $P$ | $3.1\times10^{17}$ | +0.34 | +0.04 | +0.14 | +0.28 |
| $N$ | $6.9\times10^{18}$ | +0.32 | +0.16 | +0.27 | +0.34 |
| $N$ | $2.3\times10^{19}$ | +0.37 | +0.27 | +0.35 | +0.39 |
| $N$ | $1.9\times10^{20}$ | +0.37 | +0.30 | +0.37 | +0.37 |

estimate the density of surface states in silicon to be approximately $10^{14}$ per volt per cm², when the surface has been treated in the above manner. The free silicon surface behaves in air as though the density of surface levels were increased by several orders of magnitude.

[1] W. E. Meyerhof, Phys. Rev. **71**, 727 (1947).
[2] J. Bardeen, Phys. Rev. **71**, 717 (1947).

## Evidence for Surface States on Semiconductors from Change in Contact Potential on Illumination

W. H. Brattain
*Bell Telephone Laboratories, Murray Hill, New Jersey*
July 3, 1947

ON the basis of the surface state picture[1] one expects a double layer at the free surface of a semiconductor, the excess charge in the surface states being compensated by an equal and opposite space charge in the semiconductor. At low temperatures it should take an appreciable time for this equilibrium to be established between the surface states and the space charge region. Consequently, electrons or holes excited by absorption of light near the surface should upset this equilibrium making the surface state charge more positive for $N$-type semiconductors and more negative for $P$-type semiconductors, thus changing the contact potential when the surface is exposed to light. The experiment suggested has been done on silicon surfaces of both $N$ and $P$ type and on an $N$-type germanium surface. The contact potential changes due to light exposure at approximately 120°K were +0.12 volts for $N$-type silicon, −0.08 volts for $P$-type silicon, and +0.02 volts for $N$-type germanium. The changes have the predicted sign. The change appeared to be instantaneous on exposure of the surface to light. The return to the equilibrium condition in the dark appeared to have a time constant of the order of a few seconds. No change in contact potential with exposure to light was found at room temperature. The dependence of this effect on temperature, light intensity, and a determination of the time constant are in progress.

[1] J. Bardeen, Phys. Rev. **71**, 717 (1947).

## Note on the Disintegration Energies of $Na^{24}$ and $Al^{28}$

WALTER H. BARKAS
*Office of Naval Research, San Francisco Branch, San Francisco, California*
July 7, 1947

SIEGBAHN[1] and others[2] have presented rather complete evidence that the disintegration energy of $Na^{24}$ is in the neighborhood of 5.53 Mev. It has been stated[3] that this figure is not in agreement with the writer's[4] calculations, and an alternative level scheme has been proposed which provides a disintegration energy of 4.15 Mev.

The mass of $Na^{24}$ calculated in ref. (4) is referred to the mass scale of Livingston and Bethe,[5] while ref. (3) has compared this figure with one calculated on a revised scale. For the present purpose such a comparison of absolute masses is incorrect. Relevant comparisons may, however, be made of the $Na^{24}-Mg^{24}$ mass differences.

The disintegration energy of $Na^{24}$ obtained in ref. (4) was 5.0 Mev. This was calculated as follows:

$$(N-H^1)+4L+\Delta T+\Delta C$$
$$=0.80+8.32+1.10-4.87=5.35 \text{ mMU}=5.0 \text{ Mev}.$$

In this calculation $(N-H^1)$ is the neutron-hydrogen mass difference, $L$ is the empirical function $L(A)$ derived in ref. (4), $\Delta T$ is the increment of kinetic energy entailed by the difference of isotopic spin, and $\Delta C$ is the corresponding decrement in coulomb energy. The figures for $(N-H^1)$ and $\Delta C$ are probably reliable. The divergence of 0.53 Mev between the calculated and experimental disintegration energies is accountable by assuming an error of six percent in $L$ or fifty percent in $\Delta T$ (a minor, poorly known term). Probably each is uncertain to about this degree, and Wigner and Feenberg[6] have now, in fact, obtained somewhat different estimates of these terms. Accuracy only to one mMU was originally indicated in ref. (4). Despite this amount of uncertainty, the calculated figure definitely favors the level structure of Siegbahn.

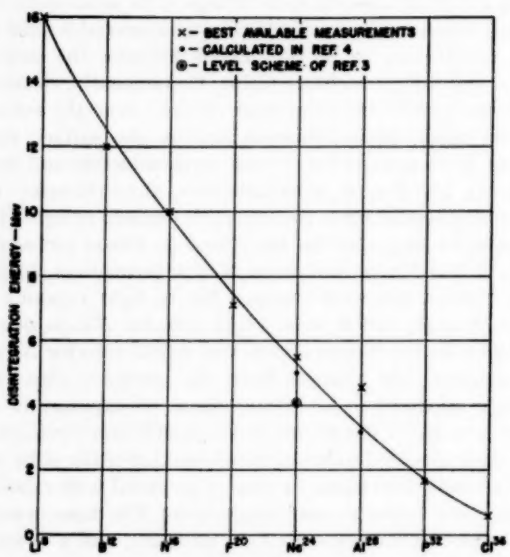


FIG. 1. Disintegration energies of nuclei decaying into products of alpha particle type. The curve is not extended to mass number forty because the existence of a shell discontinuity at that point is well known.

The question of the disintegration energy of $Na^{24}$ may also be approached by examining the behavior of adjacent nuclei having corresponding symmetry. If the basic ideas of ref. (4) approximate reality, we should expect such disintegration energies to vary smoothly with mass number, except that nuclear shells may be revealed by discontinuities.

In Fig. 1 are plotted the disintegration energies of isobars decaying into alpha-particle type nuclei. For the disintegration energies of $Li^6$, $B^{12}$, $N^{16}$, $F^{20}$, $P^{32}$, and $Cl^{36}$, there has been sufficient accord in the recent literature so that we have entered points in these instances without further discussion. It will be seen that the plotted points for these nuclei fall close to a smooth curve, and that the result of Siegbahn for $Na^{24}$ also fits in well with the general trend of disintegration energies.

While the old[6] value (3.3 Mev) for the disintegration energy of $Al^{28}$ would also fall on the smooth locus, recent results of Bleuler and Zünti[7] supported by other evidence[8] lead to a disintegration energy for $Al^{28}$ of about 4.55 Mev. The disintegration seems to consist of a beta-ray of 2.75 Mev followed by a gamma-ray of 1.8 Mev in cascade.

In summary, whereas no anomaly seems now to be presented by the disintegration energy of $Na^{24}$, recent results for the disintegration energy of $Al^{28}$ are higher than anticipated by one Mev or more. If confirmed, these data indicate either a significant deficiency in the postulates of ref. (4) or the presence of an additional unsuspected shell closure.

[1] K. Siegbahn, Phys. Rev. **70**, 127 (1946).
[2] L. G. Elliot, M. Deutsch, and A. Roberts, Phys. Rev. **61**, 99 (1942); A. Wattenberg, Phys. Rev. **71**, 497 (1947); C. E. Mandeville, Phys. Rev. **63**, 387 (1943); E. C. Barker, Phys. Rev. **71**, 453 (1947); C. S. Cook, E. Jurney, and L. M. Langer, Phys. Rev. **70**, 985 (1946).
[3] R. G. Sachs, Phys. Rev. **70**, 572 (1946).
[4] W. H. Barkas, Phys. Rev. **55**, 591 (1939).
[5] M. S. Livingston and H. A. Bethe, Rev. Mod. Phys. **9**, 245 (1937).
[6] E. P. Wigner and E. Feenberg, Reports on Progress in Physics, **VIII**, 274 (The Physical Society, London, 1941).
[7] E. Bleuler and W. Zünti, Helv. Phys. Acta **20**, 195 (1947).
[8] J. Itoh, Proc. Phys.-Math. Soc. Japan **23**, 605 (1941); Y. Watase, Proc. Phys. Math. Soc. Japan **23**, 618 (1941); S. Eklund and N. Hole, Ark. Mat. Astr. Fys. **29A**, 4 No. 26 (1943).

## Cavity Accelerator for Electrons*

H. L. SCHULTZ, R. BERINGER, C. L. CLARKE, J. A. LOCKWOOD, R. L. MCCARTHY, C. G. MONTGOMERY, P. J. RICE, AND W. W. WATSON
*Sloane Physics Laboratory, Yale University, New Haven, Connecticut*
July 5, 1947

A LINEAR electron accelerator employing a series of cavity resonators is under construction in this laboratory. Unlike accelerators thus far described, the cavities are mutually uncoupled. Frequency and phase coherence in the separate cavities are provided by a master oscillator driving a set of power amplifiers, each of which excites a single cavity. The phase of the fields in each cavity is adjustable independently of the other cavities by a phase shifter between the oscillator and the amplifier.

The system is designed for pulse operation at 580 Mc/sec., that being about the highest frequency at which high power amplifiers were available when this work was

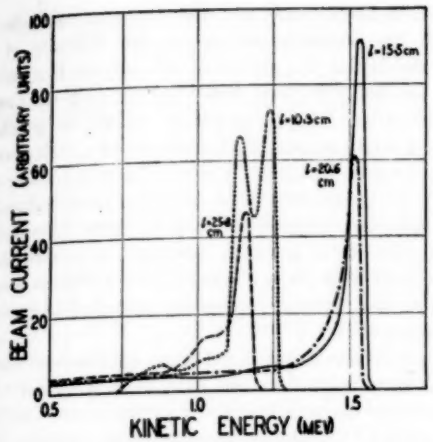


FIG. 1. Theoretical energy spectra for electrons from a $TM_{010}$ mode cavity operating at 580 Mc/sec. idealized for a constant peak power of 400 kw dissipated in the cavity; continuous injection at 10 kev; cavity lengths $l$ as noted.

begun. Grounded-grid triodes, type X126P, are being used as oscillators and amplifiers and are capable of peak powers of as much as 600 kw. These tubes and much useful design information have been generously supplied by the Federal Telephone and Radio Corporation.

The cavities are circular cylinders operating in the $TM_{010}$ mode which provides an axial accelerating field. They are mounted coaxially and form a self-supporting vacuum chamber. The electron beam will traverse the axis, passing into each cavity through a small hole in the end plate. In preliminary tests full-scale cavities have been excited with an amplifier operating at low power levels, and it is found that the frequency and phase of the exciting fields can be varied smoothly in the region of cavity resonance. Rather long pulses are contemplated in the final design to allow the cavity fields to approach their steady-state values. The initial electron injection is to be over the entire r-f cycle, using a d.c. gun of relatively low voltage (10 kv). The injection at succeeding cavities is, of course, dependent on the phase and velocity homogeneity provided by the preceding cavities.

Calculations begun about a year ago indicate that the energy increment per cavity in electron volts is at least sixty percent of the peak voltage across the cavity. With low-voltage d.c. injection a large class of electron phases result in complete traversal of the first cavity. The transition between classical and relativistic velocities under the action of sinusoidal fields leads to longitudinal or phase focusing in the first cavity which is maintained in succeeding cavities. These fields also provide fair energy homogeneity even from the first cavity. Figure 1 shows the calculated energy spectrum from the first cavity for a given set of conditions. The magnetic fields in the cavity provide transverse focusing for nearly all of the accepted electrons for short cavities, and it appears that even with longer cavities magnetic defocusing will not be serious.

* This development is being supported by the Office of Naval Research under contract N6ori-44. We are indebted to the George Sheffield Fund for a grant and to Machlett Laboratories, Inc. for several 2C39 triodes for our low power testing.

## The Isotopic Composition of Meteoritic Copper

HARRISON BROWN
*Institute for Nuclear Studies, University of Chicago, Chicago, Illinois*
AND
M. G. INGHRAM
*Argonne National Laboratory, Chicago, Illinois*
June 28, 1947

CONSTITUENTS of iron meteorites that have been previously studied for possible alterations in isotopic composition, using modern techniques, are iron[1] and carbon.[2] In neither case was a significant difference in composition between meteoritic elements and terrestrial elements observed. We have extended the work to a minor constituent of iron meteorites, copper, and have likewise observed no significant difference.

Copper is present in iron meteorites to an extent of approximately 300 parts per million.[3] One hundred grams of Canyon Diablo meteorite[4] were dissolved in HCl. The residual matter was treated with concentrated HF, following which a single treatment with $HNO_3$ served to take the residue into solution. The acid concentration was adjusted to 0.1$M$, and the copper was co-precipitated with bismuth sulfide, previously purified from copper. The bismuth sulfide was dissolved and reprecipitated several times in order to eliminate traces of nickel, following which the bismuth and copper were separated by precipitating the bismuth several times in ammonia solution. The copper was finally precipitated alone as the sulfide, dissolved in $HNO_3$, and evaporated to dryness several times with HCl.

Three samples of copper were studied with the mass spectrometer:[5] a sample of terrestrial copper as CuCl, a sample of terrestrial copper as $CuCl_2$, and the Canyon Diablo sample as $CuCl_2$. The spectrometer was equipped with an automatic recorder, thus enabling one to measure quickly and conveniently about thirty ratios on each sample. The averages are shown in Table I.

TABLE I. Abundance ratios of $Cu^{63}$ to $Cu^{65}$ for terrestrial and meteoritic copper.

| Source of copper | Form of copper | Ratio $Cu^{63}/Cu^{65}$ |
|---|---|---|
| Terrestrial | CuCl | 2.236 |
| Terrestrial | $CuCl_2$ | 2.234 |
| Canyon diablo | $CuCl_2$ | 2.244 |

It can be seen that the isotopic ratio for meteoritic copper does not differ from that of terrestrial copper by more than 0.5 percent, which we believe is within the experimental error.

The possible astrophysical implications of this isotope ratio identity in copper are discussed elsewhere in this issue.[6]

We are indebted to Col. C. C. Gregg, the Director of the Chicago Natural History Museum, and to Dr. S. K. Roy, the Curator of Geology, for their kindness in making available suitable meteorite samples.

[1] G. E. Valley and H. H. Anderson, Phys. Rev. **59**, 113 (1941).
[2] B. F. Murphy and A. O. Nier, Phys. Rev. **59**, 771 (1941).
[3] I. Noddack and W. Noddack, Naturwiss. **35**, 757 (1930).
[4] For a description of this meteorite see O. C. Farrington, Mem. Nat. Acad. Sci. **13**, 96 (1915).
[5] M. G. Inghram, Phys. Rev. **70**, 653 (1946).
[6] H. Brown, Phys. Rev. **72**, 348 (1947).

## An Experimental Method for the Estimation of the Age of the Elements

HARRISON BROWN
*Institute for Nuclear Studies, University of Chicago, Chicago, Illinois*
June 28, 1947

ALL evidence indicates that the elements were formed at some time within a period of $3\times10^9$ to $10\times10^9$ years ago. The lower limit has been set by estimates of the age of the earth's crust,[1] while the upper limit is based upon the fact that certain radioactive species still exist in nature. Further definition of the age, utilizing well-known radioactive methods of age determination, is difficult primarily because of our ignorance concerning the original isotopic composition of lead. However, recent studies of the composition of meteoritic matter, undertaken by the author, suggest a method for at least partially overcoming this difficulty.

Meteorites are composed in general of mixtures of one or more distinct phases: metallic iron-nickel, silicate, and sulfide. Elements are distributed between the phases according to rules which are as yet incompletely understood. It is generally believed, but not proved, that the elements distributed themselves between these phases during the process of planet formation.

The time elapsed since the formation of the elements can be divided into two parts: $t_1$, the time interval between the formation of the elements and the separation of elements into the various phases comprising meteoritic matter; and $t_2$, the time interval between the meteoritic phase separation and the present. The latter time interval, $t_2$, is subject to experimental determination using the uranium-lead technique.[2] It involves the determination of the isotopic composition of lead isolated both from the silicate and metallic phases, together with a determination of the lead and uranium contents of both phases. Although this is a difficult task, it is by no means impossible, as can be seen by the average abundance figures[3] given in Table I.

A direct estimate of $t_1$ is possible if we assume that when the elements were formed, essentially all possible species were formed in amounts depending upon nuclear properties such as binding energy and the number and kinds of particles in the nucleus. The short and intermediate-lived substances presumably have since decayed away, while those species with half-lives comparable to the total elapsed time still exist in nature.

If the meteoritic phase separation took place before a given radioactive species had decayed into insignificance, and if the parent and daughter elements were fractionated from one another during the phase separation, then one would expect the isotopic composition of the daughter element to differ in the two phases. In such a case, one would be able to set an upper limit to the time interval of a few half-lives.

On the other hand, if no isotopic composition difference is observed, a lower limit for the interval could be set, although less precisely because of the difficulty of estimating the initial abundance of the parent. If a series of nuclear species, possessing half-lives covering the range of $10^3$ to $10^9$ years were available, it should be possible to estimate $t_1$ fairly accurately. Unfortunately, such a series is as yet unknown, probably, in great measure, because of the difficulties of producing these species of intermediate half-life in sufficient intensity to permit their detection and identification. It is possible, however, that with the development of high energy accelerators and high intensity piles more species in this interesting range will be discovered and characterized.

TABLE I. Uranium and lead contents (parts per million).

| | Iron phase | Silicate phase | Earth's crust |
|---|---|---|---|
| Uranium | 0.1 | 0.4 | 4 |
| Lead | 56 | 2 | 16 |

The general method outlined above for the determination of $t_1$ has been applied to one case, that of copper,[4] where unfortunately the half life of the nickel parent ($Ni^{63}$) is as yet unknown.[5,6] Stability considerations indicate that it should be long lived. No isotopic abundance differences between copper isolated from an iron meteorite and earth's crust copper were observed, although the nickel-copper ratio in the first case is 200 and in the latter approximately unity. This result, when coupled with an identification of the $Ni^{63}$ half-life, should permit a rough estimate of the lower limit of $t_1$.

[1] A. Holmes, Nature **159**, 127 (1947).
[2] It should be pointed out that Paneth has determined the helium ages of a number of meteorites. F. Paneth, Zeits. f. Elektrochemie **36**, 727 (1930); Naturwiss. **19**, 164 (1931); Zeits. f. physik. Chemie (Bodenstein Festband) **145** (1931).
[3] V. M. Goldschmidt, Mat.-Naturv. Klasse, 1947, No. 4 (Oslo, 1938).
[4] H. Brown and M. G. Inghram, Phys. Rev. **72**, 347 (1947).
[5] J. A. Swartout, *et al.* Phys. Rev. **70**, 232 (1946).
[6] E. E. Conn, *et al.* Phys. Rev. **70**, 768 (1946).

## The Effect of a Direct Current Potential on the Initiation of a Radiofrequency Discharge

F. KIRCHNER
*University of Cologne, Cologne, Germany*
July 5, 1947

IN a recent number of this journal[1] an effect of a d.c. potential on the initiation of a radiofrequency discharge was described by Arthur A. Varela. He found that the application of a d.c. potential greatly impeded the formation of the discharge, and that a considerably higher r-f potential was required for the initiation of the discharge.

I should like to mention that I described the same effect in a paper[2] in which I studied the r-f potentials necessary for the initiation and maintenance of a discharge in different gases with different frequencies. I found, for instance, that the application of a d.c. potential of plus or minus 60 volts to a r-f discharge, maintained by an a.c. potential of 60 volts, caused the discharge to vanish completely.[3] As I showed in this paper, the reason for this effect is that the displacement which the electrons responsible for ionization can attain during one period of the oscillation, is of the same order of magnitude as, or is smaller than, the distance between the electrodes, and that therefore these electrons can oscillate between the electrodes and give rise to a cumulative generation of ions.

[1] A. A. Varela, Phys. Rev. **71**, 124 (1947).
[2] F. Kirchner, Ann. der Physik **77**, 287 (1925).
[3] F. Kirchner, Ann. der Physik **77**, 298 (1925).

## On the Existence of a Calcium Isotope with an 8.5 Day Period†

ROY OVERSTREET* AND LOUIS JACOBSON**
*Radiation Laboratory, Department of Physics, University of California, Berkeley, California*
June 25, 1947

WALKE, Thompson, and Holt,[1] in a study of the radioactive isotopes of calcium, have reported an isotope with an 8.5 day half-life which they have given the assignment of $Ca^{41}$. It was prepared in greatest yield by the bombardment of calcium metal with 8 Mev deuterons. Also, very low yields of the isotope were prepared by bombarding calcium oxide with fast neutrons. The authors conclude that $Ca^{41}$ decays to $K^{41}$ by K-electron capture, emitting primarily x-rays (3500 ev) but some gamma-rays and conversion electrons of high energy (1.1 Mev).

An attempt to produce $Ca^{41}$ has been made in this laboratory using higher energy particles. Although the reported fraction of gamma-rays and conversion electrons is small, it was thought that sufficiently high yields of the isotope could be obtained with 20 Mev deuterons to make feasible its use as a tracer in biological work. The following reactions were tried:

(a) $Ca^{40}(d, p)Ca^{41}$: $CaCl_2$ was bombarded with 20 Mev deuterons to the extent of 40 microampere hours. No activity with a half-life in the neighborhood of 8.5 days and electron energy greater than about 0.05 Mev (limit of the electroscope) was found in the calcium fraction. Approximately 0.3 $\mu$c of long-lived activity (>60 days) was found which presumably was due to $Ca^{45}$. This result was unexpected in view of the fact that high yields are obtained for the reaction $K^{41}(d, p)K^{42}$ at these energies (107 $\mu$c per microampere hour).

(b) $K^{41}(d, 2n)Ca^{41}$: KCl was bombarded with 20 Mev deuterons to the extent of 135 microampere hours. Thirty-six hours after the bombardment the purified calcium fraction was examined for activity. The thickness of the sample was 0.75 milligrams per square centimeter. No activity could be detected upon placing the sample inside an ionization chamber. Also the calcium fraction was examined with negative results by means of a thin window electroscope and a GM counter (window thickness = 2 mg/cm²). As a final check, an x-ray film was placed over the sample for several days. No darkening was observed.

(c) $A^{40}(\alpha, 3n)Ca^{41}$: Argon gas (2.5 liters) was bombarded with 40 Mev alpha-particles to the extent of 20 microampere-hours. The radioactive products were collected on a negatively charged copper wire extending into the gas. No measurable amount of radioactive calcium was produced. The only activity found on the wire was due to $K^{42}$. This isotope was produced in surprisingly good yield by means of the reaction $A^{40}(\alpha, pn)K^{42}$. The yield was 80 $\mu$c per microampere-hour.

In each of the above preparations appropriate inert carriers were added, and calcium was finally isolated as the oxalate. As a special precaution, barium and strontium precipitations were made in all cases. All precipitations were repeated several times in the presence of hold-back carriers in order to insure clean separations. Activities were measured with a Lauritzen electroscope. The air gap plus the electroscope window was equivalent to 4 mg/cm² of aluminum.

On the basis of the experiments described, it must be concluded that if a $Ca^{41}$ isotope exists that emits beta or gamma-rays or energetic conversion electrons, its half-life must be considerably less than one day or longer than one year. The possibility of an isotope that decays by means of K-electron capture to the ground state of the product nucleus $K^{41}$, thus emitting only very soft x-rays (3500 ev) and no gamma-rays or detectable electrons, also seems to be ruled out. On the basis of the observed yield of $Ca^{45}$ from the $(d, p)$ reaction, an 8.5 day $Ca^{41}$ should have been produced by the same bombardment in a yield of ~300 $\mu$c. This amount of activity presumably would have been detected by the instruments used, in view of the fact that 3500 ev x-rays have a half-thickness of ~1.5 mg Al/cm² or ~6 mg air/cm².

† This paper is based on work performed under Contract No. W-7405-eng-48-A with the Atomic Energy Commission, in connection with the Radiation Laboratory, University of California, Berkeley, California.
* Associate Professor of Soil Chemistry and Associate Soil Chemist in the Experiment Station, University of California.
** Assistant Plant Bio-chemist, Division of Plant Nutrition, College of Agriculture, Agriculture Experiment Station, University of California.
[1] H. Walke, F. C. Thompson, and J. Holt, Phys. Rev. **57**, 177 (1940).

---

## A New Naturally Occurring Lanthanum Isotope at Mass 138

MARK G. INGHRAM, RICHARD J. HAYDEN, AND DAVID C. HESS, JR.
*Argonne National Laboratory, Chicago, Illinois*
July 5, 1947

LANTHANUM was studied with a Nier-type mass spectrometer, using a thermal ionization source coated with the oxide, and a vibrating reed electrometer. It was known from previous experiments that the heated oxide emits primarily oxide ions at mass 155. Peaks at masses 154, 155, 156, and 157 were observed. The 155, 156, and 157-peaks were present in relative abundances characteristic of $La^{139}O^{16}$, $La^{139}O^{17}$ and $La^{139}O^{18}$. The peak at 154 was unexpected but was always present to the same relative amount in four different lanthanum samples. The possibilities that this new peak might be due to $Ce^{138}O^{16}$, $Ba^{138}O^{16}$, $Sm^{154}$, or $Gd^{154}$ were ruled out because these elements would also have given other lines. We are obliged to attribute the 154 line to an isotope of lanthanum, $La^{138}$, which is present to $0.089 \pm 0.002$ percent. This $La^{138}$ isotope has an odd number of neutrons and an odd number of protons, similar to the $K^{40}$ and $Lu^{176}$ isotopes, which are naturally radioactive. Because of this fact an investigation of the activity of normal lanthanum was made. Lanthanum oxide samples were counted with a counter with window thickness 2.6 mg/cm². The purest sample, especially purified from the usual radioactive contaminations found in the rare earths, showed no activity when 200 mg were spread over 5 square centimeters and counted at 25 percent geometry. A more complete description of this investigation will be published in the near future.

## Theoretical Evaluation of the Size-Frequency Curve of Extensive Cosmic-Ray Showers

G. Cocconi
*Istituto Di Fisica, Universita Di Catania, Catania, Italy*
June 30, 1947

SKOBELTZYN, Zatsepin, and Miller[1] recently recorded at 3860 m above sea level extensive cosmic-ray showers causing coincidences $C$ between two counter trays when the distance $D$ between them was varied from 2 to 1000 m; each tray consisted of two G.M. counters, 1.5 m apart, and of 1840 cm² efficient surface. The circled points in the figure represent the results for $D=100$, 285, 585, and 1000 meters.

Skobeltzyn and co-workers, using the formulas of the cascade theory, evaluated theoretically the behavior of the curve of fourfold coincidences *versus* distance $D$ (dotted line in Fig. 1) and reached the conclusion that the disagreement between theory and experiments is very large for the most extensive showers, so that they cannot be assumed to be generated by the known multiplicative processes.

In order to specify more exactly the amount of this disagreement, we tried to calculate not only the behavior of the curve but also the absolute value of the fourfold coincidences using Rossi and Greisen's formulas[2] for the cascade theory and Moliére's electron distribution in extensive showers.[3] We used the primary spectrum of Heisenberg[4]

$$H(E)=0.05[10^{10}/E]^{\gamma}\ \text{cm}^{-2}\ \text{sec.}^{-1}, \qquad (1)$$

where $H(E)$ represents the number of primary particles with energy $\geqslant E$ in electron-volts coming from the semi-space: we assumed tentatively $\gamma=1.6$, 1.7, 1.8. Let $w(r)$ be the probability, deduced from Moliére's curve, that a particle of a shower may fall on unit surface at a distance $r$ from the axis of the shower, then the density of particles in the shower at $r$ is:

$$\Delta(r, E, l)=w(r)N(E, l),$$

where $N(E, l)$ is the total number of particles in the shower, $E$ the energy of the primary electron generating the shower, and $l$ the air thickness crossed by the shower.

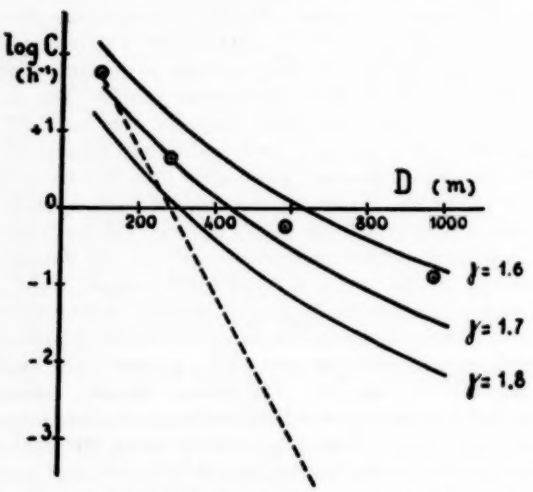


FIG. 1. Plot of the fourfold coincidence rate as a function of the separation of the counter-trays.

In order to calculate the number of fourfold coincidences when the two counter trays are $D$ meters apart, let $r_1$ and $r_2$ be the distances of the counter trays from the axis of the shower; then the probability of recording a fourfold coincidence is:

$$P(D, r_1, r_2, E, l)=[1-\exp(-\Delta_1 S)][1-\exp(-\Delta_2 S)],$$

where $\Delta_1(r_1, E, l)$ and $\Delta_2(r_2, E, l)$ are the densities of the shower at the two counter trays.

If $\nu(E)dE$ is the frequency (per cm² per sec. and per unit solid angle) of primary electrons having energies lying between $E$ and $E+dE$ (from formula (1)), the number of fourfold coincidences produced by electrons coming in such a direction as to cause the shower cross a thickness $l$ of atmosphere, results:

$$n(D, l)=\int_0^{\infty}\int_s \nu(E)P(D, r_1, r_2, E, l)dEds, \qquad (2)$$

where the integral over $ds$ goes over the position of the shower core in the horizontal plane of the counters.

The frequency $N(D)$ of the fourfold coincidences at a distance $D$ can be obtained by integrating over all semi-space. It must be taken into account that, if $l_0$ is the vertical thickness of the air above the place of measurement (in the case of the measurements in discussion $l_0=645$ g cm$^{-2}=15$ radiation lengths), the showers whose axes form an angle $\theta$ with the vertical, cross an air thickness $l=l_0/\cos\theta$ and fall on the counter set as if the two trays were at a distance $D\cos\theta$. Hence

$$N(D)=2\pi\int_0^{\pi/2} n(D\cos\theta, l/\cos\theta)\sin\theta\, d\theta. \qquad (3)$$

The computation of Eqs. (2) and (3) was carried out graphically for $D=100$, 300, 600, 1000 m and for $\gamma=1.6$, 1.7, 1.8. The results are represented by the full curves in the figure. In contrast with the conclusions of Skobeltzyn and coworkers, the agreement between theory and experiment is satisfactory both for the behavior of the curves and for the absolute values of the frequencies. The best agreement seems to be obtained for the curve with $\gamma=1.7$.

We think that the most important reason for the disagreement between Skobeltzyn's and our calculations is the fact that Skobeltzyn did not take into account that for the showers forming a great angle with the vertical the apparent counter-trays' distance, $D\cos\theta$, can be very much reduced. Owing to the fact that the most extensive showers are generated by very energetic primary particles ($10^{17}$–$10^{18}$ ev), the larger thickness of air does not appreciably affect the number of electrons in the shower; on the other hand, the apparent reduction of $D$ strongly increases the number of coincidences. When $D=1000$ m, most of the coincidences are due to showers with $\theta=50°$; the vertical showers, in this case, are about 1000 times less frequent. Therefore the results of our calculations do not confirm the disagreement between cascade theory and experiment pointed out by Skobeltzyn.

This conclusion does not necessarily mean that the cascade theory maintains its validity up to energies as high

as $10^{18}$ ev, and that the primary spectrum remains for these energies of the form (1). We only wish to call attention to the fact that up to now all measurements on the extensive cosmic-ray air showers fit this hypothesis satisfactorily.

[1] D. V. Skobeltzyn, G. T. Zatsepin and V. V. Miller, Phys. Rev. **71**, 315 (1947).
[2] B. Rossi and K. Greisen, Rev. Mod. Phys. **13**, 240 (1941).
[3] G. Moliére, *Vorträge über Kosmische Strahlung* (Berlin, 1943), p. 24.
[4] W. Heisenberg, *Vorträge über Kosmische Strahlung* (Berlin, 1943), p. 10.

## Altitude Dependence of High Energy Atmospheric Showers

HENRY L. KRAYBILL, *The University of Chicago, Chicago, Illinois*
AND
PAUL J. OVREBO, *Aircraft Radiation Laboratory, Dayton, Ohio*
June 28, 1947

MEASUREMENTS of the frequency of high energy atmospheric showers above 15,000 feet have been obtained on a B-29 plane flown by the U. S. Army Air Forces. The altitude dependence of the showers was indicated by the counting rate of a simple arrangement of counters in threefold coincidence, separated by a horizontal distance of eleven feet. The counter geometry is shown in Fig. 1.

Each counter had a sensitive area of 1 inch by 13.5 inches and was mounted just below the roof of the pressurized cabin of the airplane. An estimated 1.3 g/cm² of material consisting of aluminum and wood were above the counters. A shielded low capacity cable led from the counters to the coincidence circuit, which had a resolving time of 3 microseconds. The circuits, counters, and all batteries supplying power for the vacuum tube circuits were electrostatically shielded. The coincidences were registered by a mechanical impulse counter, which was read periodically during flight.

The variation of counting rate with altitude was determined in the vicinity of Wright Field, Dayton, Ohio, between 48° N and 51° N geomagnetic latitude. Measurements were made at five separate elevations between 15,000 feet and 33,000 feet. The results are shown in Table I.

In addition to the flights near Wright Field, data were also collected at 33,000 feet between 0° and 25° geomagnetic latitude during a flight between Wright Field and Lima, Peru. The average counting rate between 0° and 25° was $32.1 \pm 1.0$ counts per hour. The good agreement of this value with the counting rate at the same altitude between 48° N and 51° N strongly indicates that the observed showers do not show a latitude effect and hence must originate from high energy particles which do not carry an extremely high charge.[1]

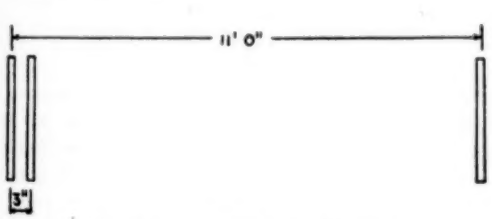


FIG. 1. Arrangement of the counters.

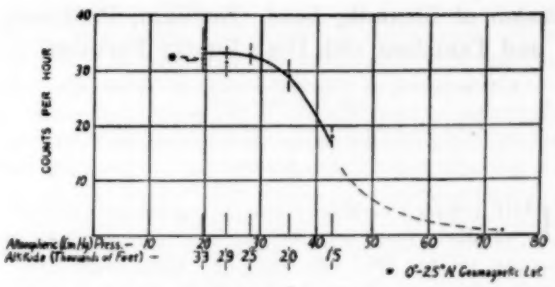


FIG. 2. Variation of the triple coincidence counting rate with the atmospheric pressure (altitude).

TABLE I. Counting rate *versus* altitude of extensive atmospheric showers.

| Altitude | Pressure | Time | Total counts | Counting rate |
|---|---|---|---|---|
| 1000 ft | 73.4 cm | 1368 hrs. | 1001 | $0.73 \pm 0.3$/hr. |
| 15,000 | 43.0 | 4.5 | 80 | $18 \pm 2$ |
| 20,000 | 35.0 | 3.0 | 86 | $29 \pm 3$ |
| 25,000 | 28.0 | 6.0 | 197 | $33 \pm 2$ |
| 29,000 | 23.6 | 3.8 | 118 | $31 \pm 3$ |
| 33,000 | 19.7 | 2.2 | 74 | $34 \pm 4$ |

Figure 2 shows the threefold counting rate plotted against atmospheric pressure. The dashed curve represents data published by Hilberry[2] between sea level and 14,300 feet. For comparison, his results have been multiplied by a constant factor in order to make his counting rate equal to our counting rate at sea level.

The solid curve shows that the counting rate first increases rapidly up to an altitude of 25,000 feet and is then constant within experimental error between 25,000 and 33,000 feet.

If one assumes that the observed showers originate from electrons near the top of the atmosphere with an integral energy spectrum of the form $E^{-1.8}$, it can be shown that showers from electrons of $10^{13}$ ev energy have insufficient particle density to contribute to the observed counting rate above 15,000 feet. Therefore, the observed showers are believed to arise predominantly from particles of energy definitely higher than $10^{12}$ ev. However, showers produced by vertically incident electrons of such high energies would reach their greatest number of electrons in regions below 33,000 feet, and would consequently produce a definite peak in the curve of counting rate *vs.* altitude at an elevation below 33,000 feet. On the other hand, particles incident from varying zenith angles will cause the region of maximum counting rate to be higher in the atmosphere and less sharply defined than for showers from vertically incident particles alone. The fact that the observed counting rate curve shows a broad plateau instead of a definite peak thus indicates that many of the observed showers arise from particles incident at large zenith angles.

We wish to thank Professor M. Schein for many helpful suggestions. Gerhard C. Willecke, Elmer Winterland, and Lt. S. H. Seeleman of Wright Field assisted in carrying out the experiments.

[1] O. Klein, Arkiv. f. mat. astr. och fysik **31A** [14] (1944–45).
[2] N. Hilberry, Phys. Rev. **60**, 1 (1941).

## Fission of Bismuth, Lead, Thallium, Platinum, and Tantalum with High Energy Particles*

I. PERLMAN, R. H. GOECKERMANN, D. H. TEMPLETON, AND J. J. HOWLAND
*Radiation Laboratory and Department of Chemistry, University of California, Berkeley, California*
June 26, 1947

THE 184-inch Berkeley frequency-modulated cyclotron produces deuterons, helium ions, and neutrons of energies up to 200, 400, and 100 Mev, respectively. Nuclear fission in elements covering the range of atomic numbers 83 (bismuth) to 73 (tantalum) has been observed with one or more of the above projectiles. Fission was determined by chemical identification of radioactive fission products.

Although a number of the fission products characteristic of slow neutron fission of uranium are found, the fission reaction on these light elements with high energy particles differs in some important respects. There is no evidence for well-defined asymmetric cleavage with a deep valley at the midpoint of the yield curve as is the case with slow neutron fission. Another difference is the appearance in good yield of light isotopes of a given element, and undoubtedly the formation of stable isotopes as primary fission products is not unusual. For example, the shielded isotope $Br^{82}$ is formed in comparable yield to $Br^{83}$ with 400 Mev helium ions and 200 Mev deuterons on bismuth, while the relative yields are 1 to $10^4$ for these isotopes in the slow neutron fission[1] of uranium. In the bombardment of bismuth and lead with 400 Mev helium ions, no measurable amount of $Ba^{140}$ (formed in highest yield with slow neutrons on uranium) was found, but an activity which is probably[2] $Ba^{132}$ was noted. This isotope is not found at all in the fission of uranium with slow neutrons as it falls well down among the lightest stable isotopes of barium.

It has not been possible, thus far, to compare accurately yields from different bombardments because of the inability to determine the beam strength. However, certain trends appear to be definite: The probability of the fission reaction for a given projectile drops off as the target atomic number decreases from bismuth to tantalum. That for a given target element the fission yield decreases as the projectile energy decreases is indicated by the decrease in yield of bromine activities from bismuth fission as the deuteron energy is varied from 200 to 50 Mev. The distribution of fission products changes in varying the projectile energy since the ratio of $Br^{83}$ to $Br^{82}$ was 2 for 200 Mev deuterons on bismuth and 100 for 50 Mev deuterons on bismuth.

Table I shows fission products found from the reaction of 400 Mev helium ions with bismuth and the relative yields of these isotopes. The radioactive properties checked reasonably well those previously reported for these isotopes.[1,2] The yields are expressed in arbitrary units. It is of interest that $Ba^{140}$ was not present in detectable amount.

TABLE I. Relative yields of fission products from 400 Mev helium ions on bismuth.

| | | | |
|---|---|---|---|
| $Ga^{72}$ | 22 | $Mo^{99}$ | 480 |
| $Br^{82}$ | 150 | $Ru^{105} \rightarrow Rh^{105}$ | 240 |
| $Br^{83}$ | 390 | $I^{131}$ | 8 |
| $Sr^{91} \rightarrow Y^{91}$ | 540 | $Ba^{132}$ | 34 |
| $Y^{90}$ | 1400 | | |

TABLE II. Summary of irradiations in which fission was observed

| Target | Projectile | Energy (Mev) |
|---|---|---|
| Bi | $\alpha$ | 400 |
| Bi | $d$ | 200, 150, 90, 70, 50 |
| Bi | $n$ | 100 |
| Pb | $\alpha$ | 400 |
| Pb | $d$ | 200 |
| Pb | $n$ | 100 |
| Tl | $\alpha$ | 400 |
| Tl | $d$ | 200 |
| Pt | $\alpha$ | 400 |
| Ta | $\alpha$ | 400 |

The conditions of irradiation that were tried and under which fission was observed in all cases are summarized in Table II.

It is of interest to speculate on the mechanism of the fission in view of the high degree of excitation of the compound nucleus. Since the probability of fission would increase with a greater (charge/mass) ratio, and since it is known[3] that large numbers of neutrons may be ejected from such highly excited nuclei, it seems likely that the actual fission reaction is preceded, on the average, by the boiling-off of a large number of neutrons. Some experimental evidence supporting this view is the appearance of light isotopes for a given element in a few cases and the finding that the most probable fission results in products the sum of whose masses lies well below that of the target mass number. However, the same observations would result if the fission reaction would occur first with the fragments still in highly excited states after dissipation of their kinetic energy.

The cooperation of Prof. R. L. Thornton, Dr. D. C. Sewell, and all those whose operation of the 184-inch cyclotron made these irradiations possible is gratefully acknowledged. We wish to thank Professor E. O. Lawrence for continued interest and Professor G. T. Seaborg for helpful discussions regarding this work.

* This paper is based on work performed under Contract No. W-7405-eng-48 with the Atomic Energy Commission in connection with the Radiation Laboratory, University of California.
[1] Plutonium Project compilation of nuclei formed in fission. J. Am. Chem. Soc. **68**, 2411 (1946).
[2] G. T. Seaborg, "Table of Isotopes," Rev. Mod. Phys. **16**, 1 (1944).
[3] B. B. Cunningham, H. H. Hopkins, M. Lindner, D. R. Miller, P. R. O'Connor, I. Perlman, G. T. Seaborg and R. C. Thompson. Paper to be given before Stanford University meeting of the American Physical Society, July 11–12, 1947.

## The Radiations from 60-Day $Ir^{192}$ and 27-Day $Pa^{233}$*

PAUL W. LEVY
*Clinton Laboratories, Oak Ridge, Tennessee*
June 25, 1947

THE 180° beta-ray spectrometer which was used in the determination of the maximum energy of the beta-ray spectrum of $C^{14}$, described in a previous letter, has been used to investigate the conversion electron and beta-ray spectrum of 27-day $Pa^{233}$. This spectrometer, and an additional photographically recording spectrograph, were

TABLE I. Gamma-rays and conversion lines in $_{91}Pa^{233}$.

| Gamma-ray | Conversion lines observed | Energy of conversion lines (Mev) | Energy of gamma-rays (Mev) |
|---|---|---|---|
| 1 | $K$ | 0.193 | 0.309 |
| | $L$ | 0.289 | 0.310 |
| | $M$ | 0.305 | 0.310 |
| 2 | $K$ | 0.222 | 0.337 |
| | $L$ | 0.318 | 0.339 |
| 3 | $K$ | 0.183 | 0.298 |
| | $L$ | 0.277 | 0.298 |
| 4 | $L$ | 0.063 | 0.084 |
| | $M$ | 0.081 | 0.083 |

employed to analyze the spectrum of the 60-day $Ir^{192}$ activity.

The data on the conversion electrons from $Pa^{233}$ are summarized in Table I. The end point of the continuous spectrum of the $Pa^{233}$ is completely masked by a conversion line, and consequently it is difficult to estimate the maximum energy more accurately than to say that it is approximately 0.2 Mev. These beta- and gamma-ray energies are in substantial agreement with the values reported by Haggstrom,[1] who found conversion lines indicative of only three gamma-rays, but suggests that a fourth might exist.

The beta-ray and conversion electron spectrum of the 60-day $Ir^{192}$ activity consists of a large number of conversion lines superimposed on what appears to be a simple continuous spectrum. The maximum energy of the spectrum, determined from a Kurie plot constructed from data taken with the 180° spectrometer, is 0.67 Mev. This value would be accurate to 2 percent if the presence of the conversion lines near the high energy end of the spectrum did not introduce the possibility of a larger error. Because of these lines the shape of the spectrum is difficult to ascertain. Consequently, one cannot exclude the possibility that the spectrum consists of several components, nor can one use it to make a theoretical analysis based on its shape.

TABLE II. Gamma-rays and conversion lines in $_{77}Ir^{192}$.

| Gamma-ray | Conversion lines observed | Estimated intensity of conversion lines | Energy of conversion lines (Mev) | Energy of gamma-rays (Mev) |
|---|---|---|---|---|
| 1 | $K$ | Very faint | 0.121 | 0.199 |
| 2 | $K$ | Very faint | 0.124 | 0.202 |
| 3 | $K$ | Faint | 0.128 | 0.205 |
| | $L$ | Very faint | 0.193 | 0.205 |
| 4 | $K$ | Medium | 0.131 | 0.209 |
| | $L$ | Faint | 0.194 | 0.208 |
| | $M$ | Faint | 0.202 | 0.205 |
| 5 | $K$ | Strong | 0.217 | 0.295 |
| | $L_{I+II}$ | Medium | 0.281 | 0.295 |
| | $L_{III}$ | Faint | 0.284 | 0.296 |
| | $M$ | Faint | 0.293 | 0.296 |
| 6 | $K$ | Strong | 0.229 | 0.307 |
| | $L_{I+II}$ | Medium | 0.295 | 0.308 |
| | $L_{III}$ | Faint | 0.297 | 0.308 |
| 7 | $K$ | Very strong | 0.237 | 0.316 |
| | $L_{I+II}$ | Medium | 0.303 | 0.317 |
| | $L_{III}$ | Faint | 0.305 | 0.316 |
| | $M$ | Faint | 0.314 | 0.316 |
| | $N$ | Very faint | 0.316 | 0.317 |
| 8 | $K$ | Strong | 0.390 | 0.468 |
| | $L_{I+II}$ | Faint | 0.456 | 0.469 |
| | $L_{III}$ | Very faint | 0.457 | 0.469 |
| 9 | $K$ | Very faint | 0.410 | 0.488 |
| 10 | $K$ | Faint | 0.513 | 0.591 |
| | $L$ | Very faint | 0.580 | 0.593 |
| 11 | $K$ | Faint | 0.529 | 0.607 |
| | $L$ | Very faint | 0.595 | 0.608 |
| 12 | $K$ | Very faint | 0.537 | 0.615 |

The conversion lines were studied with the photographic spectrograph, and the results are summarized in Table II. These results are in agreement with, but are more accurate than, those obtained with the 180° counter spectrometer. The accuracy of the gamma-ray energies for both the $Pa^{233}$ and $Ir^{192}$ is approximately 2 percent. The energy differences of the observed lines agree best with the differences between the electronic levels of Pt, and therefore it was assumed that all of the conversions take place in the Pt atom formed by beta-decay.

* A detailed description of this work and of the spectrometer used is contained in Plutonium Project Report CP-3702 which is to appear in Division IV of the Manhattan Project Technical Series as part of the contribution of Clinton Laboratories. This work was done under the auspices of Manhattan District Contract W 7405-eng 39.

[1] E. Haggstrom, Phys. Rev. **59**, 322 (1941).

## On a Connection between the Fountain Effect, Second Sound, and Thermal Conductivity in Liquid Helium II

LASZLO TISZA
*Massachusetts Institute of Technology, Cambridge, Massachusetts*
July 2, 1947

UNDER the above title, Lothar Meyer and William Band[1] advanced the assumption that "in the absence of constriction, the internal forces responsible for the fountain effect are still present, and produce an internal momentum density $M$." They conclude that there exists a wave equation for the temperature $T$ "similar" to second sound, with the velocity $c_2(T)$ increasing up to the $\lambda$-point. Since this is in conflict with experiments according to which $c_2(T)\rightarrow 0$ as $T\rightarrow T_\lambda$, Meyer and Band conclude that the disagreement is due to irreversible effects. Their reason seems to be the resemblance between the curves representing $c_2(T)$ and $\mu(T)$, the latter being the fountain pressure measured in not very thin capillaries where irreversible effects make their appearance.

The following points should be raised in connection with these ideas:

The assumption that the fountain pressure exists in helium II far from solid walls is correct,[2,3] but Eq. (1), which Meyer and Band deduce from this, is not. The correct equation should read in Meyer and Band's notation:

$$\mu\nabla T=\nabla p=-(\rho/\rho)_d d\mathbf{M}/dt. \qquad (1a)$$

Equation (1a) differs by the factor $\rho/\rho_s$ from Eq. (1) of Meyer and Band. Equation (1a) has been given[2] and derived[3] from the point of view of the theory of the Bose-Einstein liquid. Actually it can be derived also from more general assumptions with quasi-thermodynamical methods.[4] The factor $\rho/\rho_s$ assures that $c_2\rightarrow 0$ for $T\rightarrow T_\lambda$ as required by

experiment. It should be emphasized that the theoretical expression for $c_2(T)$ was not adjusted to fit the experiments but appeared as a prediction. Hence, there is no basis for postulating new effects to explain the observed values of $c_2$.

Meyer and Band's contention is that their relations are phenomenological. Actually a molecular model is introduced in a concealed fashion into their considerations. Their relations between pressure, momentum density, and heat content are not valid except in a *gas*. A condensation of the Bose-Einstein type is assumed implicitly in their sentence following Eq. (4). It should be pointed out that the author's theory[2,3] does not refer to a Bose-Einstein *gas*, but to a Bose-Einstein *liquid*. In such a system the *coupling between the normal and superfluid components is taken into account* and leads to the factor $\rho/\rho_s$ in (1a) which assures agreement with observations.

Although experiments so far have failed to show any dissipation effects in second sound,[5] such effects (absorption and dispersion) are to be expected in second approximation. The investigation of these effects would be of great interest for the solution of certain questions regarding the molecular theory[4] of helium II. However, on the basis of the present state of the theory, there is no reason to expect that irreversible phenomena would manifest themselves in a way predicted by Meyer and Band.

[1] L. Meyer and W. Band, Phys. Rev. **71**, 828 (1947).
[2] L. Tisza, C.R. Paris, Phys. Rev. **207**, 1035 (1938).
[3] L. Tisza, J. de Physique (8) **1**, 350 (1940).
[4] L. Tisza (to be published).
[5] V. Peshkov, J. Phys. **10**, 389 (1946); C. T. Lane, H. Fairbank, H. Schultz, W. Fairbank, Phys. Rev. **71**, 600 (1947).

## Production of Helium in Meteorites by Cosmic Radiation

CARL AUGUST BAUER
*Harvard College Observatory, Cambridge, Massachusetts*
June 27, 1947

THE amounts of helium, uranium, and thorium in iron meteorites have been used to compute the times since their solidification. In the application of this method it has been assumed that the helium contents are affected only by the decay (at the present observed rate) of U and Th. Paneth[1] has measured the helium content of about 50 iron meteorites. Figure 1 shows the logarithm of the mass of each of these meteorites[2] (total mass if two or more meteorites are associated) plotted against their helium content. The large helium contents appear only in the relatively small masses or, conversely, all of the large meteorites show relatively small helium contents. This relation indicates that the helium contents of meteorites are related to their pre-atmospheric masses, and in a sense is contrary to that to be expected if an appreciable leakage of helium had occurred. For a given helium content the points with the relatively small masses may represent the meteorites that were only partially recovered or that struck the atmosphere with a relatively high velocity and thus lost a large fraction of their original mass by evaporation.

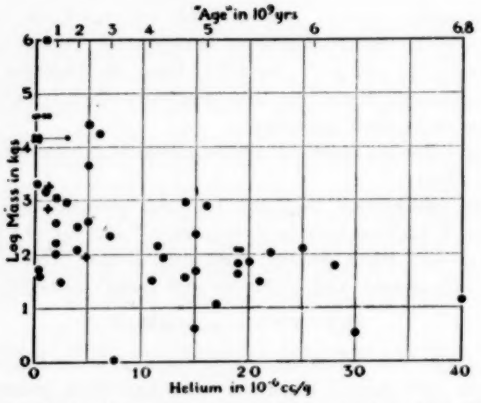


FIG. 1. The logarithm of the mass of iron meteorites plotted against their helium content. Solid circles represent measures of individual iron meteorites. Small connected solid circles represent measures of different individuals of associated meteorites. Crosses represent the iron portion of stony-iron meteorites. The scale at the top shows present assigned ages on the basis of an average U and Th content.

The explanation of Fig. 1 that appears most promising is that cosmic radiation has produced extra helium in the small meteorites. Observations show that cosmic radiation produces nuclear disruptions in which $\alpha$-particles are among the disintegration products. On the basis of published observations it appears reasonable to adopt: (1) $n=1$, the average number of $\alpha$-particles per disruption,[3] (2) $L=150$ g/cm$^2$, the mass in which a cosmic-ray particle will, on the average, produce one disruption,[4] (3) $J=1.5$, the number of primary cosmic-ray particles[5] (probably all capable of producing nuclear disruptions) crossing 1 cm$^2$ per sec. For a meteoroid with a diameter small in comparison with $L$/density (19 cm for iron) the absorption of the radiation is not important, and the rate of $\alpha$-particle formation is

$$N=nJ/L=1.5/150=10^{-2}\ \alpha\text{-particles per sec. per g of meteoroid.}$$

At this rate the disruption process will produce the maximum observed helium content ($4\times10^{-5}$ cc/g) in $3.4\times10^9$ years. If the nuclear-disruption process in iron meteoroids is comparable to that observed in the photographic emulsion and in the cloud chamber, then we can draw the important conclusion that the largest observed helium content can be produced in a small meteoroid by cosmic radiation in a time less than the present assigned age. In traversing the atmosphere, large meteoroids maintain their high cosmic velocities for a longer time and thus lose a thicker layer of material by evaporation than do small meteoroids. Therefore, the meteorites that are derived from the large meteoroids have been better shielded from cosmic radiation than the meteorites that are derived from small meteoroids.

If the absence of primary cosmic radiation with energies less than 3 Bev is attributed to the effect of the sun's magnetic field, then at greater solar distances the cut-off would occur at lower energies. The average solar distance of meteoroids can be taken as about 3 astronomical units, at which distance the cut-off would occur at about 0.3 Bev. In the observed region the number of cosmic-ray protons with energies greater then $E$ Bev is well represented by $N=(7\times10^{-10}/E^{1.9})/\text{cm}^3$. If this relation holds down to energies of 0.3 Bev, then the rate of $\alpha$-particle production in

small meteoroids may be increased by a large factor (up to $10^2$) and the time for the formation of the observed helium contents in small meteorites decreased correspondingly.

There are other observations, in addition to those of Fig. 1, that will give us valuable evidence for or against the proposed process: (1) determination of the ratios $He^3$:$He^4$ for the helium from meteorites, (2) determination of any radial variation in the helium content of meteorites, (3) measurement of the helium, uranium, and thorium contents of both the iron and stone portions of stony-iron meteorites, (4) investigation to detect any cosmic-ray radioelements (such as $C^{14}$).

I wish to express my sincere appreciation to Drs. S. C. Brown and B. Rossi of M.I.T., and to Drs. E. M. Purcell and F. L. Whipple of Harvard for valuable discussions and suggestions.

[1] F. Paneth, Nature **149**, 235 (1942).
[2] The masses are from: H. H. Nininger, *Our Stone-Pelted Planet*, Appendix; A. D. Nininger, Pop. Astron. **45**, 449 (1937); **47**, 209 (1939); **48**, 555 (1940), and F. C. Leonard, Pop. Astron. **51**, 161 (1943). For the two crater-producing meteorites a somewhat low estimate of the mass has been adopted.
[3] W. E. Hazen, Phys. Rev. **65**, 67 (1944); M. M. Shapiro, Rev. Mod. Phys. **13**, 58 (1941); H. Wambacher, Sitzungsberichte Akad. Wiss. Wien **149**, 2a (Nos. 3–4), 157 (1940); **149**, 2a (Nos. 5–6), 231 (1940).
[4] H. Bridge and B. Rossi, Phys. Rev. **71**, 379 (1947).
[5] For $E=3$ Bev the equation $N=(7\times10^{-10}/E^{1.9})/\text{cm}^2$ leads to $J=2.6/\text{cm}^2\text{-sec}$.

## Erratum: On the Alleged Gamma Ray of $N^{13}$

[Phys. Rev. **71**, 906 (1947)]

L. M. Langer, C. S. Cook, and M. B. Sampson
*Indiana University, Bloomington, Indiana*

THE Editor regrets that Fig. 1 of the above Letter to the Editor was badly distorted in reproduction. Its correct appearance is as follows:

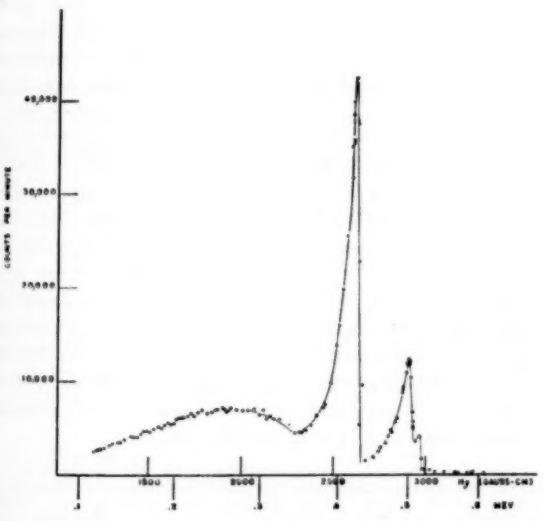

FIG. 1. Momentum distribution of photo and Compton electrons ejected from a Pb radiator by the radiation from $N^{13}$.

## On the High Energy Neutron-Proton Scattering

J. Leite Lopes
*Faculdade Nacional de Filosofia, University of Brazil, Rio de Janeiro, Brazil*

June 23, 1947

IN a previous paper,[1] we calculated the cross section for the inelastic scattering of neutrons by protons with production of isobars, according to the point of view of the meson field theory of nuclear forces with strong coupling. The cross section depends on the isobar energy $E_i$ of a nucleon; the value that we assumed for $E_i$ was 45 Mev, as indicated by Wentzel's[2] attempt to adjust the theory to Amaldi's measurements of the angular distribution of 14 Mev neutrons scattered by protons. Recently, however, Villars[3] showed that if the theory with strong coupling is to give the correct energy levels of the triplet and singlet states of the deuteron, then $E_i$ should be larger[4] than 200 Mev. In this case, the production of isobars is possible only if the kinetic energy $E_0$ of the bombarding neutrons is larger than 400 Mev in the laboratory system. In Table I

TABLE I. Cross sections of the inelastic and elastic $n-p$ scattering at high energies.

| $E_i$ | $E_0$ | $\sigma_{in}(\text{cm}^2)$ | $\sigma_{el}(\text{cm}^2)$ | $R$ |
|---|---|---|---|---|
| 100 Mev | 250 Mev | $1.05\cdot10^{-27}$ | $1.44\cdot10^{-25}$ | 0.007 |
| 150 | 350 | $0.40\cdot10^{-27}$ | $1.03\cdot10^{-25}$ | 0.004 |
| 200 | 450 | $0.24\cdot10^{-27}$ | $0.80\cdot10^{-25}$ | 0.003 |
| 250 | 550 | $0.84\cdot10^{-28}$ | $0.66\cdot10^{-25}$ | 0.001 |
| 300 | 650 | $0.50\cdot10^{-28}$ | $0.55\cdot10^{-25}$ | 0.0009 |
| 350 | 750 | $0.33\cdot10^{-28}$ | $0.48\cdot10^{-25}$ | 0.0007 |
| 400 | 850 | $0.15\cdot10^{-28}$ | $0.42\cdot10^{-25}$ | 0.0003 |

we give the values of the inelastic cross section $\sigma_{in}$ on the symmetrical Møller-Rosenfeld theory with strong coupling,[5] corresponding to several high values of the isobar energy. For comparison we also give the values of the elastic cross section $\sigma_{el}$ as derived from the same theory with weak coupling, i.e., from the potential:

$$V=(\tau_I\cdot\tau_{II})\{g_1^2+g_2^2(\sigma_I\cdot\sigma_{II})\}e^{-\mu r}/r,$$

where the symbols have the usual meaning and $g_1^2=0.05$, $g_2^2=0.09$. Both cross sections were evaluated in the first Born approximation; $R$ is the ratio $\sigma_{in}/\sigma_{el}$.

It is seen that $\sigma_{in}$ decreases more rapidly than $\sigma_{el}$ with increasing energy; the ratio $R$ is already very small for $E_0=250$ Mev. Our results show that such high values of the isobar energy make it still more difficult to check the strong coupling theory directly, at least with a nucleon-nucleon collision experiment. In the same paper,[1] it was stated that the triplet cross section of the elastic scattering of neutrons by protons as calculated by Hulthén[6] in the pseudoscalar theory was not correct. Hulthén's formula is, however, correct[4] and agrees with ours except for a factor 3 by which our formula has to be divided if we use the usual expression:

$$\sigma=\tfrac{1}{4}\sigma_s+\tfrac{3}{4}\sigma_t.$$

The elastic cross section in this theory is $0.18\cdot10^{-24}$ cm² for 100 Mev neutrons; also $R=0.16$ and not 0.05, for $E_i=45$ Mev, as was indicated in our paper.

Calculations are being carried out for high energy proton-proton scattering and will be published elsewhere.

[1] J. Leite Lopes, Phys. Rev. **70**, 5 (1946).
[2] G. Wentzel, Helv. Phys. Acta **18**, 430 (1945).
[3] F. Villars, Helv. Phys. Acta **19**, 323 (1946).
[4] I am indebted to Dr. L. Hulthén for having called my attention to this point.
[5] Ref. 1, section 5.
[6] L. Hulthén, Arkiv. Mat. Astr. Fysik **31A** [15] (1944).

## Quantitative Alpha-Particle Counting by the Emulsion Technique

HERMAN YAGODA AND NATHAN KAPLAN
*National Institute of Health, Laboratory of Physical Biology, Bethesda, Maryland*
June 25, 1947

EXPERIMENTS with weighed thin films of radiochemically pure $U_3O_8$ exposed to fine grained emulsions[1] show that the rate of disintegration $\delta$ can be computed accurately by microscopic evaluation of the number of alpha-particle tracks $n_\tau$ recorded by the emulsion. For films having an equivalent air thickness $\tau$ emitting alpha-particles of average range $\bar{R}$:

$$\delta = 2n_\tau/[1-(\tau+2l)/2(\bar{R}-e)] = n_\tau k_w.$$

When the distance between the source and the emulsion $l$ is less than 0.05 cm, about 98 percent of the tracks are confined to an area on the emulsion equal to that of the source, and $n_\tau$ can be evaluated by counting tracks in sampled portions of this area with a precision of 2 percent. At magnifications exceeding 500×, employing dark field illumination, the tracks of alpha-particles striking the emulsion at normal incidence are readily discernible from the background fog (Fig. 1). Measurements with a collimated source of polonium alpha-particles reveal that the minimum residual air range $e$ recorded in the emulsion as a distinct track is 0.84 air cm. The equivalent air thickness of the source $\tau$ is computed from its atomic composition with the aid of the Bragg-Kleeman stopping power law. For films of $U_3O_8$, $\tau = 0.2288w$, where $w$ is the film thickness in mg per sq. cm. The track-disintegration conversion factor

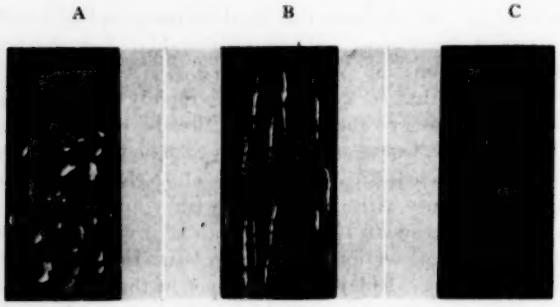


FIG. 1. Dark-field photomicrographs (44× obj. +15× ocular) of tracks from collimated monoenergetic alpha-particles (RaF) at varying obliquities.
A: Perpendicular Incidence. Geometric considerations indicate that these tracks should be dimensionless. After fixation the residual gelatin dries to a very thin layer and the vertical tracks may be tilted slightly. Their visibility is also enhanced by the light scattered from the compressed column of silver grains.
B: 45° Incidence. Using sources weighing less than 1 mg./sq. cm., over 90 percent of the tracks have obliquities typical of visibility class *B*.
C: Oblique tracks of minimum discernibility ($e = 0.84$ air cm.) produced by alpha particles which spent 80 percent of their energy in traversing the source and air gap.

TABLE I. Rate of disintegration in $U_3O_8$ films.*

| Film | $w$ | $k_w$ | Track count | $\delta$ per g of U per sec. |
|---|---|---|---|---|
| *A* | 0.61 | 2.12 | 6604 | $2.51\times10^4$ |
| *B* | 0.75 | 2.14 | 11,600 | 2.48 |
| *C* | 1.43 | 2.23 | 13,500 | 2.37 |
| *D* | 2.32 | 2.36 | 13,874 | 2.34 |
| | | | average: | $2.43\pm.07\times10^4$ |
| Comparative determinations: | | | | |
| Geiger and Rutherford,** from scintillations | | | | $2.37\times10^4$ |
| Kovarik and Adams,*** alpha-pulses | | | | 2.48 |
| Schiedt,† alpha-pulses | | | | 2.53 |
| Kovarik and Adams,†† alpha-pulses | | | | 2.50 |

* The $U_3O_8$ was isolated and purified from a sample of Great Bear Lake pitchblende containing 51.0 percent U, 0.005 percent Th and 10.1 percent Pb. The Pb/U ratio of 0.198 indicates that the specimen (U. S. Nat. Mus. R6736) is probably of the same age ($1.3\times10^9$ yr) as found in the investigations of Marble[5] and Nier.[3] The measurements of Rutherford and Kovarik were made on uranium oxide isolated by Boltwood from Norwegian uraninite of similar geologic age,[3] $1.1\times10^9$ yr.
** H. Geiger and E. Rutherford, Phil. Mag. (6) **20**, 691 (1910).
*** A. F. Kovarik and N. I. Adams, Jr., Phys. Rev. **40**, 718 (1932).
† R. Schiedt, Sitz. Akad. Wiss. Wien, Math.-naturw. Kl. Abt IIa **144**, 175–211 (1935).
†† A. F. Kovarik and N. I. Adams, Jr., J. App. Phys. **12**, 296 (1941).

$k_w$ was evaluated for an air gap of 0.05 cm, using 2.93 cm for $\bar{R}$ (the weighted average of the mean ranges of the alpha-particles emitted by U*I*, U*II* and AcU based on the measurements of Rayton and Wilkins[2] and the activity ratios of Nier).[3]

Preliminary results on sources of varying thickness prepared by the ether-sedimentation method are recorded in Table I. The average on the four films corresponds to a disintegration rate of $2.43\pm0.07\times10^4$ alpha-particles per sec. per g of U. This is in good agreement with other experimental determinations of this constant and indicates the general validity of the method as a quantitative tool. Track counts from electrolytically deposited extra-thin films of uranium may lead to a more precise determination of the value of this fundamental constant.

The principal applications of the method reside in the estimation of low levels of alpha-ray activity, the track population increasing linearly on extended exposure until the fading of the latent image[4] of the older tracks becomes pronounced. Preliminary experiments on an exposure identical with *B* of Table I, but whose development was delayed for 10 days, gave a track count 9.2 percent lower than that of the undelayed control. With the brief exposures of 25 to 10 minutes employed in conjunction with sources *A* to *D* this factor is entirely negligible. However, in the analysis of a radiochemically purified carrier containing only 0.01 percent uranium, a 10 day exposure is desirable, and the track count would be about 5 percent low as a result of partial fading of the older tracks. Experiments on the mechanism and rate of fading in progress at present are expected to yield data on the fading factors covering exposures of 100 days duration for alpha-particles of diverse energy. A comprehensive report covering the technical details of the method is in preparation.

[1] Eastman fine grain alpha-particle emulsion No. 340,388 was employed. Our analyses indicate a composition of 84 percent silver halide and 16 percent gelatin. Their stopping power relative to air is 1680 for alpha-particles of 4.7 to 6.9 Mev. The value of $e$ is dependent on the emulsion composition and must be determined for each lot of plates.
[2] W. M. Rayton and T. R. Wilkins, Phys. Rev. **51**, 818 (1937).
[3] A. O. Nier, Phys. Rev. **55**, 150–163 (1938).
[4] H. Yagoda and N. Kaplan, Phys. Rev. **71**, 910 (1947).
[5] J. P. Marble, J. Am. Chem. Soc. **58**, 434 (1936).